
# Advanced Photon Source Upgrade Project

## Final Design Report

**May 2019**

## Chapter 4: Experimental Facilities

Document Number : APSU-2.01-RPT-003
ICMS Content ID : APSU_2032071

# Table of Contents

# List of Figures

# List of Tables

## Acronyms and Abbreviations

| | |
|---|---|
| 2D | Two Dimensional |
| 3D | Three Dimensional |
| ADR | Accelerator Detector Research |
| ALARA | As Low As Reasonably Achievable |
| ALD | Atomic Layer Deposition |
| AML | Activated Materials Laboratory |
| APS | Advanced Photon Source |
| APS-U | Advanced Photon Source Upgrade |
| Argonne | Argonne National Laboratory |
| ASD | (ANL) Accelerator Systems Division |
| BDA | Beam Defining Aperture |
| BCDI | Bragg Coherent Diffraction Imaging |
| BES | Office of Basic Energy Sciences |
| BESAC | Basic Energy Science Advisory Committee |
| BSC | Beam Conditioning System |
| CD-n | DOE Critical Decision (n = 0, 1, 2, 3, 4) |
| CDI | Coherent Diffractive Imaging |
| CHEX | Coherent High-Energy X-ray |
| CIGS | Cu(In, Ga)Se2 |
| CMR | Colossal Magnetoresistance |
| CNM | Center for Nanoscale Materials |
| COR | Center of Rotation |
| CRL | Compound Refractive Lens |
| CSE | Chemical Sciences and Engineering Division |
| CSSI | Coherent Surface Scattering Imaging |
| CVD | Chemical Vapor Deposition |
| DBA | Diffracted-Beam Aperture |
| DCM | Double Crystal Monochromator |

| | |
|---|---|
| DMM | Double Multilayer Monochromator |
| DOE | U.S. Department of Energy |
| DWBA | Distorted Wave Born Approximation |
| EBSD | Electron Backscatter Diffraction |
| EDD | Energy Dispersive Detectors |
| EE | Experimental Enclosure |
| ER | Error Reduction |
| ES | Experimental Station |
| ESAC | Experimental System Advisory Committee |
| FE | Front End |
| ff-HEDM | far-field high-energy x-ray diffraction microscopy |
| FFT | Fast Fourier Transform |
| FOE | First Optics Enclosure |
| FPGA | Field Programmable Gate Array |
| FWHM | Full Width Half Maximum |
| GA | Generic Algorithm |
| GB | Gigabyte ($10^9$ bytes) |
| GISAXS | Grazing-Incidence Small-Angle X-ray Scattering |
| GIXPCS | Grazing-Incidence X-ray Photon Correlation Spectroscopy |
| GUI | Graphical User Interface |
| H | Horizontal |
| H-BDA | Horizontally Beam Defining Aperture |
| HE | High Energy |
| HEDM | high-energy x-ray diffraction microscopy (prefixes nf-, ff-, and vff- denote near-field, far-field, and very-far-field technique variants) |
| HERIX | High Energy Resolution Inelastic X-ray Spectrometer |
| HEXM | High-Energy X-Ray Microscope beamline |
| HGVPU | Horizontal Gap Vertically Polarized Undulator |
| HHL | High Heat Load |

| | |
|---|---|
| HIO | Hybrid Input-Output |
| HV | High Vacuum |
| ID | Insertion Device |
| ISF | Intermediate Scattering Function |
| ISN | *In Situ* Nanoprobe |
| KB | Kirkpatrick-Baez |
| KL | Kinoform Lens |
| LDRD | Laboratory-Directed Research and Development |
| LLD | Lower Level Discrimination |
| LN2 | Liquid Nitrogen |
| $\mu$-CT | computed micro-tomography |
| MBA | Multi-Bend Achromat |
| MBE | Molecular Beam Epitaxy |
| MDI | Materials Discovery Institute |
| MH | Mini Hutch |
| MLL | Multilayer-Laue-Lens |
| MM-PAD | Mixed-Mode Pixel Array Detector |
| NA | Numerical Aperture |
| nf-HEDM | near-field high-energy x-ray diffraction microscopy |
| NFO | Nanofocusing Optic |
| NMPZ | Non-Minimum Phase Zero |
| NNSA | National Nuclear Safety Administration |
| NSLS-II | National Synchrotron Light Source II |
| NSUF | Nuclear Science User Facilities |
| PAD | Pixel Array Detector |
| PCS | Photon Correlation Spectroscopy |
| ph | photon |
| PLD | Pulsed Laser Deposition |
| R&D | Research and Development |

| | |
|---|---|
| RIXS | Resonant Inelastic X-ray Scattering |
| rms | Root Mean Square |
| RSS | Radiation Safety System |
| SAC | Scientific Advisory Committee |
| SA-XPCS | Small-Angle X-ray Photon Correlation Spectroscopy |
| SAXS | Small-Angle X-ray Scattering |
| SC | Superconducting |
| SCU | Superconducting Undulator |
| SCAPE | Superconducting Arbitrarily Polarized Emitter |
| SCM | Single-Crystal Monochromator |
| SEM | Scanning Electron Microscope |
| SF | Spatial Filter |
| SME | Subject Matter Experts |
| SMS | Sample Manipulation System |
| SNR | Signal-to-Noise Ratio |
| SOE | Second Optics Enclosure |
| SR | Storage Ring |
| SSA | Secondary Source Aperture |
| ST | Scattering Tomography |
| TB | Terabyte ($10^{12}$ bytes) |
| TBD | To Be Determined |
| TEM | Transmission Electron Microscope |
| TM | Transition Metal |
| TXM | Transmission X-ray Microscope |
| UFXC | Ultra Fast X-ray Camera |
| UHV | Ultra-High Vacuum |
| V | Vertical |
| V-BDA | Vertically Beam-Defining Aperture |
| vff-HEDM | very-far-field high-energy x-ray diffraction microscopy |

| | |
|---|---|
| VIPIC | Vertically Integrated Photon Imaging Chip |
| WA-XPCS | Wide-Angle X-ray Photon Correlation Spectroscopy |
| WAXS | Wide-Angle X-ray Scattering |
| WB | White Beam |
| WBS | Work Breakdown Structure |
| XBIC | X-ray Beam Induced Current |
| XBIV | X-ray Beam Induced Voltage |
| XEOL | X-ray Excited Optical Luminescence |
| XFEL | X-ray Free Electron Laser |
| XMAT | eXtreme MATerials beamline concept/initiative |
| XMCD | X-ray Magnetic Circular Dichroism |
| XMLD | X-ray Magnetic Linear Dichroism |
| XPCS | X-ray Photon Correlation Spectroscopy |
| XRD | X-ray Diffraction |
| XRF | X-ray Fluorescence |
| XRIM | X-ray Reflection Interfacial Microscopy |
| XRMS | X-ray Resonant Magnetic Scattering |
| XSD | (ANL) X-ray Science Division |
| YAG | Yttrium Aluminum Garnet |
| ZP | Zone Plate |

# 4 Experimental Facilities

## 4-1 Experimental Facilities Overview

The U2.04 Experimental Facilities portion of the APS-U Project covers activities directly related to beamlines. Specifically, it consists of two major areas: 1) Feature Beamlines and 2) Beamline Enhancements. The Feature Beamlines portion of the Project includes all APS-U beamlines that are either entirely new, or are existing APS beamlines that are being significantly modified. The Beamline Enhancements are upgrades to existing beamlines that are more modest in scope, but that will have a significant impact on that beamline to allow it to more fully utilize the capabilities of the APS-U storage ring.

A brief overview of the experimental system scope is described in this section followed by more detailed description in the rest of this chapter.

### 4-1.1 Feature Beamlines

For nearly twenty years there have been workshops concerning possible new beamlines for the APS. The decision to pursue a low-emittance, storage-ring lattice directed the focus of these workshops to beamlines that would take advantage of the vastly increased coherence of the APS-U storage ring. In particular, a set of well-attended workshops in May, 2015 generated formative plans for specific beamline needs and contributed many ideas to the APS-U science case as presented in the APS-U Preliminary Design Report.

After an extensive selection process, nine beamlines covering a wide range of science were chosen to be designed as part of the feature beamline scope of the experimental system of the APS-U project. The APS currently has only two open ID ports that have not been built out. A roadmap was developed to locate these nine beamlines on either new or existing ports. This roadmap was further confined due to the need for two long beamlines that will extend outside the existing facility. The location of the two long beamlines are adjacent to each other to take advantage of the infrastructure needs. Table 4.1 shows the programs and the associated beamline locations in the APS-U storage ring.

The two long beamlines are ISN and HEXM, shown in Table 4.1, located in 19-ID and 20-ID respectively. Unfortunately, 19-ID and 20-ID are currently occupied and two existing programs require relocation. This process is currently underway, with the program in 20-ID (ASL) being relocated to 25-ID (one of the two open ID ports). The 19-ID beamline is currently occupied by SBC-CAT and negotiations are in progress to resolve that situation.

The specifications for the design of the feature beamlines are defined in the Functional Requirement and Interface Control Document. For each of the Feature Beamlines a set of requirements are used in turn to define the three types of Engineering Specification documents. The three types of Engineering specification document are the Photon Delivery System, Optics, and the beamline experimental Instrument. Interfaces specific to the type of front ends and source are defined in a set

*Table 4.1. APS-U Feature Beamlines*

| **Name** | **Location** | **Proposal Title** | **Technique** |
|---|---|---|---|
| CHEX | 28-ID | Coherent High Energy X-ray Sector for In Situ Science | *In situ*, surface high-energy coherent scattering |
| Polar | 4-ID | Polarization modulation spectroscopy | Magnetic spectroscopy |
| HEXM | 20-ID | A High-Energy X-ray Microscope | High-energy microscopies & CDI |
| XPCS | 8-ID | Development of a Small-Angle X-ray Photon Correlation Spectroscopy Beamline for Studying Dynamics in Soft Matter<br>Wide-Angle X-Ray Photon Correlation Spectroscopy and Time-Resolved Coherent X-Ray Scattering Beamline | Small-angle XPCS, Wide-angle XPCS |
| PtychoProbe | 33-ID | PtychoProbe | Ultimate resolution, forward scattering ptychography/spectromicroscopy |
| ISN | 19-ID | In Situ Nanoprobe Beamline | *In situ*, forward scattering ptychography/spectromicroscopy Long working distances |
| CSSI | 9-ID | Coherent Surface Scattering Imaging Beamline for Unraveling Mesoscopic Spatial-Temporal Correlations | Coherent GISAXS,XPCS |
| ATOMIC | 34-ID | Atomic – A beamline for extremely high resolution coherent imaging of atomistic structures | Diffraction microscopy & CDI Bragg CDI |
| 3DMN | 34-ID | 3D Micro & Nano Diffraction | Upgrade of current 34-ID-E |

of ICDs for each of the 35 ID beamlines as discussed in the next chapter. All these documents were appropriately reviewed and approved and are stored in the APS document management system (ICMS). Table 4.2 is a comprehensive list of the documents for the various feature beamlines. The rest of this chapter will provide summaries from these documents for each of the beamlines. In addition, the same set of documents have also been generated for the ASL beamlines as well.

*Table 4.2. Feature Beamline Documentation*

| **Beamline** | **Function Requirements & Interface Control** | **Engineering Specifications** | | |
|---|---|---|---|---|
| | | **Photon Delivery** | **Optics** | **Instrument** |
| CHEX | APSU_2014855 | APSU_2012715 | APSU_2030439 | APSU_2030642 |
| Polar | APSU_2025911 | APSU_2012709 | APSU_2030433 | APSU_2030618<br>APSU_2030619 |
| HEXM | APSU_2012428 | APSU_2012713 | APSU_2030437 | APSU_2030616 |
| XPCS | APSU_2011244 | APSU_2012710 | APSU_2030434 | APSU_2030643<br>APSU_2030654 |
| PtychoProbe | APSU_2022855 | APSU_2012716 | APSU_2030440 | APSU_2032313 |
| ISN | APSU_2012171 | APSU_2012712 | APSU_2030436 | APSU_2030615 |
| CSSI | APSU_2012429 | APSU_2012711 | APSU_2030435 | APSU_2030647 |
| ATOMIC & 3DMN | APSU_2021728/ APSU_2022854 | APSU_2012717 | APSU_2030441 | APSU_2032343<br>APSU_2030818 |
| ASL | APSU_2024251 | APSU_2012714 | | |

### 4-1.2 Long Beamline Building

With the siting of the two long beamlines for ISN and HEXM at 19-ID and 20-ID, an architectural firm was engaged to develop the preliminary design for the long beamline building. The end stations for HEXM and ISN will be located in this building. Two long corridors will connect the long beamline building to the APS storage ring building. The two corridors will be mainly for the beam transport. The beam transport for these long beamlines will pass through some of the LOM laboratories and offices. Along the HEXM beamline corridor a row of offices will be built to accommodate the LOM offices displaced by the two long beamlines. The space between the two end stations has sufficient space for a sample preparation laboratory. The ISN end station requirements for high vibrational stability will be addressed as part of the final design of the building.

### 4-1.3 Beamline Enhancements

The APS-U Feature Beamline scope is designed to deliver a relatively small number of new or significantly upgraded beamlines that will be recognized as world-leading or world-class in performance, and are explicitly designed to capitalize on the strengths of the APS-U storage ring. What should not be overlooked is that the current APS has over sixty operating beamlines, many of which are state-of-the-art for a particular x-ray technique. A relatively small investment in key areas such as

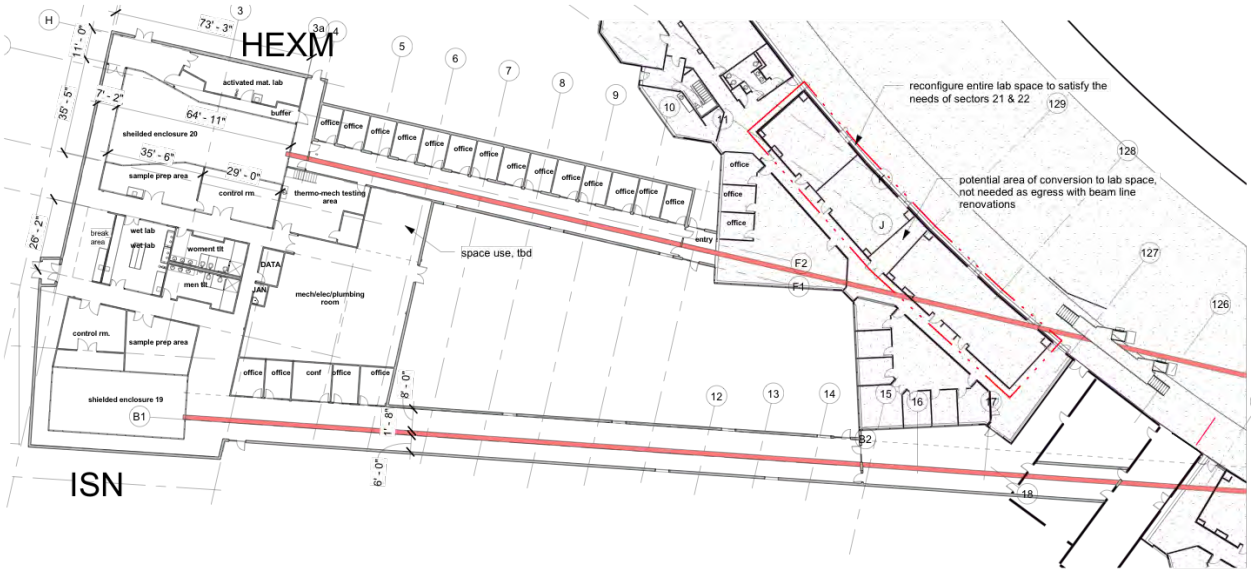


*Figure 4.1. Plan view of long beamline building for ISN and HEXM beamlines along with the corridor connecting to the APS building. Beam transport is shown is red lines traveling from left to right. The ISN beamline is shown in the bottom of the figure and the HEXM beamline at the top of the figure.*

beam delivery (X-ray optics) and endstation instrumentation allows for many beamlines to utilize the improved emittance of the APS-U storage ring and tremendously leverages the APS-U Project.

The APS-U Beamline Enhancements process and scope is designed to address the opportunity that exists to make relatively minor investments in existing beamlines with resultant large increases in a beamline's ability to utilize the improvements of the APS-U. Two guiding principles were used for the Beamline Enhancements: 1) No beamline should lose ground in its performance after the APS-U is finished – "do no harm," and 2) it is prudent to make relatively minor investments that significantly improve a beamlines performance – "bang for the buck." For the APS-U Beamline Enhancements process, the do-no-harm items that fall under the first principle are considered "Non-Discretionary," and those that fall under the second bang-for-the-buck principle as "Discretionary."

For the "Non-Discretionary" portion, few key items were identified and based on evaluation certain funds have been set aside for:

- Realignment of bending-magnet beamlines
- Shielding enhancements
- Beam choppers for bunch separation
- Optics (typically needed because of heat-load performance)
- High-heat-load safety components (e.g., stops, shutters)
- Beamline canting components

Based on a proposal process as discussed in the preliminary design report a list for beamline enhancements were identified to be part of the APS-U scope to be developed and built. Table 4.3 is the list of the beamline enhancement scope. For all the beamline enhancements a Functional

Requirements document (FReD) has been created to document the requirements. The ICMS document numbers for the FReDs are shown in the Table 4.3 as well. The engineering specifications are also in the process of being generated. Some of the items identified in this list were picked as part the CD-3B LLP items and have been procured or is in the process of being procured.

*Table 4.3. Beamline Enhancement Scope*

| Beamline | FReD | Enhancement | Deliverable |
|---|---|---|---|
| 1-ID | APSU_2022135 | 1-ID-A Beam Delivery | High-Energy Horizontally Deflecting Laue Monochromator |
| | | 1-ID-C Instrumentation | Sample manipulation system with hexapod and tilt stage |
| | | 1-ID-E Instrumentation | Enhanced SAXS resolution detector distance extension |
| 2-ID | APSU_2022398 | 2-ID-A Beam Delivery | Two vertical focusing mirrors |
| | | 2-ID-D Instrumentation | 10 nm Resolution Bionanoprobe-II with<br>Polycapillary detector collimator<br>Upgraded scanning stages<br>Upgraded rotation stage<br>Upgraded laser interferometer system<br>Vacuum chamber<br>Delta tau control system<br>High-resolution and high-efficiency zone plate optics |
| | | 2-ID-E Instrumentation | Enhanced microprobe with<br>Beam Defining Aperture<br>Figured KB mirrors mounted inside vacuum chamber<br>Compact laser interferometers, two on each KB mirror<br>High-stiffness fast-scanning sample stages |
| 3-ID | | 3-ID-C Beam Delivery | KB-mirror system |
| 5-ID | APSU_2022416 | 5-ID-A Beam Delivery | Refurbished Horizontal Mirror System<br>Upgraded HHL Monochromator |
| 6-ID | APSU_2024247 | 6-ID-B/C Beam Delivery | Beryllium paraboloid CRL lenses with transfocator |
| | | 6-ID-D Beam Delivery | Aluminum paraboloid CRL lenses with transfocator |
| 7-ID | APSU_2022857 | 7-ID-A Beam Delivery | HHL mirror for diffraction branch |
| | | 7-ID-C Beam Delivery | Nanofocusing KB mirror system |
| | | 7-ID-C Instrumentation | Detector arm |
| 11-ID | APSU_2024237 | Beamline Canting Reconfiguration | Photon stop<br>Two tungsten collimators with masks<br>High-heat-load canted slits<br>Shielding modifications |
| | | 11-ID-A Beam Delivery | Double multilayer monochromator |
| | | 11-ID-A/D Beam Delivery | Multiple sets of compound refractive lenses |
| 12-ID | APSU_2022861 | 12-ID-MH1 Beam Delivery | CRL transfocator system |
| | | 12-ID-C Instrumentation | 12-meter-Long SAXS tube/enclosure upgrade<br>USAXS Facility Upgrade |

| Beamline | FReD | Enhancement | Deliverable |
|---|---|---|---|
| 13-ID | APSU_2022866 | 13-ID-C/D Beam Delivery | Repolish KB mirrors (1000 mm) |
| | | 13-ID-D Beam Delivery | Repolish KB mirrors (350 mm) |
| | | 13-ID-E Beam Delivery | New dual horizontal mirrors (500 mm) |
| | | | Repolish two sets of KB mirrors (250 mm) |
| | | | Double crystal monochromator enhancement |
| | | 13-ID-E Instrumentation | Table stability upgrade |
| 15-ID | APSU_2022870 | 15-ID-A Beam Delivery | New dual-mirror vertical focusing system |
| | | | 2D CRL focusing system |
| | | 15-ID-D Beam Delivery | New single harmonic rejection mirror system |
| 25-ID | APSU_2024251 | 25-ID-B Beam Delivery | $LN_2$ silicon/multilayer monochromator |
| | | 25-ID-C Instrumentation | LERIX spectrometer |
| 26-ID | APSU_2022873 | 26-ID-A Beam Delivery | New M1 mirror system |
| | | 26-ID-B Beam Delivery | Rebuild of double crystal monochromator |
| | | 26-ID-C Beam Delivery | Stacked zone plate optics |
| | | 26-ID-C Instrumentation | High-speed high-range Nanoprobe scanning upgrade |
| 27-ID | APSU_2018288 | 27-ID-B Beam Delivery | Extension of the high-energy-resolution monochromator |
| | | 27-ID-B Instrumentation | RIXS spectrometer upgrade |
| 30-ID | APSU_2018288 | 30-ID-A Beam Delivery | Cryogenic conversion of Kohzu monochromator |
| | | 30-ID-B Beam Delivery | New cryogenic high-energy resolution monochromator |
| 32-ID | APSU_2022884 | Beamline Canting | White beam shutter and mask |
| | | | White beam slits |
| | | | Filters |
| | | | Be windows |
| | | | Aluminum pipes and adapters |
| | | | Slightly modification to the manual shutter |
| | | | Slightly modified end shutter |
| | | 32-ID-C Beam Delivery | Pair of small deflecting multilayer (ML) mirrors and hardware |
| | | | Double vertical mirrors |
| | | | CRLs and transfocator |
| | | | Two sets of KB, with ML optimized for 25 keV and 12 keV |
| | | 32-ID-C Instrumentation | Dual-beam instrument |
| | | | Nano-CT instrument |

## 4-2 CHEX 28-ID

### 4-2.1 Scientific Objective

The Coherent High energy X-ray (CHEX) sector for in situ science beamlines will advance the frontier for in situ, real-time studies of dynamics using the unprecedented coherence of the high-energy X-ray beams provided by the APS Upgrade. Such research promises breakthroughs in discovering, developing, and understanding the materials and processes that are needed to address our global challenges in energy, environment, health, and security. The scientific impact of the proposed facility for coherent high-energy, in situ studies will be broad, cutting across sections of the APS-U Early Science document [1] on advanced materials, chemistry, condensed-matter physics, and environmental science, and bringing together researchers in these areas with common underlying scientific questions and technical approaches. Here we focus on two major areas: in situ materials synthesis and transformations under real conditions.

#### 4-2.1.1 In Situ Studies of Materials Synthesis:

Not only do we need to understand the proper arrangements of atoms in materials and nanostructures that give desired functionality, but we also need to learn how to synthesize and stabilize these arrangements. Rather than a trial-and-error approach, developing the science underlying materials synthesis promises the most extensive and sustainable progress. New capabilities provided by the APS Upgrade will dramatically impact the science of synthesis. The orders-of-magnitude increase in X-ray brightness at high energies will enable in situ coherent X-ray studies of synthesis mechanisms down to the atomic scale with sub-microsecond time resolution. As described below, coherent imaging and correlation spectroscopy techniques will reveal unprecedented detail regarding atomic arrangements and dynamics. In parallel, orders-of-magnitude increases in computing power are enabling ab initio simulations not just of ground-state materials structure and properties, but also of the competing chemical reactions and materials kinetics that occur during synthesis. Both coherent X-ray techniques and atomic scale modeling enable us to see beyond the average behavior of a fluctuating system and reveal the microscopic arrangements, correlations, and dynamics underpinning the synthesis process. The combination of in situ observation of structure and dynamics during synthesis with advanced computational studies will usher in a powerful new framework for discovering, isolating, and optimizing desired growth pathways and outcomes.

#### 4-2.1.2 Transformations under Real Conditions:

The need for in situ studies of materials and chemical transformations spans across a wide range of research activities. These include the atomic-scale understanding of advanced lithographic processes such as reactive ion etching and additive manufacturing, complementary to the science of thin-film synthesis; understanding the relationship between surface-site structure and reactivity during heterogeneous catalysis, and the evolution of the catalyst structure; the formation mechanisms of metastable microstructures under extreme conditions such as ion irradiation; as well as heterogeneous phase transitions and chemical reactions in energy storage and geochemical systems. The power of coherent, high-energy X-ray techniques to image and observe dynamics at the nanoscale under operating conditions provides a transformational opportunity in all of these areas.

### 4-2.2 Beamline Requirements for the Insertion Devices (IDs)

This beamline will be configured to operate two independent branches fed by two independent insertion devices. There will be a 1.85 cm period superconducting magnet undulator for the outboard canted branch directed along the tunable-energy X-ray branch (28-ID-A/B/C) and a 1.85 cm period superconducting magnet undulator for the inboard canted branch directed along the fixed-energy x-ray branches (28-ID-A/D/E, 28-ID-A/F, and 28-ID-A/G).

*Table 4.4. CHEX Source Parameters*

| **Undulator** | **Period** *(mm)* | **Length** *(m)* | **Location** | **Max Power** *(W)* |
|---|---|---|---|---|
| SCU | 18.5 | 1.3 | 1.25 m upstream of the center of the straight section | 698 W[1] |
| SCU | 18.5 | 1.3 | 1.25 m downstream of the center of the straight section | 843 W[1] |

[1] Through the Front End Mask 2x1 $mm^2$ @ 25.4 m with the undulator SCU18.5 Ky = 2.291.

### 4-2.3 Beamline Requirements for the Front End

The CHEX will have a canted undulator (CU) front end capable of handling two beams separated by 1 mrad canting angle and 10 kW power each. The beamline will have a windowless exit configuration with a 2 mm x 1 mm (H x V) exit aperture for each branch.

A detailed description of the CHEX Front End and Insertion devices can be found in the APS-U 28-ID Beamline Front End and Insertion Devices Interface Control Document (ICMS Content ID: APSU_190956).

### 4-2.4 Beamline Layouts

The CHEX beamlines will provide a tunable-energy branch (28-ID-A/B/C) at the energy range of 5-60 keV and three fixed energy branches (28-ID-A/D/E, 28-ID-A/F, and 28-ID-A/G). The layout of the beamlines is shown below.

#### 4-2.4.1 CHEX Beamline Component Table

Table 4.5 shows all the major optics, instrument, and detector positions.

*Table 4.5. Major Optics, Instruments and Detctor locations in the CHEX beamline stations.*

| **Station 28-ID-** | **B** | **C** | **D** | **E** | **F/1** | **F/2** | **G/1** | **G/2** |
|---|---|---|---|---|---|---|---|---|
| Monochromators (m) | 35.0 | 35.0 | 28.3 | 28.3 | 38.3 | 38.3 | 40.2 | 40.2 |
| CRL 1 (m) | 50.0 | 50.0 | 29.8 | 29.8 | 40.0 | 40.0 | 42.0 | 42.0 |
| CRL 2 (m) | 63.0 | 70.0 | 34.0 | 41.5 | 44.0 | 48.0 | 49.5 | 54.5 |
| Instruments (m) | 64.5 | 72.0 | 35.5 | 43.0 | 45.5 | 49.5 | 52.0 | 56.0 |
| Detectors (m) | 65.5-68.5 | 73.0-76.5 | 36.5-39.5 | 44.0-47.5 | 46.5-48.5 | 50.5-53.5 | 53.0-55.0 | 57.0-60.0 |

Table Table 4.6 shows the major beamline components for A/B/C branch beamline. Table Table 4.7

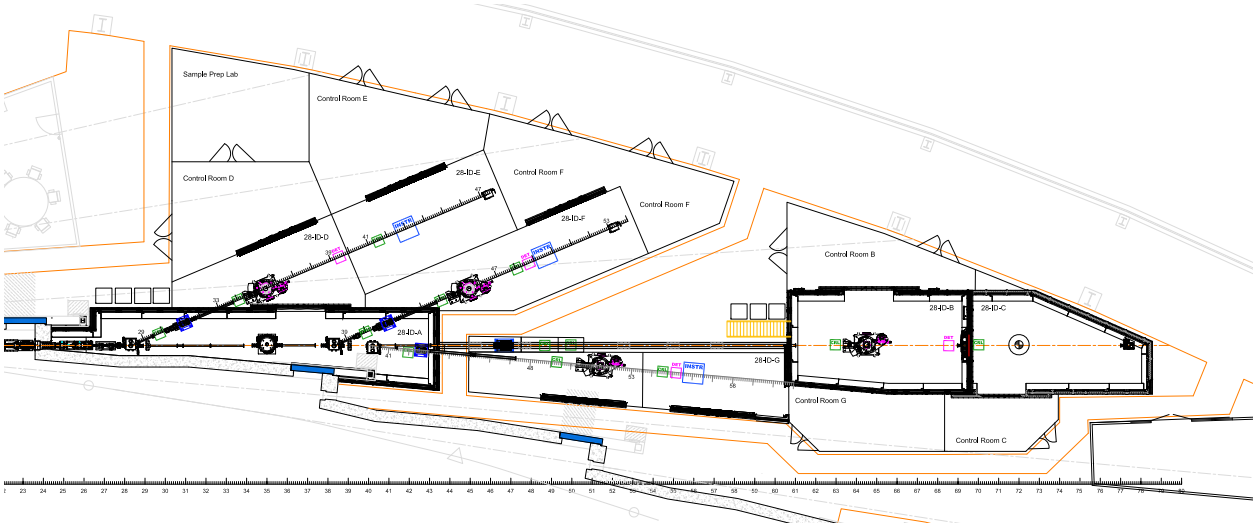


*Figure 4.2. Layout of the CHEX beamlines.*

shows the major beamline components for A/D/E branch beamline. Table Table 4.8 shows the major beamline components for A/F branch beamline. Table Table 4.9 shows the major beamline components for A/G branch beamline. A detailed description of the CHEX beamlines can be found in the CHEX 28-ID Photon Delivery System ESD (ICMS Content ID: APSU_2012715).

### 4-2.5 Optics Overview

Each experimental station (28ID-B-G) will have two sets of CRLs to provide variable focal spots. Table 4.10 shows the expected flux and focal spot sizes of the beamline.

#### 4-2.5.1 Detailed Optical Layout

#### 4-2.5.2 Optical Simulation and Tolerances

The zoom focusing capabilities of the CHEX beamline are shown in Figure 4.4 and Figure 4.5 using station B and D as examples for the tunable branch and the fixed energy branch, respectively.

ShadowOui was used to verify the zoom focusing of the CRLs. Figure 4.6 shows the simulated (largest and smallest) focal spots at the sample position in station B.

**HHL Double Crystal Monochromator/Multilayer** The HDCM is a standard double-crystal monochromator with two liquid-nitrogen cooled crystals Si(111) and Si(311) and fixed exit operation.

**HHL Single Crystal Monochromator** The SCMs are horizontally deflecting single-crystal monochromators with liquid-nitrogen cooled crystals and fixed angle geometries.

*Table 4.6. List of all beamline components in the CHEX A/B/C branch beamline*

| Position (m) | Component | Designation | Description/Comments |
|---|---|---|---|
| 25.6 | FE Exit Mask | | Standard CU front-end exit mask<br>2 mm x 2 mm aperture |
| 26.0 | FE Collimator | | Standard CU front-end exit collimator.<br>5 mm x 5 mm aperture |
| 26.8 | CU WB Slits | 28ID-SL-1 | CU variable aperture photon absorber<br>with tungsten edge inserts |
| 27.3 | CU WB Slits | 28ID-SL-2 | CU variable aperture photon absorber<br>with tungsten edge inserts |
| 29.1 | Collimator, Secondary | 28ID-SC-1 | Collimator after the first single crystal<br>monochromator |
| 32 | Diagnostic | 28ID-BD-1 | Beam visualization monitor for alignment |
| 33.8 | Collimator | 28ID-BC-1 | Collimator |
| 35 | Monochromator | 28ID-MN-1 | Horizontal double crystal monochromator |
| 39 | Collimator, Secondary | 28ID-SC-2 | Collimator after the second single crystal<br>monochromator |
| 43.5 – 60.6 | Shielded Transport | 28ID-ST-1 | White beam shielded transport |
| 48.2 – 52.2 | Shielded Enclosure (mini) | 28ID-SE-1 | White beam shielded enclosure |
| 48.7 | Mask | 28ID-PM-1 | Photon mask |
| 49.1 | Collimator | 28ID-BC-2 | Collimator |
| 49.7 | Slits | 28ID-SL-3 | Monochromatic beam conditioning slits for CRL unit |
| 50 | CRL1 B/C | 28ID-CR-1 | Transfocator unit 1 for 28-ID-B and 28-ID-C stations |
| 51.4 | Shutter | 28ID-SH-1 | P4-40 Shutter |
| 62 | Diagnostic | 28ID-BD-2 | Beam visualization monitor for alignment |
| 62.7 | Slits | 28ID-SL-4 | Monochromatic beam conditioning slits for CRL unit |
| 63 | CRL2 B | 28ID-CR-2 | Transfocator unit 2 for 28-ID-B station |
| 63.3 | Window | 28ID-WN-1 | Diamond or Be window |
| 69.3 | Moveable WB stop | 28ID-BS-1 | Moveable white beam stop at the<br>end of the 28-ID-B station (motorized) |
| 69.7 | Slits | 28ID-SL-5 | Monochromatic beam conditioning slits for CRL unit |
| 70 | CRL2 C | 28ID-CR-3 | Transfocator unit 2 for 28-ID-C station |
| 70.3 | Window | 28ID-WN-2 | Diamond or Be window |
| 77.4 | Beam stop | 28ID-BS-2 | White beam stop at the end of the 28-ID-C station |

*Table 4.7. List of all beamline components in the CHEX A/D/E branch beamline*

| Position (m) | Component | Designation | Description/Comments |
|---|---|---|---|
| 28.3 | SCM | 28ID-MN-2 | Single crystal monochromator (diamond) for 28-ID-D/E branch |
| 29.3 | Slit | 28ID-SL-6 | Monochromatic beam conditioning slits for CRL unit |
| 29.8 | CRL1 D/E | 28ID-CR-4 | CRL unit 1 for 28-ID-D and 28-ID-E stations |
| 30 | Diagnostic | 28ID-BD-3 | Beam visualization monitor for alignment |
| 31 | P8-20 Shutter | 28ID-SH-2 | Monochromatic beam shutter |
| | Shielded Pipe through A Station | 28ID-ST-2 | White beam shielded transport |
| 33.7 | Slit | 28ID-SL-7 | Monochromatic beam conditioning slits for CRL unit |
| 34 | CRL2 | 28ID-CR-5 | CRL unit 2 for 28-ID-D station |
| 34.3 | Window | 28ID-WN-3 | Diamond or Be window |
| 39.9 | Moveable beam stop | 28ID-BS-3 | Moveable monochromatic beam stop at the end of the 28-ID-D station (manual) |
| 41.2 | Slit | 28ID-SL-8 | Monochromatic beam conditioning slits for CRL unit |
| 41.5 | CRL2 | 28ID-CR-6 | CRL unit 2 for 28-ID-E station |
| 41.8 | Window | 28ID-WN-4 | Diamond or Be window |
| 48 | Beam stop | 28ID-BS-4 | Monochromatic beam stop at the end of the 28-ID-E station |

*Table 4.8. List of all beamline components in the CHEX A/F branch beamline*

| Position (m) | Component | Designation | Description/Comments |
|---|---|---|---|
| 38.3 | SCM | 28ID-MN-3 | Single crystal monochromator (diamond) for 28-ID-F branch |
| 39.5 | Slit | 28ID-SL-9 | Monochromatic beam conditioning slits for CRL unit |
| 40 | CRL1 | 28ID-CR-7 | CRL unit 1 for 28-ID-F station |
| 40.2 | Diagnostic | 28ID-BD-4 | Beam visualization monitor for alignment |
| 41 | P8-20 Shutter | 28ID-SH-3 | Monochromatic beam shutter |
| | Shielded Pipe through A Station | 28ID-ST-3 | White beam shielded transport |
| 43.7 | Slit | 28ID-SL-10 | Monochromatic beam conditioning slits for CRL unit |
| 44 | CRL2 | 28ID-CR-8 | CRL unit 2 for 28-ID-F station experiment position 1 |
| 44.3 | Window | 28ID-WN-5 | Diamond or Be window |
| 47.7 | Slit | 28ID-SL-11 | Monochromatic beam conditioning slits for CRL unit |
| 48 | CRL2 | 28ID-CR-9 | CRL unit 2 for 28-ID-F station experiment position 2 |
| 48.3 | Window | 28ID-WN-6 | Diamond or Be window |
| 54.3 | Beam stop | 28ID-BS-5 | Monochromatic beam stop at the end of the 28-ID-F station |

*Table 4.9. List of all beamline components in the CHEX A/G branch beamline*

| Position (m) | Component | Designation | Description/Comments |
|---|---|---|---|
| 40.2 | SCM | 28ID-MN-4 | Single crystal monochromator (silicon) for 28-ID-G branch |
| 41.5 | Slit | 28ID-SL-12 | Monochromatic beam conditioning slits for CRL unit |
| 42 | CRL1 | 28ID-CR-10 | CRL unit 1 for 28-ID-G station |
| 42.3 | Diagnostic | 28ID-BD-5 | Beam visualization monitor for alignment |
| 42.6 | P8-20 Shutter | 28ID-SH-4 | Monochromatic beam shutter |
| | Shielded Pipe through A Station | 28ID-ST-4 | White beam shielded transport |
| 49.2 | Slit | 28ID-SL-13 | Monochromatic beam conditioning slits for CRL unit |
| 49.5 | CRL2 | 28ID-CR-11 | CRL unit 2 for 28-ID-G station experiment position 1 |
| 49.8 | Window | 28ID-WN-7 | Diamond or Be window |
| 54.2 | Slit | 28ID-SL-14 | Monochromatic beam conditioning slits for CRL unit |
| 54.5 | CRL2 | 28ID-CR-12 | CRL unit 2 for 28-ID-G station experiment position 2 |
| 54.8 | Window | 28ID-WN-8 | Diamond or Be window |
| 60.5 | Beam stop | 28ID-BS-6 | Monochromatic beam stop at the end of the 28-ID-G station |

*Table 4.10. The expected flux and focal spot sizes for the CHEX beamlines*

| Station | B | C | D | E | F/1 | F/2 | G/1 | G/2 |
|---|---|---|---|---|---|---|---|---|
| E min (keV) | 15 | 15 | 15 | 15 | 15 | 15 | 45 | 45 |
| H focusing range ($\mu$m) | 0.9-9.8 | 1.1-14 | 1.5-6.4 | 1.3-15 | 1.2-4.8 | 1.1-7.8 | 1.8-8.1 | 1.0-11 |
| V focusing range ($\mu$m) | 0.3-3.4 | 0.4-4.7 | 0.5-2.2 | 0.5-5.3 | 0.4-1.7 | 0.4-2.7 | 0.5-2.3 | 0.3-3.2 |
| Flux range[1] ($10^{11}$ph/s) | 68-370 | 58-370 | 44-100 | 32-100 | 26-64 | 23-65 | 29-110 | 16-120 |
| E max (keV) | 60 | 60 | 35 | 35 | 35 | 35 | 105 | 105 |
| H focusing range ($\mu$m) | 0.8-8.1 | 1.0-14 | 1.5-6.4 | 1.3-15 | 1.2-4.7 | 1.1-8.1 | 1.7-8.1 | 1.0-11 |
| V focusing range ($\mu$m) | 0.3-2.3 | 0.3-4.1 | 0.4-1.8 | 0.4-4.3 | 0.3-1.4 | 0.3-2.3 | 0.5-2.1 | 0.3-2.8 |
| Flux range[1] ($10^{11}$ph/s) | 42-110 | 36-110 | 4.9-7.0 | 3.9-7.0 | 2.6-5.2 | 2.3-5.2 | 0.21-1.2 | .097-1.3 |

[1]A 2 mm graphite filter is applied for branches D/E, F and G.

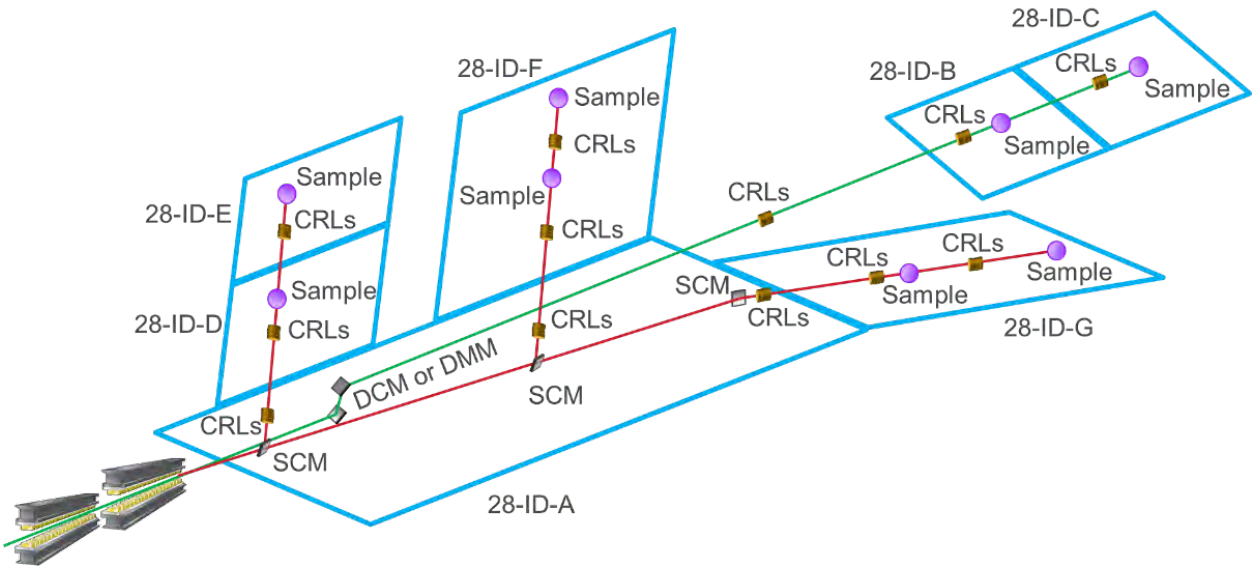


*Figure 4.3. Basic optical layout of the CHEX beamlines.*

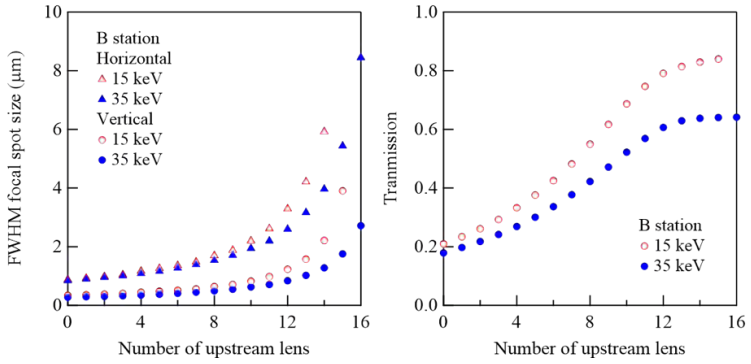


*Figure 4.4. Station B: (left) The achievable horizontal and vertical focal spot sizes (FWHM). (right) The transmission of the focusing system.*

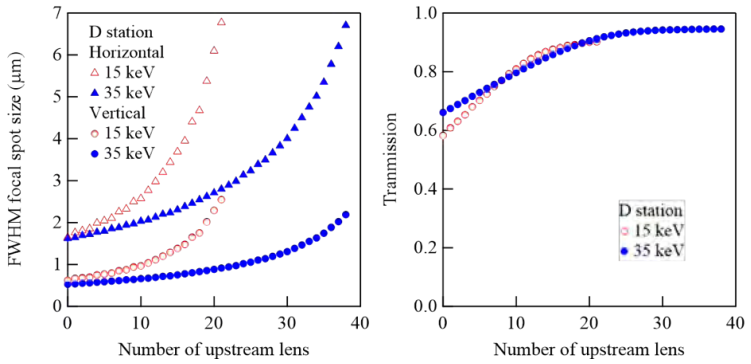


*Figure 4.5. Station D: (left) The achievable horizontal and vertical focal spot sizes (FWHM). (right) The transmission of the focusing system.*

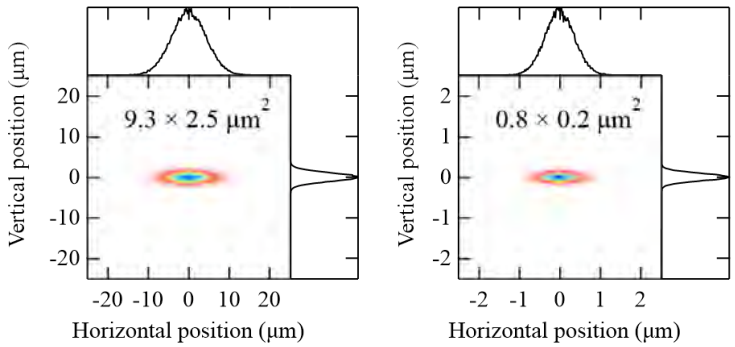


*Figure 4.6. Largest (left) and smallest (right) focal spots at the sample position of station B (64.5 m). The sizes shown in the figure are the FWHM. The calculation was performed at 35 keV with ideal CRLs.*

**Transfocators** Variable numbers and types (radii) of CRLs are required to achieve the focusing requirements for the CHEX beamline. Transfocators are the device selected for achieving this. Requirements for the transfocator are UHV compatibility, x/y/z translations, and pitch/yaw rotations, and the ability to precisely remove and insert variable numbers of lenses. The arrangement of individual lenses of the transfocator systems for station B is shown in the Table 4.11 as an example.

*Table 4.11. Arrangement of transfocator systems for station B.*

| **CRL-1** | | | | | | | | | | | | | | |
|---|---|---|---|---|---|---|---|---|---|---|---|---|---|---|
| Stack | 1 | 2 | 3 | 4 | 5 | 6 | 7 | 8 | 9 | 10 | 11 | 12 | 13 | |
| Type | 2D | 2D | 2D | 2D | 2D | 2D | 2D | 2D | 2D | 2D | 1D | 1D | 1D | |
| *N* | 1 | 1 | 1 | 1 | 1 | 2 | 4 | 8 | 16 | 16 | 1 | 1 | 2 | |
| *R*, µm | 1000 | 500 | 300 | 200 | 100 | 100 | 100 | 100 | 100 | 100 | 1000 | 500 | 500 | |
| **CRL-2** | | | | | | | | | | | | | | |
| Stack | 1 | 2 | 3 | 4 | 5 | 6 | 7 | 8 | 9 | 10 | 11 | 12 | 13 | 14 | 15 |
| Type | 2D | 2D | 2D | 2D | 2D | 2D | 2D | 2D | 2D | 2D | 2D | 2D | 1D | 1D | 1D |
| *N* | 1 | 1 | 1 | 1 | 1 | 2 | 4 | 8 | 16 | 32 | 64 | 64 | 1 | 2 | 4 |
| *R*, µm | 1000 | 500 | 200 | 100 | 50 | 50 | 50 | 50 | 50 | 50 | 50 | 50 | 50 | 50 | 50 |

The maximum number of lenses for each experimental station is shown in Table 4.12. If not specified, Be lenses are used.

*Table 4.12. Maximum numbers of lenses for each station.*

| **Station:** | **B** | **C** | **D** | **E** | **F/1** | **F/2** | **G/1** | **G/2** |
|---|---|---|---|---|---|---|---|---|
| CRL 1 apex R ($\mu$m) | 100 | 100 | 50 | 50 | 50 | 50 | 50 (Ni) | 50 (Ni) |
| CRL 1 number of lenses | 47 | 35 | 19 | 10 | 19 | 12 | 19 | 15 |
| CRL 2 apex R ($\mu$m) | 50 | 50 | 50 | 50 | 50 | 50 | 50 (Ni) | 50 (Ni) |
| CRL 2 number of lenses | 180 | 136 | 64 | 64 | 63 | 63 | 66 | 107 |

### 4-2.5.3 Heat Load Considerations

Table 4.13 and Table 4.14 summarize the maximum powers expected to be absorbed by the monochromators.

*Table 4.13. Power Calculations for the HDCM.*

| **Und** | **K** | **Mono Energy** *(keV)* | **1st crystal Angle** *(keV)* | **Beam Size at Mono (HxV)** *(mm x mm)* | **Beam Footprint (HxV)** *(mm x mm)* | **Power absorbed** *(W)* | **Power Density** *($W/mm^2$)* |
|---|---|---|---|---|---|---|---|
| SCU | 2.291 | 5.1 (1st) | 23.0° | 2.72 x 1.36[1] | 7.0 x 1.36 | 697 | 77.5 |
| SCU | 2.291 | 5.1 (1st) | 23.0° | 1.0 x 1.0[2] | 2.6 x 1.0 | 192 | 77.5 |

[1] Through the Front End Mask 2x1 $mm^2$ @ 25.4 m
[2] Operation condition

The HDCM deformation is minimized by optimizing the $LN_2$ cooling. The SCM deformation is

*Table 4.14. Power Calculations for the SCM of branch D/E.*

| **Diamond crystal thickness** | **Graphite filter thickness** | **Power absorbed**[1] *(W)* | **Power Density** *($W/mm^2$)* |
|---|---|---|---|
| 200 µm | 0 | 68.7 | 6.9 |
| 100 µm | 0 | 55.6 | 5.6 |
| 200 µm | 2 mm | 16.4 | 1.9 |
| 100 µm | 2 mm | 8.8 | 1.1 |

[1]Through the Front End Mask 2x1 $mm^2$ @ 25.4 m

minimized by applying filters. The remaining thermal deformation on the monochromator can be corrected by adding 1D CRLs.

A detailed description of the CHEX optics can be found in the CHEX 28-ID Optics ESD (ICMS Content ID: APSU_2030439).

### 4-2.6 Instrument Overview

#### 4-2.6.1 Scientific Scope

The CHEX beamline will operate with a combination of integrated and shared instruments. Integrated instruments will be specially designed for a particular project. These shared instruments will be designed to provide a versatile and stable platform for positioning chambers and samples for high energy coherent x-ray scattering measurements.

#### 4-2.6.2 Instrument Definition

Each CHEX shared endstation instrument includes a central diffractometer, upstream optical table, upstream flight path optics, downstream flight path, a Long Distance Detector Positioner (LDDP), pixel array detectors (PADs), a scintillator CCD detector module, motor drivers, and motor cables.

A visualization of the shared diffractometer component of the instrument is shown in Figure 4.7. A conceptual layout for the LDDP is shown in Figure 4.8.

#### 4-2.6.3 Instrument Location

There will be one shared instrument in each of the CHEX branchline hutches, which include 28-ID-D, 28-ID-F, and 28-ID-G as well as one shared instrument in the front hutch of the tunable line 28-ID-B. Figure 8 shows a layout of Sector 28 with the fixed energy hutches marked by the green dashed boxes. The front hutch of the tunable line is marked by the blue dashed box.

#### 4-2.6.4 Instrument Operating Modes

The instruments will have two principle operating modes:

- **Alignment/Imaging Mode:** In this mode the beam will be delivered to the diffractometers

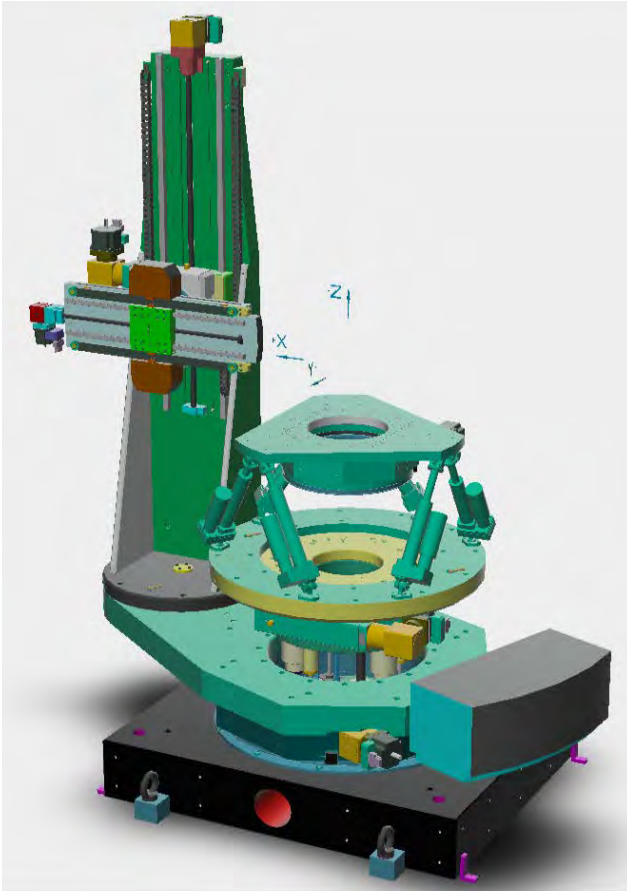


*Figure 4.7. Conceptual schematic of the diffractometer for the shared branchline instruments.*

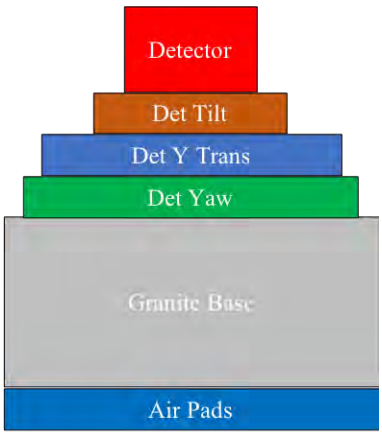


*Figure 4.8. Conceptual schematic of the LDDPs for each shared instrument.*

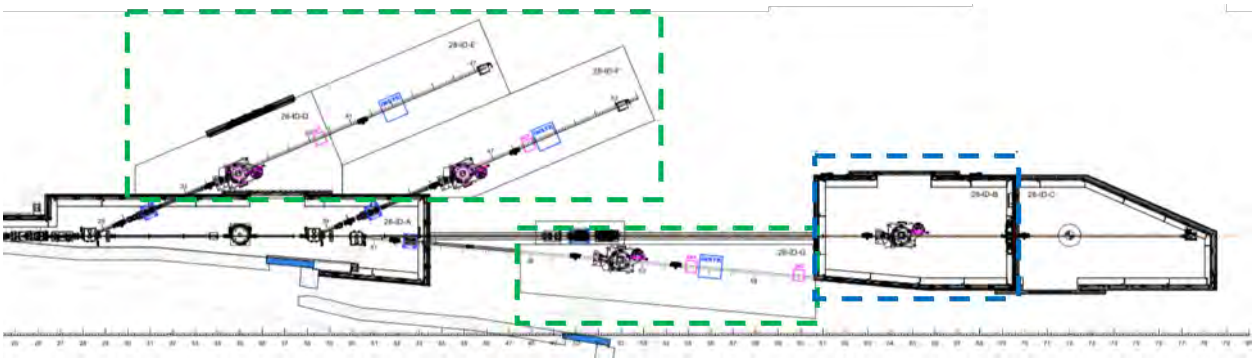

*Figure 4.9. 28-ID station layout. Fixed energy stations are marked with green dashed boxes. The front station of the tunable line is marked by the blue dashed box.*

and measurements will be performed with a detector mounted on the detector arm or the LDDP.

- **Beam-pass Mode:** In this mode beam will be transported past the diffractometer and the LDDP and delivered to dedicated instruments in the rear of the branchline hutches. This mode requires that all elements of the shared instruments have a range of motion that accommodates the insertion of a beampipe to transport beam to the rear instruments.

#### 4-2.6.5 Experimental Methods

There will be three configurations in which measurements will be performed:

- **Alignment Configuration:** In this configuration a PAD will be positioned using the diffractometer detector arm with a sample-to-detector distance of ~1-2m.
- **Imaging Configuration:** In this configuration the PAD will be positioned using the LDDP with a sample-to-detector distance of ~2m-4m.
- **XRIM Configuration:** X-ray reflection interface microscopy is a real space imaging technique in which an x-ray objective downstream of the sample will be used to project a real space image of a sample surface on to a PAD. In this configuration the PAD will be mounted on the LDDP and an x-ray zone plate with positioning stages will be mounted on the detector arm of the diffractometer.

A detailed description of the CHEX Endstation instruments can be found in the 28-ID CHEX Endstation Instrumentation ESD (ICMS Content ID: APSU_2030642).

## 4-3 Polar 4-ID

### 4-3.1 Scientific Objective

Competing interactions in correlated electron systems oftentimes lead to nearly degenerate ground states resulting in quantum critical points or spontaneous electronic phase separation at low temperatures [2, 3]. By virtue of proximity to degeneracy, these complex ground states are highly responsive to external stimuli providing a path to manipulating and ultimately controlling complex electronic matter. The latter is required if these novel ground states are to be used in next generation information storage and data processing technologies, including some forms of quantum computing. Polar will leverage two key properties of APS-U, namely, brilliant x-ray beams and round insertion device vacuum chambers to enable studies of mesoscale electronic and magnetic inhomogeneities by means of resonant techniques coupled with tunable x-ray polarization. Particular emphasis is placed on tuning and controlling competing ground states and electronic inhomogeneity with extreme high-pressures in simultaneous low temperature and high magnetic field conditions.

#### 4-3.1.1 High pressure studies of quantum criticality

Proximity to electronic degeneracy is often achieved by chemical doping making the system responsive to small changes in energy density. The latter can be achieved with a number of external stimuli such as low pressures, high magnetic fields, or temperature changes. Extrinsic doping leads to chemical inhomogeneity affecting electronic texture and preventing a thorough understanding of the driving forces behind intrinsic electronic heterogeneity. Advances in high-pressure methodologies, however, now allow reaching multi-Mbar pressures and large changes in energy density [4, 5], bringing pure, undoped compounds to the regime of quantum degeneracy/criticality via tuning of Coulomb interactions, electronic bandwidth, hybridization, and crystal fields, triggering electronic order (magnetic, ferroelectric, superconducting, Kondo lattice), electronic disorder (mixed/fluctuating valence, Kondo screening, magnetic frustration, spin liquids), or competing/segregated phases at the nano/meso-scale [6, 7, 8].

#### 4-3.1.2 Unraveling the nature of electronic heterogeneity

Polarization dependent x-ray probes such as x-ray magnetic circular/linear dichroism (XMCD/XMLD) and x-ray resonant magnetic scattering (XRMS), coupled with high-flux nm-to-μm sized beams, large coherence fraction, and extreme sample environments, provide a unique route to unraveling the nature of electronic heterogeneity and drive discovery of novel quantum phases. The polarization dependence of resonant absorption/scattering couples to charge, spin, and orbital degrees of freedom, allowing to probe their intertwined responses. Hard x-rays enable studies in extreme environments where penetrating radiation is required. In the case of extreme pressures, polarized x-rays are a unique probe of electronic matter providing element-specific information on valence state, orbital occupancies, hybridization, charge transfer and electronic/magnetic ordering [9, 10, 11]. The ability to probe most types of electronic/magnetic orders and their spatial inhomogeneity using real- and reciprocal-space mapping with polarized brilliant x-ray beams at the extremes of high pressure in high magnetic fields at low temperatures is unique to low-emittance synchrotron radiation sources and will remain so for the foreseeable future.

### 4-3.2 Beamline Requirements for the Insertion Devices (IDs)

The Polar beamline is designed to operate over the energy range of 2.75-27 keV with variable polarization. The photon source included in the project scope is two phased planar undulators providing linear-horizontal polarization. Phase retarding optics will be used to generate circular and linear-vertical polarization in the 2.75-14 keV range. The APS-U project scope for this beamline is two planar devices. Following the competion of the project the plan is to replace this source with two in-line superconducting SCAPE devices. These devices provide L-H, L-V and CP polarization up to 27 keV.

*Table 4.15. Polar beamline source paramteres*

| **Unduator** | **Period** *(mm)* | **Length** *(m)* | **Location** | **Max Power*** *(W)* |
|---|---|---|---|---|
| Linear | 30 | 2x2.3 | SSC | 432 |
| SCAPE | 35# | 2x1.3# | Upstream and downstream from SSC | 158 |

SSC: Straight section center.
* Horizontal linear through white beam slit 0.92x0.92 $mm^2$ @ 27.0 m with the undulator tuned to emit 2.8 keV radiation
# Based on conservative estimates. Smaller period (30 mm) and longer (up to 1.8 m) devices may be possible.

### 4-3.3 Beamline Requirements for the Front End

The Polar beamline will utilize the new standard MBA High Heat-Load Front End capable of handling a maximum power of 21 kW. The beamline will have a windowless exit configuration with a 2 mm x 2 mm (H x V) exit mask aperture.

A detailed description of the Polar Front End and Insertion devices can be found in the APS-U 4-ID Beamline Front End and Insertion Devices Interface Control Document (ICMS Content ID: APSU_190932).

### 4-3.4 Beamline Layout

The physical layout of the Polar beamline utilizes existing hutch infrastructure at sector 4 with modifications to meet functional requirements. It consists of 4 enclosures: a FOE (4-ID-A), a SOE (4-ID-E), and two end stations (4-ID-B and 4-ID-G). 4-ID-B and 4-ID-G end stations will operate one at a time.

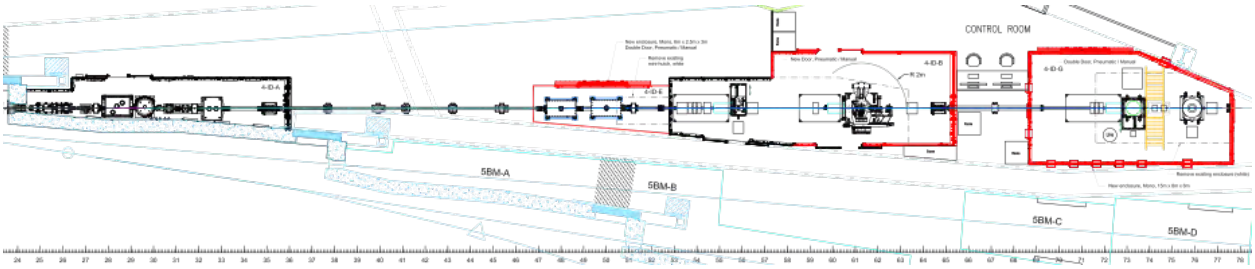


*Figure 4.10. Physical layout utilizes enclosure infrastructure at sector 4 with modifications*

### 4-3.4.1 Beamline Component Table

Table 4.16 shows all major beamline components. For a complete list of components, see the layout drawing bill of materials.

A detailed description of the Polar beamline can be found in the Polar 4-ID ESD (ICMS Content ID: APSU_2012709).

## 4-3.5 Optics Overview

Each experimental station (4-ID-B,G) will have one new KB-mirror system to provide focal spots in the 100-300 nm range. 4-ID-B will have a transfocator with CRLs for variable focal spot size. Large spot sizes are achieved with the toroidal mirrors also used for higher harmonic suppression.

Table 4.17 and Table 4.18 show the expected flux and focal size for circularly polarized beams at 10 keV for experimental stations 4-ID-B and 4-ID-G. The calculations are for brightness mode using two phased planar devices as the photon source and include attenuation by a 500 microns C(111) phase plate.

### 4-3.5.1 Detailed Optical Layout

Figure 4.11 shows the different focusing schemes for the two experimental stations 4-ID-B and 4-ID-G.

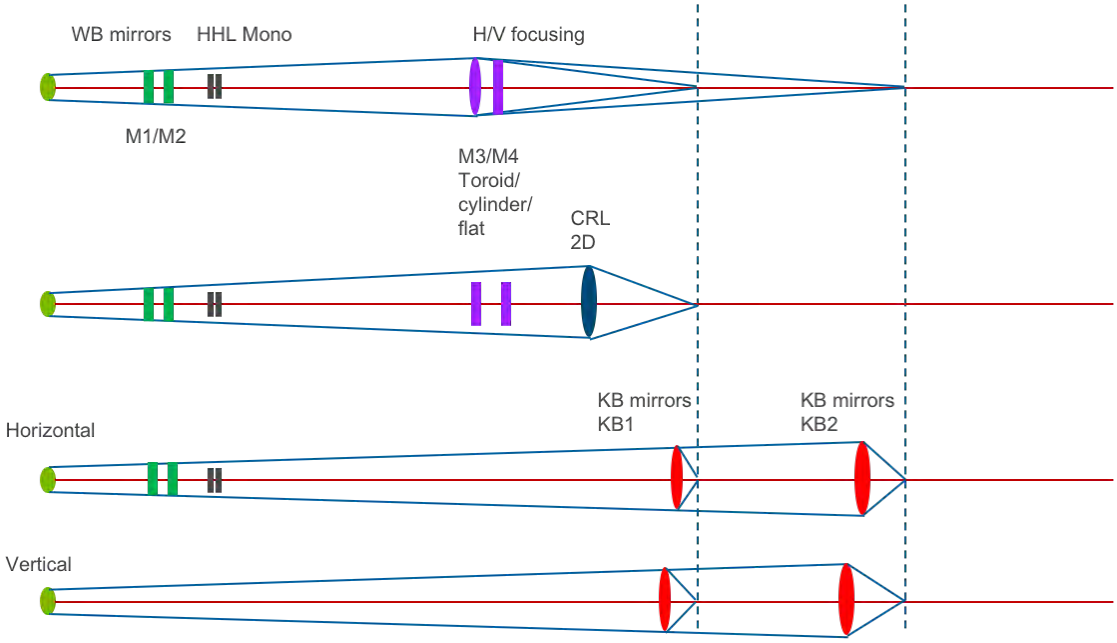


*Figure 4.11. Basic optical layout of the Polar beamline. M1/M2 (white beam mirrors) and M3/M4 (toroidal/flat mirrors) are horizontally reflecting mirrors. HHL mono is a horizontal-bounce double crystal monochromator, CRL are the compound refractive lenses and KB1 and KB2 are the fixed-curvature K-B mirrors.*

*Table 4.16. Polar beamline component table*

| **Distance from source** *(m)* | **Component** | **Description/Comments** |
|---|---|---|
| 25.4 | FE Exit Mask | Standard HHL Front-End exit mask<br>2x2 aperture |
| 26.1 | FE Collimator | Standard HHL Front-End Exit Collimator,<br>5x5 aperture |
| 27.0 | HHL WB Slits | HHL WB Slits w/ Tungsten Edge inserts, 4ID-SL-1 |
| 28.5 | Dual Mirror System | Mirror, Horizontal, Flat<br>& Mirror, Horizontal, Bendable, 4ID-MR-6 |
| 29.3 | Photon Mask | Photon Mask / PB Stop, 4ID-PM-1 |
| 30.0 | HDCM | Double Crystal Monochromator, Horizontal, 4ID-MN-1 |
| 31.1 | Slits | Slits, Mono, 4ID-SL-2 |
| 31.3 | Collimator | Collimator, Secondary, 4ID-SC-1 |
| 31.7 | Photon Mask | Photon Mask / WB Stop, 4ID-PM-2 |
| 32.0 | Collimator | Collimator, primary Bremsstrahlung, 4ID-BC-1 |
| 33.2 | Phase Retarder Tank | Phase Retarder Tank, 4ID-PR-1 |
| 35.1 | Shutter | Shutter, Mono, 4ID-SH-1 |
| 47.3 | Slits | Slits, Mono, 4ID-SL-3 |
| 48.0 | Mirror | Mirror, Horizontal,<br>Double Toroid/flat stripes + Bender,4ID-MR-1 |
| 50.0 | Mirror | Mirror, Horizontal,<br>Double Flat/cylinder stripes, 4ID-MR-2 |
| 50.8 | Window | Window, Be or diamond, 4ID-WN-1 |
| 53.4 | Polarimeter | In Situ Polarimeter, 4ID-EX-1 |
| 53.7 | Slits | Slits, Mono, 4ID-SL-4 |
| 54.0 | XBPM | XBPM, Mono, Diamond, 4ID-BD-1 |
| 54.1 | Attenuators | Attenuators, 4ID-FL-1 |
| 54.5 | Chopper | Chopper, In-Vacuum, 4ID-CH-1 |
| 55.1 | Mirrors | Mirrors, K-B, Bendable, 4ID-MR-3 |
| 55.5 | Monitor Detector | Monitor Detector (IO), 4ID-BD-4 |
| 55.8 | 2T Electromagnet | 2 T Electromagnet, 4ID-MG-1 (existing) |
| 56.5 | Detector Photodiode | Detector Photodiode (I), 4ID-BD-5 (existing) |
| 59.3 | Transfocator | Transfocator, 4ID-TR-1 |
| 59.4 | Slits | Slits, Mono, 4ID-SL-5 |
| 61.0 | Mirrors | Mirrors, K-B, Fixed Curvature, 4ID-MR-4 |
| 61.3 | 2T Magnet | 2 T Magnet, 4ID-EX-2 |
| 61.3 | Diffractometer | Diffractometer, 4ID-EX-3 |
| 62.0 | Detector | Detector, Pixel Array, 4ID-DT-2 |
| 62.0 | Polarization Analyzer | Polarization Analyzer, 4ID-BD-3 |
| 64.6 | Shutter | Shutter, Mono, 4ID-SH-2 |
| 71.5 | XBPM | XBPM, Mono, Diamond 4ID-BD-2 |
| 71.7 | Slits | Slits, Mono, 4ID-SL-6 (existing) |
| 71.9 | Attenuators | Attenuators, 4ID-FL-1 |
| 72.6 | Mirrors | Mirrors, K-B, Fixed Curvature, 4ID-MR-5 |
| 72.8 | Monitor Detector | Monitor Detector (IO), 4ID-BD-4 |
| 73.3 | 10T Magnet | 10 T Superconducting Magnet, 4ID-EX-4 |
| 73.3 | Raman Support | Raman Support, 4ID-EX-6 |
| 73.3 | Raman Spectrometer | Raman Spectrometer, 4ID-EX-7 |
| 73.3 | Interferometer | Interferometer, 3-channel 4-ID-EX-8 |
| 74.2 | Detector | Detector, Multielement Florescence, 4ID-DT-1 |
| 74.4 | Transmission Detector | Transmission Detector (I), 4ID-BD-5 |
| 75.9 | 4T magnet | Small bore 4 T magnet (existing) |
| 77.5 | Beam Stop | Beam Stop, 4ID-BS-1 |

*Table 4.17. Flux and spot size in 4-ID-B. A 0.5x0.5 $mm^2$ aperture at 25 m is used (20x20 $\mu rad^2$ acceptance) and all relevant optical elements are included (white beam mirrors, DCM, focusing optics).*

| **Mode** | **Energy** *keV* | **Focusing optic** | **Flux** *(ph/s/0.1%BW)* | **Focal size FWHM (HxV)** |
|---|---|---|---|---|
| Flux, High brightness | 10 | K-B | $1.3x10^{13}$ | 120x115 $nm^2$ |
| Flux, Coherent | 10 | K-B + slit | $1.4\ x10^{12}$ | 200x200 $nm^2$ |
| Flux, medium spot | 10 | CRL | $1.4x10^{13}$ | $\geq$ 1.2x0.4$\mu m^2$ |
| Flux, large spot | 10 | Toroid | $3x10^{13}$ | 34x4 $\mu m^2$ |

*Table 4.18. Flux and spot size in 4-ID-G. A 0.5x0.5 $mm^2$ aperture at 25 m is used (20x20 $\mu rad^2$ acceptance) and all relevant optical elements are included (white beam mirrors, DCM, focusing optics).*

| **Mode** | **Energy** *keV* | **Focusing optic** | **Flux** *(ph/s/0.1%BW)* | **Focal size FWHM (HxV)** |
|---|---|---|---|---|
| Flux, High brightness | 10 | K-B | $2.1x10^{13}$ | 330x230 $nm^2$ |
| Flux, Coherent | 10 | K-B + Slit | $1.7x10^{12}$ | 555x370 $nm^2$ |
| Flux, large spot | 10 | Toroid | $3x10^{13}$ | 70x8 $\mu m^2$ |

### 4-3.5.2 Optical Simulation and Tolerances

Optical simulations were carried out using the ShadowOui program in the Oasys environment. The figure errors required to obtain the spot sizes shown in Figure 4.12 and Figure 4.13 are listed together with other mirror parameters in various tables. For focusing with K-B mirrors the combined figure errors specified in the tables (white beam mirrors + K-B) do not increase the spot size by more than 10% relative to the ideal case neglecting FE and SE. Intensity profiles for focused beams at the sample position in 4-ID-B for the three mirror modes listed in Table 4.17 are shown in Figure 4.12. The simulations use the brightness filling mode and the x-ray energy is 10 keV.

Intensity profiles for focused beams at the position of the high-field magnet in 4-ID-G for the three modes listed in Table 4.18 are shown in Figure 4.13. The simulations use the brightness filling mode and the x-ray energy is 10 keV.

### 4-3.5.3 Optics Specifications

**HHL Slits** Total power from the insertion device when tuned to 2.8 keV in linear mode is 16 kW. The power density on slits, located at 27 m, is ~ 512 W/$mm^2$ (see ICD document APSU_190932).

**HHL Mirrors** The water-cooled high-heat load mirrors will be the first optical components of the Polar beamline. They will be co-located in a single vacuum vessel in enclosure A and operate at a reflection angle of 3 mrad in the horizontal plane. The first mirror will be flat with the notch designed to reduce the thermal induced deformation. The second mirror is bendable to correct for the deformation of the first crystal in the DCM. These mirrors will each have three reflecting stripes (bare Si, Rh, and Pt) to provide harmonic rejection and cover the operational energy range. Vertical

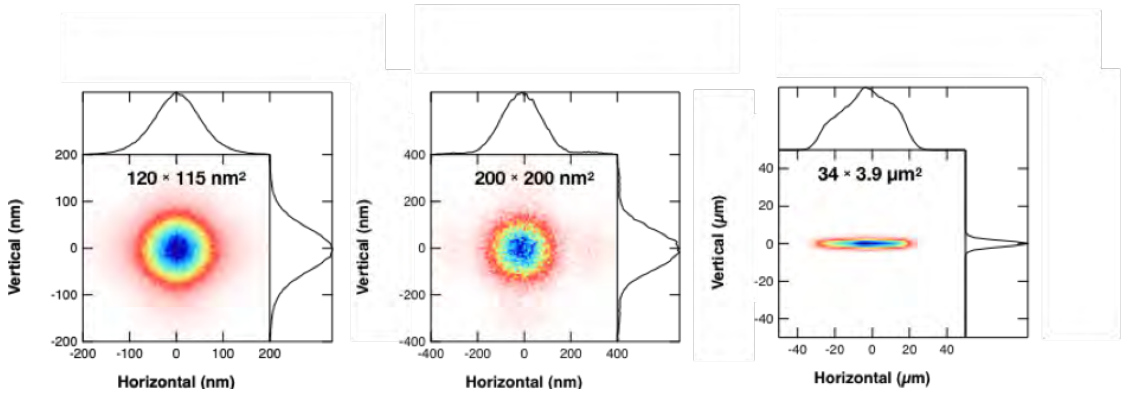


*Figure 4.12. Focal spot at the sample location in 4-ID-B for the high-brightness mode (left); coherence mode (middle) and large spot (right). Corresponding flux values are given in Table 4.17 .*

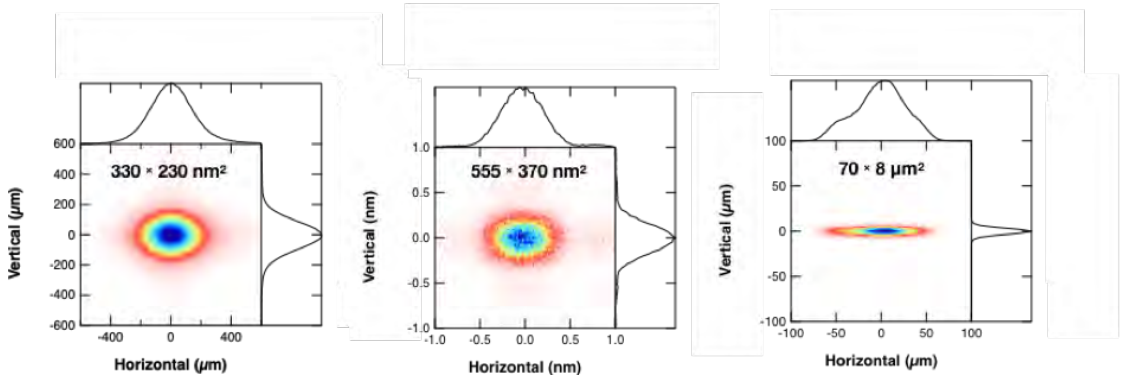


*Figure 4.13. Focal spot at the sample location in 4-ID-G for the high-brightness mode (left); coherence mode (middle) and large spot (right). Corresponding flux values are given in Table 4.18 .*

translation is required to change the reflecting stripe used. The mirror specifications are given in Table 4.19.

*Table 4.19. Specifications of white beam mirrors*

| | **Mirror 1** | **Mirror 2** |
|---|---|---|
| Material | Single Crystal Si | Single Crystal Si |
| Shape | Flat | Meridional Bendable |
| Radius of Curvature | $\infty$ | -50 to 50 km |
| Angle of incidence | 3 mrad | 3 mrad |
| Deflection | Horizontal | Horizontal |
| Length | 320 mm | 320 mm |
| Thickness | 30 mm | 30 mm |
| Three Optical Coatings | Pt, Rh, bare Si | Pt, Rh, bare Si |
| Width each coating | 5 mm | 5 mm |
| Active length | 300 mm | 300 mm (98% at 2.8 keV) |
| Power absorbed | 254 W | 118 W |
| Meridional Figure error RMS | <0.8 nm | <0.8 nm |
| Meridional Slope error | <0.1 µrad | <0.1 µrad |
| Sagittal Figure error RMS | <10 µrad | <10 µrad |
| RMS Roughness (1-100 µm) | <0.2 nm | <0.2 nm |

**HHL Double Crystal Monochromator** The Polar beamline will have a horizontally deflecting double-crystal monochromator (HDCM) operating in the energy range of 2.75-27 keV. The DCM uses Si(111) crystals and is cryogenically cooled ($LN_2$). 6H-SiC crystals mounted either on a second crystal cage or on the primary Si(111) crystals with a vertical offset from the center of the crystals will be used for operation in the 2.75-3.3 keV range.

**Toroidal and Cylindrical Mirrors** These horizontal-bounce mirrors provide a large spot size in the tens of microns range for experiments at either one of the two experimental stations that cannot use very small beams. They also provide additional suppression of higher order harmonics emitted by the insertion device. The first mirror can be bent along its meridional direction. It has two sagittal cylinders and one flat region. The second mirror has two flat regions and a sagittal cylinder. The mirror specifications are listed in Table 4.20 for the first mirror M3 and in Table 4.21 for the second mirror M4.

**Transfocator** A transfocator equipped with parabolic 2D compound refractive lenses (CRLs) will be located 2 m upstream of the sample position in the diffractometer at 61.3 m. The transfocator has 7 stacks of lenses with the number and radii of lenses shown in Table 4.22.

**Experimental 4-ID-B K-B and 4-ID-G KB Mirror System** The nano-focusing K-B mirrors for 4-ID-B and 4-ID-G operate at a reflection angle of 3.0 mrad. Both mirrors sets will have a prefigured elliptical cylinder with Pt and Rh coatings. Mirror specifications are given in Table 4.23 and Table 4.24.

*Table 4.20. Specifications for mirror M3*

| | **Si** | **Pd (Cr binding)** | **Pt (Cr binding)** |
|---|---|---|---|
| Material | | Single crystal Si | |
| Shape | Sagittal Cylinder | Flat | Sagittal Cylinder |
| Sagittal Radius | 83.1±1 mm | $\infty$ | 79±1 mm |
| Width | 10 mm | 10 mm | 10 mm |
| Active width | 5 mm | 5 mm | 5 mm |
| Deflection | | Horizontal plane | |
| Angle of incidence | | Variable 2 - 4 mrad | |
| Active Length | | 520 mm | |
| Length | | 540 mm | |
| Meridional Radius | | Variable: 4 – 100 km | |
| Thickness | | Allowing 4 km radius of curvature | |
| RMS Meridional Slope error on cylinders | | 0.3 µrad | |
| RMS Meridional Slope error on flat | | 0.2 µrad | |
| RMS Sagittal Slope error. | | 10 µrad | |
| RMS Roughness | | 0.15 nm | |

*Table 4.21. Specifications for mirror M4*

| | **Si** | **Pd (Cr binding)** | **Pt (Cr binding)** |
|---|---|---|---|
| Material | | Single crystal Si | |
| Shape | Flat | Sagittal Cylinder | Flat |
| Sagittal Radius | $\infty$ | 69.9±1 mm | $\infty$ |
| Width | 10 mm | 10 mm | 10 mm |
| Active width | 5 mm | 5 mm | 5 mm |
| Angle of incidence | | Variable 2 - 4 mrad | |
| Active Length | | 520 mm | |
| Length | | 540 mm | |
| Meridional Radius | | >100 km | |
| Thickness | | 40 mm | |
| RMS Meridional Slope error on cylinder | | 0.3 µrad | |
| RMS Meridional Slope error on flats | | 0.2 µrad | |
| RMS Sagittal Slope error. | | 10 µrad | |
| RMS Roughness | | 0.15 nm | |

*Table 4.22. Number and radii of lenses for stack 1 to 7 in transfocator*

| Stack | 1 | 2 | 3 | 4 | 5 | 6 | 7 |
|---|---|---|---|---|---|---|---|
| Type | 2D | 2D | 2D | 2D | 2D | 2D | 2D |
| $N$ | 1 | 1 | 2 | 4 | 8 | 8 | 8 |
| $R$, µm | 500 | 200 | 200 | 200 | 200 | 100 | 50 |

*Table 4.23. Specifications of 4-ID-B K-B mirrors KB1*

| | **VFM** | **HFM** |
|---|---|---|
| Shape | Elliptical cylinder | Elliptical cylinder |
| Angle of incidence | 3 mrad | 3 mrad |
| Distance to source* | 60900.5 mm | 61105.5 mm |
| Distance to Image* | 362.5 mm | 157.5 mm |
| Length | 275 mm | 115 mm |
| Thickness | 30 mm | 30 mm |
| Width | 30 mm | 30 mm |
| Active length | 255 mm | 95 mm |
| Active width | 12 mm | 12 mm |
| Figure error PV (RMS) | <2 nm (< 0.5 nm) | <2 nm (< 0.5 nm) |
| RMS Roughness | 0.15 nm | 0.15 nm |
| Material | Single crystal Si | Single crystal Si |
| Optical Coating | Pt & Rh (5 mm each, Cr binding) | Pt & Rh (5 mm each, Cr binding) |

*Table 4.24. Specifications of 4-ID-G KB mirrors KB2*

| | **VFM** | **HFM** |
|---|---|---|
| Shape | Elliptical cylinder | Elliptical cylinder |
| Angle of incidence | 3 mrad | 3 mrad |
| Distance to source* | 72458.5 mm | 72778.5 mm |
| Distance to Image* | 827.5 mm | 507.5 mm |
| Length | 405 mm | 215 mm |
| Thickness | 30 mm | 30 mm |
| Width | 30 mm | 30 mm |
| Active length | 385 mm | 195 mm |
| Active width | 12 mm | 12 mm |
| Figure error PV (RMS) | <2 nm (< 0.5 nm) | <2 nm (< 0.5 nm) |
| RMS Roughness | 0.15 nm | 0.15 nm |
| Material | Single crystal Si | Single crystal Si |
| Optical Coating | Pt & Rh (5 mm each, Cr binding) | Pt & Rh (5 mm each, Cr binding) |

### 4-3.5.4 Heat Load Considerations

The HHL mirrors will reduce the power passed on to the monochromator. Table 4.25 below summarizes the maximum power expected to be absorbed by various components when the HHL slits are tuned to accept the full undulator radiation at 2.8 keV and 10 keV (third harmonic). The first mirror has an optimized notch design to minimize its meridional deformation. The ray tracings using the FEA show that the increase in the spot size due to the deformations of the optical elements can be fully cancelled.

*Table 4.25. Power absorbed on optical elements with slits tuned to accept the full monochromatic beam at two energies (0.59x0.59 $mm^2$ at 10 keV and 0.92x0.92 $mm^2$ at 2.8 keV)*

| **Undulator** | **K** | **Mono Energy** *(keV)* | **Power absorbed on M1** *(W)* | **Mirror coating** | **Power absorbed by M2** *(W)* | **Mirror coating** | **Power absorbed on DCM** *(W)* | **Power Density on DCM** *($W/mm^2$)* |
|---|---|---|---|---|---|---|---|---|
| 2xU30 | 2.49 | 2.8 | 254 | Pt | 118 | Si | 50 | 46 (SiC) |
| 2xU30 | 2.2 | 10 ($3^{rd}$) | 88 | Pt | 44 | Si | 27 | 13.3 |

Figure 4.14 shows the focal spot at 4-ID-B without and with thermal induced deformations as well as the correction by changing the radius of curvature of the second HHL mirror. The photon energy is 10 keV and the mirrors coatings and their absorbed power are listed in Table 4.25.The mirrors do not include the FE due to manufacture. The correction is done by bending the second mirror with a convex radius of curvature of -77 km and a rotation of the vertical KB by 0.35 µrad.

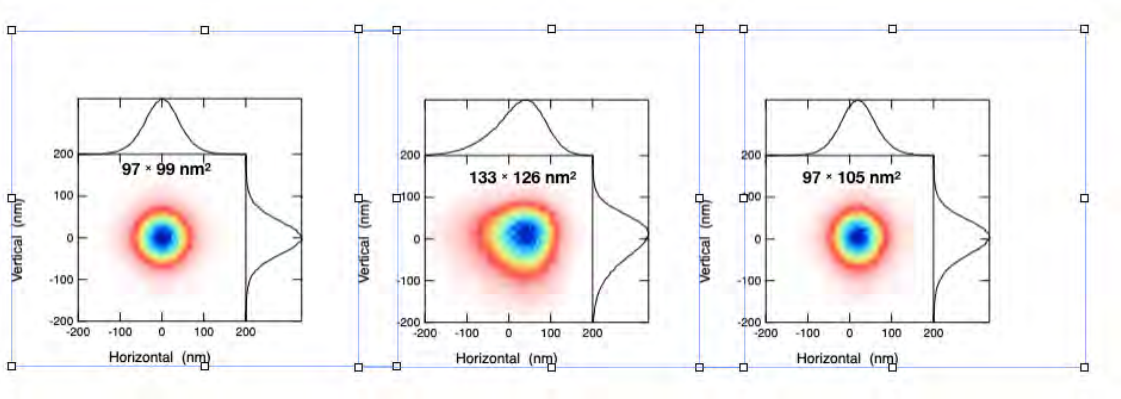


*Figure 4.14. Focal spot at the sample location on 4-ID-B for the high brightness mode neglecting deformation of HHL optical components (left); including optical elements deformation (middle) and after correction (right).*

A detailed description of the Polar optics can be found in the Beamline Optics ESD Polar (ICMS Content ID: APSU_2030433).

## 4-3.6 Instrument Overview

### 4-3.6.1 Scientific Scope

The 4-ID-B enclosure at the Polar beamline will house a dedicated instrument for performing X-ray resonant magnetic reflectivity (XRMR) as well as resonant hard X-ray ptychography and diffraction experiments at extreme pressures ($<$ 7 Mbar) making use of the highly brilliant and coherent beam provided by the APS-U storage ring as well as the unique polarizing insertion device that will be available at this beamline.

The 4-ID-G hutch at the Polar beamline will have a dedicated instrument for x-ray absorption spectroscopy, including linear and circular magnetic/natural dichroic measurements (XAS, XLD, XCD, XMLD, XMCD), under extreme static pressure conditions ($<$ 7 Mbar) in simultaneous low-temperature ($>$ 1 K) and high magnetic field ($>$ 7 Tesla) environments.

### 4-3.6.2 XRD Instrument in 4-ID-B

### 4-3.6.3 Instrument Definition

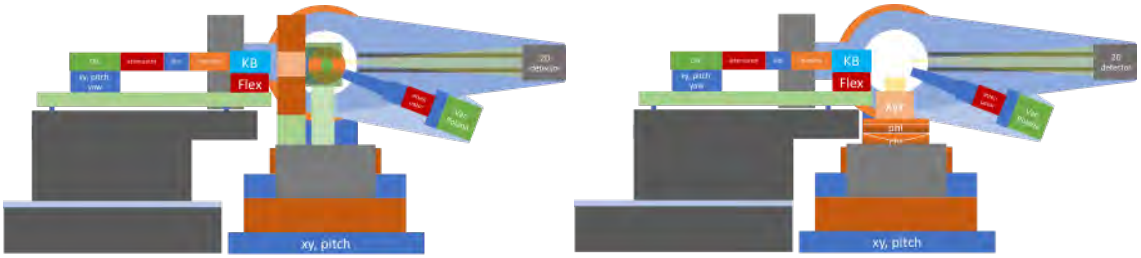


*Figure 4.15. Schematic of 4-ID-B-XRD instrument with Eulerian cradle (left) and double tilt goniometer (right).*

The 4-ID-B-XRD instrument includes a flexible diffractometer with Eulerian cradle for high Q-range access. It includes a compact 2 T superconducting magnet. The Eulerian cradle is removable and allows installation of heavy-load, high-precision rotation and translation stages for ptychographic coherent diffraction imaging experiments. The detector arm carries an in vacuum polarization analyzer for polarization dependent studies and an area detector for coherent imaging experiments. The instrument includes an in-vacuum polarization analyzer for polarization dependent studies and an area detector for coherent imaging experiments. The instrument includes K-B mirrors for nm-sized focused beam and a transfocator for more relaxed focus size. It also includes attenuators both upstream of the diffractometer and on the detector arm as well as a granite optical table for beam conditioning and support of the beamline optics upstream of the diffractometer. A separate table for placing a detector at 3 m distance to the sample on the diffractometer is positioned downstream of the diffractometer. A sketch of this instrument is shown in Figure 4.15.

### 4-3.6.4 Instrument operating modes

The instrument will have three configurations. The Eulerian-cradle configuration will be used for resonant scattering experiments together with a cryostat, a 2 T magnet, and pressure cells. In the

second mode the Eulerian cradle on the diffractometer is replaced by a combination of rotation and XYZ stages with small sphere of confusion and a removable air bearing rotation stage on top. Both modes will use the variable length detector arm for detector positioning between 1.5 and 2 m. Finally, in the beam pass mode beam will be delivered through the 4-ID-B hutch to the 4-ID-G hutch for XMCD and spectroscopy measurements.

#### 4-3.6.5 High-Field-Magnet in 4-ID-G

#### 4-3.6.6 Instrument Definition

The 4-ID-G-XMCD instrument is built around a large-bore high-field superconducting magnet capable of accommodating a non-magnetic CuBe diamond anvil cell (DAC) fitted with helium gas compression/decompression membranes for in-situ pressure control. The magnet has 3 split pair coils for producing longitudinal and transverse fields. The magnet includes reentrant room temperature bores in both transverse directions for placement of optical elements of a Raman system, energy-dispersive multi-element solid state, and optical elements for interferometry-based sample positioning. The DAC assembly includes nano-positioning stages and photodiode array detector for x-ray fluorescence measurements in backscattering geometry. The instrument includes magnet support structure, motorized table and rotation stage for magnet translations and rotation about vertical direction, motorized translation and rotation of the sample insert, K-B mirrors, granite block supporting both K-B mirrors and magnet structure, intensity monitors, an upstream optical table with beam conditioning components including diamond XBPM, attenuators and defining slits, sample loading platform.

#### 4-3.6.7 Instrument operating modes

The instrument will have 3 operating modes. A brightness mode uses the K-B mirrors to generate a 330x230 $nm^2$ spot size for high pressure experiments and 2D mapping experiments. A high-flux mode uses the 70x4$\mu m^2$ spot size from the toroidal mirror in 4-ID-E for ambient pressure experiments. A beam pass mode requires the magnet to be translated in the inboard direction to allow beam into the back of the hutch (e.g. for use with existing cryogen-free magnet).

The operating modes are summarized in Table 4.26.

*Table 4.26. Operating modes with beam size and focusing optics*

| Beam size | Mirrors | Experiment |
|---|---|---|
| 330x230 $nm^2$ | K-B | High pressure |
| 330x230 $nm^2$ | K-B | 2D mapping |
| 70x4 $\mu m^2$ | Toroidal | Ambient pressure |

#### 4-3.6.8 Instrument Location

The diffractometer will be located in 4-ID-B at 61.3 m and the high-field magnet will be located in 4-ID-G at 73.4 m from the source. Figure 4.17 shows a layout of the experimental stations at Sector 4.

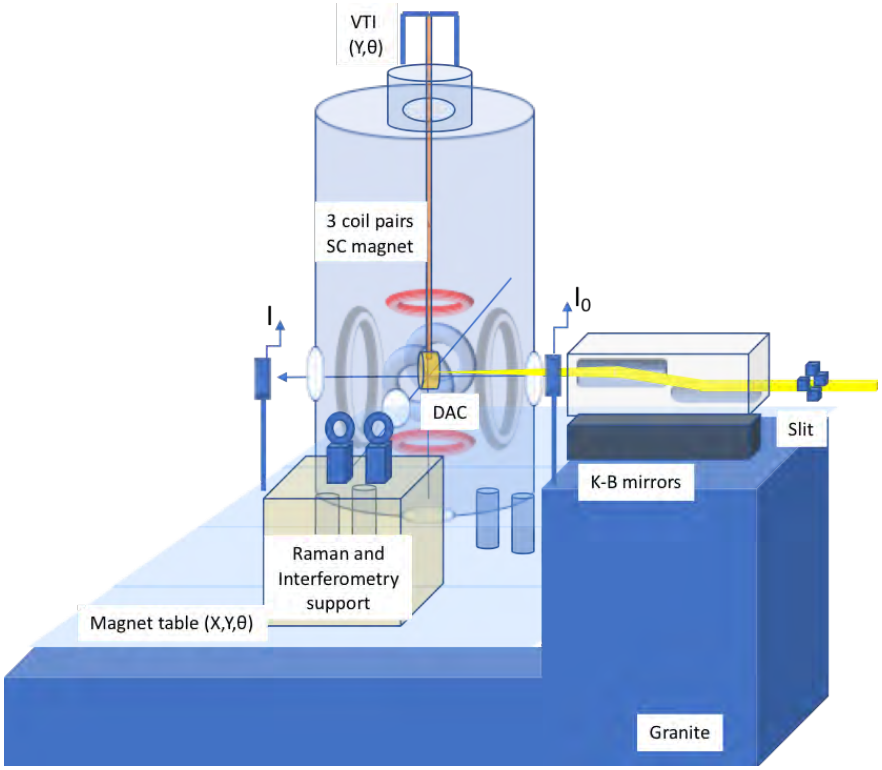


*Figure 4.16. Schematic of 4-ID-G-XMCD instrument. Optical table upstream of the mirrors is not shown.*

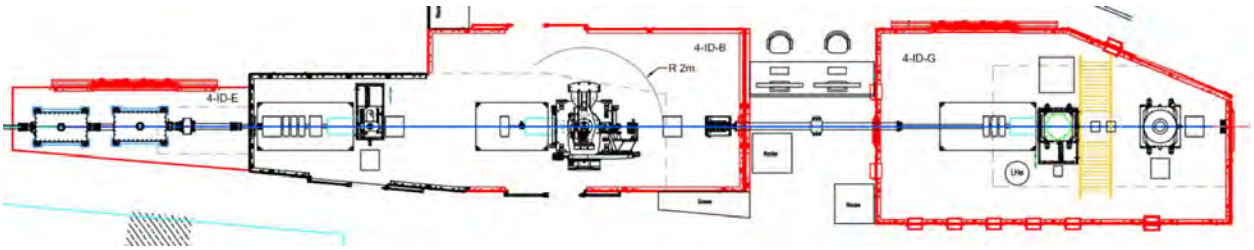


*Figure 4.17. 4-ID hutch layout. The 4-ID-B hutch is the middle hutch and the 4-ID-G hutch is the last hutch.*

A detailed description of the Polar Endstation instruments can be found in the 4-ID Endstation Instrumentation ESDs (ICMS Content ID: APSU_2030618 and APSU_2030619).

## 4-4 HEXM 20-ID

### 4-4.1 Introduction

The High-Energy X-Ray Microscope (HEXM) will be a long beamline at APS-20-ID. Operating in the monochromatic 35 - 120 keV range and also being white-beam capable, it will receive radiation from a superconducting-undulator (SCU) source. HEXM will consist of a first-optics enclosure (FOE) and two experimental end-stations – one at approximately 70 m (within the main experimental floor) and one at 180 m (in an external building) from the source. The external building will be shared with another long APS-U beamline (the In-Situ Nanoprobe [ISN] located at 19-ID).

HEXM will investigate structure and evolution within bulk materials, often in extreme environments, with both the enhanced high-energy x-ray scattering techniques used today (e.g., at 1-ID) and with novel coherence-based techniques enabled by the low-emittance APS-U multi-bend-achromat (MBA) lattice.

### 4-4.2 Scientific Objective

High-energy x-rays interact with matter with low attenuation, small scattering angles (giving large reciprocal space access), and the validity of the single-scattering approximation. These features, when combined with a brilliant source like the APS-U at high energies, make such x-rays the scattering probe of choice for interrogating bulk material structure. Such a combination of penetration capability with high spatial, reciprocal-space, and temporal resolution, enables these x-rays to measure phase, texture, and strain distributions nondestructively under complex sample environments.

HEXM will apply these principles by combining the low-emittance MBA lattice, a superconducting-undulator source, and a long beamline with a large end-station, as shown in Figure 4.18. The high-energy x-rays (35 - 120 keV) will be applied through multi-modal techniques such as high-energy diffraction microscopy (HEDM), wide- and small-angle scattering (WAXS/SAXS), micro-tomography (μ-CT), scattering tomography (ST), transmission x-ray microscopy (TXM), and Bragg coherent-diffraction imaging (BCDI) – available at the same sample location (E station). Hence, HEXM will have the ability to probe length scales covering many orders of magnitude during a single experiment. Materials subjected to these techniques would be of relevance to mechanical engineering, biophysics, irradiation/nuclear energy, energy storage, and advanced manufacturing.

The primary experimental station (E) will be ∼20 m in length, with samples and environments located at 180-m distance from the source. The long beamline enables:

A. focusing down to small spot sizes at larger working distances that are more convenient from the standpoint of sample environments, focusing optics fabrication, and divergence;
B. efficient performance of expansion optics when large beams in one or both dimensions are needed (e.g., near-field-HEDM, μ-CT); and
C. producing relatively large, coherent focal spots (tens of μm for BCDI) through low source-demagnification or magnification geometries.

Furthermore, the long end-station enables distances greater than 15 m between the sample and some detectors to optimize direct or reciprocal space resolutions in certain techniques (very-far-

field-HEDM, BCDI, SAXS, TXM). Finally, being away from the main APS experimental hall, the external building that houses the E station will be compatible with unique facilities like activated-materials handling.

### 4-4.3 Beamline Requirements for the Insertion Devices (IDs)

HEXM desires the highest brilliance over its operating energy range, with full spectral coverage. A superconducting undulator is planned, with parameters listed in Table 4.27. Due to possibly not needing a phasing magnet between the two undulator segments, the total magnetic length might be increased from 3.5 m to 3.8 m.

The HHLFE exit mask/window is planned to be 2 x 1 $mm^2$, 0.5 mm thick Be.

*Table 4.27. Source Parametersfor HEXM*

| **Unduator** | **Period** *(mm)* | **Length** *(m)* | **$K_{max}$** | **Power*** *(kW)* | **Power Density*** *($kW/mrad^2$)* |
|---|---|---|---|---|---|
| SCU | 16.5 | 3.5 | 1.63 | 1.6 | 600 |

* Through the Front End Mask, 2 x 1 $mm^2$ @ 25.4 m with a 0.5 mm Be window.

### 4-4.4 Beamline Requirements for the Front End

The HEXM beamline will utilize the new standard MBA High Heat-Load front end capable of handling a maximum power of 21 kW. The beamline will require a 2 mm x 1 mm (H x V) exit mask aperture with a Be window.

A detailed description of the HEXM Front End and Insertion devices can be found in the APS-U 20-ID Beamline Front End and Insertion Devices Interface Control Document (ICMS Content ID: APSU_190948).

### 4-4.5 Beamline Layout

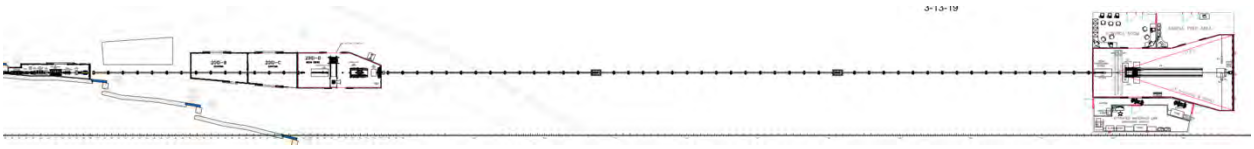

*Figure 4.18. Layout for HEXM beamline.*

The High-Energy X-Ray Microscope (HEXM) will be one of two long beamlines built at the APS. Located at APS-20-ID, HEXM beamline will extend beyond the current exterior walls of the facility and terminate with a sample position at approximately 180m.

#### 4-4.5.1 Beamline Component Table

The following Table 4.28 shows all major beamline components.

*Table 4.28. HEXM beamline component table*

| **Distance from source***(m)* | **Component** | **Designation** | **Description/Comments** |
|---|---|---|---|
| 25.4 | FE Exit Mask | | Front-End exit mask<br>2(H)x1(V) $mm^2$ aperture |
| | FE Window | | Diamond Window |
| 26.1 | FE Collimator | | HHL Front-End Exit Collimator<br>5x5 $mm^2$ aperture |
| 26.5 | Filter | 20ID-FL-1 | White Beam Filter |
| 27.5 | HHL WB Slits | 20ID-SL-1 | HHL Variable Aperture Photon<br>Absorber w/ Tungsten Edge inserts |
| 28.5 | L1 Optics | 20ID- | L1 - WB refractive optics |
| 29.5 | Monochromator | 20ID-MN-1 | Laue-Laue High Energy Monochromator,<br>Horizontal offset (25-35 OB) |
| 30.3 | Window | 20ID-WN-1 | Diamond Window |
| 30.7 | L2 Optics | | Not in Project Scope |
| 31.8 | Monochromator | 20ID-MN-2 | High Resolution Monochromator, No offset |
| 33.0 | L3 Optics | 20ID- | Not in Project Scope |
| 33.9 | Window | 20ID-WN-2 | Be Window |
| 34.0 | Photon Mask | 20ID-PM-1 | Photon Mask |
| 34.4 | Collimator | 20ID-BC-1 | Tungsten Collimator |
| 35.0 | Shutter | 20ID- | WB/Bremsstrahlung Shutter, P4-80 |
| 36.0 -65.3 | Shielded Transport | 20ID-ST-1 | White Beam Shielded Transport |
| 66.2 | Photon Mask | 20ID-PM-2 | Photon Mask |
| 66.5 | Collimator | 20ID-BC-2 | Tungsten Collimator |
| 66.8 | Be Window | 20ID- | Be Window |
| 67.3 | Slits | 20ID-SL-3 | Multi-beam Slits |
| 68.0 | Fast Shutter | 20ID-FS-1 | |
| 68.3 | L4 Optics | | Not in Project Scope |
| 69.3 | Slits | 20ID-SL-4 | Multi-beam Slits |
| 70.2 | Instrumentation | 20ID-BI-1 | 20-ID-D station Instrumentation |
| 72.5 - 75 | Detector | 20ID-BI-2 | Dexela 2923 or equivalent |
| 75.7 | Slits | 20ID-SL-5 | Multi-beam Slits |
| 76.0 | L5 Optics | | Not in Project Scope |
| 76.7 | Beam Stop | 20ID-BS-1 | Movable White Beam / Bremsstrahlung Stop |
| 77.0 | Window | 20ID-WN-3 | In shielded box downstream of 20-ID-D |
| 77.0-177.5 | Shielded Transport | 20ID-ST-2 | White Beam Shielded Transport |
| 177.7 | Window | 20ID-WN-4 | In shielded box downstream of 20-ID-D |
| 178.2 | Slits | 20ID-SL-7 | WB Slits (TEMP) |
| 178.8 | L6 Optics | | Not in Project Scope |
| 180.0 | Window | 20ID-WN-5 | Window Be (TEMP) |
| 180.7 | | 20ID-BI-3 | 20-ID-E Endstation Instrumentation |
| 183.3-192.5 | Detector | 20ID-DT- | Robot Arm with Dexela 2923 or equivalent |
| 197.0 | Beam Stop | 20ID-BS-2 | White Beam Stop, Fixed |

A detailed description of the HEXM beamline can be found in the HEXM 20-ID Photon delivery system ESD (ICMS Content ID: APSU_2012713).

## 4-4.6 Optics Overview

### 4-4.6.1 Beam Delivery Specifications

HEXM will operate in a monochromatic mode over the 35–120 keV energy range and also in white beam mode (denoted as "broadband" in the table). Numerous optics configurations will be available, many of which are listed in the Table 4.29, with expected performance parameters assuming the brightness-lattice of the APS-U storage ring. The broadband cases pertain to delivering a focused single spectral harmonic of the undulator to the experiment.

*Table 4.29. Performance parameters, not including the filters, for various optics configurations under the APS-U brightness mode. Refer to Figure 4.19 for an explanation of the focusing optics.*

| **Configuration: station, delivery optics** | **Energy, Mode (keV)** | **Beam Size FWHM (h x v, $\mu$m)** | **Flux (ph/s/200 mA)** | **Energy Spread ($\Delta$E / E)** |
|---|---|---|---|---|
| E unfocused | 70, mono | 2.5 x 2.2 | $1 \times 10^{14}$ | $10^{-3}$ |
| E focused, L6 optics | 70, mono | 0.43 x 0.21 | $4 \times 10^{11}$ | $10^{-3}$ |
| E focused, L5 optics | 70, mono | 48 x 13 | $6.5 \times 10^{13}$ | $10^{-3}$ |
| E focused, L3 optics | 70, mono | 155 x 40 | $8 \times 10^{13}$ | $10^{-3}$ |
| E focused, L1 optics | 70, broadband | 182 x 47 | $4.8 \times 10^{14}$ | $6 \times 10^{-3}$ |
| E, coherence for BCDI (see Figure 4.20) | 40, mono | 48 x 31 | $3.8 \times 10^{9}$ | $2 \times 10^{-6}$ |
| D unfocused | 70, mono | 1 x 0.9 | $1 \times 10^{14}$ | $10^{-3}$ |
| D focused, L4 optics | 70, mono | 0.96 x 0.87 | $2.7 \times 10^{12}$ | $10^{-3}$ |
| D focused, L3 optics | 70, mono | 39 x 10 | $8 \times 10^{13}$ | $10^{-3}$ |
| D focused, L1 optics | 70, broadband | 50 x 13 | $4.8 \times 10^{14}$ | $6 \times 10^{-3}$ |

### 4-4.6.2 Detailed Optical Layout

A schematic of the HEXM x-ray optics layout is shown in Figure 4.19, from which all the implementations of configurations in Table 4.29 are clear, with the exception of the BCDI configuration, which is shown in Figure 4.20.

### 4-4.6.3 Optical Performance

Table 4.30 shows focal spot contributions and sizes expected in short-focal-length configurations in the D and E stations, using the L4 and L6 optics, respectively, for both the brightness and timing modes of APS-U. In the brightness mode, the 2 m focal length in the in the E station achieves 200 nm vertical focusing. (Note that the $f = 2$ m, brightness mode parameters in Table 4.30 correspond the rows 2 [L6 focusing] and 8 [L4 focusing] in Table 4.29.) Focusing to 100 nm vertically is possible with a shorter focal length of 1 m, with high-resolution monochromatization (to reduce chromatic aberration) and larger focusing aperture (e.g., with a kinoform lens, to reduce the diffraction limit). Kinoform calculations assume the conservative $f \sim 1/\lambda^2$ chromaticity.

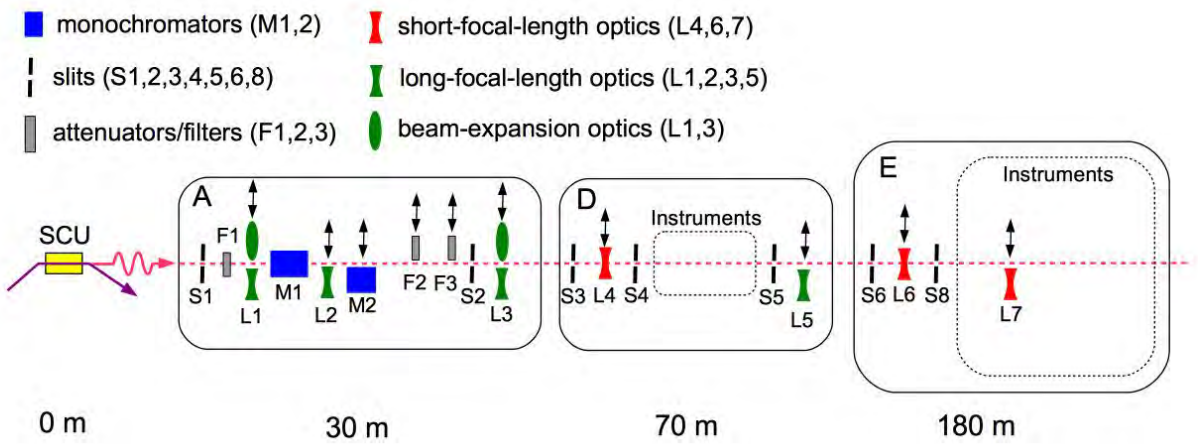


*Figure 4.19. HEXM x-ray optical layout (plan view)*

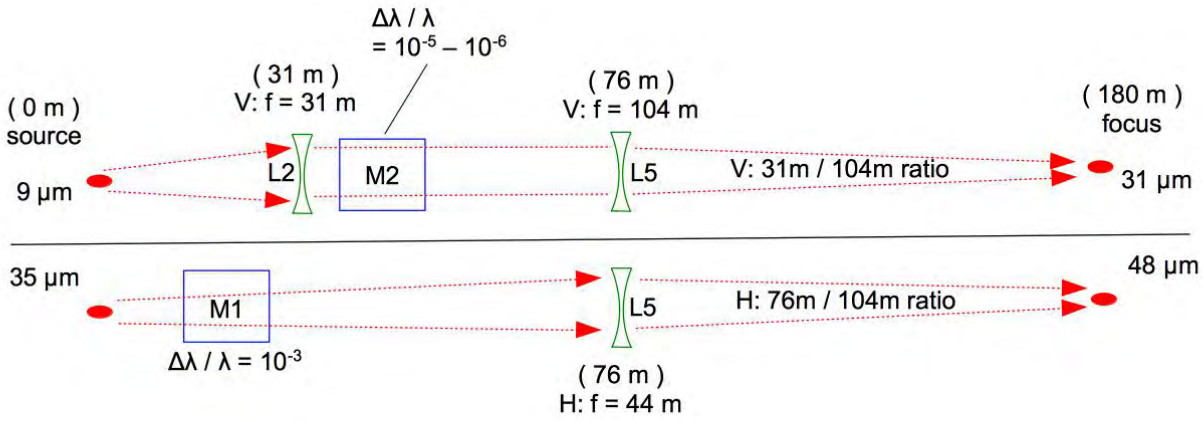


*Figure 4.20. Optics configuration (vertical/upper, horizontal/lower) for enabling the BCDI technique.*

*Table 4.30. Focal spot contributions and sizes at 70 keV for 2 m and 1 m focal lengths, for both brightness (and timing) APS-U beam modes.*

| **Station and distance (m)** | **$f$ = 2 m, 150 $\mu$m aperture refractive lens $\Delta\lambda/\lambda$ = 0.001 at 70 keV** | | | | **$f$ = 1 m, 400 $\mu$m aperture kinoform $\Delta\lambda/\lambda$ = 0.00014 at 70 keV** | | | |
|---|---|---|---|---|---|---|---|---|
| | combined (nm) | source demag (nm) | chrom. aberr. (nm) | diffr. limit (nm) | combined (nm) | source demag (nm) | chrom. aberr. (nm) | diffr. limit (nm) |
| E, 180 m vert. | 209 (281) | 99 (212) | 152 | 104 | 77 (121) | 49 (106) | 56 | 20 |
| E, 180 m horiz. | 432 (396) | 391 (350) | | | 203 (184) | 194 (174) | | |
| D, 70 m vert. | 319 (587) | 259 (556) | 154 | | 141 (281) | 128 (274) | 57 | |
| D, 70 m horiz. | 1041 (936) | 1024 (917) | | | 508 (456) | 504 (452) | | |

### 4-4.6.4 Optics Specifications

**High-Heat Load Slits (S1)** Slits S1 have been designed (Doc. A300-SL0200). They offer a maximum opening aperture of 2 x 2 $mm^2$, which is more than sufficient to pass the full central cone at x-ray energies, with the size-broadening from the electron beam chromaticity in the MBA lattice (Figure 4.21).

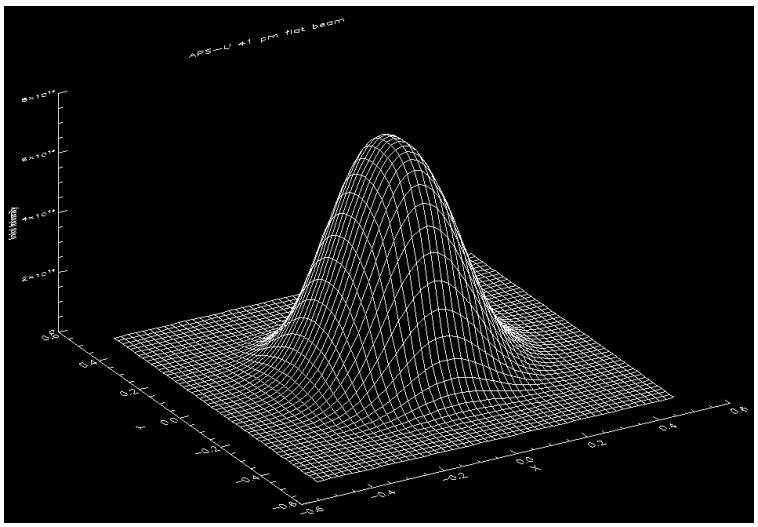


*Figure 4.21. 70 keV undulator central cone at 29 m over a 1 x 1 $mm^2$ area for the brightness mode.*

**High-Heat-Load Filters (F1)** The fixed/static set of filters F1 should withstand the maximum power load passed by the HHLFE and S1 slits, and subject the monochromator M1 to a reduced thermal load of $< 60$ W deposited (photo-electrons and Compton recoil electrons) into a 2.5 mm thick Si crystal, to permit cryogenic ($LN_2$) cooling that will sufficiently mitigate perturbation of the source phase-space. The thermal load reduction requirements onto M1 should be achieved with minimal sacrifice at energies $> 35$ keV, but can assume slits S1 operating at 0.6 x 0.6 $mm^2$, which is just enough to pass the central radiation cone. A sequence of diamond and Si filters is planned (Table 5), sharing the same vacuum tank and stand (SP-1) as the L1 optics.

**White Beam Refractive Lenses (L1 Optics)** The diamond CRLs comprising the L1 optics are currently under R&D (outside of APS-U scope) in a collaboration between APS and external companies. The detailed mounts and cooling design will be completed when the R&D reaches a more mature phase. Changing the number of CRL elements will be achieved by manual access. The L1 optics mechanics specifications are described in Table 6. These optics will share the same tank and stand (SP-1) as the F1 filters.

**High-Heat-Load Bent Double-Laue Monochromator (M1)** The monochromator will consist of two bent Laue crystals in a sequential/nested inverse-Cauchois configuration (i.e., Rowland geometry with Laue crystals) with respect to the source, with parameters given in Table 8. A

monochromator of this type has already been in operation at the APS-1-ID high-energy x-ray beamline. It has the feature of phase-space compensation, wherein the 2nd crystal corrects the phase space distortion incurred by the 1st crystal. However, to further mitigate possible perturbation of the vertical emittance provided by the MBA lattice, particularly in the brightness mode, the planned monochromator will diffract in the horizontal plane. In routine operation, M1 would not be exposed to an S1 aperture larger than 0.6 x 0.6 $mm^2$. The associated vacuum tank and support are considered part of M1, with requirements given in Table 9.

**High-Resolution-Monochromator (M2)** The four-reflection high-resolution monochromator system will provide energy resolution at two levels. One will be at $\delta E/E \sim 10^{-4}$ for vff-HEDM applications, very similar to the one that has been operating in APS-1-ID. The other will be at $10^{-5}$ – $10^{-6}$ for BCDI. Conversion to the higher energy resolution will be accomplished by replacing two sets of parallel-crystal-pairs on weak-link flexure plates from low-order to high-order reflections. Apertures are needed after the 2nd and 4th reflections to mask out spurious beams.

It might be possible to incorporate both the vff-HEDM and BCDI crystals into a single flexure assembly, reducing the flexure number from 4 to 2, thereby avoiding mechanical changeovers. This would entail side-by-side crystal mounts with different surface heights to accommodate both the energy ranges within the travel of the M-SDS positioners. Monolithic Si side-by-side crystals could address the problem of preserving the tilt alignment between the two high-resolution modes.

**Monochromatic Attenuators and Foils (F2, F3)** The mechanism for actuating the monochromatic attenuators and foil are already designed, with prototypes that have been in operation at APS 1-ID. The attenuators (F2) are for flux reduction under experimental or optical alignment configurations, to avoid detector saturation or damage. The elemental foils (F3) are for x-ray beam energy calibration and drift monitoring. They are operated by rotating a wheel to bring in the desired attenuator or foil into (or out of) the beam. The 3 wheels can be positioned so that the total Z-space taken is not 3 times the length of one assembly, but far less—for example, by placing two of them with their shafts parallel on either side of the beam (separated in X), and the third with its shaft parallel to but above the beam.

**Monochromatic Focusing Optics (L2, L3, L4, L5, L6, L7 Optics)** The monochromatic focusing refractive optics will entail saw-tooth lenses, kinoforms, CRLs, and zone plates (Table 12), currently under R&D (outside of APS-U scope, e.g., through separate DOE funding, APS operations funding, and in collaboration with external companies). However, the stacks of motion stages for these optics are fully designed up to the kinematic mounts that will hold the optical element, permitting flexible interchanges.

The number of stage stacks for the different focusing systems is given in Table 4.31. Short-focal-length two-dimensional focusing with saw-tooth refractive lenses requires four stage stacks.

**Monochromatic Slits (S2, S3, S4, S5, S6, S8)** Monochromatic slits will be on stage stacks of two varieties, those with motorized rotations, and those with manual rotations. Rotations are

*Table 4.31. Number of stage stacks for the monochromatic focusing systems.*

| Focusing Optics | Number of stage stacks |
|---|---|
| L2, 3, 5, 7 | 2 |
| L4, 6 | 4 |

desired to precisely orient the overall slit assembly with respect to the beam. These are expected to be a one-time adjustment, making manual operation sufficient. However, for S3 and S4, motorization for very precise remote adjustability is desirable, as these slits might be used to define secondary virtual-source apertures for focal spot stability or for transverse coherence tuning in focal spot for BCDI.

**Portable End-Station White Beam Slits (S7)** This portable set of slits is intended to be installed temporarily in the D or E end-station, on support SP-7 or SP-9, respectively, as the final aperture for white beam experiments using a full undulator harmonic focused by the L1 optics (broadband focusing). They will be subject to less power than the S1 slits for various reasons, such as the beam having passed through the F1 filters and the typically reduced aperture of the S1 slits to no more than 0.6 x 0.6 $mm^2$. However, S7 could experience elevated power density due to the broadband focusing, with the worst case being that of 27 keV focused into the D station.

### 4-4.6.5 Heat Load Considerations

The optical components subject to thermal loads are the white beam slits S1, filters F1, diamond refractive optics L1, the monochromator M2, and the portable white beam slits S7. The white beam slits S1, located right after the HHLFE, have been designed to handle the power load. Routine beamline operation will entail using S1 with an aperture no larger than 0.6 x 0.6 $mm^2$, which is sufficient to pass the full undulator radiation central cone. The filters F1 (4-4.6.4) need to be able to withstand larger beams, up to 1 x 1 $mm^2$, with less than 100 W power dissipation conditions per filter element, and together having higher than 85% transmission at 40 keV. Under 0.6 x 0.6 $mm^2$ conditions they should reduce the power load onto the monochromator M1 such that a 2.5 mm thick Si crystal will need no more than 55 W dissipated through cryogenic cooling (4-4.6.4). A beam stop, part of M1, will have to stop the white beam after the $1^{st}$ crystal. The L1 optics (4-4.6.4), still under R&D for focusing performance, will be designed for thermal management at a later stage. The slits S7 (4-4.6.4), although not receiving high power, might be exposed to a significant power density due to their use near broadband focal spots in the end stations.

A detailed description of the HEXM optics can be found in the HEXM 20-ID Optics ESD (ICMS Content ID: APSU_2030437).

## 4-4.7 Instrument Overview

### 4-4.7.1 Scientific Scope

The HEXM 20-ID-D and 20-ID-E end station instruments will enable world-leading high-energy x-ray imaging capabilities, using both direct- and diffracted-beam x-rays. A key overarching feature

is the ability to zoom-in and zoom-out of materials for multi-scale investigations using penetrating high-energy x-rays. The 20-ID-D instrument will be located as far downstream as possible inside the experimental hall, while 20-ID-E will be outside of the APS experimental floor, as one of the two long beamlines at the APS. Highlights of the instruments include:

- Delivery of both white beam and monochromatic high-energy x-rays between 35-120 keV using a superconducting undulator, with beamsizes ranging from sub-micron to several mm.
- Direct-beam imaging capabilities will include radiography/tomography (largest field-of-view) and transmission x-ray microscopy (highest resolution).
- Diffraction-based imaging capabilities will include high-energy diffraction microscopy (largest field of view) and coherent diffraction imaging (highest resolution).
- The instrument will be configured to allow straightforward switching between these imaging modalities.
- The end-stations will be configured with multiple sample-manipulation systems, to allow for switching between experiments requiring the highest resolutions and those requiring more bulky in-situ 'extreme' environments, such as large mechanical loads, temperatures and the like.
- The 20-ID-E instrument will be located adjacent to a planned Activated Materials Laboratory (AML), which is outside the APS-U scope, to enable studies of activated materials at the beamline.
- More information about the scientific scope and purpose of the HEXM beamline can be found in the FRED HEXM document.

### 4-4.7.2 Instrument Definitions

The HEXM 20-ID-D and 20-ID-E instruments are defined as a combination of the following components and sited in the 20-ID-D and 20-ID-E end-stations, respectively:

- Sample configuration, including stages and sample environment.
- Optical configuration, including optical stages and optical elements both before and after sample.
- Detectors and supporting motion systems for diffraction and direct-space imaging measurements.
- Metrology for monitoring sample, optic and detector motions.
- All connected auxiliary hardware such as cables, motor drivers, utilities, etc.

### 4-4.7.3 HEXM 20-ID-D and 20-ID-E Design Scope

The 20-ID-D and 20-ID-E instruments will be comprised almost exclusively of newly designed and purchased components. The instruments will enable the scientific scope outlined in several documents including the HEXM white-paper.

**Instrument Locations** The instruments shall reside in the 20-ID-D and 20-ID-E end-stations. Details and descriptions of these locations can be found in the HEXM 20-ID Photon delivery system ESD (ICMS Content ID: APSU_2012713).

**Experimental Techniques – 20-ID-D** The following techniques will be supported at 20-ID-D:

1. Wide-angle x-ray scattering (white/mono)
2. Small-angle x-ray scattering (white/mono)
3. Full-field imaging (white/mono)

**Experimental Techniques – 20-ID-E** The following x-ray techniques will be supported at 20-ID-E:

1. Wide-angle x-ray scattering (white/mono)
2. High-energy diffraction microscopy (mono) – Near-field, far-field, coherence-enhanced
3. Small-angle x-ray scattering (white/mono)
4. Full-field imaging (white/mono)
5. Transmission x-ray microscopy (mono)

A detailed description of the HEXM Endstation instrument can be found in the 20-ID HEXM Endstation Instrumentation ESD (ICMS Content ID: APSU_2030616).

## 4-5 XPCS 8-ID

### 4-5.1 Introduction

X-ray photon correlation spectroscopy (XPCS) characterizes fluctuations in condensed matter at a combination of mesoscale length scales and timescales not otherwise accessible. Signal strengths depend on the x-ray beam coherence and minimum accessible time scales inversely with the square of the source brilliance – so it is clear that XPCS will benefit tremendously from APS-U. In this document, we describe the functional requirements for a beamline facility fully dedicated to state-of-the-art wide and small-angle XPCS (WA-XPCS and SA-XPCS, respectively) that fully leverages the outstanding gains in brilliance, B, provided by APS-U. Using WA-XPCS, the beamline will advance studies in a host of key areas in physics and materials science and engineering that include dynamic heterogeneity, structural dynamics in super-cooled liquids and fluctuations associated with competing mesoscale interactions in emergent materials. Using SA-XPCS, the beamline will enable dynamics-related studies in areas as diverse as in situ rheometry, nano-fluidic flow, and high pressure that will significantly impact key problems in soft matter and advance their potential applications in technologies across an array of sectors, from energy and transportation to health, agriculture, and national defense. Features of the beamline include uniquely high time-averaged coherent flux, access to time delays as short as 100 ns and access to higher coherent flux at energies up to ~ 25 keV for penetration into diverse samples.

### 4-5.2 Scientific Objective

Understanding, and ultimately controlling, matter increasingly requires measurements of not only time-averaged or instantaneous properties, but also dynamic behavior. This exact theme has been articulated in the most recent version of the DOE Grand Challenges document entitled Challenges at the Frontiers of Matter and Energy [12], that states:

> "Many real materials are inherently heterogeneous across spatial and temporal scales, as evidenced by their compositional, spatial/structural, and temporal fluctuations and disorder. .... Yet we often have considered materials in idealized, 'frozen' states or as represented by their spatially or temporally averaged structures. These overly simplistic models do not capture the nuances of structure and dynamics that often drive desired functional behavior."

Photon correlation spectroscopy (PCS) provides exactly this information by characterizing fluctuations in condensed matter across a broad range of length and time scales while x-ray scattering provides sensitivity to order and motion at scales spanning the mesoscale to the atomic scale. A general subset of the areas of scientific investigation that will be pursued at the beamline include the role of fluctuations and dynamic heterogeneity in the properties of phase-change materials, understanding structural relaxations in super-cooled liquids and their connection to glass formation, the effect of interfaces and confinement on nanoparticle dynamics, and the connection between dynamics and relaxation of shear-thinned and shear-thickened states. In the following two paragraphs, we provide, first, a little more detail on a specific area of investigation that will be enabled by SA-XPCS and, second, by WA-XPCS.

The properties of surface-active species at or near liquid-liquid and liquid-solid interfaces have considerable technical and scientific importance [13, 14, 15]. Typically, these systems involve the assembly and ordering of monolayers or sub-monolayers that are buried between two fluids or between a fluid and solid, making characterization of their structure and dynamics intrinsically difficult [16]. One area of specific investigation in interfacial science concerns nanoparticle ordering and assembly at fluid-fluid interfaces [13, 17, 18]. While considerable information about micrometer-scale colloids at fluid-fluid interfaces has been obtained by confocal microscopy [19], the energy scales of adsorption and the interactions of nanoparticles at fluid interfaces are much smaller, making their behavior fundamentally different. In the small-angle scattering geometry, the XPCS beamline's small, bright, coherent, high-energy beams will provide detailed understanding of these interfacial phenomena as well as the nature of other nanoscale interfacial processes important for applications such as the use of surfactant-based solvent extraction methods to clear toxic metals and other impurities from water [14], drug delivery, and enhanced energy-storage capacity of nascent flow-cell batteries.

Amorphous metal alloys are diverse and technologically relevant materials that are also rich areas for fundamental study using WA-XPCS at the APS-U. Bulk metallic glasses (BMGs) are an important class of materials in this family [20, 21, 22, 23]. BMGs are relatively new members of the glass family – solid-like materials with liquid-like order – and have emerged as particularly exciting materials because they display many of the outstanding physical properties such as high elasticity, hardness, fracture toughness, and corrosion resistance found in other amorphous metals, but with many advantages over both more traditional "splat" glasses or regular (semi-crystalline) metal alloys. Many aspects of BMGs and metallic glasses, however, remain poorly understood and hinder rational design and control of their characteristics. These include such questions as the local atomic structure of BMGs, the physical mechanisms for BMG formation, and the correlation between – so-called $\alpha$ relaxations and glass forming ability [24]. Questions like these are well suited to investigations at the proposed XPCS beamline, but are currently impossible because of limited coherent flux. Moreover, the "zoom" focusing capability of the WA-XPCS station will provide optimizable sensitivity to motion at across a span of relevant length (and time) scales.

### 4-5.3 XPCS Beamline Insertion Devices (IDs)

The XPCS beamline will require the highest brilliance over its energy range of 8-25 keV. The source will be two inline revolver undulators (total length of 4.6 m) with period lengths of 21 mm and 25 mm (two different periods for each revolver).

*Table 4.32. Source Parameters for XPCS beamline*

| Undulator | Period [mm] | Length [m] | Location | Max Power |
|---|---|---|---|---|
| Revolver | 21/25 | 4.6 | Center of Straight Section | 2.0/2.2 kW[1] |

[1] Through the Front End Mask 2x2 $mm^2$ @ 25.4 m with the undulator U21 Ky = 1.287 and U25 Ky = 1.902.

### 4-5.4 XPCS Beamline Front End

The XPCS beamline will utilize the new standard MBA High Heat-Load front end capable of handling a maximum power of 21 kW. The beamline will have a windowless exit configuration with

a 2 mm x 2 mm (H x V) exit mask aperture.

A detailed description of the XPCS Front End and Insertion devices can be found in the APS-U 8-ID Beamline Front End and Insertion Devices Interface Control Document (ICMS Content ID: APSU_190936).

### 4-5.5 Beamline Layout

The XPCS beamline geometry is an inline tandem ID. The XPCS beamline is a facility fully dedicated to state-of-the-art WA-XPCS and SA-XPCS that fully leverages the outstanding gains in brilliance provided by APS-U.

The wide-angle (diffraction) XPCS experiments will be performed in the 8-ID-E end station. This enclosure will be compatible with pink and monochromatic x-ray beams and will operate over the energy range of 8 - 25 keV.

The small- and medium-angle regime XPCS experiments will be performed in the 8-ID-I end station. This enclosure will be compatible with pink and monochromatic x-ray beams and will operate over the energy range of 8 - 25 keV.

The 8-ID-E and 8-ID-I end stations will operate one at a time. The layout of the XPCS beamline is shown in Figure 4.22.

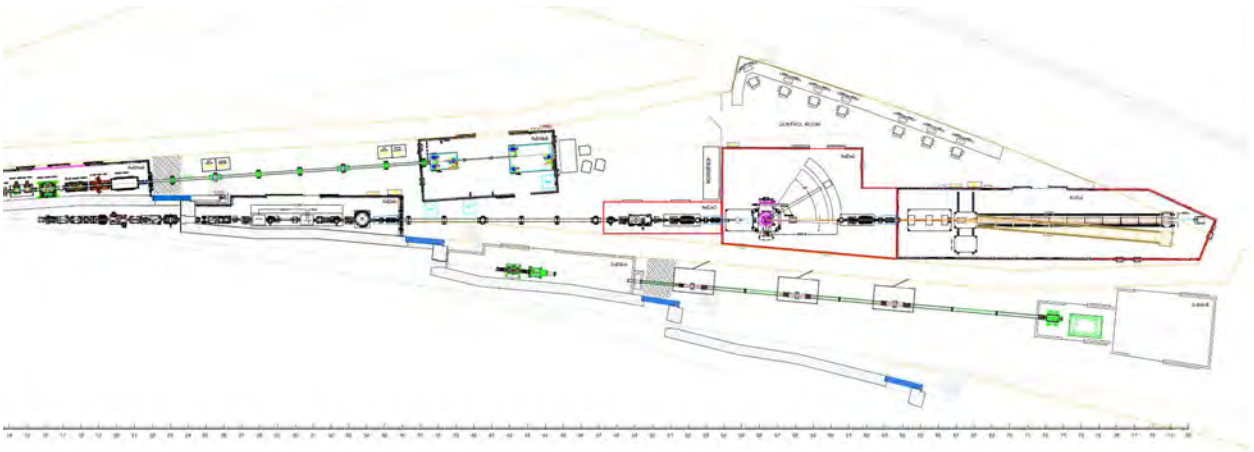

*Figure 4.22. Layout of XPCS beamline*

#### 4-5.5.1 Beamline Component Table

The following table shows all major beamline components. For a complete list of components, see the layout drawing bill of materials.

A detailed description of the XPCS beamline can be found in the XPCS 8-ID Photon Delivery System ESD (ICMS Content ID: APSU_2012710).

*Table 4.33. XPCS list of beamline components.*

| Distance from source (m) | Component | Description/Comments |
|---|---|---|
| 25.4 | FE Exit Mask | Standard HHL Front-End exit mask. 2 mm x 2 mm aperture |
| 26.1 | FE Collimator | Standard HHL Front-End Exit Collimator; 5 mm x 5 mm aperture |
| 27.1 | Slits, HHL | HHL WB Slits w/ Tungsten Edge inserts, 8ID-SL-1 |
| 28.0 | Mirror | Mirror, Horizontal, Flat, 8ID-MR-1 |
| 28.6 | Diagnostics | Diagnostics, WB/PB, 8ID-BD-1 |
| 30.0 | Mask | Mask, WB Stop, 8ID-PM-1 |
| 30.6 | Mirror | Mirror, Horizontal, Focusing, 8ID-MR-2 |
| 31.4 | Collimator | Collimator, Secondary, 8ID-SC-1 |
| 31.8 | Mask | PB Mask, PB Stop, 8ID-PM-2 |
| 32.1 | Collimator | Collimator, 8ID-BC-1 |
| 32.4 | Diagnostics | Diagnostics, WB/PB, 8ID-BD-2 |
| 32.9 | Slits | Slits, PB, H+V, 8ID-SL-2 |
| 33.7 | Monochromator | Monochromator, Horizontal, DCM, 8ID-MN-1, 8ID-MN-2 |
| 34.4 | Mask | Mode Switch Mask, 8ID-PM-3 |
| 35.0 | Shutter | Shutter, Pink, 8ID-SH-1 |
| 35.6 | Collimator | Collimator, Secondary, 8ID-SC-2 |
| 36.0 – 47.0 | Shielded Transport | Shielded Transport, 8ID-ST-1, 8ID-ST-2 |
| 47.5 | Diagnostics | Diagnostics, PB, 8ID-BD-3 |
| 48.1 | PB Slits | Slits, PB, H+V, 8ID-SL-3 |
| 49.0 | Monochromator | Monochromator, DMM, 8ID-MN-3; 4; 5 |
| 51.0 | Mask | Mode Switch Mask, 8ID-PM-4 |
| 51.3 | Slits | Slits, PB, H+V, 8ID-SL-4 |
| 52.0 | Transfocator | Transfocator / CRL-1, 8ID-TR-1 |
| 52.5 | Diagnostics | Diagnostics, PB, 8ID-BD-4 |
| 53.2 | Shutter | Shutter, Pink, 8ID-SH-2 |
| 54.8 | Slits | Slits, MB, H+V, 8ID-SL-5 |
| 55.3 | Mirror | Mirror, Kirkpatrick-Baez bendable, 8ID-MR-3 |
| 55.7 | Window | Window, Be, 8ID-WN-1 |
| 55.9 | MB Slits | Slits, MB, H+V, 8ID-SL-6 |
| 56.3 | Diffractometer | Diffractometer, 8ID-BI-1 |
| 56.3 | Sample Environment | Sample Environment, 8ID-BI-3 |
| 58.0 | Flight Path | Exit flight path, 8ID-BI-2 |
| 60.0 | Detector | Detectors, 8ID-DT-1 |
| 57.3-61.0 | Transport | Vacuum Pipe, removable, 8ID-VP-2 |
| 61.0 | Diagnostics | Diagnostics, PB, 8ID-BD-5 |
| 61.3 | Slits | Slits, PB, H+V, 8ID-SL-7 |
| 62.3 | Transfocator | Transfocator / CRL-2, 8ID-TR-2 |
| 63.3 | Shutter | Shutter, Pink, 8ID-SH-3 |
| 63.7 | Shielded Transport | Shielded Transport, 8ID-ST-3 |
| 64.5 | Slits | Slits, PB, H+V, 8ID-SL-8 |
| 65.5 | Slits | Slits, PB, H+V, 8ID-SL-9 |
| 66.4 | Slits | Slits, PB, H+V, 8ID-SL-10 |
| 66.6 | Window | Window, Be, 8ID-WN-2 |
| 67.5 | Sample Environment | Sample Environment, 8ID- BI -6 |
| 67.5 | Motion System | Motion System, 8ID- BI -4 |
| 68.0 | Flight Path | Adjustable Flight Path, 8ID-BI-5 |
| 79.0 | Detector | Detectors, 8ID-DT-2 |
| 80.6 | Beam Stop | Beam Stop, PB, 8ID-BS-1 |

## 4-5.6 Optics Overview

### 4-5.6.1 Beam Delivery Specifications

The XPCS beamline will operate over the energy range of 8-25 keV. The beamline will deliver a (partially) coherent beam with variable focal spot sizes to two enclosures, the WA- and SA-XPCS stations. In the WA-XPCS station, the spot size at the sample location (56.5 m) will be tunable from 0.3 to 3 µm with the combination of CRL1 (52 m) and KB mirrors (55.3 m). In the SA-XPCS station, the spot size at the sample location (67.5 m) will be tunable from 3 to 10 µm with the combination of CRL1 (52 m) and CRL2 (62.3 m). The table below shows the expected flux and focal spot sizes of the beamline at 8.8 keV and 23.7 keV. The source parameters are for the brightness mode in the APS-U PDR (APSU_1705610). The optical design and optics specification are listed in this document. The optical layout of the XPCS beamline is shown in Figure 4.23.

*Table 4.34. Expected flux and focal spot sizes of the beamline.*

| | **Energy (keV)** | **Coherent mode size ($\mu$m)** | **Smallest focal spot size ($\mu$m)** | **Flux (ph/s/0.1%BW)** | **Largest focal spot size ($\mu$m)** | **Flux (ph/s/0.1%BW)** |
|---|---|---|---|---|---|---|
| WA-XPCS | 8.8 | 1 | 0.4x0.3 | $1.6x10^{13}$ | 6.2x2.6 | $1.5x10^{13}$ |
| WA-XPCS | 8.8 | 10 | 0.2x0.3 | $6.9x10^{13}$ | 4.1x3.3 | $8.7x10^{13}$ |
| WA-XPCS | 23.7 | 1 | 0.4x0.2 | $8.7x10^{11}$ | 5.6x1.6 | $9.1x10^{11}$ |
| WA-XPCS | 23.7 | 10 | 0.2x0.1 | $6.3x10^{12}$ | 2.8x1.6 | $7.0x10^{12}$ |
| SA-XPCS | 8.8 | 1 | 5.6x4.0 | $1.7x10^{13}$ | 22x11 | $1.7x10^{13}$ |
| SA-XPCS | 8.8 | 10 | 3.0x1.5 | $9.6x10^{13}$ | 19x21 | $1.1x10^{14}$ |
| SA-XPCS | 23.7 | 1 | 5.2x1.8 | $1.2x10^{12}$ | 18x5.2 | $1.2x10^{12}$ |
| SA-XPCS | 23.7 | 10 | 2.6x1.1 | $8.2x10^{12}$ | 10x6.7 | $8.9x10^{12}$ |

### 4-5.6.2 Detailed Optical Layout

### 4-5.6.3 Optical Simulation and Tolerances

Optical simulations were carried out using the ShadowOui program in the Oasys environment. The zoom focusing capability of the SA-XPCS and WA-XPCS stations is shown in Figure 4.24.

The figure error on the KB mirrors is the most important optical parameter that affects the focal spot size. Figure 4.25 shows the calculated RMS focal size and relative peak intensity as a function of the RMS figure height errors. To keep both the focal size broadening and the peak intensity drop by less than 10%, the RMS figure error has to be smaller than 1.5 nm and 1.0 nm for KB(h) and KB(v), respectively.

### 4-5.6.4 Optics Specifications

**HHL Mirrors** Two horizontally deflecting mirrors will comprise the first optical components of the XPCS beamline. They will be located in enclosure A and operate at a reflection angle of 3.0 mrad. Both mirrors will be flat with the notch design to reduce the thermal induced deformation. A mechanical or thermal bending mechanism may be required for the second mirror to correct wavefront distortions created by the first mirror or the DCM (downstream). The mirrors will each have four reflecting stripes (bare Si, Cr, Rh, and Pt) to provide harmonic rejection over the

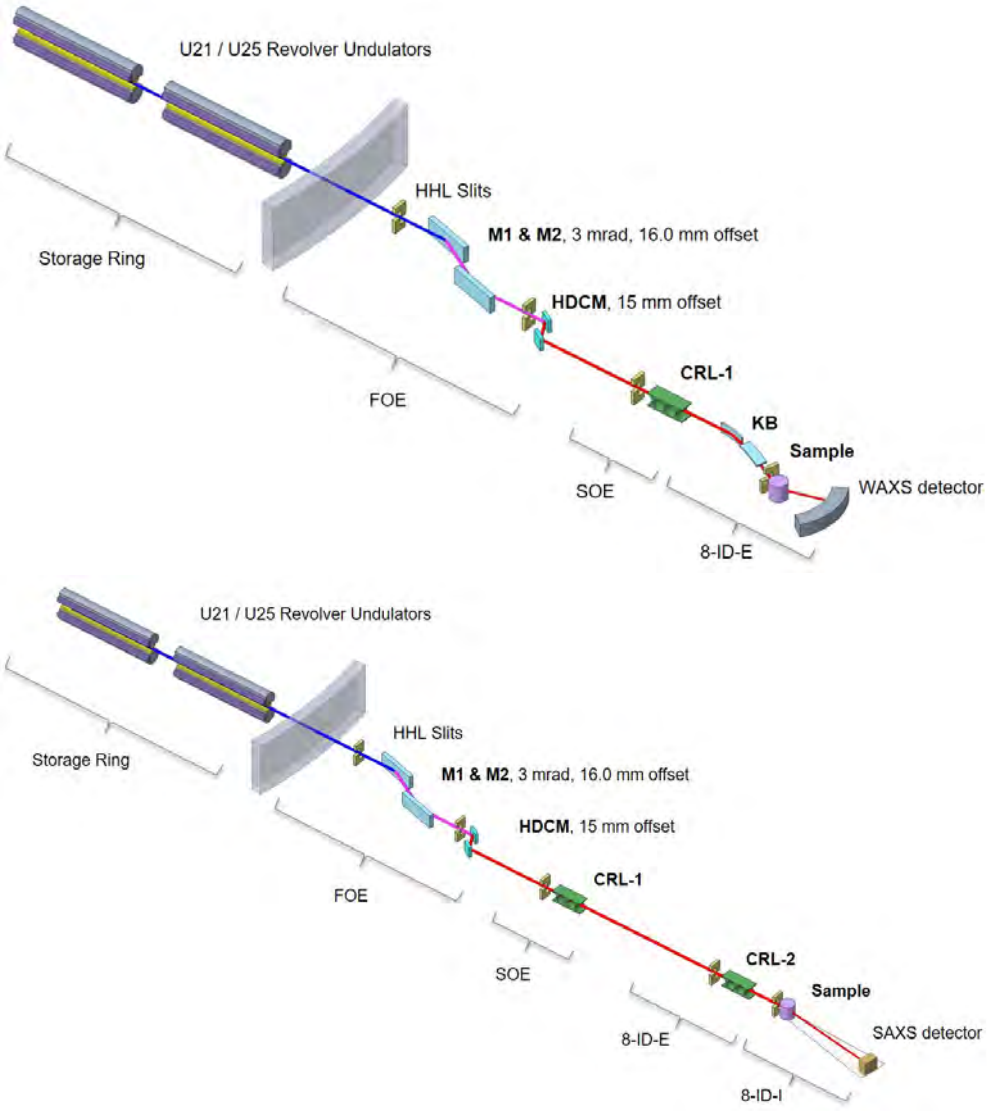


*Figure 4.23. Basic optical layout of the WA-XPCS (top) and SA-XPCS (bottom) beamline. M1 and M2 are high heat load HHL mirrors, HDCM is a horizontally deflecting double-crystal monochromator, CRLs are the compound refractive lenses and a Kirtpatrick-Baez (KB) mirror pair.*

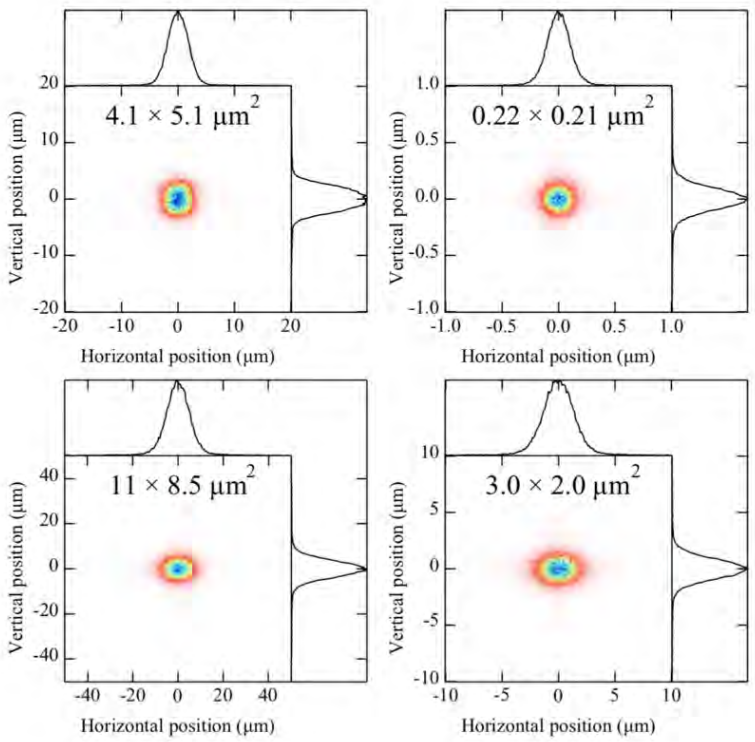


*Figure 4.24. Largest (left) and smallest (right) focal spot at the sample location for (top) the WA-XPCS setup (56.3 m) and (bottom) the SA-XPCS setup (67.5 m). The sizes shown in the figure are the FWHMs. The calculation was performed at 14.2 keV in the 3.2(H)x3.2(V) coherence modes.*

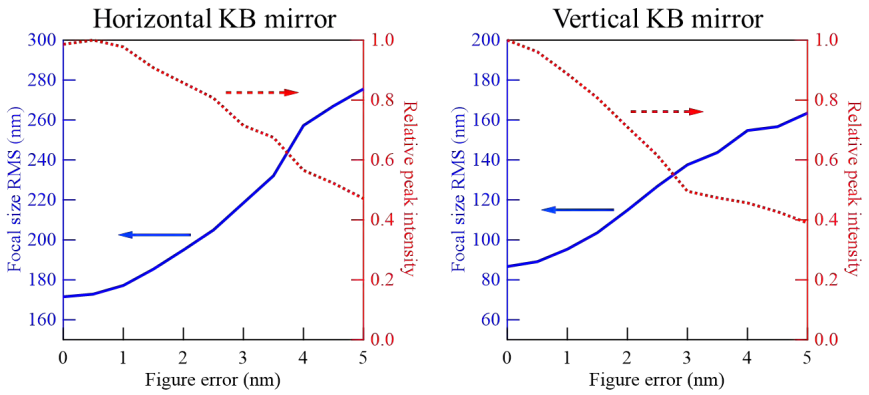


*Figure 4.25. Effects of KB mirror figure errors on the focal spot.*

operational energy range. Vertical translations are required to change the reflecting stripes used.

**HHL Double Crystal Monochromator/Multilayer** The HDCM is a standard Si(111) and Si(113) double-crystal monochromator with liquid-nitrogen cooled crystals, and fixed exit operation. The HDCM will require precision positioners with typical specifications given in the table below. It will also require closed loop (encoder) feedback of position and diagnostics such as capacitive sensors and interferometers for determining the crystal gap and stage vibrations.

**Transfocators** Variable numbers and types (radii) of CRLs are required to achieve the focusing requirements for the XPCS beamline. In the two beamline locations where CRLs are specified, a so-called transfocator is the device selected for achieving this. Requirements for the transfocator are UHV compatibility, x/y/z translations, and pitch/yaw rotations, water cooling of the lens stack for pink-beam compatibility and the ability to precisely remove and insert variable numbers of lenses. The arrangement of individual lenses of both the 8ID-TR-1 and 8ID-TR-2 transfocator systems can be the same are shown in the table below.

*Table 4.35. Arrangement of individual lens for end stations*

| **Stack** | **1** | **2** | **3** | **4** | **5** | **6** | **7** | **8** | **9** | **10** | **11** | **12** |
|---|---|---|---|---|---|---|---|---|---|---|---|---|
| Type | 2D | 2D | 2D | 2D | 2D | 2D | 2D | 2D | 2D | 1D | 1D | 1D |
| $N$ | 1 | 1 | 1 | 1 | 1 | 2 | 4 | 8 | 8 | 1 | 2 | 4 |
| $R$, µm | 1000 | 500 | 300 | 200 | 100 | 100 | 100 | 100 | 100 | 1000 | 1000 | 1000 |

**Experimental Station KB Mirror System** The KB mirrors will be located in the end-station E and operate at a reflection angle of 2.5 mrad. Both mirrors will be bendable flat mirrors with Pt coating. The vertical KB (horizontal KB) mirror located 500 mm (350 mm) upstream of the sample location focuses the beam vertically (horizontally).

### 4-5.6.5 Heat Load Considerations

The HHL mirrors (M1 and M2) will reduce the power passed on to the downstream optics. Tables below summarize the maximum powers expected to be absorbed by various components with the closed gap U21 and U25 undulator.

*Table 4.36. Power Calculations for M1 and M2.*

| **Und** | **K** | **Mono Energy (keV)** | **Incident power on M1* (W)** | **Power absorbed by M1 (W)** | **Power Density on M1 (W/mm$^2$)** | **Power absorbed by M2 (Watts)** | **Power Density on M2 (W/mm$^2$)** |
|---|---|---|---|---|---|---|---|
| U21 | 1.305 | 8.8 (1$^{st}$) | 552 | 370 | 1.0 | 10 | 0.024 |
| U25 | 1.939 | 14.2 (3$^{rd}$) | 591 | 425 | 1.1 | 18 | 0.055 |

* Based on the mirror acceptance of 1.08 x1.08 mm$^2$.

*Table 4.37. Power Calculations for HDCM.*

| Und | K | Mono Energy (keV) | 1st crystal Angle | Beam Size at Mono (HxV) (mm x mm) | Beam Footprint (HxV) (mm x mm) | Power absorbed (W) | Power Density ($W/mm^2$) |
|---|---|---|---|---|---|---|---|
| U21 | 1.305 | 8.8 ($1^{st}$) | 13.0° | 1.2 x 1.3 | 5.1 x 1.3 | 155 | 25 |
| U25 | 1.939 | 14.2 ($3^{rd}$) | 8.0° | 1.2 x 1.3 | 8.3 x 1.3 | 132 | 13 |

The HHL mirror deformation can be reduced by an order of magnitude by adding a notch to the mirror side. The HDCM deformation is minimized by optimizing the LN2 cooling. Figure 4.26 shows the smallest focal spot at the sample location (56.4 m) for the XPCS-WA setup with and without thermal induced deformations on HHL mirrors and HDCM. The broadening on the focal spot is within the tolerance. The zoom CRL-KB system can also be used to improve the focus.

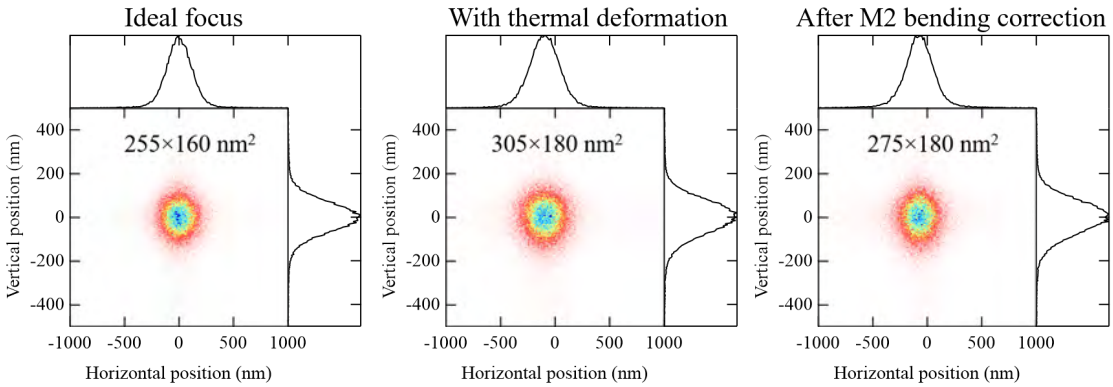


*Figure 4.26. Beam profile (with FHWM sizes) at the sample location without (left) and with (middle) thermal deformations on all HHL mirrors and HDCM, and with bending correction on M2 (right) at 14.2 keV.*

A detailed description of the XPCS optics can be found in the XPCS 8-ID Optics ESD (ICMS Content ID: APSU_2030434).

## 4-5.7 Instrument Overview 8-ID-E

### 4-5.7.1 Scientific Scope

The 8-ID-E hutch at the XPCS beamline will have a dedicated instrument for performing Wide Angle X-ray Photon Correlation Spectroscopy (WA-XPCS) measurements across a range of length and time scales. The engineering requirements for this instrument are described below.

### 4-5.7.2 Instrument Definition

The 8-ID-E WA-XPCS instrument includes the principle diffractometer, a Long Distance Detector Positioner (LDDP), a flight path assembly, sample environment modules, an upstream optical table

and detectors. A schematic of the instrument is shown in Figure 4.27.

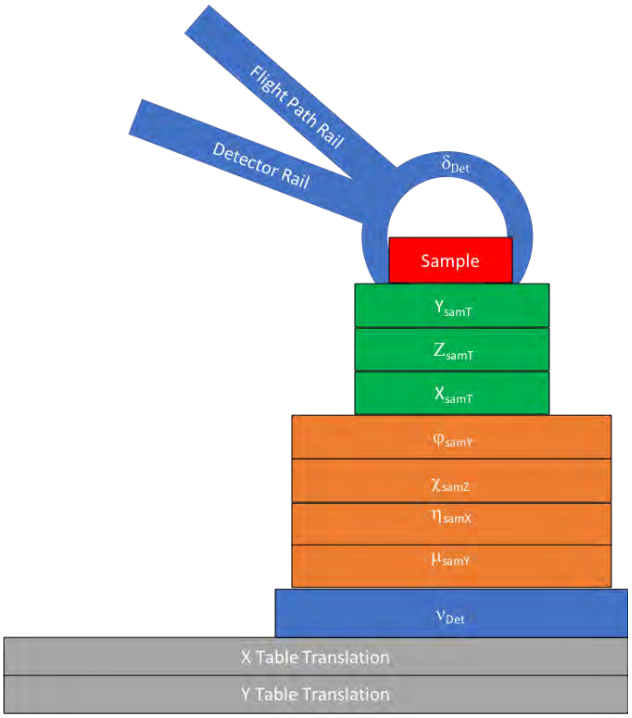


*Figure 4.27. Conceptual schematic of 8-ID-E diffractometer.*

### 4-5.7.3 Instrument Location

The dedicated WA-XPCS instrument will be located in the 8-ID-E hutch of the XPCS beamline as indicated in Figure 4.28.


*Figure 4.28. 8-ID hutch layout. The 8-ID-E hutch is enclosed by the green dashed box.*

**Instrument Operating Modes** The instrument will have three operating modes:

- **WA-XPCS mode:** In this mode, beam will be delivered to the WA-XPCS instrument and experiments will be performed in the 8-ID-E hutch.
- **Beam pass mode:** In this mode, beam will be delivered through the 8-ID-E hutch to the 8-ID-I hutch for SA-XPCS measurements. This mode requires that the WA-XPCS instrument have sufficient space and range of motion such that a beampipe can be easily installed to

transport beam to the 8-ID-I hutch. This mode must be compatible with pink beam or mono beam illumination. The ability to transmit pink beam to the 8-ID-I hutch in beam-pass mode requires that all windows in the 8-ID-E hutch be able to withstand the full flux of the pink beam. In many cases this will require water cooling. Any windows that serve as an interface between vacuum and gas environments require an $N_2$ purge to minimize damage and deposition on the windows.

- **Pinhole U-SAXS Mode:** In this mode, samples will be located in the 8-ID-E hutch and positioned with the 8-ID-E instrument but the detector will be located in the 8-ID-I hutch. The specifications for the sample positioning requirements of this mode are contained in this ESD. The detector and detector positioning requirements for this mode are contained in the 8-ID-I endstation instrumentation ESD.

**Experimental Methods** There will be three configurations in which WA-XPCS alignment and measurements will be performed:

- **Short sample-to-detector WA-XPCS:** In this configuration, the detector in use will be positioned on the diffractometer detector arm at a sample-to-detector distance of 1.5-2m.
- **Long sample to detector WA-XPCS:** In this configuration, the detector in use will be positioned using the LDDP at a sample-to-detector distance of up to 4m.
- **Pinhole U-SAXS:** In this configuration, the detector will be positioned in the 8-ID-I hutch with a sample to detector distance of up to ~22 m.

A detailed description of the XPCS 8-ID-E instrument can be found in the XPCS 8-ID-E endstation instrumentation ESD (ICMS Content ID: APSU_2030643).

### 4-5.8 Instrument Overview 8-ID-I

#### 4-5.8.1 Scientific Scope

The 8-ID-I hutch at the XPCS beamline will have a dedicated instrument for performing Small Angle X-ray Photon Correlation Spectroscopy (SA-XPCS) and pinhole Ultra-Small Angle X-ray scattering (U-SAXS) measurements across a range of length and time scales.

#### 4-5.8.2 Instrument Definition

The 8-ID-I instrument includes an upstream optical table with beam conditioning optics, a mobile support table for sample environments, long distance movable flight tube, and x-ray detectors.

#### 4-5.8.3 Instrument Location

The SA-XPCS/U-SAXS instrument will be located in the 8-ID-I hutch of the XPCS beamline as indicated in Figure 4.29.

**Instrument Operating Modes** The instrument will have two operating modes:

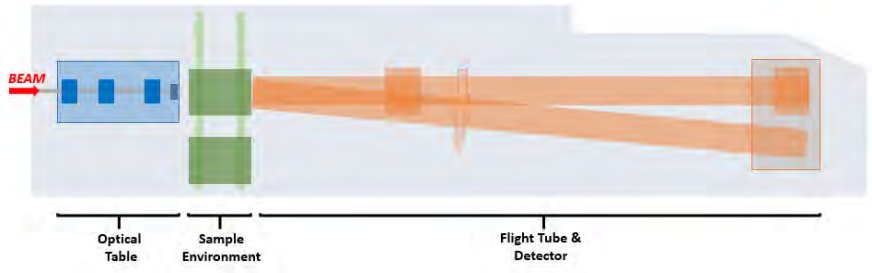


*Figure 4.29. Schematic of 8-ID-I instrument.*

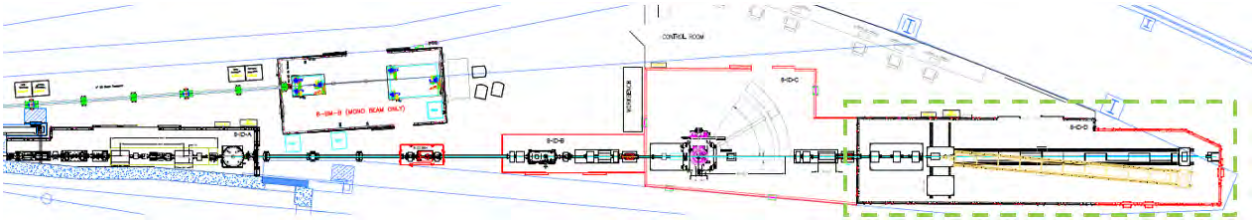

*Figure 4.30. 8-ID hutch layout. The 8-ID-I hutch is enclosed by the green dashed box.*

- **SA-XPCS mode:** In this mode, beam will be delivered to the SA-XPCS instrument and experiments will be performed in the 8-ID-I hutch.
- **Pinhole U-SAXS Mode:** In this mode, samples will be located in the 8-ID-E hutch and positioned with the 8-ID-E instrument but the detector will be located in the 8-ID-I hutch.

A detailed description of the XPCS 8-ID-I instrument can be found in the XPCS 8-ID-I endstation instrumentation ESD (ICMS Content ID: APSU_2030654).

## 4-6 PtychoProbe 33-ID

### 4-6.1 Introduction

The race is on for chemical and structural x-ray imaging with nanoscale resolution. There currently are substantial efforts underway at hard x-ray synchrotron facilities worldwide that aim to improve the spatial resolution and chemical sensitivity of x-ray microscopes. The excitement of the scientific community on the development of these techniques is clearly evident by the ever-growing number of research teams working toward this aim. The PtychoProbe project we describe here is unique, because it will enable the world's first general user program for 5-nm focusing with ultra-fast scanning, facilitated through the APS upgrade. It will give nanoscientists unprecedented capabilities to accelerate the discovery of complex materials and establish the APS as the go-to place for hard x-ray high-resolution microscopy. There is a lot at stake in this competitive landscape. Nevertheless, the PtychoProbe beamline will guarantee U.S. leadership for years to come.

The goal of the PtychoProbe (x-ray fluorescence Nanoprobe + Ptychography) beamline is to realize the highest possible spatial resolution x-ray microscopy both for structural and chemical information. The unprecedented brightness of the APS MBA lattice will be exploited to produce a nm beam of focused hard x-rays to achieve the highest possible sensitivity to trace elements. Ptychography will be used to further improve the spatial resolution for structural components to its ultimate limit. The beamline will enable high-resolution, two- and three-dimensional imaging of thick objects, bridging the resolution gap between contemporary x-ray and electron microscopy. Pushing x-ray microscopy into the nanoscale is crucial for understanding complex hierarchical systems on length scales from atomic up to meso- and macroscales, so as to be applicable to scientific questions ranging from biology to earth and environmental materials science to electrochemistry to catalysis and corrosion and beyond.

The main goal of the PtychoProbe is to realize the highest possible spatial resolution x-ray microscopy of samples, both with structural and chemical information. In order to reach this goal, it sacrifices working distance between optics and sample, and therefore only supports a limited set of *in situ* and *operando* environments. Nevertheless, based of comparable working distances present in electron microscopy or soft x-ray microscopy the PtychoProbe is expected to be able to address important high impact questions as laid out in the science case. The PtychoProbe focusses primarily on attaining the highest spatial resolution for chemical information, *i.e.*, using x-ray fluorescence contrast. This is achieved by using diffractive optics such as either Multilayer-Laue-Lenses (MLLs) or Fresnel zone plates (ZP). This information is supplemented by adding phase and absorption contrast information at spatial resolution beyond the diffraction limit via ptychography. In addition, the instrument will support 'ptychography-poly' mode where much larger sample areas can be scanned rapidly with a comparatively large beam (100 nm - micron sized) and ptychography is used to recover structural detail down to the nm level. Ptychography decouples the microscope's spatial resolution from the focused beam size and extends it to the diffraction limit. Spatial resolution below 10 nm has already been demonstrated using ptychography. With the flux density that is achievable assuming even modest focusing it may be possible to achieve nearly atomic resolution for radiation hard sample. X-ray fluorescence (XRF) offers exquisite sensitivity for measuring elemental concentration. Collecting the photon stimulated secondary fluorescence signal with an energy resolving detector will add elemental contrast complemented by structural contrast from ptychography. Through combination with ptychography, additional improvements in spatial reso-

lution beyond the native XRF elemental maps can be achieved using deconvolution techniques. In addition, the microscope can be operated in spectroscopic mode to yield chemical state contrast (chemical state mapping, by scanning a sample at well-defined incident energies). Assuming the technology matures sufficiently, as seems plausible based on recent results, the PtychoProbe plans to incorporate superconducting spectrometers for emission spectroscopy. The 'holy grail' would be to combine elemental mapping with emission spectroscopy, to fully characterize chemically (elements and speciation) the sample at the 5-nm spatial resolution level.

### 4-6.2 Scientific Objective

Macroscopic material properties like material strength and or carrier mobility are phenomena that result from the complex interaction of constituent elements across many length scales. However, scientific measurements have historically been targeted at investigating a single length scale, often with a single contrast mechanism. Limiting the field of view to just one length scale inhibits discoveries that come more naturally from considering the material system holistically. The PtychoProbe will realize the highest possible spatial resolution hard x-ray nanoprobe to deliver trace elemental mapping with sensitivities down to a few atoms, complemented by structural information via ptychography only limited in its resolution by the radiation hardness of the sample. Additionally, using fast scanning, large areas can be scanned quickly allowing to put the fine-grained information into the coarser scale context.

The multiscale visualization enabled through the PtychoProbe will be utilized to tailor materials for specific applications in energy conversion and storage, catalysis, nano-electronics, and construction. It will also open up new opportunities in several areas of environmental and life sciences.

### 4-6.3 Beamline Requirements for the Insertion Devices (IDs)

The PtychoProbe beamline will operate over the energy range of 5-30 KeV. As a nanoprobe, it will require the highest brilliance possible throughout this range. A revolver undulator of 4.6 m length with two periods (21 mm and 25 mm) is currently planned.

**Table 4** Source parameters

*Table 4.38. Source Parameters*

| **Unduator** | **Period** *(mm)* | **Length** *(m)* | **Location** | **Max Power*** *(kW)* |
|---|---|---|---|---|
| Revolver | 21/25 | 4.6 | Center of straight section | 2.28 |

* Through the Front End Mask 2x2 mm @ 25.4 m with the undulator Ky = 1.939.

### 4-6.4 Beamline Requirements for the Front End

The PtychoProbe beamline will utilize the new standard MBA High Heat-Load front end capable of handling a maximum power of 21 kW. The beamline will a windowless exit configuration with a 2 mm x 2 mm (H x V) exit mask aperture.

A detailed description of the PtychoProbe Front End and Insertion devices can be found in the APS-U 33-ID Beamline Front End and Insertion Devices Interface Control Document (ICMS Content ID: APSU_190961).

### 4-6.5 Beamline Layout

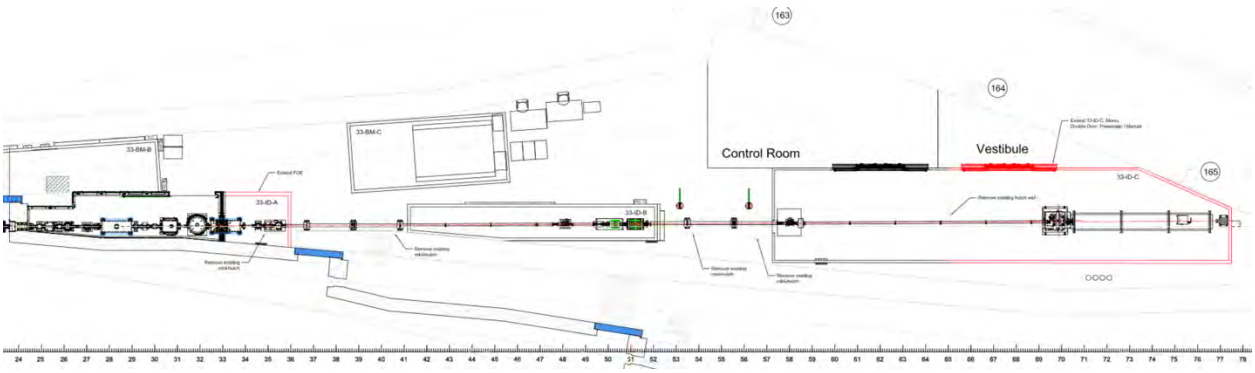


*Figure 4.31. Layout of the PtychoProbe Beamline.*

In order for the PtychoProbe to realize the highest possible spatial resolution in lens-less imaging mode, and to minimize distortion due to drifts in scanning-probe mode, the key requirement is to maximize the amount of coherent photons on the sample per unit time. The design of the PtychoProbe is intended to utilize the unprecedented low emittance of the APS-U storage ring to do exactly that.

#### 4-6.5.1 Beamline Component Table

Table 4.39 shows all major beamline components and their general location along the beamline.

A detailed description of the PtychoProbe beamline can be found in the Ptycoprobe 33-ID ESD (ICMS Content ID: APSU_2012716).

### 4-6.6 Optics Overview

#### 4-6.6.1 Beam Delivery Specifications

The goal of the PtychoProbe beamline is to realize the highest possible spatial-resolution for x-ray microscopy to determine both structural and chemical information. The optical-design calculations and optics specifications for the beamline are listed in this document. The source parameters used are taken from Michael Borland's presentation at the DOE/SC CD-2 Review of the APS Upgrade Project (October 10-12, 2018). Wave-Optics calculations with SRW (Synchrotron Radiation Workshop) software have been performed to compute the coherence length of the radiation at the secondary source aperture (SSA1). Simulations were carried out using the Oasys program environment and executed on parallel-computing resources in the ANL-LCRC cluster (http://www.lcrc.anl.gov). The tables below show results for 10 and 25 keV. The SSA1 is positioned at 48 m for best focus size. In addition, SSA2 at 58 m will allow to tune flux versus resolution if desired in the experiment.

*Table 4.39. List of Ptychoprobe beamline components*

| Distance from source (m) | Component | Designation | Description/Comments |
|---|---|---|---|
| 25.4 | FE Exit Mask | | Standard HHL Front-End exit mask. 2x2 $mm^2$ aperture |
| 26.1 | FE Collimator | | Standard HHL Front-End Exit Collimator 5x5 $mm^2$ aperture |
| 27.0 | HHL WB Slits | 33ID-SL-1 | HHL Variable Aperture Photon Absorber w/ Tungsten Edge inserts |
| 28.3 | Mirror (M1) | 33ID-MR-1 | Horizontal Focusing Mirror |
| 29.2 | Secondary Collimator | 33ID-SC-1 | Lead Secondary Scattering Collimator |
| 29.6 | Photon Mask | 33ID-PM-1 | Pink Beam mis-steering Mask |
| 30.0 | Diagnostic | 33ID-BD-1 | BPM / Fluorescent Flag |
| 30.6 | Monochromator (DCM) | 33ID-MN-1 | Horizontal Double Crystal Monochromator, 1mm offset |
| 31.9 | Monochromator (MLM) | 33ID-MN-2 | Horizontal Multilayer Monochromator, 1mm offset |
| 33.1 | Mirror (M2) | 33ID-MR-2 | Vertical Focusing Mirror |
| 34.6 | Diagnostic | 33ID-BD-2 | BPM / Fluorescent Flag |
| 35.1 | Photon Mask | 33ID-PM-2 | Photon White Beam Stop |
| 35.5 | Bremsstrahlung Collimator | 33ID-BC-1 | Bremsstrahlung Tungsten Beam Stop |
| 35.7-41.5 | Shielded Transport | 33ID-ST-1 | Pink / Mono Shielded Transport |
| 47.9 | Secondary Source Aperture 1 (SSA1) | 33ID-SL-2 | Beam Defining Aperture (Slits) for best focus |
| 49.7 | Photon Mask | 33ID-PM-3 | Pink Beam Mask |
| 50.2 | Shutter | 33ID-SH-1 | Pink Beam Shutter |
| 51.2 | Shutter | 33ID-SH-2 | Tungsten Mono Shutter |
| 51.8-57.5 | Shielded Transport | 33ID-ST-2 | Pink / Mono Shielded Transport |
| 57.8 | Secondary Source Aperture (SSA2) 2 | 33ID-SL-3 | Beam Defining Aperture (Slits) for flux vs resolution |
| 69.7 | Velociprobe / sample stack | 33ID-BI-1 | Granite air bearing manipulator with precision stages |
| 70.0-76.5 | Flight Tube | 33ID-BI-2 | In-vacuum adjustable flight tube |
| 75.3 | Detector | 33ID-DT-1 | Jungfrau / Hitachi ME-4 |
| 77.1 | Beam Stop | 33ID-BS-1 | Pink Beam |

*Table 4.40. Coherence length*

| | Energy (keV) | Value (HxV) |
|---|---|---|
| Coherence Length | 25 | 0.8 x 1.0 µm |
| Coherence Length | 10 | 2.9 x 3.0 µm |

The coherent fraction is determined by the ratio of the Flux at SSA1 with the slits opened to the coherence length given above to the total Flux. The calculation has been performed using both Si(111) and Si(311) DCM reflections.

*Table 4.41. Coherent fraction*

| | Energy (keV) | DCM | Coherent Flux (ph/s) | Total Flux (ph/s) | Value |
|---|---|---|---|---|---|
| Coherent Fraction | 25 | Si(311)<br>Si(111) | $5.5x10^{10}$<br>$2.5x10^{11}$ | $9.4x10^{12}$<br>$4.7x10^{13}$ | 0.54% |
| Coherent Fraction | 10 | Si(311)<br>Si(111) | $7.5x10^{11}$<br>$5.1x10^{12}$ | $1.8x10^{13}$<br>$1.2x10^{14}$ | 4.16% |

The Table 4.42 below shows the expected flux and focal spot sizes for 10 KeV and 25 KeV at the final focus position, for both the DCMs. The (Coherent) Flux at the focus is computed by opening the slits to $\Delta = \frac{z\lambda}{\pi D} = 4.82$ µm ($z$ is the SSA to zone plate distance, $D$ is the diameter of the zone plate).

*Table 4.42. Coherent flux at 10 and 25 keV*

| **Energy** *(KeV)* | **DCM** | **$\delta r_N$** *(nm)* | **D** *(µm)* | **Flux** *(ph/s)* | **Focal spot size RMS (HxV)** | **Focal spot size FWHM* (HxV)** |
|---|---|---|---|---|---|---|
| 25 | Si(311)<br>Si(111) | 4<br>16 | 72<br>72 | $1.1x10^{10}$<br>$5.2x10^{10}$ | 4x4 $nm^2$<br>8x8 $nm^2$ | 5x5 $nm^2$<br>10x10 $nm^2$ |
| 10 | Si(311)<br>Si(111) | 4<br>16 | 180<br>180 | $3.1x10^{10}$<br>$1.8x10^{11}$ | 3x3$nm^2$<br>7x7 $nm^2$ | 4x4 $nm^2$<br>10x10 $nm^2$ |

### 4-6.6.2 Detailed Optical Layout

### 4-6.6.3 Optical Simulation and Tolerances

Optical simulations were carried out using the ShadowOui program in the Oasys environment. The ideal focusing at 70 m at 10 and 25 KeV is shown in Figure 4.33.

### 4-6.6.4 Optics Specifications

**HHL Mirror** A horizontally deflecting mirror (M1) will be the first optical component of the PtychoProbe beamline. It will be located in enclosure A and operate at a reflection angle of 2.5 mrad. The mirror will be bendable to focus the beam horizontally at the SSA1 or SSA2 locations and allow for correcting the thermal induced distortions on M1 and Horizontally Deflecting Double-Crystal Monochromator (HDCM). The mirror will have three reflecting stripes (bare Si, Rh, and Pt) to provide harmonic rejection and cover the operational energy range. Vertical translation is required to change the reflecting stripe used. The mirror will require a meridional slope error of less than 0.1 µrad under the full heat load of the undulator after correcting for the thermal bump. The radius of the second mirror will be as small as approximately 10 km.

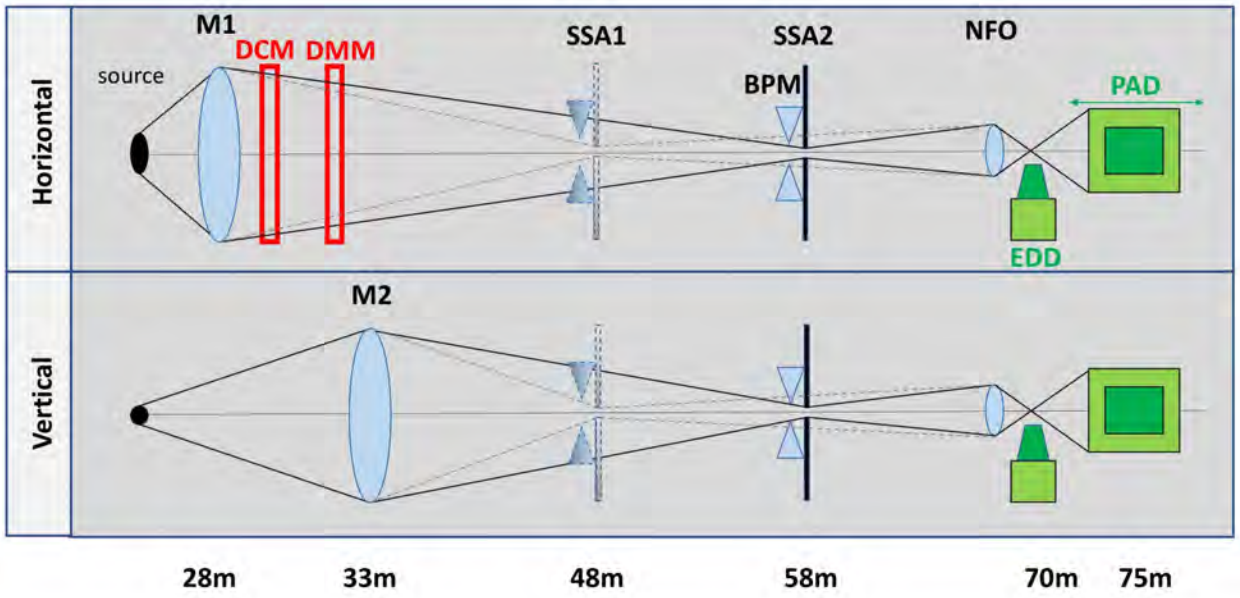


*Figure 4.32. Basic optical layout of the PtychoProbe beamline. M1 (high-heat-load mirror HHL) and M2 are horizontally and vertically reflecting mirrors, respectively. The DCM/DMM is a double crystal/multilayer monochromator, the SSAs are secondary source apertures with integrated beam positioning monitors. Nanofocusing optics focus the x-ray beam onto the sample. The resulting fluorescence and ptychography signals are measured by an energy-dispersive detector and pixel area detector, respectively.*

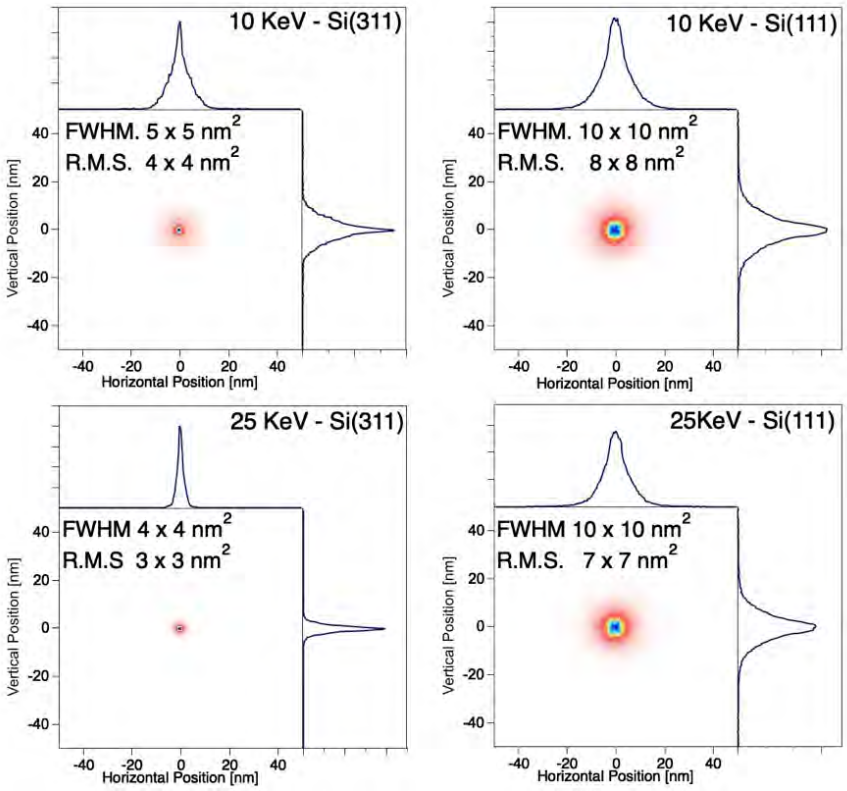


*Figure 4.33. : Simulated ideal focal spot at the sample location (70 m from source) for the two configurations (Si(111) (right) and Si(311) (left) DCMs) for 10 keV (top) and 25 keV (bottom).*

**HHL Double Crystal Monochromator/Multilayer** The HDCM is a standard Si (111) double-crystal monochromator with liquid nitrogen cooled crystals and fixed exit operation.

The purpose of the HDMM is to maximize flux for ptychography experiments in which the obtainable spatial resolution is determined by the signal to noise ratio at highest diffraction angles. The HDMM used in this study is a 25 Å d-spacing Mo/B4C multilayer (9 Å/16 Å) with 300 bilayers. A more conservative configuration is a 20 Å d-spacing Mo/B4C multilayer (9 Å/11Å) with 600 bilayers, providing a 40% smaller bandwidth and reflectance reduced by 15% factor.

The number of motions for each multilayer is minimized to maximize angular stability between the first and second multilayer. Flexures will be used for most motions. Multilayers properties are summarized in the Table 4.43.

*Table 4.43. Multilayer parameters*

| **Multilayer Parameters** | **Value** |
|---|---|
| Substrate Material | Silicon |
| Nominal d-spacing | 20-25 Å |
| Substrate surface roughness | $<$ 1 Å |
| Substrate Flatness [RMS] | $<$ 1 µrad |
| Clamped Crystal Flatness [RMS] | $<$ 2 µrad |
| Clamped Sagittal Twist | $<$ 0.2 µrad/cm |

**Vertically, focusing mirror (M2)** M2 is a vertically deflecting mirror located in enclosure A and operate at a reflection angle of 2.5 mrad. The mirror will be bent to focus the beam vertically at the SSA1 or SSA2 locations. The mirror will have three reflecting stripes (bare Si, Rh, and Pt) to provide harmonic rejection and cover the operational energy range. Vertical translation is required to change the reflecting stripe used. The mirror will require a meridional slope error of less than 0.05 µrad. The radius of the mirror will be as small as approximately 11 km.

**Secondary Source Aperture** The SSA1 and SSA2 are located at 48 m and 58 m from the source in the enclosure B and C, respectively. Both SSA will need to be water cooled. The SSA specifications are given in Table 4.44 below

*Table 4.44. Secondary source specifications*

| | **SSA1 and SSA2** |
|---|---|
| Range | ±50 µm |
| Resolution | 100 nm |
| Repeatability | 100 nm |

**Nanofocuing Optics** Nanofocusing optics (NFOs) such as Fresnel zone plates (ZPs) and multilayer Laue lenses (MLLs) will be located in the PtychoProbe endstation instrument. Generally, ZPs will be utilized for focusing at low energies, while MLLs are preferred for high energies (>13 keV). Examples of ideal ZP specifations are shown in Table 4.45.

*Table 4.45. Ideal zone plate specifications*

| **Zone Plate:** | **5 nm** | **20 nm** | **5 nm** | **20 nm** |
|---|---|---|---|---|
| Energy | 10 KeV | 10 KeV | 25 KeV | 25 KeV |
| Outer zone width | 4 nm | 16 nm | 4 nm | 16 nm |
| Diameter | 180 µm | 180 µm | 72 µm | 72 µm |
| Focal length | 5.8 mm | 23.25 mm | 5.81 mm | 23.25 mm |
| Thickness/efficiency | 1900 nm /33% | 1900 nm / 33% | 4400 nm / 33% | 4400 nm / 33% |
| Number zones | 11250 | 2812 | 4500 | 1125 |

The zone plate module will require at least 5 degrees of freedom, 3 transverse and 2 angular. Larger ranges for the transverse directions would assist in operation as long as the stability and resolution are not affected. The third angular degree of freedom is not needed.

### 4-6.6.5 Heat Load Considerations

**HL Mirror and DCM-1 Crystal** The HL mirrors (M1) will reduce the power passed on to the downstream optics. Table 4.46 and Table 4.47 summarize the maximum powers expected to be absorbed by various components. The heat load absorbed by M1 and DCM-1 Crystal was calculated using SRCalc for Si mirrors.

*Table 4.46. Power Calculations for DCM-1.*

| **K (U25)** | **Mono Energy** *(keV)* | **Power absorbed by DCM-1** *(Watts)* | **Power Density on DCM-1** *($W/mm^2$)* |
|---|---|---|---|
| 1.862 | 5.0 | 89.2 | 41.4 |

*Table 4.47. Power Calculations for M1*

| **Undulator** | **K** | **Mono Energy** *(keV)* | **Incident power on M1*** *(W)* | **Power absorbed by M1** *(W)* | **Power Density on M1** *($W/mm^2$)* |
|---|---|---|---|---|---|
| U21 | 1.305 | 8.8 ($1^{st}$) | 504 | 332 | 0.89 |
| U25 | 1.939 | 4.7 ($1^{st}$) | 540 | 454 | 1.16 |

* Based on the mirror acceptance of 1.0 x1.0 $mm^2$

The mirror deformation can be reduced by an order of magnitude by adding a notch to the mirror side and applying cooling above the notch, as visible in Figure 4.34.

When using the HL mirror with a notch, the thermal effects can be compensated for by acting on the curvature of the M1 and M2, as visible in Figure 4.35.

The correction of the radius of curvature is $\Delta$ R1 $\cong$ 14% and $\Delta$ R2 $\cong$ 7% for M1 and M2, respectively. The flux change within a 4.82 µm SSA is ~15%, while the increase in focal size is 9% x 5% (H x V). Effects of Thermal Deformation can be further mitigated by optimizing the notch design around the most common desired energies.

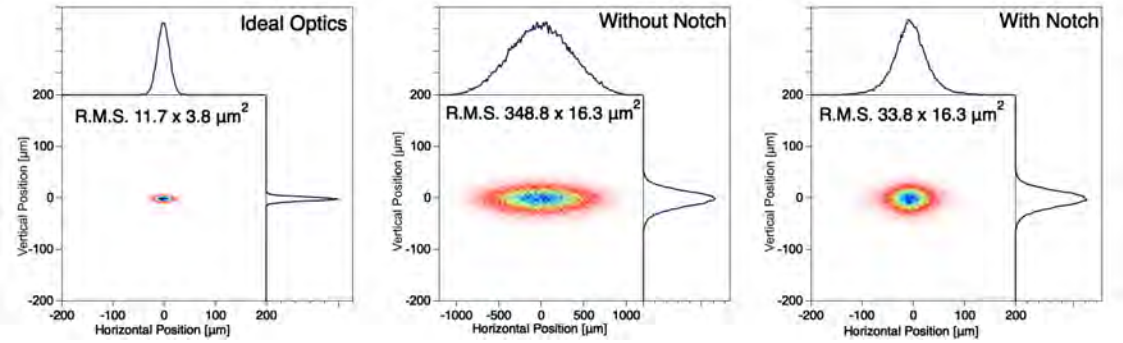


*Figure 4.34. Beam profile at the SSA1 location without thermal load (left), with thermal load on DCM-1 and HL Mirror without the notch (center), with thermal load on DCM-1 and HL Mirror with the notch (right), at 5 keV.*

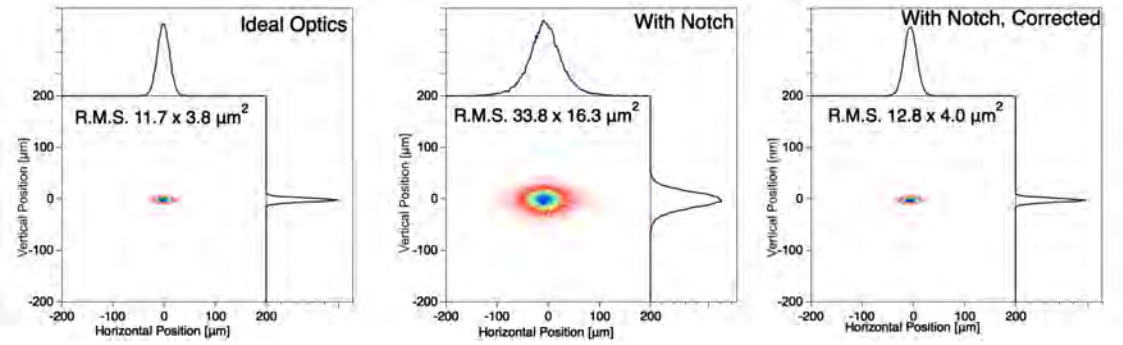


*Figure 4.35. Beam profile at the SSA1 location without thermal load (left), with thermal load on DCM-1 and HL Mirror with the notch (center), with thermal load on DCM-1 and HL Mirror with the notch and correction applied to mirrors curvature (right), at 5 keV.*

**Secondary Source Aperture** The SSA, while not operated in the optimal setup, could be subjected to a radiation with a significant amount of power density, being at focal position. For this reason, the power density has been calculated in a worst-case configuration:

- Beam filling the full angular acceptance by mirrors M1 and M2
- Energy Source at 17 KeV, producing the highest value of monochromatic energy
- Simulation performed with Si(311)/Si(111) DCM and Mo/B4C Double-Multilayer Monochromator(DMM)

The calculation has been performed by coupling SRW (to accurately compute the radiation from the source) and Shadow (to transport the radiation) within the Oasys program environment using an iterative process and an accurate sampling of the energy spectrum.

Figure 4.36 shows the results for the DCM (Si(311), Si(111)), and the DMM with the WBS fully opened (2x2 $mm^2$) and closed at 0.5x0.5 $mm^2$. The total incident power on SSA1 is 44 mW and 225 mW, respectively, for the two DCM reflections and 12.14 W and 10.14 W for the two DMM slit settings. The peak power density with the DMM is lowered by a ~10% by closing the WBS indicating the radiation focused at SSA1 is dominated by the central cone of the undulator harmonic. It is noted that the power density cannot be reduced without losing coherent photons.

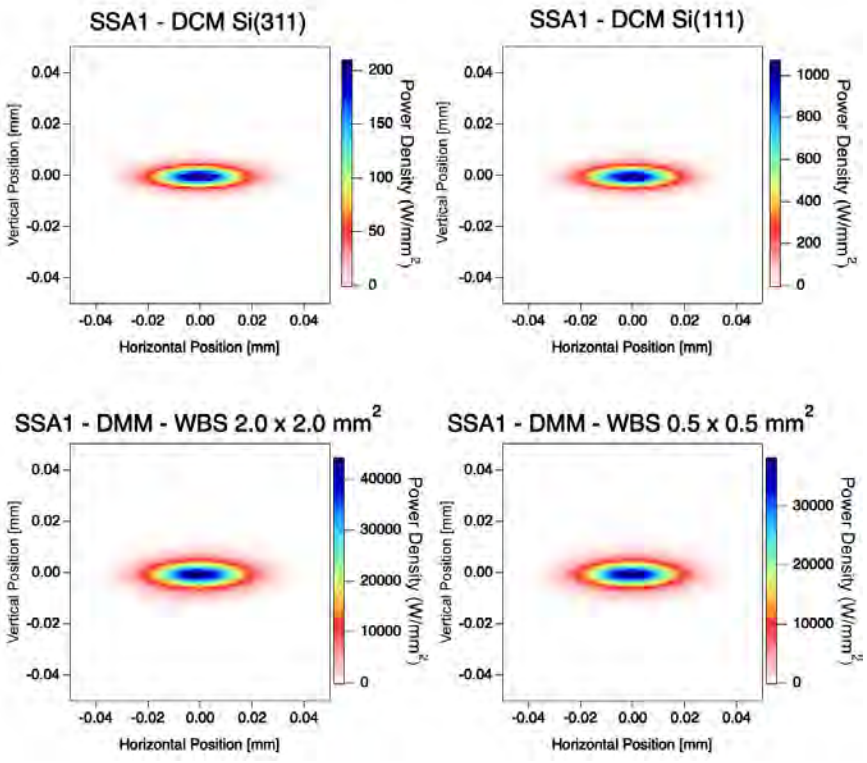


*Figure 4.36. Power Density distribution at the SSA1 location with Si(311) DCM (top-left), Si(111) DCM (top-right), Mo/$B_4C$ DMM and WBS = 2x2 $mm^2$ and Mo/$B_4C$ DMM and WBS = 0.5x0.5 mm2. The incident total power on SSA1 is 44 mW, 225 mW and 12.14 W and 10.14 W, respectively.*

Due to the large power densities produced by the focused beam and the power loads in the DMM condition, an incident surface with a maximum of 5 degrees is required if the SSA is produced from Glidcop AL-15. Other materials such as CuCrZr will need to have an incident surface of much less than 5 degrees. The incident face will need to have a beam defining tungsten blade at defining edge of the aperture.

A detailed description of the Ptychoprobe optics can be found in the Ptychoprobe 33-ID Optics ESD (ICMS Content ID: APSU_2030440).

## 4-6.7 Instrument Overview

### 4-6.7.1 Scientific Scope

The PtychoProbe is to realize the highest possible spatial resolution combining structural and chemical information. This will be achieved with 5 nm-focusing diffractive optics. Chemical information obtained using X-ray fluorescence (XRF) on all relevant elemental edges between 5 keV and 30 keV will be obtained with the 5 nm optics. These chemical information will be combined with structural information obtained using ptychography. The PtychoProbe will offer two- and three-dimensional, multimodal, thick-sample capability and bridge the gap between contemporary X-ray microscopes and electron microscopy. The APS-U flux combined with the nm-scale focusing will provide unprecedented sensitivity to trace elements. Fast scanning of large areas will allow for setting the fine-grained information into the coarse-scale context. However, at the high resolution, working distances will be sacrificed, with the instrument supporting a limited set of in situ and operando environments. Experiments will be carried out either in air, vacuum, or inert gas environment. The high-resolution, chemical sensitivity, and fast scanning will provide users with a world-leading instrument with which to investigate macroscopic properties that result from the complex interaction of constituent elements across length scales.

Key scientific aspects can be summarized as:

- Highest possible focusing capability (5 nm)
- XRF and ptychography capability
- Ability to combine structural and chemical information for two- and three-dimensional imaging
- Fast scanning to enable imaging of large areas
- *In situ* and *in operando* capabilities at highest resolution

### 4-6.7.2 Instrument Definition

The scientific objectives can be addressed with a PtychoProbe instrument that consists of the following 12 main items:

1. a stiff support structure,
2. a vacuum chamber,
3. a set of stages for manipulating the optics,
4. nanofocusing optics,
5. a set of stages for positioning and scanning the sample,
6. sample environment(s),

7. optics and sample metrology,
8. dynamic control system,
9. instrument control system,
10. an energy dispersive spectrometer (EDS) for XRF measurements,
11. a pixel array detector (PAD) for ptychographic measurements, and
12. a flight path.

To best address the scientific scope, a minimum set of degrees of freedom (DOF) necessary to both align the instrument and conduct measurements shall be provided. Redundant degrees of freedom increase compliance (and resulting vibration). In addition, metrology measurement points will be as close to the points of interest on the optics and sample as possible, thereby including as much of the instrument in the measurement loop as possible. Figure 4.37 shows a simplified schematic of the PtychoProbe instrument, less detectors. Approximately 26 motorized axes are required to provide the necessary alignments and motions (detector axes are not counted in total). The stiff support

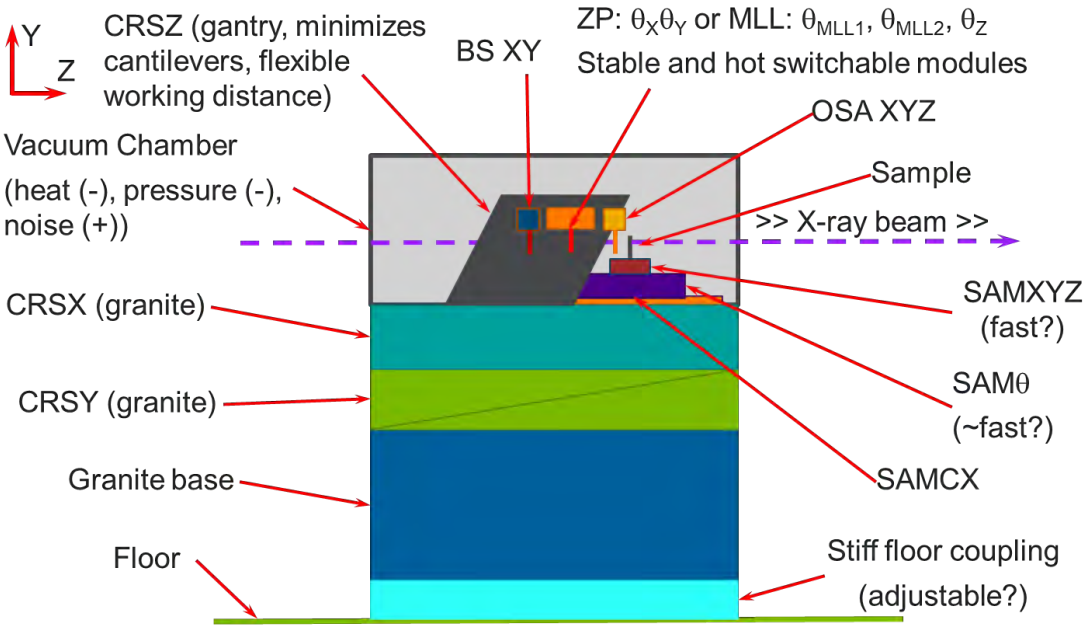


*Figure 4.37. Schematic of the Ptychoprobe instrument showing the vacuum chamber and basic motions. 17 axes of motion are required. The metrology system, XRF detector and imaging detector are not shown.*

structure will be similar to that of the Velociprobe. The support structure consists of, from the floor to the top, coupling between floor and granite base, a granite base, a granite coarse vertical (Y) axis, a granite coarse transverse (X) axis, and a coupling to the vacuum chamber. The floor coupling needs to be stiff and allow for adjustment to bring the instrument optic axis parallel to the X-ray beam axis. The granite base supports the Y and X axes above. The vacuum chamber will interface to the top of the granite X axes. It will be bolted or clamped to the granite surface and simple lateral and longitudinal adjustments may be provided.

The vacuum system encloses both the optics assembly and the sample assembly. Adequate access is necessary to change samples and perform maintenance. The instrument may be operated in air,

in vacuum, or in an inert gas environment. Sufficient pumping will be provided to achieve quick pump down and maintain a minimum of 100 mPa. The chamber needs to allow access for the EDS and PAD. The EDS and PAD require specific solid angles of clear space to operate. For low energy operation, the PAD detector may need to be as close as 50 mm downstream of the sample.

The optics assembly resides in the upstream position in the vacuum chamber. Sufficient DOF are required to support either 5 nm-class multilayer Laue lenses (MLLs) or Fresnel zone plates (ZPs). These MLL and ZP modules will reside on a gantry. The use of a gantry allows for minimizing cantilevered components while providing sufficient travel along the beam axis (Z) to accommodate the focal length of 5 keV to 30 keV optics. Off-focus use for ptychography will also be accommodated. The use of the MLLs or the ZPs can be effected through a the coarse X motion of the support and sufficient travel in sample coarse X. Depending on the instrument operation scheme, the optics stages may have short-range, fast-scanning capability as would be needed in a sample/slow, optics/fast scanning scheme. This choice will be made as design progresses. Both types of nanofocusing optics will be mounted in the instrument simultaneously. A number of zone plates to cover a specified energy range will be mounted to a carrier. The carrier will simultaneously accommodate four zone plates for the energy ranges 5-8, 8-12, 12-18, and 18-30 keV. The MLL optics will be mounted on a separate carrier. Both the ZP and MLL carriers will be mounted to the gantry. The availability of monolithic MLLs or the need for 2 separate MLLS for two-dimensional focusing will be considered in the design process.

The sample assembly resides in the downstream position in the vacuum chamber, it will accommodate a small set of sample environments. The scientific scope includes tomography, as such a rotation axes is a requirement. One X DOF is required to bring this rotation axis in alignment with the (previously aligned) optics. Additional DOF are required to move the region of interest on a 3 mm or 10 mm 2D size sample into the rotation axis. The sample will need to be scanned at sufficient speed to make the best use of the available photons and detector rate. The upper limit may be found if we assume a 1 MHz image acquisition rate, and 66% overlap with a 20 nm spot. The maximum tangential speed would be about 7 mm/s. The method in which this is carried out will inform the type and number of these DOF above the rotation stage. The method of metrology will affect the choice of stages. If sufficiently accurate metrology can be done at the sample, the mechanical requirements can possibly be relaxed on the sample stages. The scientific scope specifies in situ and operando environments. All necessary cabling and hoses will need to pass to the sample through or across the rotation axis.

A small set of sample environments will be accommodated. These may include cooling, a flow cell, electrical connections, and others. In addition to providing conditions of interest from the scientific context, the use of sample cooling may extend the use of the PtychoProbe for samples that are less radiation hard. The use of a sample environment will necessary limit the type of optics used and type of experiments performed. This is mainly due to the working distance constraint of ZP optics.

The optics and sample metrology system determine the relative positions of the optics and sample and are critical for enabling both the data acquisition and the dynamic control of the motion system. Ideally, the exact location of the X-ray beam on the sample would be measured. However, in practice, the actual measurement point is some distance away from the actual interaction point. The further this metrology system is from the ideal case, the larger will be the influence of drifts and errors due to unmeasured angular change of the optics and sample stacks. The metrology

system may consist of both interferometers and capacitive distance measuring systems. The exact scheme is being investigated. The scientific scope specifies the use of 5 nm focusing. This constrains the resolution of the relative position measurement. The relative position measurement should be about .5 nm to 1 nm to enable adequate dynamic control and data acquisition. The actual position error will have contributions from sensor noise, out-of-measurement-loop drifts, and any kinematic errors resulting from unmeasured tilts and translations. To minimize these effects low-noise sensors should be selected and the relative position measurement should occur as close to the point of interest on the optics and sample as possible. Nazaretski [25] has shown depending on conditions and measurement bandwidth, the noise floor of one brand of fiber-optic interferometer was found to be between .3 and 1 nm.

As previously mentioned, the scientific scope requires tomography. At 5 nm resolution, tomography requires 40 µrad (.0023 degree) angular resolution. The included rotation angle will span from -180 degrees to 180 degrees. Currently there exists no off-the-shelf interferometery solution that can measure a rotating target that translates more than a few microns. It is not reasonable to expect fast scanning if the maximum field that can be scanned is small. There are three possible ways to address this. One way is to employ interferomenters with a non-rotating reference as Holler et al. at the Swiss Light Source do through the use of a so-called anti-rotation stage. A second way is to move the interferometer to keep the beam pointing at the center of a spheroid reference, also by Holler [26]. In this case, a position sensitive detector is used to measure the small motion of the interferometer beam and drive a stage which maintains the pointing of the interferometers. The interferometer moves, but the reference does not, thereby making the interferometer insensitive to the alignment motions. A third way is to employ a set of interferometers that rotate with the sample to measure sample motions with respect to a rotating reference, then use a set of capacitive micrometers to measure the translations and tilts of the rotating reference as done on ESRF ID19 instrument [27]. These capacitive micrometers can be mounted on the optics common fixed reference.

The optics stack and sample stack motion will be controlled with a dynamic control system. The *dynamic control system* is distinct from the *instrument control system*. The purpose is to provide the best baseline-mechanical dynamic performance possible. The dynamic control enables the fast scanning, rejects vibration, rejects in-loop drifts, and makes the system robust to variation in configuration. This system may incorporate both feedback and feedforward components. The system may be implemented on the instrument control system or may be a distinct piece of hardware.

Scan control, overall instrument control, and data acquisition will performed with an instrument control system. This system will handle all high-level control, including providing virtual coordinates and axes to suit the experiment and instrument operation. The system will acquire the optic and sample position information at the highest rate reasonable, such that these information can be used for X-ray data post processing. The instrument control system will manage detector triggering. High level control screens will be provided. Real-time low-resolution reconstruction may be provided.

The EDS detector shall be positioned 90 degrees to the incident beam and as close as possible to intercept the largest solid angle. The PAD detector needs to be positioned from a close distance of 50 mm to a far distance of 5 m downstream of the sample. There will be a ”close” detector range to handle detector distances between 50 mm and 300 mm. There will be a ”far” detector range to handle detector distance from 300 mm to 5 m. The far detector will be coupled to the instrument with a flight tube. The close and far detectors will be the same detector.

### 4-6.7.3 Instrument Location

The Ptychoprobe will be located at 33-ID-D, at about 70 m from the source. This can be seen in Figure 4.38.

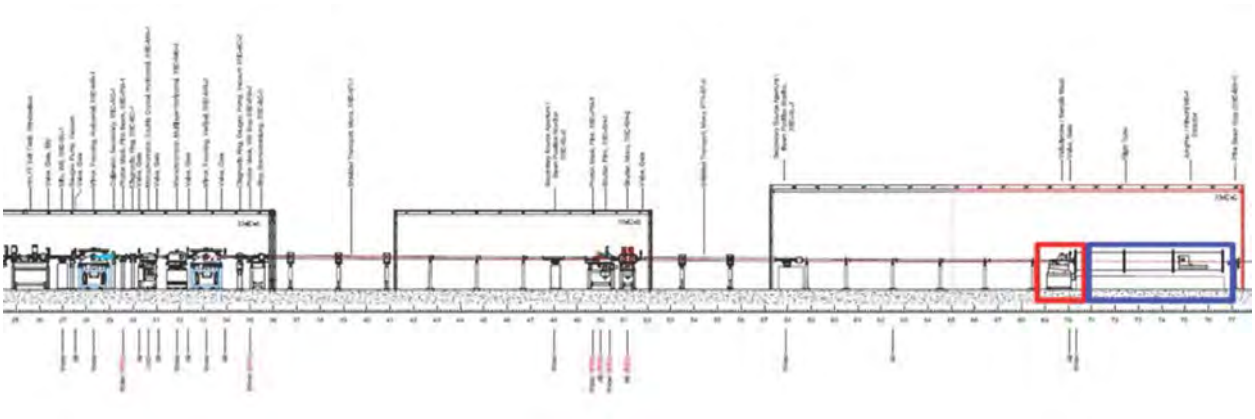

*Figure 4.38. Sector 33 beamline layout, showing the PtychoProbe location (in red square) at the end of the beamline, in the C hutch. Also located in the D hutch is the flight path linking the instrument and detector (in blue square).*

A detailed description of the Ptychoprobe Endstation instruments can be found in the 33-ID Ptychoprobe Endstation Instrumentation ESD (ICMS Content ID: APSU_2032313).

## 4-7 In situ Nanoprobe 19-ID

### 4-7.1 Introduction

The upgrade of the Advanced Photon Source with an MBA storage-ring lattice, APS-U, will provide massively increased coherent x-ray flux in the hard x-ray range, and a 20X reduction in source size in the horizontal dimension. This will make the APS ideally suited to bring to bear coherent methods to a broad range of questions from fields such as materials and condensed matter science, chemical science, and environmental science. Both nanofocusing approaches and coherence-based techniques benefit directly from the high brilliance and the new source geometry, by (i) achieving diffraction-limited spot sizes of 20 nm and below, (ii) dramatically increased speed of data acquisition, that in turn enables multiscale imaging of complex systems, and (iii) enabling high time resolution for the study of dynamic processes, such as defect formation and growth, and fluctuations. At the same time, the brilliance gain at high photon energies significantly enhances the essential capabilities of hard x-rays to penetrate gases, fluids, windows, and matrices, enabling very high spatial resolution imaging and nanospectroscopy under in-situ conditions, and access to K and L absorption edges for most elements in the periodic system. The ISN is designed exploit these transformative source properties to study complex materials systems under in-situ and operando conditions across many lengths scales, using x-ray fluorescence (XRF) for composition and trace contaminants, XRF nanospectroscopy for local composition and chemical state, x-ray beam induced currents and voltages for electronic properties, and coherent methods such as ptychography for structural imaging and coherent diffraction to study slow dynamics.

### 4-7.2 Scientific Objective

The ISN uses x-rays with photon energies between 4.8 and 30 keV, and focuses them into a diffraction-limited hard x-ray spot with a size of 20 nm. This enables quantitative nano-spectroscopy at the K and L edges of transition metals and rare-earth metals. High photon energies will allow penetration through environments and windows, and into materials to sites where active processes are taking place. To enable the study of materials under actual synthesis and operating conditions, the ISN will provide a very large working distance of 55 mm. This enables deployment of a large range of in-situ environments, namely low, high, and variable temperatures, flow of gases and fluids, varying pH, high pressure, and application of external fields. It also provides added flexibility to integrate advanced detectors, such as emission spectrometers. The scientific focus of the ISN beamline is the investigation of complex, functional materials and materials systems, such as catalysts, batteries, photovoltaic systems, and nanoscale earth and environmental samples, during synthesis, operation, and under actual environmental conditions. The ISN is designed to study these systems across many lengths scales, in 2D and 3D, under in situ conditions. The ISN will use x-ray fluorescence (XRF) to determine composition and trace contaminants, XRF nanospectroscopy for local composition and chemical state determination, X-ray induced current and voltage (XBIC/XBIV), and X-ray excited optical luminescence for APSU-2.04.03.19.01-FRD-0012 electronic properties measurements. Coherent methods will be used for structural imaging, and to study slow dynamics. As such, the ISN will provide qualitatively new insight into the properties of advanced, complex materials, and provide guidance for materials design through understanding of defect evolution under various environmental conditions.

### 4-7.3 Beamline Requirements for the Insertion Devices (IDs)

The ISN beamline will operate over the energy range of 4.8-30 keV. As a nanoprobe, it will require the highest brilliance possible throughout this range. A revolver undulator of 4.6 m length with two periods (21 mm and 25 mm) is currently planned. Undulator specifications used in this docuemnt are not controlled by this document. For the most recent values, see the ICDs for the ISN beamline.

*Table 4.48. Source Parameters for ISN beamline*

| Undulator | Period [mm] | Length [m] | Location | Max Power |
|---|---|---|---|---|
| Revoler | 21/25 | 4.6 | Center of Straight Section | 2.28 kW[1] |

[1] Through the Front End Mask 2x2 $mm^2$ @ 25.4 m with the undulator Ky = 1.939.

### 4-7.4 Beamline Requirements for the Front End

The ISN beamline will utilize the new standard MBA High Heat-Load front end capable of handling a maximum power of 21 kW. The beamline will use a windowless exit configuration with a 2 mm x 2 mm (H x V) exit mask aperture.

A detailed description of the ISN Front End and Insertion devices can be found in the APS-U 19-ID Beamline Front End and Insertion Devices Interface Control Document (ICMS Content ID: APSU_190947).

### 4-7.5 Beamline Layout

*Figure 4.39. Layout of ISN beamline.*

The ISN beamline is one of the two "long beamlines" being developed for the APS upgrade. Located at sector 19-ID, the ISN beamline will extend beyond the EAA floor and LOMs and terminate at a separate building that will house the In Situ Instrument.

#### 4-7.5.1 Beamline Component Table

The following table shows all major beamline components and their general location along the beamline.

A detailed description of the ISN beamline can be found in the ISN 19-ID Photon Delivery System ESD (ICMS Content ID: APSU_2012712).

*Table 4.49. List of ISN beamline components*

| **Distance from source** *(m)* | **Component** | **Designation** | **Description/Comments** |
|---|---|---|---|
| 25.4 | FE Exit Mask | | Standard HHL Front-End exit mask<br>2x2 $mm^2$ aperture |
| 26.1 | FE Collimator | | Standard HHL Front-End Exit Collimator<br>5x5 $mm^2$ aperture |
| 27.0 | HHL WB Slits | 19ID-SL-1 | HHL Tilting type |
| 27.3 | Pump stand | | Small standard pump stand for pump out of slits,<br>RGA, gauges |
| 28.0 | Mirror, Vertical, Flat | 19ID-MR-1 | Downward reflecting, water-cooled,<br>white beam mirror |
| 29.0 | Mirror, Vertical, Focusing | 19ID-MR-2 | Upward reflecting, water-cooled,<br>pink beam focusing mirror |
| 29.7 | Secondary Collimator | 19ID-SC-1 | Secondary Bremsstrahlung collimator |
| 30.0 | Beam Diagnostic | 19ID-BD-1 | Diagnostic flag assembly |
| 29.7 | Photon Mask, WB Stop | 19ID-PM-1 | Pink beam aperture / white beam stop Vertical offset |
| 30.9 | Slits, Pink beam | 19ID-SL-2 | Pink Slits, CUFE tilting type |
| 31.7 | DCM | 19ID-MN-1 | Horizontally deflecting inboard, $LN_2$ cooled |
| 32.7 | DMM | 19ID-MN-2 | Horizontally deflecting inboard, $LN_2$ cooled |
| 33.6 | Photon Mask | 19ID-PM-2 | Pink beam missteering mask |
| 34.2 | Bremsstrahlung Collimator | 19ID-BC-1 | Primary Bremsstrahlung Collimator, Lead |
| 34.4 | Slits, Pink | 19ID-SL-3 | Pink Slits, tilting type |
| 35.0 | Mirror, Horizontal, Focusing | 19ID-MR-3 | Inboard deflecting mirror.<br>Focuses horizontally on beam-defining aperture at 64 m.<br>Accepts monochromatic beam from DCM or DMM. |
| 35.8-48.2 | Shielded Transport | 19ID-ST-1 | White beam shielded transport from 19-ID-A to 19-ID-B |
| 49.1 | Photon Mask | 19ID-PM-3 | Pink beam missteering mask |
| 49.5 | Bremsstrahlung Collimator | 19ID-BC-2 | Primary Bremsstrahlung Collimator / Stop, Lead |
| 55.0 | Beam Defining Aperture Vertical | 19ID-SL-4 | Defines the vertical size of intermediate x-ray source.<br>Resolution, accuracy and stability must be consistent<br>with a smallest aperture size of ~ 4 $\mu$m. |
| 64.0 | Beam Defining Aperture Horizontal | 19ID-SL-5 | Defines the horizontal size of intermediate x-ray source.<br>Resolution, accuracy and stability must be consistent<br>with a smallest aperture size of ~ 4 $\mu$m. |
| 65.0 | Photon Shutter | 19ID-SH-1 | P9-50 water cooled pink beam shutter |
| 65.5-213.0 | Shielded Transport | 19ID-ST-2 | Mono beam shielded transport from 19-ID-D to 19-ID-E |
| 95, 124,<br>153, 183 | Shielded ion pump station | | Shielded mini enclosures to house ion pumps<br>along 100 meter transport to endstation |
| 213.0 | Window | 19ID-WN-1 | Double Si3N4 |
| 213.2 | Filter | 19ID-FL-1 | |
| 215.8 | Shutter, Fast | 19ID-FS-1 | |
| 220.0 | ISN Instrument | 19ID-BI-1 | ISN instrument with high-resolution focusing optics,<br>in-situ environment, energy-dispersive detector,<br>area detectors , control and motion systems. |
| 227.0 | Beamstop | 19ID-BS-1 | Mono Beamstop |

## 4-7.6 Optics Overview

### 4-7.6.1 Beam Delivery Specifications

The ISN beamline will focus the coherent fraction of the undualtor beam to a focal spots of 20 nm and at nominal energies of 10 and 25 keV. The source parameters are from Michael Borland's presentation at the DOE/SC CD-2 Review of the APS Upgrade Project (October 10-12, 2018). The optical design and optics specifications are listed in this document. Wave-optics calculations with SRW (Synchrotron Radiation Workshop) software have been performed to compute the lateral coherence length of the radiation at each secondary source (BDA-H, BDA-V). Simulations have been prepared within the Oasys program environment and were executed by using parallel computing in the LCRC cluster (http://www.lcrc.anl.gov). Table 4.50 and Table 4.51 show the results for photon energies of 10 keV and 25 keV.

*Table 4.50. Beam defining aperture sizes*

| | Energy | BDA-V | BDA-H |
|---|---|---|---|
| Coherence Length | 25 keV | 1.8 µm | 1.3 µm |
| Coherence Length | 10 keV | 5.8 µm | 3.1 µm |

The coherent fraction is determined by the ratio of the flux at BDAs to the flux with the slits opened and are given in the Table 4.51 as the coherent flux and the total flux.

*Table 4.51. Flux and coherent fraction*

| | Energy | Coherent Flux (ph/s) | Total Flux (ph/s) | Value |
|---|---|---|---|---|
| Coherent Fraction | 25 keV | $4.7 \times 10^{11}$ | $5.0 \times 10^{13}$ | 0.94% |
| Coherent Fraction | 10 keV | $7.2 \times 10^{12}$ | $1.3 \times 10^{14}$ | 5.58% |

Table 4.52 shows the expected flux and focal spot sizes at 10 keV and 25 keV at the final focus position. The coherent flux at the focus is computed by opening the slits to the coherence length determined by the NF mirror's angular acceptance and by comparing/matching the flux value at the focus with the coherent flux calculated after the BDAs.

*Table 4.52. Flux and focal spot sizes*

| | Energy | Value (ph/s) | Focal size FWHM (HxV) |
|---|---|---|---|
| Total Flux | 25 keV | $3.1 \times 10^{12}$ | 24x30 $nm^2$ |
| Coherent Flux | 25 keV | $3.4 \times 10^{11}$ | 16x16 $nm^2$ |
| Total Flux | 10 keV | $8.9 \times 10^{12}$ | 43x52 $nm^2$ |
| Coherent Flux | 10 keV | $3.5 \times 10^{12}$ | 39x39 $nm^2$ |

### 4-7.6.2 Detailed Optical Layout

### 4-7.6.3 Optical Simulation and Tolerances

Optical simulations were carried out using the ShadowOui program in the Oasys environment. The ideal focusing at 220 m at 25 keV is shown in Figure 4.41.

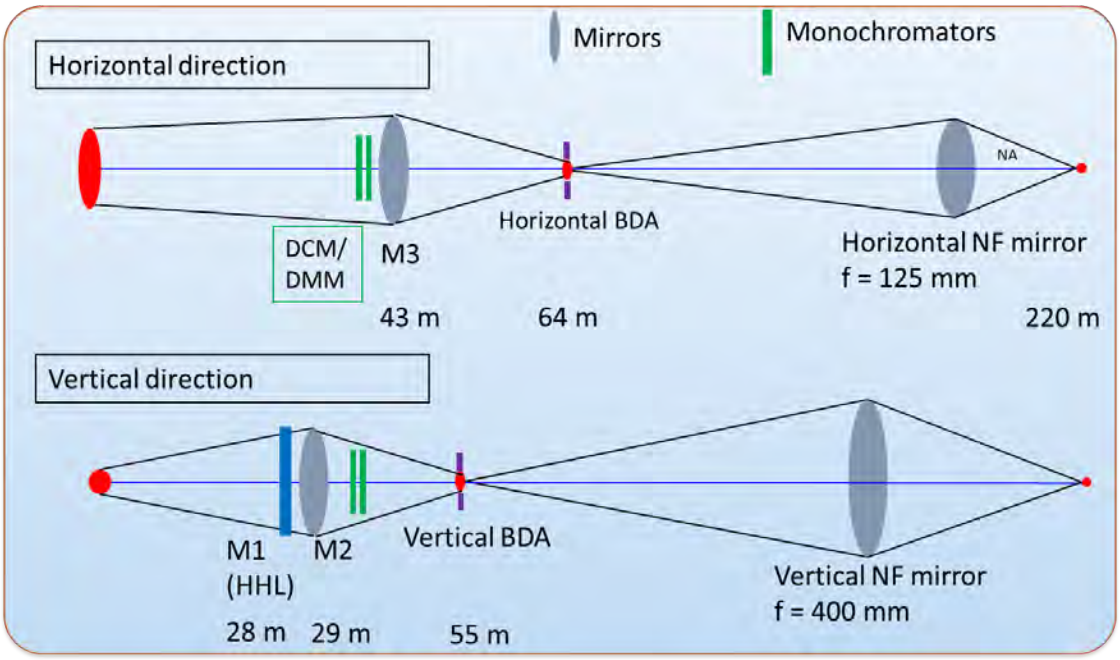


*Figure 4.40. Basic optical layout of the ISN beamline. M1 (high heat load mirror HHL, flat) and M2 (pink-beam mirror, vertically focusing) are vertically reflecting mirrors, M3 is a horizontally reflecting, horizontally focusing pink beam mirror. DCM and DMM are a double-crystal monochromator and a double-multilayer monochromator, respectively. BDA is the beam defining aperture, consisting of a vertically defining and a horizontally defining component. NF mirrors are the nanofocusing mirrors.*

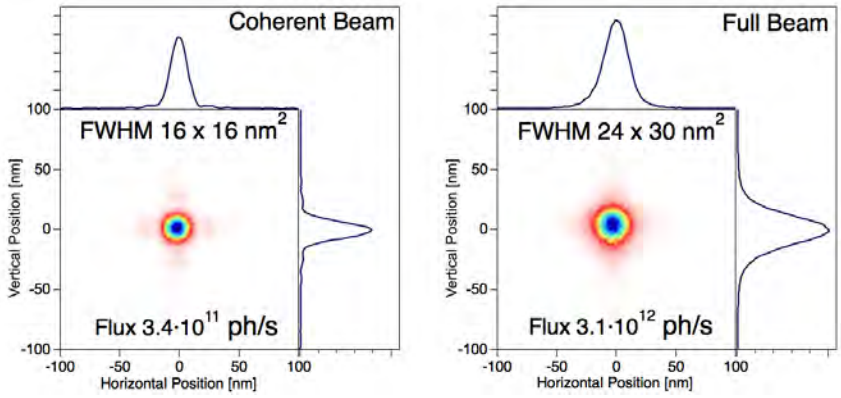


*Figure 4.41. Ideal focal spot at the sample location (220 m from source) for (left) a coherent beam defined by the BDA size of 13.0x4.1 $\mu m^2$ and (right) the full beam with BDA removed.*

The figure error on the NF mirrors is the most important optical parameter that affects the focal spot size. Figure 4.42 shows the effects of NF mirror figure errors on the focal spot. Visual inspection indicates that the side peaks need to be minimized. FWHM size is not a good measure, instead, the RMS size needs to be used.

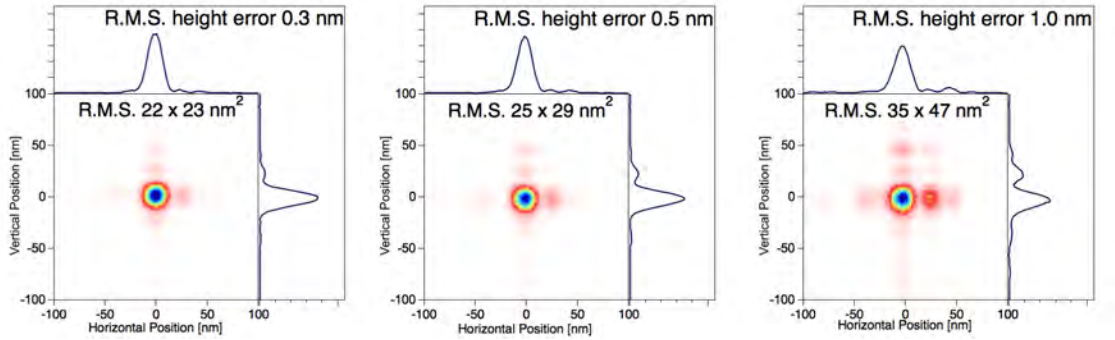


*Figure 4.42. Effects of NF mirror figure errors on the focal spot.*

Figure 4.43 shows the calculated RMS focal spot size and relative peak intensity as a function of the RMS figure height errors. To keep both the focal spot size broadening and the peak intensity drop to less than 10%, the RMS figure error has to be smaller than 0.45 nm and 0.38 nm for NF(h) and NF(v), respectively.

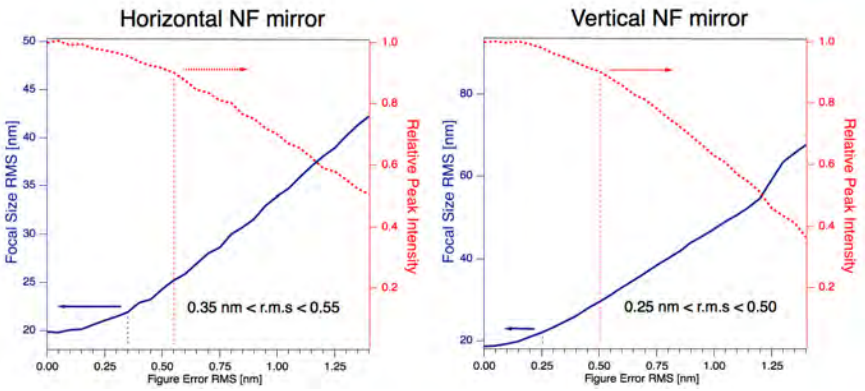


*Figure 4.43. Effects of NF mirror figure errors on the focal spot on (left) the NF(h) mirror and (right) the NF(v) mirror.*

The pitch alignment error (or angular vibration) of the NF mirrors is studied and shown in Figure 4.44. To keep both the focal size broadening and the peak intensity drop less than 10%, the pitch misalignment has to be smaller than 100 nrad and 70 nrad for NF(h) and NF(v), respectively.

### 4-7.6.4 Optics Specifications

**HHL Mirrors** Two vertically deflecting mirrors will be the first optical components of the ISN beamline. They will be located in enclosure A and operate at a reflection angle of 2.5 mrad. The first mirror will be flat, while the second will be bent to focus the beam vertically at the BDA(v) in enclosure C and allow for correcting the thermally induced distortions on both mirrors. These mirrors will each have three reflecting stripes (bare Si, Cr, and Pt) to provide harmonic rejection

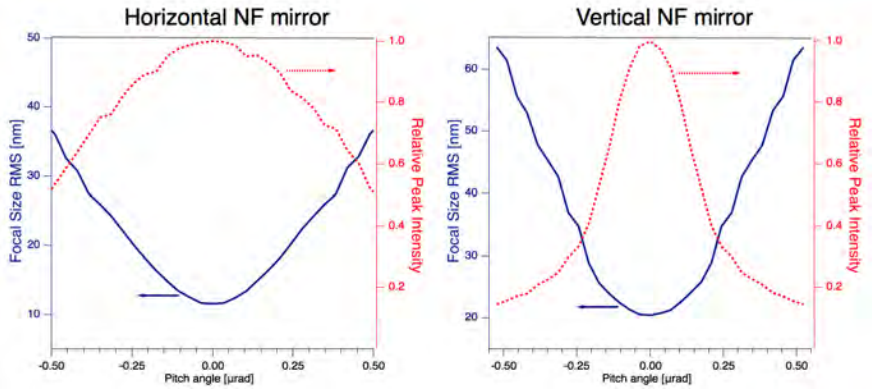


*Figure 4.44. Pitch alignment error (or angular vibration) of the NF mirrors*

and cover the operational energy range. Horizontal translation is required to change the reflecting stripe used. The mirrors will each require a meridianal slope error of less than 0.05 µrad under the full heat load of the undulator after correcting for the thermal bump. The radius of the second mirror will be as small as approximately 10 km.

**HHL Double Crystal Monochromator/Multilayer** The HDCM is a small offset Si (111) double-crystal monochromator with liquid nitrogen cooled crystals and fixed exit operation. The number of motions of each crystal is minimized to maximize angular stability between the first and second crystal.

The purpose of the HDMM is to provide more coherent flux in the high-energy range, where the undulator flux gets smaller. The HDMM used in this study is a 25 Å d-spacing Mo/$B_4C$ multilayer (9 Å/16 Å) per 300 bilayers with liquid nitrogen cooled multilayers and fixed exit operation. A more conservative configuration is a 20 Å d-spacing Mo/$B^4C$ multilayer (9 Å/11 Å) per 600 bilayers, providing a 40% smaller bandwidth and reflectance reduced by 15% factor. The number of motions of each multilayer is minimized to maximize angular stability between the first and second multilayer. Flexures will be used for most motions of multilayers.

**Horizontal focusing mirror (M3)** M3 is a horizontally deflecting mirror located in enclosure A and operated at a reflection angle of 2.5 mrad. The mirror will be bent to focus the beam horizontally at the BDA(h) in enclosure D. The mirror will have Pt coating to accept the full range photon energies in the operational energy range. Vertical translation is required to change the reflecting stripe used. The mirror will require a meridianal slope error of less than 0.1 µrad. The radius of the mirror will be as small as approximately 11 km.

**Beam Defining Aperture** The BDA(v) and BDA(h) are located at 55 m and 64 m from the source in the enclosure C and D, respectively. Both BDAs will need to be water cooled. The vertically defining aperture must allow a smallest aperture size of 3.5 micrometers, with less than 99% of 30 keV photons blocked outside the nominal aperture.

**Experimental Station NF Mirror System** The nano-focusing (NF) mirrors will be located in the end-station E and operate at a reflection angle of 2.5 mrad. Both mirrors will be pre-shaped elliptical cylinders with Pt coating. The NF(v) [NF(h)] mirror located 400 mm (125 mm) upstream of the sample location focuses the beam vertically (horizontally).

### 4-7.6.5 Heat Load Considerations

**HHL Mirrors** The HHL mirrors (M1 and M2) will reduce the power passed on to the downstream optics. Table 4.53 and Table 4.54 summarize the maximum powers expected to be absorbed by various components. The heat load absorbed by M1 and M2 was calculated using SRCalc for Si mirrors.

**Table 19:** Power Calculations for HHL Mirrors

*Table 4.53. Power Calculations for HHL Mirrors*

| **Thermal and vacuum Management** | **M1** | **M2** |
|---|---|---|
| Maximum **operational** absorbed power (W)[1] | 455 | 13 |
| Peak operational power density on the mirror surface ($W/mm^2$)[1] | 1.16 | 0.034 |
| Maximum incident total power (W)[2] | 2275 | 2275 |
| Peak normal incidence power density ($W/mm^2$)[2] | 536 | 500 |
| Allowable thermal induced slope error (μrad) | <0.05 | <0.05 |

[1]1x1 mm aperture before M1 with the undulator Ky = 1.939
[2]Through the Front End Mask 2x2 $mm^2$ @ 25.4 m with the undulator Ky = 1.939.

*Table 4.54. Power Calculations for M1 and M2.*

| **K (U25)** | **Mono Energy** *(keV)* | **Power absorbed by M1** *(W)* | **Power Density on M1** *($W/mm^2$)* | **Power absorbed by M2** *(W)* | **Power Density on M2** *($W/mm^2$)* |
|---|---|---|---|---|---|
| 1.862 | 5.0 | 429 | 1.1 | 11 | 0.027 |
| 1.833 | 5.1 | 418 | 1.1 | 10 | 0.026 |

The mirror deformation can be reduced by an order of magnitude by adding a notch to the mirror side and applying cooling above the notch. The notch dimensions on M1 were optimized for power absorbed at 5 keV. Figure 6 shows the focal spot at the BDA(v) location when scanning undulator energy from 5 keV (Ky=1.862) to 5.1 keV (Ky=1.833). The notch design shows a change in focal size from 17.2 to 17.0 μm going from 5 keV to 5.1 keV, respectively. The flux change within a 10 μm BDA(v) is less than 2%, which is required for the spectroscopy experiments at the ISN beamline. The power load on DCM is shown in Table 4.55.

**Beam Defining Apertures** The BDA(v) and BDA(h), while not operated in the optimal setup, could be subjected to a radiation with a significant amount of power density, being at focal position. For this reason, the power density has been calculated in a worst-case configuration:

- Beam filling the full angular acceptance by mirrors M1, M2 and M3

*Table 4.55. Power Calculations for DCM.*

| K (U25) | Power after mirrors (W) | Mono Energy (keV) | 1st crystal Angle | Beam Size at Mono (HxV) (mm x mm) | Beam Footprint (HxV) (mm x mm) | Power Density ($W/mm^2$) |
|---|---|---|---|---|---|---|
| 1.862 | 79 | 5.0 | 23.3° | 1.13 x 0.98 | 2.86 x 0.98 | 34.31 |
| 1.833 | 81 | 5.1 | 22.8° | 1.13 x 0.98 | 2.92 x 0.98 | 161.51 |

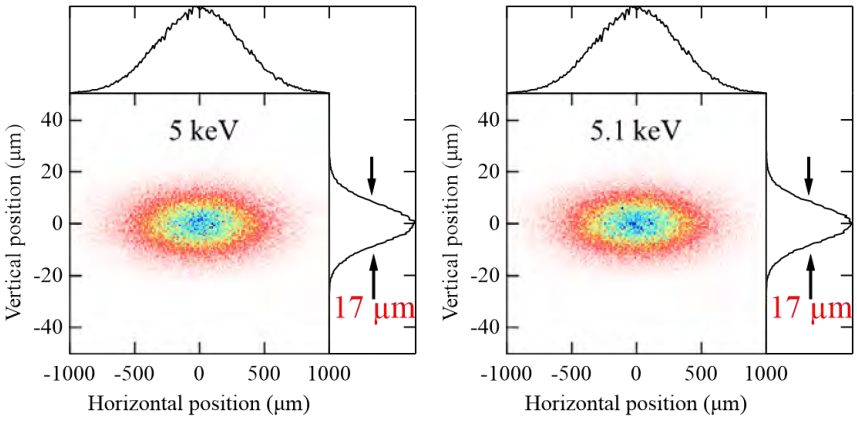


*Figure 4.45. Beam profile at the BDA(v) location with thermal load at (left) 5 KeV and (right) 5.1*

- Energy Source at 17 keV, producing the highest value of monochromatic energy
- Simulation performed with Si(111) DCM and Mo/$B_4C$ (d=25 Å) DMM

The calculation has been performed by coupling SRW (to accurately compute the radiation from the source) and Shadow (to transport the radiation) within the Oasys program environment using an iterative process and an accurate sampling of the energy spectrum.

Figure 4.46 shows the results with DCM. The incident total power on each BDA is 200 mW. Initial calculations show a localized heat rise of about 1.2 degrees Kelvin in the area that is incident on the beam. This thermal distribution presents no danger of damaging the BDA and thermal deformation should be limited to less than 20 nm depending on geometry and material of the final design.

Figure 4.47, instead, shows the results with DMM, with WBS fully opened (2x2 $mm^2$) and closed at 0.5x0.5 $mm^2$. The incident total power on each BDA is 11.55 W and 9.81 W, respectively. The peak power density is lowered by a ~10% by closing the WBS, indicating that the radiation focalized at BDAs is dominated by the central cone of the undulator harmonics, and power density cannot be reduced without losing coherent photons.

Both the horizontal and vertical BDA will not be able to withstand these spot sizes and intensities at normal incidence. Initial calculations show that the BDA would exceed 850 K and would thus destroy the BDA. A larger slit be used that has a low angle incident surface such that the incident beam would be spread out distributing the heat load. Keeping a normal or near normal incidence

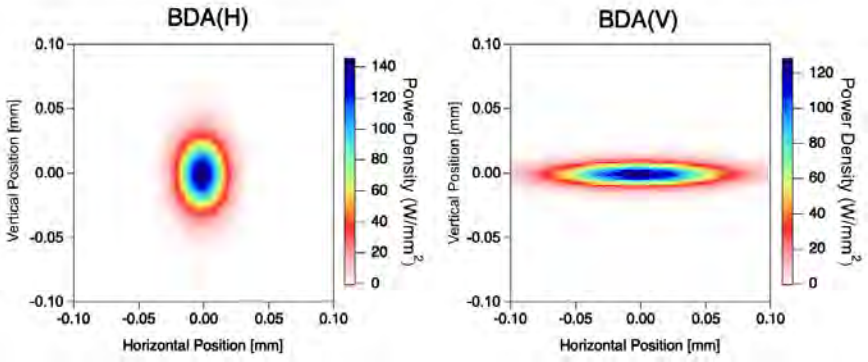


*Figure 4.46. Power Density distribution at the BDA(h) (left) and BDA(v) location (right), with Si(111) DCM. The incident total power on each BDA is 200 mW.*

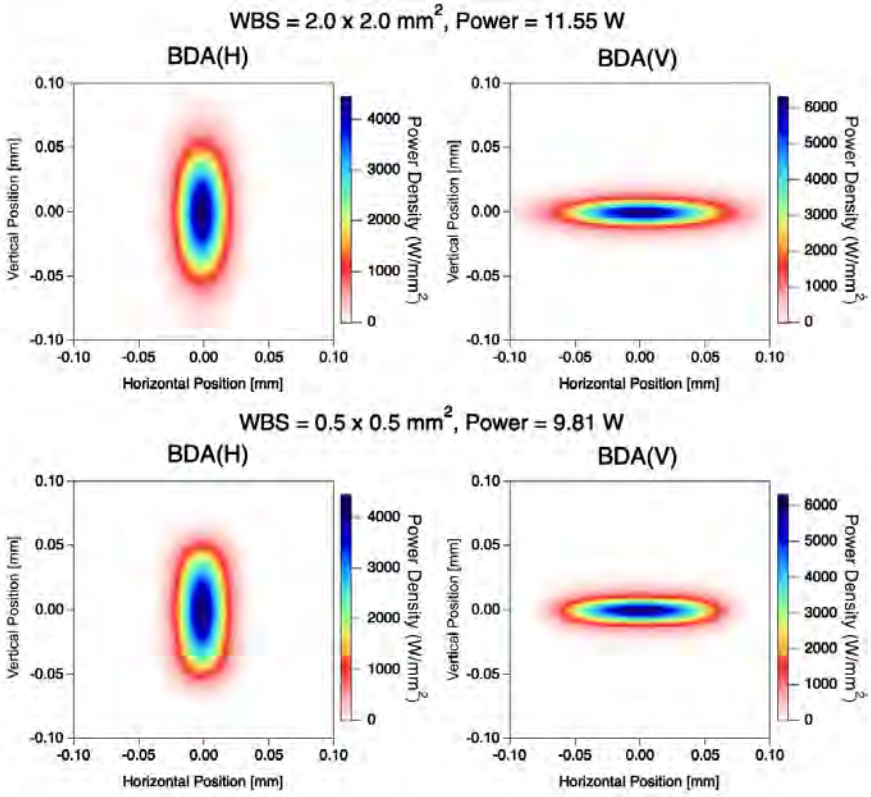


*Figure 4.47. Power Density distribution at the BDA(h) (top-left) and BDA(v) location (top-right), with Mo/$B_4C$ DMM and WBS = 2x2 mm$^2$ and at the BDA(h) (bottom-left) and BDA(v) location (bottom-right), with Mo/$B_4C$ DMM and WBS = 0.5x0.5 mm$^2$. The incident total power on each BDA is 11.55 W and 9.81 W, respectively.*

BDA will fail in this beam.

A detailed description of the ISN optics can be found in the ISN 19-ID Optics ESD (ICMS Content ID: APSU_2030436).

## 4-7.7 Instrument Overview

### 4-7.7.1 Scientific Scope

The In Situ Nanoprobe (ISN) uses x-rays with photon energies between 4.8 and 30 keV, and focuses them into a diffraction-limited hard x-ray spot with a size of 20 nm. The high brilliance provided by the upgraded APS ring will enable very high focused flux, with diffraction-limited resolution. This enables quantitative chemical imaging using the K and L emission lines of transition metals and rare-earth metals. High photon energies will allow penetration through environments and windows, and into materials to sites where active processes are taking place. To enable the study of materials under actual synthesis and operating conditions, the ISN will provide a very large working distance of 55 mm. This enables deployment of a large range of in-situ environments, namely low, high, and variable temperatures, flow of gases and fluids, varying pH, high pressure, and application of external fields. It also provides added flexibility to integrate advanced detectors, such as emission spectrometers.

The scientific focus of the ISN beamline is the investigation of complex, functional materials and materials systems, such as catalysts, batteries, photovoltaic systems, and nanoscale earth and environmental samples, during synthesis, operation, and under actual environmental conditions. The ISN is designed to study these systems across many lengths scales, in 2D and 3D, under in-situ conditions. The ISN will use x-ray fluorescence (XRF) to determine composition and trace contaminants, XRF nano-spectroscopy for local composition and chemical state determination, ptychography for high-resolution imaging of transparent samples with sub-10 nm resolution, X-ray induced current and voltage (XBIC/XBIV), and X-ray excited optical luminescence for electronic properties measurements. Coherent methods will be used for structural imaging, and to study slow dynamics. As such, the ISN will provide qualitatively new insight into the properties of advanced, complex materials, and provide guidance for materials design through understanding of defect evolution under various environmental conditions.

### 4-7.7.2 Instrument Definition

The In Situ Nanoprobe will consist of nanofocusing optics, nanopositioners for optics and sample, detectors and related positioners, a support structure that minimizes enhancement of floor vibrations, an instrument chamber that houses optics and sample, in situ metrology and feedback of optics and sample position, and in situ environments for the sample. The ISN instrument will reside in a temperature-stabilized enclosure with low vibration background. The ISN instrument will furthermore include a controls and data acquisition system, and data preprocessing and analysis capabilities, including interface to a computer cluster.

### 4-7.7.3 ISN Instrument Design Scope

The design scope of the ISN feature beamline instrument is a complete, from scratch design of a new instrument located in a new satellite building (building 444). The new instrument will be designed to provide the scientific scope given in section 3.1.

**Instrument Location** The In Situ Nanoprobe instrument will be located 220 m from the source of the 19-ID beamline in 19-ID-E enclosure, which is in a satellite station (building 444). The shielded enclosure will provide temperature stabilization, and be designed to minimize vibrations. The satellite building will also be designed to minimize vibrations and thermal drifts around the ISN enclosure.

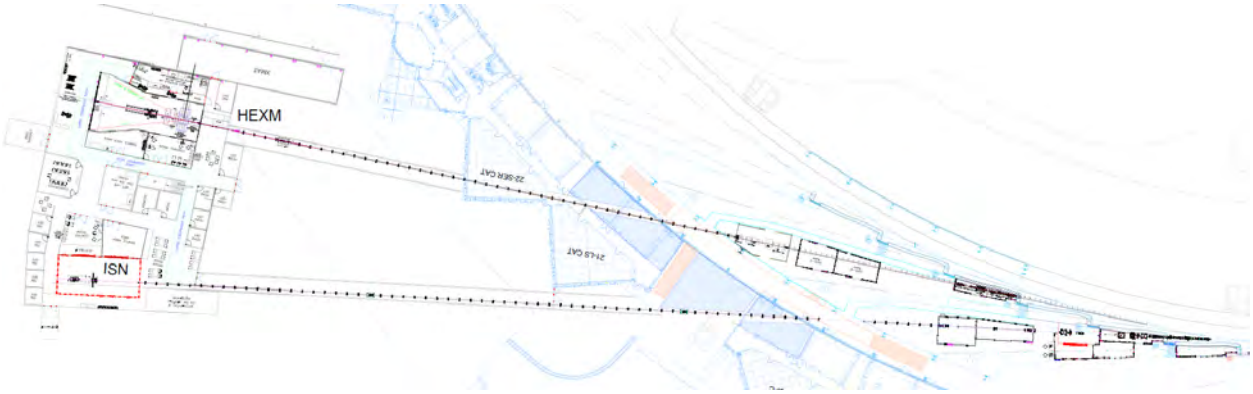


*Figure 4.48. Location of the ISN instrument. The instrument will be located at 220 m from the source in a new shielded enclosure (marked ISN in drawing).*

### 4-7.7.4 Instrument Operating Modes

**Beamline Modes** The ISN instrument will operate in a fixed exit K-B focused monochromatic nano beam mode only (4.8-30 keV). The instrument is also fixed in location.

**Experimental Methods** The following imaging modes will be used at the ISN instrument

Primary Imaging

- 2D/3D XRF mapping
- 2D/3D ptychography

Auxiliary Imaging

- XBIC/XBIV
- X-ray excited optical luminescence
- Structural imaging

### 4-7.7.5 Instrument Specifications

**Optics** The instrument will use a K-B mirror system, which includes the optics stages, metrology, and mirrors, to nano focus the beam to a 20 nm x 20 nm FWHM spot size at 25 keV, see Figure 4.49. To keep the nano focused spot within 10% of its central peak a 5 nrad stability of position is needed. The working distance will be a nominal 60 mm (reduced to 55 mm when including enclosure of K-B mirror system) from the end of the horizontal focusing mirror, see Figure 4.50. Orientation and dimensions of the mirrors is as shown in Figure 4.50.

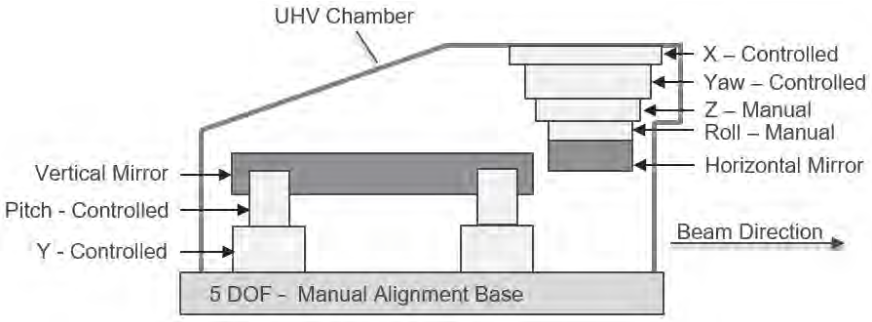


*Figure 4.49. Schematic of the general arrangement of K-B mirror system. The stages are shown in their respective mounting order, designated either controlled or manual, and have their direction of motion stated. See section 1.2 for coordinate frame.*

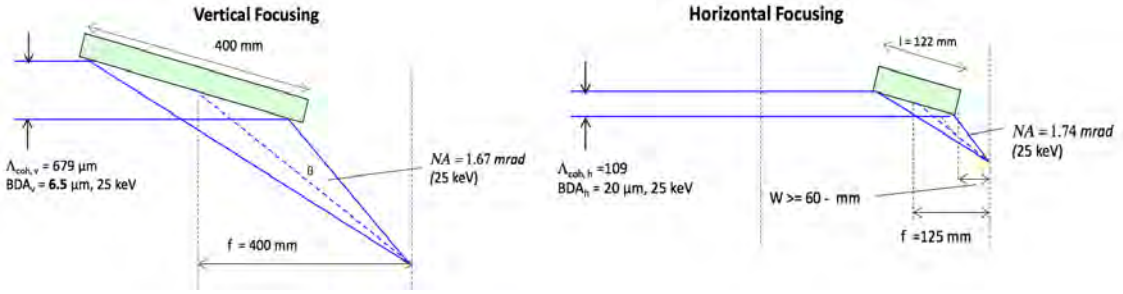


*Figure 4.50. Schematic of the K-B mirror system showing orientation and working distance. Vertical focusing is the first upstream mirror followed by the horizontal focusing mirror.*

A detailed description of the ISN Endstation instrument can be found in the 19-ID ISN Endstation Instrumentation ESD (ICMS Content ID: APSU_2030615).

## 4-8 CSSI 9-ID

At the center stage of the scientific topics, surface/interface phenomena are of great interest to scientists in a variety of fields. Imaging techniques provide ideal tools to directly observe surface/interface structures and monitor their dynamic evaluation responding to changes in external conditions. Much progress has been made in the development of hard x-ray sources and tools, including the development of storage-ring sources and x-ray free-electron-laser sources. Among all, grazing-incidence x-ray scattering and x-ray photon correlation spectroscopy (XPCS) exhibit unique advantages for exploring the surface/interface problems that are challenging to solve using other imaging techniques dynamics probes. The APS Upgrade will increase brightness by a factor of 100 to 1000 – clearly high-brightness and coherence are the cornerstones of the upgraded source. The x-ray beams from the upgraded source possesses a large coherent fraction, which is well suited for measuring the spatiotemporal evolution of structures in complex systems with the highest precision at surfaces and interfaces. A new beamline for coherent surface-scattering imaging (CSSI) takes advantage of the much improved x-ray beam coherence and is ideal for probing and understanding mesoscopic spatial-temporal correlations by integrating the coherence-based surface x-ray probe with state-of-the-art coherence-preserving optics and advanced x-ray detectors.

### 4-8.1 Scientific Objective

Surface/interface phenomena are of great interest to scientists in a variety of fields. More specifically, these challenging topics include, but are not limited to: evolution of biological membranes and supramolecules in aqueous environments, thin film and quantum dot growth at surfaces and interfaces, assembly of planner polymer nanocomposites, and structural analysis of three-dimensional (3D) nanoscaled electronic circuits using additive manufacturing. The temporal and spatial resolution promised by the upgraded sources such as the proposed APS low-emittance upgrade ideally matches the challenges of understanding mesoscaled structure and dynamics from nm to mm and ns to s. A few examples of scientific interests will be introduced in this section to show that coherent surface-scattering imaging technique can provide much needed structural and dynamical information to answer the following questions:

1. Hierarchical assembly of functional materials: how physical and chemical processes and dynamics are involved to lead to hierarchical order in mesoscopic structures and the functionalities;
2. How to advance nanopatterning using combination of top-down and bottom-up techniques for the controlled fabrication of complex and multicomponent nanomaterials that are needed for advanced functional applications;
3. How to control the morphology of thin-film based photovoltaic to optimize the efficiency of the devices; and
4. How do the dynamics at every level of the hierarchical structures control the complexity and specific functionalities of mesoscopic systems?

Those questions often need to be addressed in association with processes that involve non-equilibrium temporal evolution of structural complexity at molecular, nanoscopic, and mesoscopic scales [28]. More specifically, the CSSI beamline will be the prime user facility for the research will be include:

- Self-assembly of mesoscale structures at surfaces and interfaces,
- Three-dimensional surface nanopatterning and nanofabrication,
- Three-dimensional morphology of photovoltaic thin films,
- Dynamics at surfaces and interfaces revealed by GI-XPCS structure and dynamics,
- Capillary instability in confined geometry, and
- At-wavelength and in situ metrology for X-ray coherence preserving reflective optics.

Coherent surface-scattering imaging (CSSI) [29] will satisfy the needs for non-destructive, *in-situ* structure characterization with three-dimensional high resolution and temporal resolution afforded by the intense coherent x-ray beam from the upgraded APS. In the meantime, GI- XPCS is a complementary way to understand the interplay between the dynamics and structure in order to gain the control of the structure evolution in the materials processing.

### 4-8.2 Beamline Requirements for the Insertion Devices (IDs)

The source will be two inline undulators (each has a length of 2.3 m): one revolver with a period length of 21 mm / 25 mm (two different periods for each revolver), and one planner undulator with a period of 21 mm.

*Table 4.56. Source Parameters*

| **Unduator** | **Period** *(mm)* | **Length** *(m)* | **Location** | **Max Power*** *(kW)* |
|---|---|---|---|---|
| Revolver+planner | 21 | 4.6 | Center of the straight section | 2.10 [1] |
| Revolver | 25 | 2.3 | 1.25 m downstream of the center of the straight section | 0.81 [2] |

[1]Through the Front End Mask 2x2 $mm^2$ @ 25.4 m with Ky = 1.305.
[2]Through the Front End Mask 2x2 $mm^2$ @ 25.4 m with Ky = 1.939.

### 4-8.3 Beamline Requirements for the Front End

The CSSI beamline will utilize the new standard MBA High Heat-Load front end capable of handling a maximum power of 21 kW. The beamline will use a windowless exit configuration with a 2 mm x 2 mm (H x V) exit mask aperture.

A detailed description of the CSSI Front End and Insertion devices can be found in the APS-U 9-ID Beamline Front End and Insertion Devices Interface Control Document (ICMS Content ID: APSU_190936).

### 4-8.4 Beamline Layout

The design of the beamline aims to preserve the coherence properties and the wave front of the beam from 6 to 30 keV suitable for samples at both air-solid (or liquid) and liquid-liquid interfaces. The only wave front modifying optics will be focusing devices that deliver highest coherent photons to the samples in a diffraction limited micro-meter beam size in both monochromatic and pink forms. A long sample-to-detector distance ($>$ 20 m) is ensured to achieve sufficient speckle oversampling by pixel array detectors.

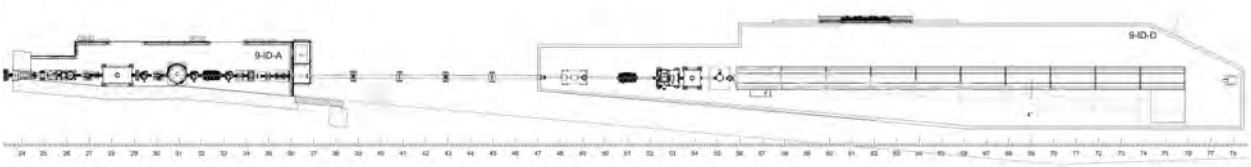

*Figure 4.51. Layout of CSSI beamline.*

### 4-8.4.1 Beamline Component Table

Table 4.57 shows all major beamline components.

*Table 4.57. CSSI beamline components*

| Distance from source (m) | Component | Description/Comments |
|---|---|---|
| 25.4 | FE Exit Mask | Standard HHL Front-End exit mask<br>2x2 $mm^2$ aperture |
| 26.1 | FE Collimator | Standard HHL Front-End Exit Collimator<br>5x5 $mm^2$ aperture |
| 27.1 | Slits, HHL | HHL WB Slits w/ Tungsten Edge inserts , 9ID-SL-1 |
| 28.25 | Mirror | Mirror, Horizontal, cooled , 9ID-MR-1 |
| 29.1 | Collimator | Collimator, Secondary, 9ID-SC-1 |
| 29.5 | Diagnostics | Diagnostics, WB/PB, 9ID-BD-1 |
| 29.9 | Slits | Slits, PB, H+V, 9ID-SL-2 |
| 30.65 | DCM, DMM | Monochromator, DCM / DMM, 9ID-MN-1 |
| 31.5 | Diagnostics | Diagnostics, PB/MB, 9ID-BD-2 |
| 32.4 | Transfocator | Transfocator / CRL-1, 9ID-TR-1 |
| 33.1 | Diagnostics | Diagnostics, PB/MB, 9ID-BD-3 |
| 33.8 | Mask | Mask, WB Stop, 9ID-PM-1 |
| 34.2 | Collimator | Collimator, 9ID-BC-1 |
| 35.5 | Shutter | Shutter, Pink, 9ID-SH-1 |
| 47.7 | Slits | Slits |
| 48.2 | Filters | Filters |
| 51.0 | Transfocator | Transfocator / CRL-2, 9ID-TR-2 |
| 54.0 | Mirror | Mirror, KB, 9ID-MR-2 |
| 55.0 | Sample Stage | Solid Sample Diffractometer and nanopositioning stages |
| 57.0 | Liquid Diffractometer | Liquid Diffractometer |
| 58.0-76.0 | Flight Path | In-vacuum flight path |
| 78.0 | Beam Stop | Beam Stop, PB, 8ID-BS-1 |

A detailed description of the CSSI beamline can be found in the CSSI 9-ID Photon Delivery System ESD (ICMS Content ID: APSU_2012711).

## 4-8.5 Optics Overview

### 4-8.5.1 Beam Delivery Specifications

The CSSI beamline will operate at the energy range of 6-30 keV. Three sets of optics, namely CRL-1, CRL-2 and KB mirrors, are placed at different locations, 33.2 m, 51 m and 54 m, respectively, to focus at the solid sample position of 55 m and liquid sample at 57 m. The Table 4.58 shows the

expected flux and focal spot sizes of the beamline at 8.8 keV and 26.4 keV at 55 m. The optical design and optics specification are listed in this document.

*Table 4.58. Expected flux and focal spot sizes of the beamline*

| **Energy** *(keV)* | **Optics** | **Coherent mode** | **Focal spot size** *μm* | **Flux** *(ph/s/0.1%BW)* |
|---|---|---|---|---|
| 8.8 | CRL-1: 1x0.2mm + 1x0.3mm+1x2mm | Full beam | 29x16 | $3.4x10^{14}$ |
| 8.8 | CRL-2: 1x0.05mm + 1x0.1mm | 3x2 | 3.5x1.7 | $9.4x10^{13}$ |
| 8.8 | KB | 3x2 | 0.75x0.42 | $9.2x10^{13}$ |
| 26.4 | CRL-1: 4x0.05mm | Full beam | 27x12 | $3.2x10^{13}$ |
| 26.4 | CRL-2: 14x0.05mm | 3x2 | 3.0x1.2 | $3.7x10^{12}$ |
| 26.4 | KB | 3x2 | 0.66x0.35 | $3.9x10^{12}$ |

### 4-8.5.2 Detailed Optical Layout

The optical layout scheme of CSSI beamline is shown in Figure 4.52.

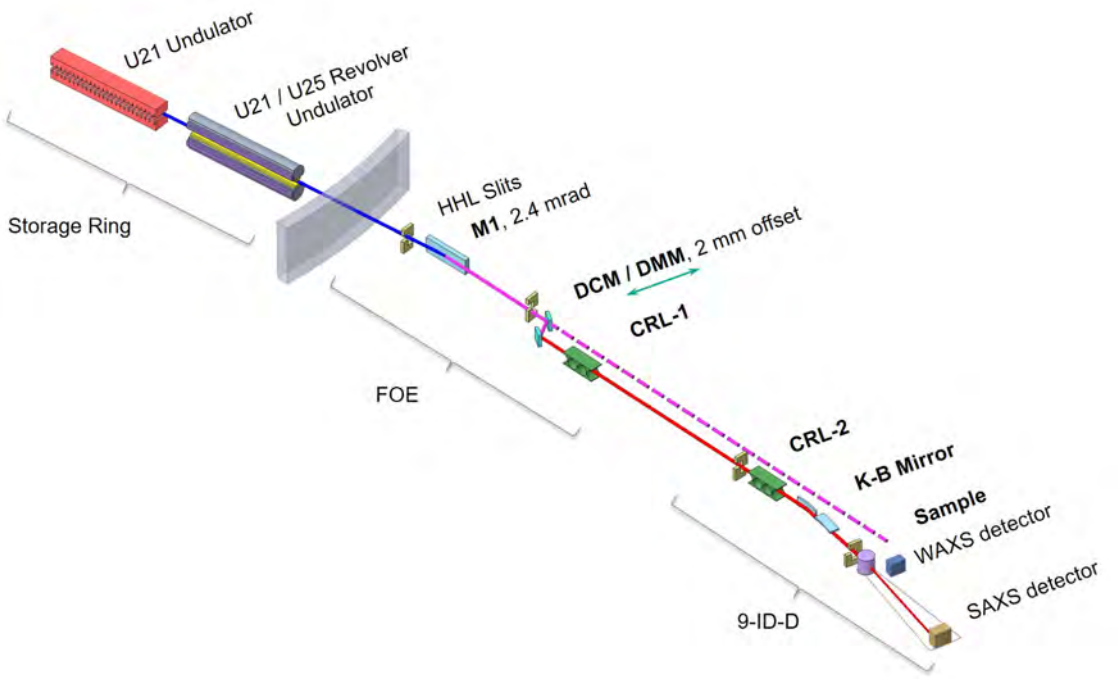


*Figure 4.52. Basic optical layout of the CSSI beamline*

### 4-8.5.3 Optical Simulation and Tolerances

Optical simulations were carried out using the ShadowOui program in the Oasys environment. The focal spot profiles of the CSSI beamline are shown in Figure 4.53.

The figure error on the KB mirrors is the most important optical parameter that affects the focal

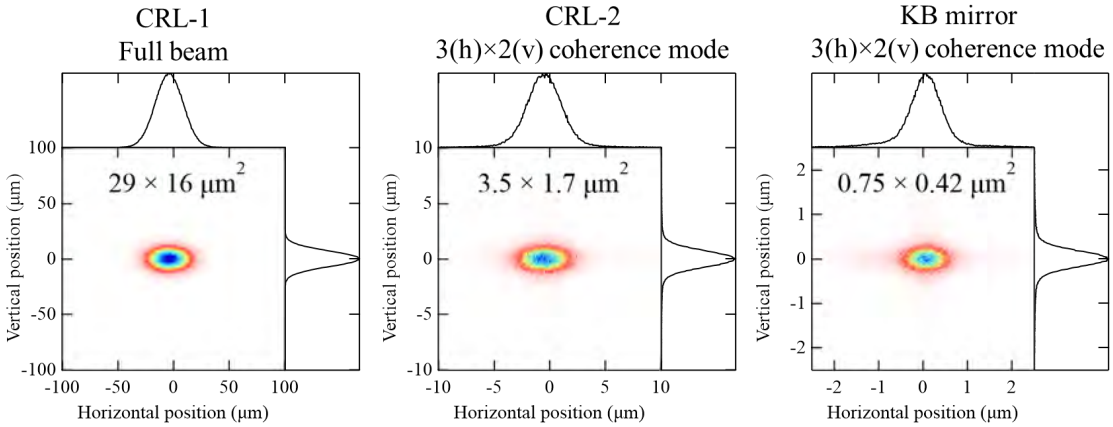


*Figure 4.53. Focusing optics layout of the CSSI beamline. Focal spots at the sample location (55 m) using (left) CRL-1 (32.4 m), (middle) CRL-2 (51 m) and (right) KB mirrors (54 m) of the CSSI beamline. The calculation was performed at 8.8 keV with (left) the full beam and (middle and right) a coherence mode of 3 (H)x2(V).*

spot size. Figure 4.54 shows the calculated RMS focal size and relative peak intensity as a function of the RMS figure height errors. To keep both the focal size broadening and the peak intensity drop less than 3%, the RMS figure error has to be smaller than 0.3 nm and 0.2 nm for KB(h) and KB(v) combined.

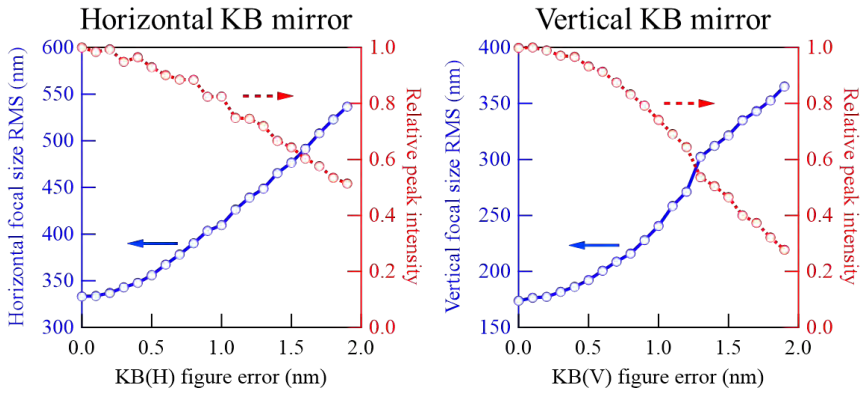


*Figure 4.54. Effects of KB mirror figure errors on the focal spot.*

### 4-8.5.4 Optics Specifications

**HHL Mirrors** The horizontally deflecting mirror will be the first optical component of the CSSI beamline. It will be located in enclosure A and operate at a reflection angle of 2.4 mrad. The mirror will be flat with the notch design to reduce the thermal induced deformation. The mirror will have three reflecting stripes (bare Si, Pd, and Pt) to provide harmonic rejection and cover the operational energy range. Vertical translation is required to change the reflecting stripe used.

**HHL Double Crystal Monochromator** The HDCM is a standard double-crystal monochromator with a pair of pseudo channel cut liquid-nitrogen cooled crystals Si(111), and fixed exit operation. The HDCM will require precision positioners with typical specifications given in the table below.

**Transfocators** Variable numbers and types (radii) of CRLs are required to achieve the focusing requirements for the CSSI beamline. In the two beamline locations where CRLs are specified, a so-called transfocator is the device selected for achieving this. Requirements for the transfocator are UHV compatibility, x/y/z translations, and pitch/yaw rotations, and the ability to precisely remove and insert variable numbers of lenses. The arrangement of individual lenses of the 9ID-CL-1 and 9ID-CL-2 transfocator systems is shown in the table below.

*Table 4.59. Arrangement of individaul lenses of the transfocator*

| CRL-1 | | | | | | | | | | | | |
|---|---|---|---|---|---|---|---|---|---|---|---|---|
| Stack | 1 | 2 | 3 | 4 | 5 | 6 | 7 | 8 | 9 | 10 | 11 | 12 |
| Type | 2D | 2D | 2D | 2D | 2D | 2D | 2D | 2D | 2D | 1D | 1D | 1D |
| $N$ | 1 | 1 | 1 | 1 | 1 | 1 | 2 | 4 | 4 | 1 | 1 | 2 |
| $R$, µm | 2000 | 1000 | 500 | 300 | 200 | 100 | 100 | 100 | 100 | 2000 | 1000 | 1000 |
| CRL-2 | | | | | | | | | | | | |
| Stack | 1 | 2 | 3 | 4 | 5 | 6 | 7 | 8 | 9 | 10 | 11 | 12 |
| Type | 2D | 2D | 2D | 2D | 2D | 2D | 2D | 2D | 2D | 2D | 1D | 1D |
| $N$ | 1 | 1 | 1 | 1 | 1 | 1 | 2 | 4 | 8 | 8 | 1 | 2 |
| $R$, µm | 1000 | 500 | 300 | 200 | 100 | 50 | 50 | 50 | 50 | 50 | 1000 | 1000 |

**Experimental Station KB Mirror System** The KB mirrors will be located in the end-station E and operate at a reflection angle of 2.5 mrad. Both mirrors will be bendable flat mirrors with Pt coating. The vertical KB (horizontal KB) mirror located 1000 mm (800 mm) upstream of the sample location focuses the beam vertically (horizontally). Each mirror will require precision positioners with specifications given in the table below

### 4-8.5.5 Heat Load Considerations

The HHL mirror will reduce the power passed on to the downstream optics. Table 4.60 and Table 4.61 summarize the maximum power expected to be absorbed by various components with the closed gap U21 undulators.

*Table 4.60. Power Calculations for M1 with the Si stripe.*

| **Undulator** | **K** | **Mono Energy** *(keV)* | **Incident power on M1*** *(W)* | **Power absorbed by M1** *(W)* | **Power Density on M1** *(W/mm$^2$)* |
|---|---|---|---|---|---|
| U21 | 1.305 | 8.8 (1$^{st}$) | 474 | 311 | 0.82 |

*Based on the mirror acceptance of 0.96 x1.0 mm$^2$.

*Table 4.61. Power Calculations for HDCM.*

| **Undulator** | **K** | **Mono Energy** *(keV)* | **1st crystal Angle** | **Beam Size at Mono (HxV)** *(mm x mm)* | **Beam Footprint (HxV)** *(mm x mm)* | **Power absorbed** *(W)* | **Power Density** *($W/mm^2$)* |
|---|---|---|---|---|---|---|---|
| U21 | 1.305 | 8.8 ($1^{st}$) | 13.0° | 1.04 x 1.08 | 4.65 x 1.08 | 163 | 34.2 |

The HHL mirror deformation can be reduced by an order of magnitude by adding a notch to the mirror side. The HDCM deformation is minimized by optimizing the $LN_2$ cooling. Figure 4 shows the smallest focal spot at the sample location with and without thermal induced deformations on HHL mirror and HDCM. The broadening on the focal spot is within the tolerance. The zoom CRL-KB system can be also used to improve the focus.

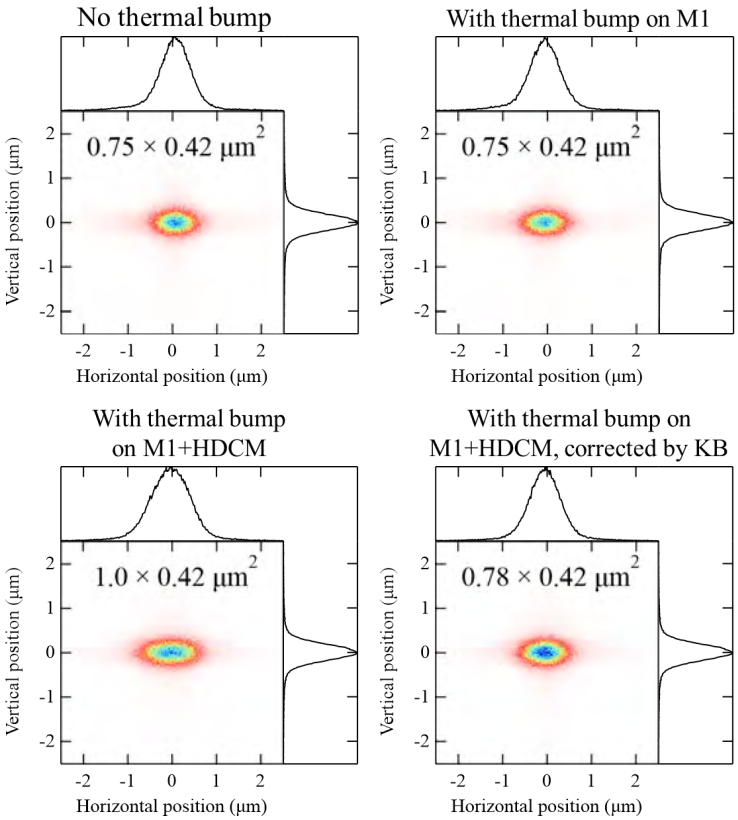


*Figure 4.55. Beam profile at the sample location without thermal deformation (top left) and with thermal deformations on M1 (top right) and on both M1 and HDCM (bottom left), and after correction by the bendable KB mirrors and CRL's (bottom right).*

A detailed description of the CSSI optics can be found in the CSSI 9-ID Optics ESD (ICMS Content ID: APSU_2030435).

## 4-8.6 Instrument Overview

### 4-8.6.1 Scientific Scope

This instrument is dedicated to surface coherent scattering and imaging techniques:

- Coherent Surface-Scattering Imaging (CSSI)
- Grazing Incidence X-ray Photon Correlation Spectroscopy (GIXPCS)
- Grazing Incidence Small-Angle and Wide-Angle X-ray Scattering (GISAXS/WAXS)

These imaging techniques will provide observations of surface structures and liquid/liquid or liquid/gas interface structures. The dynamic evolution of these structures and their response to changes in external conditions will also be observed. The increased brightness and coherence of the beam provide by the APS Upgrade will allow for non-destructive, in-situ structure characterization with high three-dimensional resolution and high temporal resolution.

Prime areas of research for the instrument:

- Self-assembly of mesoscale structures at surfaces and interfaces
- Three-dimensional surface nano-patterning and nano-fabrication
- Three-dimensional morphology of photovoltaic thin films
- Dynamics at surfaces and interfaces revealed by GI-XPCS structure and dynamics
- Capillary instability in confined geometry
- At-wavelength and in-situ metrology for X-ray coherence preserving reflective optics.

### 4-8.6.2 Instrument Definition

The end-station instrument consist of the following components of:

- Local Beam Conditioning
- Solid Sample coherent scattering imaging Assembly
- Liquid Sample coherent scattering imaging Assembly
- long beam path between sample and the detectors
- Metrology and supporting hardware for monitoring sample and optic motion

### 4-8.6.3 Instrument Location

### 4-8.6.4 Instrument Operating Modes

The instrument will operate with mono and pink beam of reduced size and power at a fixed height of 1400 mm.

A detailed description of the CSSI Endstation instrument can be found in the 9-ID CSSI Endstation Instrumentation ESD (ICMS Content ID: APSU_203064).

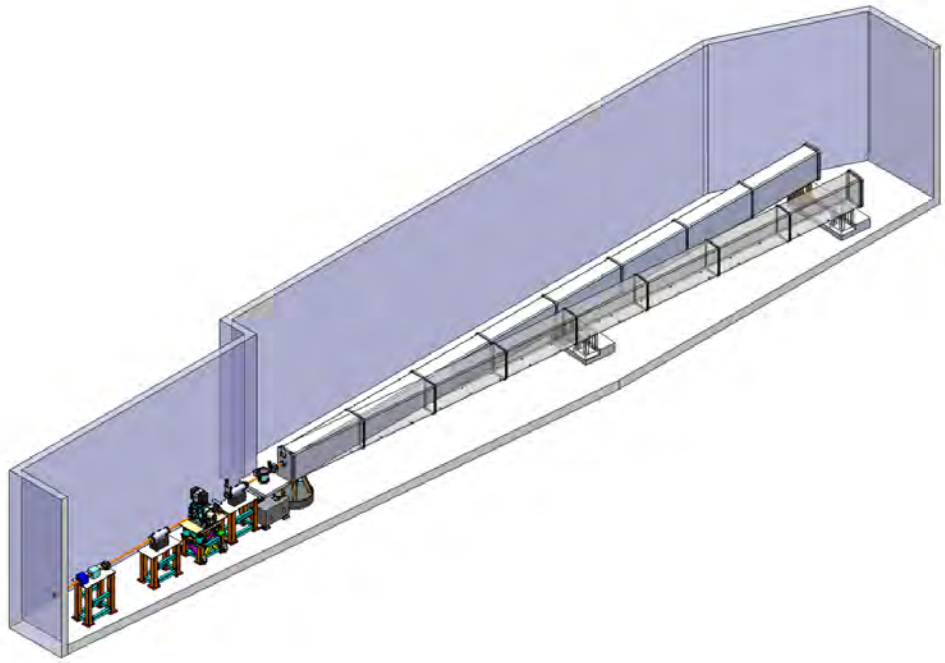

*Figure 4.56. End-Station instrument Layout*

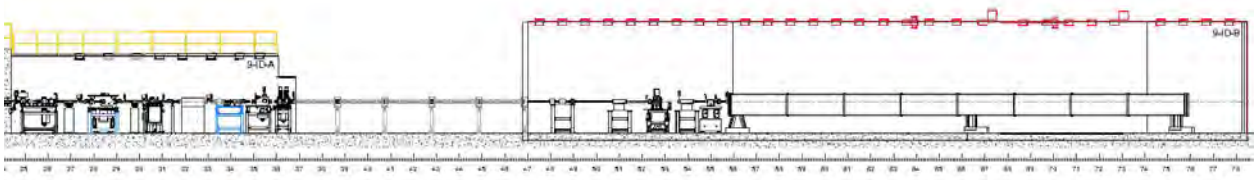

*Figure 4.57. Beamline layout and location of the CSSI instrument at 9-ID-B, shown in the red dashed box.*

# 4-9 3DMN/ATOMIC 34-ID

## 4-9.1 Introduction

The 3D Micro & Nano Diffraction (3DMN) and ATOMIC beamlines share a canted front end at Advanced Photon Source (APS) beamline 34-ID. This document includes information on the 3DMN/ATOMIC beamline and its associated end station.

## 4-9.2 Scientific Objective 3DMN

In the first part of the last century, great advances were made in understanding the mechanical and electrical properties of materials by assuming a simple perfect crystal structure. However, it was always recognized that the real properties of a material often depend critically upon the defects and spatial inhomogeneities that were either induced or inherent in the material. For example, the strength of copper changes drastically with even the simplest work hardening, and in strongly correlated electron systems, local phase separation and competition give rise to exotic macroscopic electronic properties such as colossal magnetoresistance or ferroelectric domains, to name just two. For these and many other examples, just knowing the average strain or the average structure is not good enough to understand new and interesting properties; one needs to know the local spatial distribution of strain and structure. The common theme in all of these cases is that inhomogeneous local interactions give rise to fundamentally interesting and technologically important physical phenomena. Moreover, in all of these cases, the "3D micro- and nano-diffraction" capabilities specified here provides critically needed, previously unavailable, quantitative descriptions of these local mesoscopic interactions. Illuminating the underlying microstructural mechanisms is imperative for understanding materials behavior, guiding the development of new materials, improving processing techniques, and developing predictive modeling capabilities.

The 3DMN beamline is designed to directly attack a wide range of spatially inhomogeneous materials problems at the mesoscopic length scale. These are problems in materials science, physics, geoscience, and most other fields of science where previous x-ray diffraction techniques are insufficient due to the short length scale of the inhomogeneities in the materials. This inhomogeneity is an important or intrinsic part of the material's properties, and so must be studied on the short length scale of the actual structure; large perfect samples are either impossible to make or do not represent the real material. Due to the current extreme difficulty or impossibility of making these measurements, the bright multi-bend achromat (MBA) APS Upgrade source will be utilized to provide small, intense x-ray spots (50-200 nm) to investigate the important spatial variations and correlations of strain and structure that define this wide range of scientifically and technologically important materials.

The 3DMN beamline provides users with scientific access to a suite of scanning-diffraction instruments unique in the world. These instruments use highly focused beams to measure the local lattice structure, orientation, and strain tensor with point-to-point spatial resolution. The size of the focused x-ray beams in the micro-/nano-diffraction station range from ~50 nm to 200 nm in size, enabling the user to match the probe size to the fundamental scale of the diffraction problem with a minimum of angular divergence in order to provide the highest possible resolution in both reciprocal space and real space. The ability to easily alternate between polychromatic (Laue) and tunable monochromatic diffraction modes is a key feature enabling users to study a much wider range of

randomly oriented or polycrystalline "real" materials. Because the station is physically located at a large distance from the x-ray source, the focusing optics have sufficient working distance to permit the use of the sample environments that are an important part of the scientific case including control of pressure, sample temperature, electric and magnetic fields, and mechanical forces. Finally, the ability to obtain spatially resolved structural information in all three dimensions (i.e., quantitative, nanoscale-resolution, three-dimensional structural microscopy) enables scientific investigations that cannot be accomplished with other experimental techniques

The proposed MBA lattice for the APS storage ring is primarily designed to increase the source brightness by a factor of ~100. Since the focused beam envisioned in this proposal is a direct image of the source, the focused spot size and intensity improves linearly with the brightness. The sub-50-nm resolution dramatically improves the ability to identify dislocations and other defects. Simultaneous measurement of strain and dislocation motion are directly compared to calculations of dislocation dynamics. With the direct use of brightness, this beamline is almost ideally matched to the MBA upgrade.

### 4-9.3 Scientific Objective ATOMIC

The ATOMIC beamline allows study of materials using coherent diffraction techniques, with a spatial resolution of 1 nm or below. As such the beamline is designed to extract and propagate a coherent wavefront from the front-end exit window onto the sample. The beamline also allows "zooming", enabling x-ray spot sizes of 50 nm–1.5μm to match the beam size to the requirements of an experiment. The x-ray optics of beamline and instrument are designed to provide a working distance of ~50 mm, enabling a broad range of *in situ* and *operando* capabilities for materials studies under applied external fields, under gases and fluids, and with variable temperature.

The ATOMIC beamline enables high-resolution studies of the interrelated structural, chemical, and physical properties exhibited by advanced functional materials. Few structural techniques possess sensitivity to local atomic structure across the range of 10s of nanometers to micrometers of sample volume and also permit *in situ* and *operando* investigations1. Typically, atomic and mesoscale information is gathered by a variety of techniques on micrometer- and millimeter-size samples. Modeling and simulation are then employed to extract a plausible narrative of the structural and functional properties of that sample. There is a strong need for a single technique that can acquire atomistic structural information across many length scales in full three-dimensional detail. The combination of that capability with *in situ* and *operando* environmental cells promises to have a transformative impact on many disciplines of science.

The ATOMIC beamline provides this capability by using x-ray coherent-diffractive imaging, both measured around Bragg peaks of a crystalline sample for strain sensitivity and pushed to its ultimate limit of atomic resolution. It is inherently a probe of atomic structure, as the wavelengths of hard x-rays are on the scale of atoms. At the deepest level, the x-rays are either scattered or absorbed as they interact with the electron density surrounding atoms. This electron density can be imaged within the sample with any form of contrast giving rise to a coherently scattered signal. Coherent diffractive imaging permits a remarkable gain in image resolution over that achieved through optics by carefully measuring interference patterns formed from waves scattered by a sample. The ultimate resolution of the image is not governed by the short working distances of high-resolution x-ray optics. It is this fact that enables *in situ* and *operando* experiments.

### 4-9.4 Beamline Requirements for the Insertion Devices (IDs)

34ID will have a 2.8 cm period planar undulator for the outboard canted branch (3DMN) and a 2.5 cm / 2.1 cm period revolver undulator for the inboard canted branch (ATOMIC).

*Table 4.62. 3DMN/ATOMIC Source Parameters*

| Beamline | Undulator | Period *(mm)* | Length *(m)* | Location | Max Power *(W)* |
|---|---|---|---|---|---|
| 3DMN | Planar | 28 | 2.1 | Upstream | 777 [1] |
| ATOMIC | Revolver | 21/25 | 2.1 | Downstream | 763/738 [2] |

1 Through the Front End Mask 2x2 $mm^2$ @ 30 m with Ky = 2.459.
[2] Through the Front End Mask 2x2 $mm^2$ @ 30 m with Ky = 1.939/1.305.

### 4-9.5 Beamline Requirements for the Front End

The 3DMN/ATOMIC 34ID beamline will have a canted undulator (CU) front end capable of handling two beams separated by 1 mrad canting angle and 10 kW power each. The beamline will have a windowless exit configuration with a 2 mm x 2 mm (H x V) exit aperture for each branch.

A detailed description of the 3DMN/ATOMIC 34ID Front End and Insertion devices can be found in the APS-U 34-ID Beamline Front End and Insertion Devices Interface Control Document (ICMS Content ID: APSU_190962).

### 4-9.6 Beamline Layout

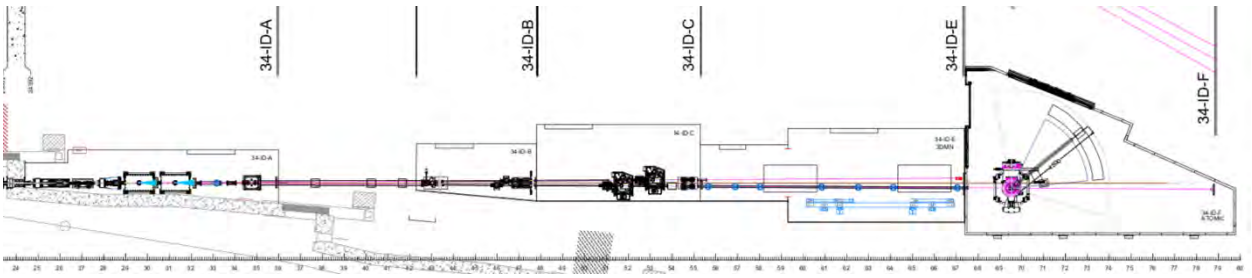


*Figure 4.58. Layout of 3DMN/ATOMIC beamline.*

#### 4-9.6.1 Beamline Component Table

The following table shows all major beamline components and their general location along the beamline.

A detailed description of the 3DMN/ATOMIC beamline can be found in the 3DMN/ATOMIC 34-ID Photon Delivery System ESD (ICMS Content ID: APSU_2012717).

*Table 4.63. 3DMN/ATOMIC Beamline Component Table*

| **Distance from source** *(m)* | **Component** | **Designation** | **Description/Comments** |
|---|---|---|---|
| 25.4 | FE Exit Mask | | Standard canted front-end exit mask<br>2X 2x2 $mm^2$ aperture |
| 26.1 | FE Collimator | | Standard canted front-end exit collimator<br>2X 5x5 $mm^2$ aperture |
| 26.8 | CUFE WB Slits (Inboard) | 34ID-SL-1 | Canted Undulator Variable Aperture<br>Photon Absorber w/ Tungsten Edge inserts |
| 27.3 | CUFE WB Slits (Outboard) | 34ID-SL-2 | Canted Undulator Variable Aperture<br>Photon Absorber w/ Tungsten Edge inserts |
| 28.4 | Collimator | 34ID-BC-1 | Tungsten Collimator |
| 28.7 | Collimator | 34ID-BC-2 | Lead Collimator |
| 29.6 | Mirror | 34ID-MR-1 | Mirror, Flat, Horizontal, Outboard (3DMN) |
| 30.3 | Secondary Collimator | 34ID-SC-1 | Secondary Bremsstrahlung Collimator |
| 31.3 | Mirror | 34ID-MR-2 | Mirror, Flat, Horizontal, Inboard (Atomic) |
| 32.2 | Secondary Collimator | 34ID-SC-2 | Secondary Bremsstrahlung Collimator |
| 32.5 | Beam Diagnostic | 34ID-BD-1 | Diagnostic Flag |
| 34.0 | Photon Mask | 34ID-PM-1 | Pink Photon Mask / WB Stop |
| 36.0 – 42.5 | Shielded Transport | 34ID-ST-1 | Existing WB shielded Transport |
| 46.9 | Photon Mask | 34ID-PM-2 | Photon Mask (Inboard, Pink Beam) |
| 46.9 | Photon Mask | 34ID-PM-3 | Photon Mask (Outboard, Pink Beam) |
| 47.3 | Collimator | 34ID-BC-3 | Lead Collimator / Bremsstrahlung Stop |
| 49.7 | Beam Diagnostic | 34ID-BD-2 | BPM (Inboard, Atomic) |
| 50.3 | Slits | 34ID-SL-3 | Slits (Inboard, Atomic) |
| 51.0 | Monochromator | 34ID-MN-1 | DCM Monochromator (Atomic) |
| 52.0 | K-B Mirror | 34ID-MR-3 | K-B Mirror (Atomic) |
| 52.7 | Beam Diagnostic | 34ID-BD-3 | BPM (Outboard, 3DMN) |
| 53.1 | Slits | 34ID-SL-4 | Slits (3DNano) |
| 53.8 | Monochromator | 34ID-MN-2 | DCM Monochromator (3DMN) |
| 54.8 | Photon Shutter | 34ID-SH-1 | Pink Beam Shutter (Inboard, Atomic) |
| 54.8 | Photon Shutter | 34ID-SH-2 | Pink Beam Shutter (Outboard, 3DMN) |
| 55.1 - 67.5 | Shielded Transport | 34ID-ST-2 | Shielded pipe through 34-ID-E to deliver beam to Atomic endstation, 34-ID-F |
| 60.0 | Endstation Instrumentation | 34ID-BI-1 | 3D Micro Endstation Instrument |
| 65.5 | Endstation Instrumentation | 34ID-BI-2 | 3D Nano Endstation Instrument |
| 66.9 | Beam Stop | 34ID-BS-1 | Beam Stop, Pink, Outboard |
| 68.1 | Mirror | 34ID-MR-4 | K-B Mirror (Atomic) |
| 69.5 | Endstation Instrumentation | 34ID-BI-3 | Atomic Endstation Instrument |
| 78.7 | Beam Stop | 34ID-BS-2 | Beam Stop, Pink, Inboard |

## 4-9.7 Optics Overview

### 4-9.7.1 Beam Delivery Specifications

The 3D Micro & Nano Diffraction and ATOMIC beamlines will share a canted front end at 34-ID. Both beamlines will operate at the energy range of 5.3-30 keV.

The 3DMN beamline will deliver a pink or monochromatic beam with fixed spots (200 and 50 nm) at two sample locations with the micro-focusing and nano-focusing setups. Table 4.64 shows the expected flux and focal sizes of the 3DMN beamline at 14 keV.

*Table 4.64. The expected flux and focal sizes of the 3DMN beamline at 14 keV.*

| **3DMN** | **Mode** | **Horizontal size** *(nm)* | **Vertical size** *(nm)* | **Flux (ph/s/0.1%BW)** |
|---|---|---|---|---|
| Micro-focusing | Brightness | 103 | 68 | $4.9 \times 10^{12}$ |
| | Timing | 91 | 100 | $4.0 \times 10^{12}$ |
| Nano-focusing | Brightness | 37 | 37 | $4.9 \times 10^{11}$ |
| | Timing | 38 | 37 | $3.9 \times 10^{11}$ |

The ATOMIC beamline will deliver a coherent beam with variable focal spot sizes of 50 nm – 2$\mu$m. The table below shows the expected flux at 8.7 keV with variable focal spot sizes.

*Table 4.65. The expected flux at 8.7 keV with variable focal spot sizes for ATOMIC beamline.*

| **ATOMIC** | **Zoom focusing condition** | **Flux** *(ph/s/0.1%BW)* |
|---|---|---|
| Brightness mode | 50 nm | $3.1 \times 10^{12}$ |
| | 2 $\mu$m | $4.6 \times 10^{12}$ |
| Timing mode | 50 nm | $1.8 \times 10^{12}$ |
| | 2 $\mu$m | $2.5 \times 10^{12}$ |

### 4-9.7.2 Optical Simulation and Tolerances

Optical simulations were carried out using the ShadowOui program in the Oasis environment. Figure 4.59 is an optical layout of both the 3DMN and ATOMIC beamlines.

**3DMN beamline** The 3DMN beam profiles in the micro-focusing and nano-focusing setups are shown in Figure 4.60.

The figure error on the KB mirrors is the most important optical parameter that affects the focal spot size. Figure 4.61 shows the calculated RMS focal size and relative peak intensity as a function of the RMS figure height errors on the micro-focusing and nano-focusing KB mirrors. To keep both the focal size broadening and the peak intensity drop by less than 10%, the RMS figure error has to be smaller than 0.75 nm and 0.5 nm for the micro-focusing KB(h) and KB(v) and smaller than 0.5 nm and 0.4 nm for the nano-focusing KB(h) and KB(v), respectively.

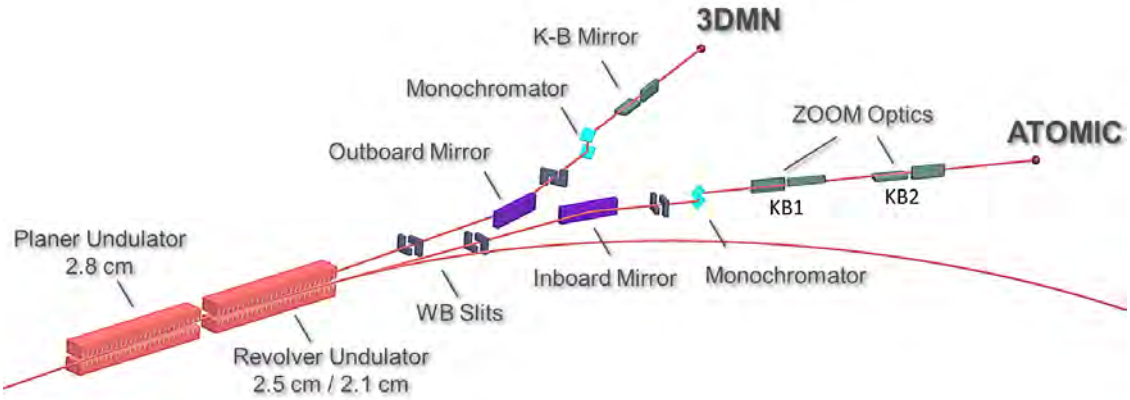


*Figure 4.59. Optical layout of 3DMN and ATOMIC beamlines.*

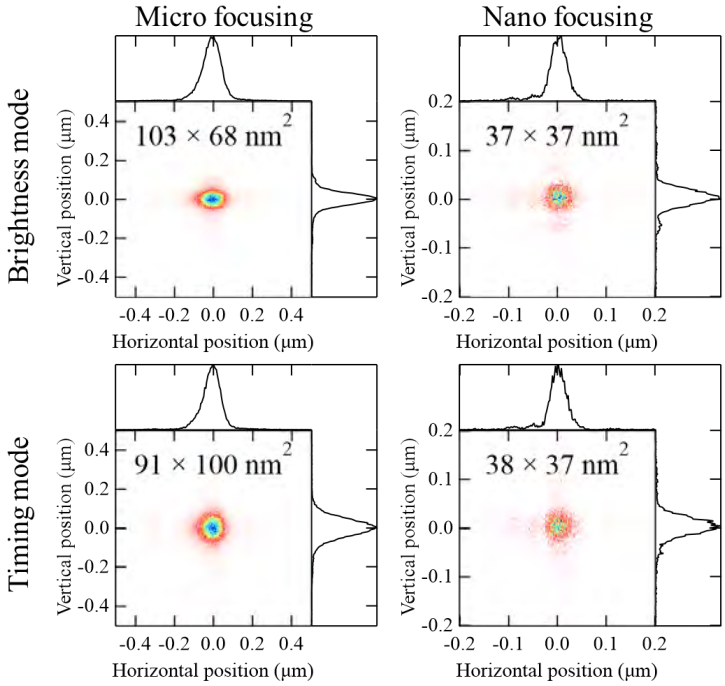


*Figure 4.60. Focal spots at (left) the micro-focusing setup (60 m) and (right) the nano-focusing setup (65 m) for the brightness (top) and the timming (bottom) mode of the machine for the 3DMN beamline. The calculation was performed at 14 keV. All mirrors were simulated with the specified figure.*

### 4-9.7.3 ATOMIC beamline

The zoom focusing capability of the ATOMIC beamline is shown in Figure 4.62.

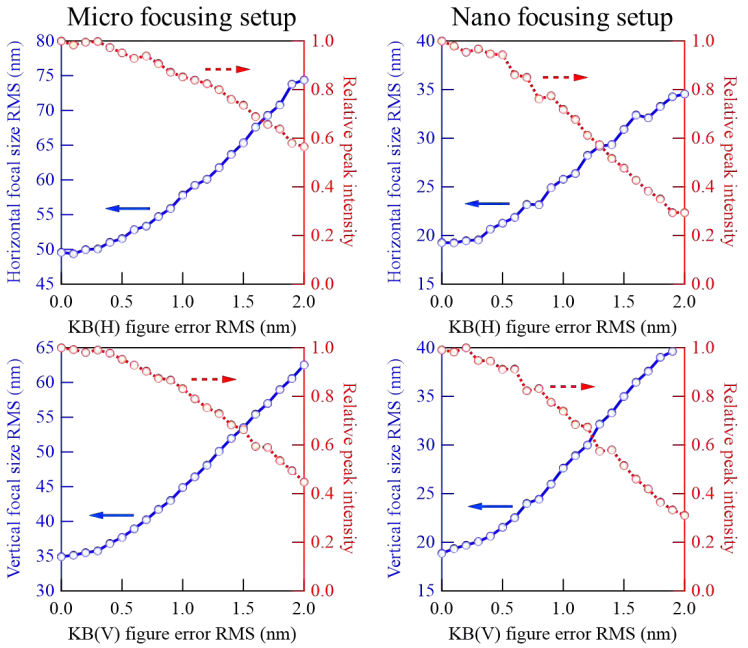


*Figure 4.61. Effects of KB mirror figure errors on the focal spot at (left) the micro-focusing setup (60 m) and (right) the nano-focusing setup (65 m) for the 3DMN beamline. The calculation was performed at 14 keV. The RMS slope error on OM is 0.1 μrad.*

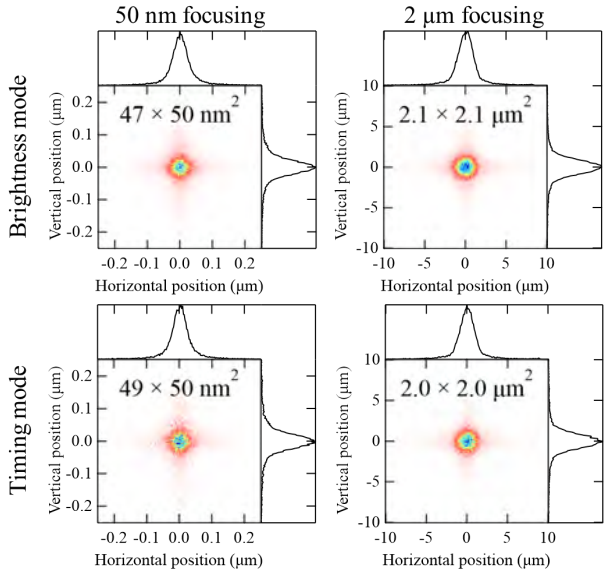


*Figure 4.62. The ATOMIC beamline will provide variable focal spot sizes from 50 nm (left) to 2μm (right) with both the brightness (top) and the timming (bottom) mode of the machine. The calculation was performed at 8.7 keV.*

Figure 4.63 shows the calculated RMS focal size and relative peak intensity as a function of the RMS figure height errors on the two KB mirror pairs. To keep the focal size broadening and the peak intensity drop to less than 10%, the RMS figure error has to be smaller than 1.0 nm for all KB mirrors.

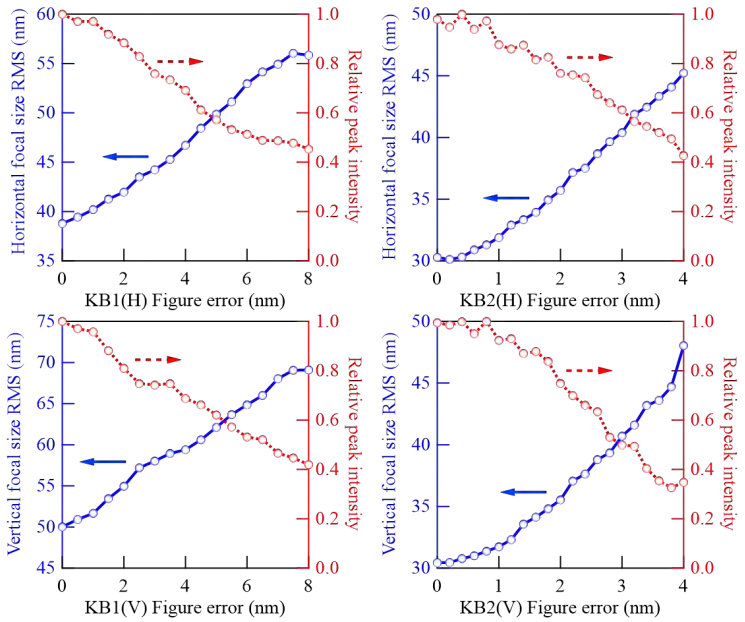


*Figure 4.63. Effects of KB mirror figure errors on the focal spot for the ATOMIC beamline.*

### 4-9.7.4 Optics Specifications

**HHL Mirror** The inboard mirror (IM) and outboard mirror (OM) will be the first optical components of the ATOMIC and 3DMN beamlines, respectively. They will be located in enclosure A and operate at a reflection angle of 3.0 mrad in the horizontal plane. Both mirrors will be flat with the notch design to reduce the thermal induced deformation. These mirrors will each have three reflecting stripes (bare Si, Rh, and Pt) to provide harmonic rejection and cover the operational energy range. Vertical translation is required to change the reflecting stripe used.

**Double Crystal Monochromator** Both the 3DMN and ATOMIC beamlines will have a horizontally deflecting double-crystal monochromator (HDCM) operating in the energy range of 5.3-30 keV. The monochromator is an unusual type with a very small offset (~1.1 mm).

Both beamlines require that the monochromator have a pink-beam bypass mode. A typical experiment employs a pink-beam Laue diffraction measurement to index the Bragg peaks from the sample. This is followed by a monochromatic measurement of a single Bragg peak for known reflection determined by the indexed pink-beam data. In order to accomplish this, the pink and monochromatic beams must intersect and intercept the sample at a fixed position. To achieve this, a heater is placed under the second monochromator crystal to control its lattice parameter by taking advantage of the thermal expansion of silicon. This way the angle of outgoing monochromatic beam can be tuned relative to the pink-beam such that it intersects the pink beam at the sample position. For this

technique, typical temperature differences between the first and second crystals are ~60°K.

**3DMN KB mirrors** The micro-focusing and nano-focusing KB mirrors for 3DMN beamline will be located in the end-station E at 60 m and 65.5 m, respectively, and operate at a reflection angle of 3.0 mrad. Both pairs of mirrors will be prefigured elliptical cylinder with Pt coating. Each mirror will require precision positioners with specifications given in the table below.

**ATOMIC zoom KB mirrors** The zoom KB system for the ATOMIC beamline contains two pairs of bendable KB mirrors. The first KB pair will be located in station C at 54 m, and the second KB pair will be located in the end-station F at 69 m. Each mirror will require precision positioners with specifications given in the table below.

The maximum and minimum profiles for each mirror operating at 3 mrad incidence are shown in Figure 4.64. The mirrors will most likely have a pre-figure at an optimal profile and be deformed in both directions to achieve the full range of focal spot sizes. The pre-figure will give a predetermined spot size with no active actuation of the mirror shapes. To improve the transmission of the optical system at lower x-ray energies the KB mirrors can be operated at greater incidence angle. The extremum profiles required for a 50 nm beam at 5 mrad are shown in Figure 4.65 compared with the profiles required at 3 mrad.

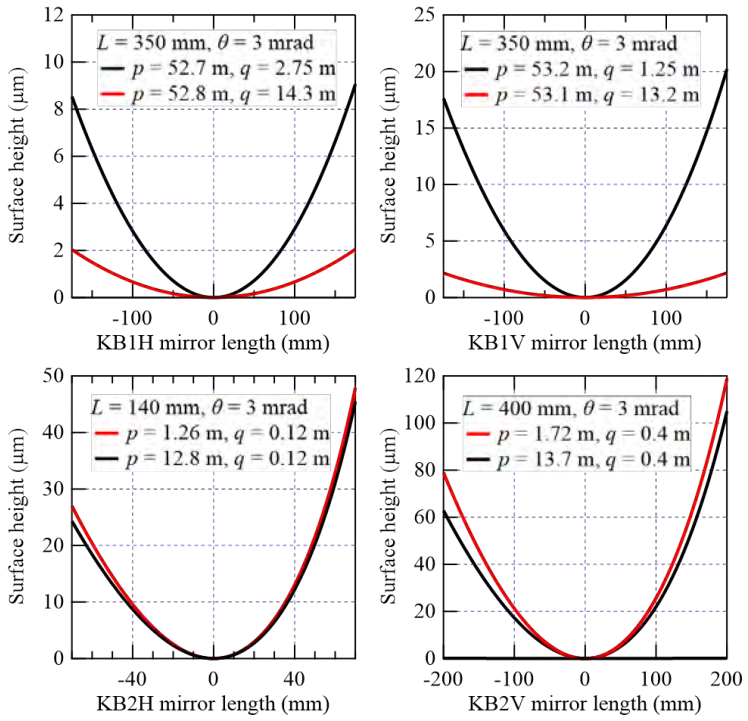


*Figure 4.64. The maximum and minimum bending profiles of each mirror to achieve zoom focusing from 50 nm to 2 μm at 3 mrad incidence.*

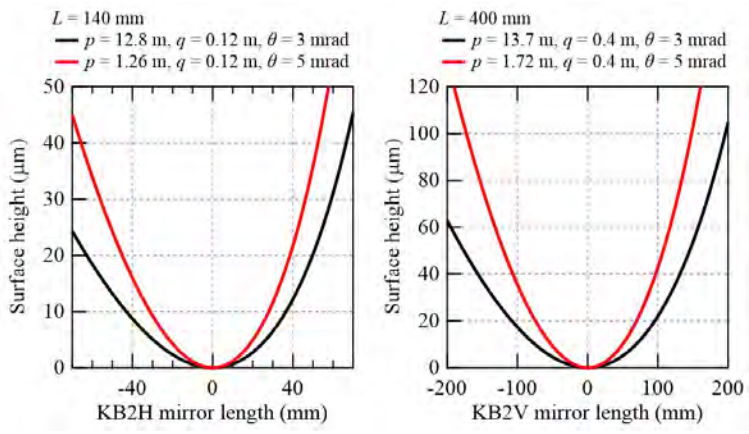


*Figure 4.65. The maximum and minimum bending profiles of each mirror to achieve 50 nm focussing at 3 and 5 mrad incidence.*

### 4-9.7.5 Heat Load Considerations

The HHL mirrors will reduce the power passed on to the downstream optics. The thermal management of both beamlines is very similar. Here we take the worst case of the 3DMN beamline as an example. Table 4.66 and Table 4.67 summarize the maximum power expected to be absorbed by various components.

*Table 4.66. Power Calculations for the OM (1 mm x 1 mm acceptance) of the 3DMN beamline.*

| **Undulator** | **K** | **Mono Energy (keV)** | **Incident power on M1 (W)** | **Mirror coating** | **Power absorbed by OM (W)** | **Power Density on OM (W/mm²)** |
|---|---|---|---|---|---|---|
| U28 | 2.459 | 9.1 ($3^{rd}$) | 226 | Si | 189 | 0.48 |
| U28 | 2.231 | 10.5 ($3^{rd}$) | 204 | Rh | 120 | 0.30 |

*Table 4.67. Power Calculations for the HDCM with 0.3 mm x 0.3 mm acceptance of the 3DMN beamline.*

| **Undulator** | **K** | **Mono Energy Mono Energy (keV)** | **1st crystal Angle** | **Beam Footprint (HxV) (mm x mm)** | **Power absorbed (W)** | **Power Density (W/mm²)** |
|---|---|---|---|---|---|---|
| U28 | 2.459 | 9.1 ($3^{rd}$) | 12.5Âř | 1.4 ÃŮ 0.3 | 0.94 | 2.24 |
| U28 | 2.231 | 10.5 ($3^{rd}$) | 10.9Âř | 1.6 ÃŮ 0.3 | 2.24 | 4.84 |

The HHL mirror deformation can be reduced by an order of magnitude by adding a notch to the mirror side. Figure 4.66 shows the focal spot at the micro-focusing and nano-focusing setups without and with thermal induced deformations on the OM. The mirror deformation has negligible effects owing to the notch design.

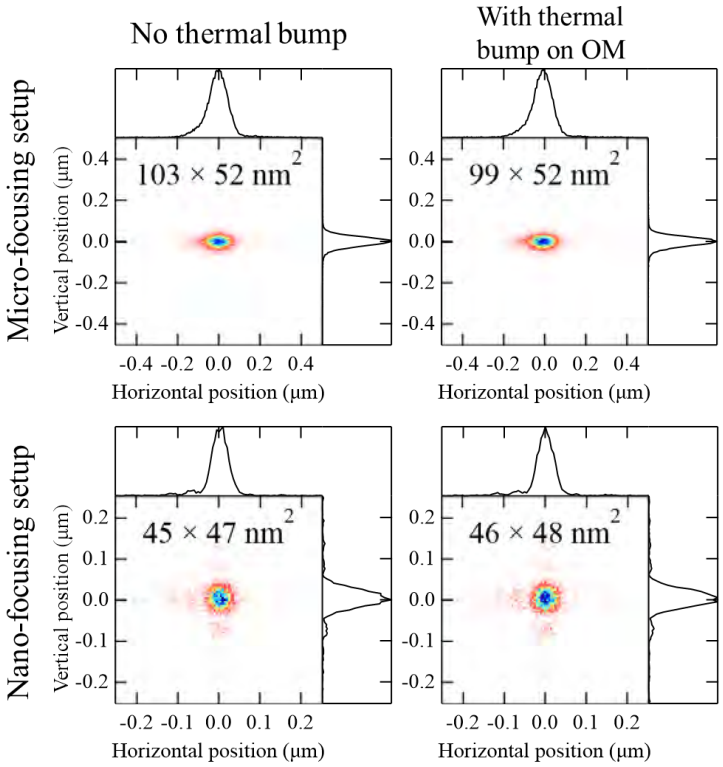


*Figure 4.66. Beam profiles at the micro-focusing (top) and nano-focusing (top) stations without (left) and width (right) thermal deformations on OM.*

A detailed description of the 3DMN optics can be found in the 3DMN/ATOMIC 34-ID Optics ESD (ICMS Content ID: APSU_2030439).

## 4-9.8 Instrument Overview 3DMN

### 4-9.8.1 Scientific Scope

The 3DMN instrument will use highly focused beams to measure the local lattice structure, orientation, and strain tensor with point-to-point spatial resolution utilizing focused x-ray beams in the micro-/nano-diffraction station range from ~50 nm to 200 nm in size. This instrument will also provide the ability to easily alternate between polychromatic (Laue) and tunable monochromatic diffraction modes is a key feature enabling users to study a much wider range of randomly oriented or polycrystalline "real" materials.

### 4-9.8.2 Instrument Definition

The 3DMN instrument consists of two experimental stations. The first micro-diffraction station includes a base table and instrument stabilization structure, sample and knife edge scanning stages, final K-B mirror focusing optics, multiple near field area detectors, and a far-field BCDI detector.

The second nano-diffraction station includes an ultra-stable optical table, a thermal enclosure, nanoscale sample and knife edge scanning stages, final K-B mirror focusing optics, multiple near field area detectors. The design of the nano-diffraction instrument is shown in Figure 4.67.

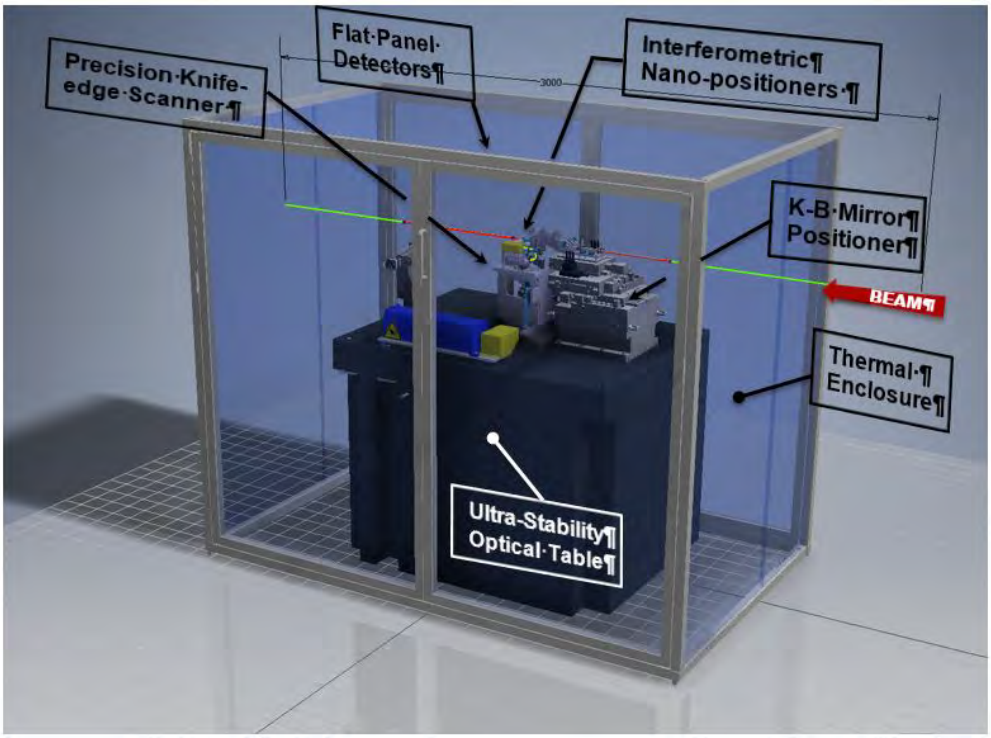


*Figure 4.67. Nano-diffraction instrument conceptual design.*

### 4-9.8.3 Instrument Location

The 3DMN experiment stations will be located in the 34-ID-E hutch as indicated in Figure 4.68

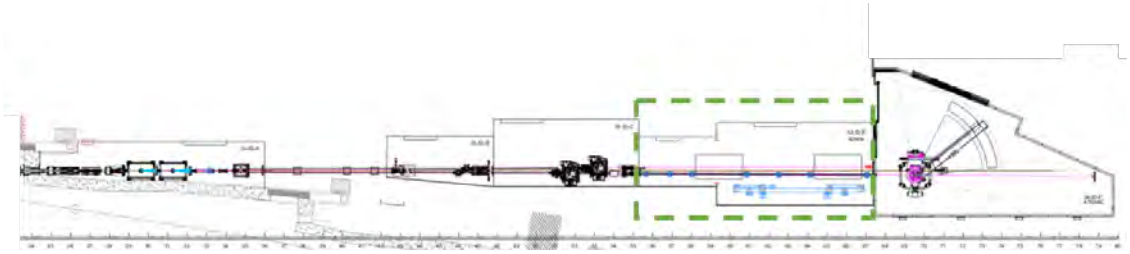

*Figure 4.68. 34-ID station layout. The 34-ID-E station is enclosed by the green dashed box.*

The 3DMN instrument will have four operational modes that will function independently of the ATOMIC endstation instruments.

- **Monochromatic micro-diffraction mode:** In this mode, focused monochromatic beam will be delivered to the upstream micro-diffraction experimental station.

- **Pink micro-diffraction mode:** In this mode, focused pink beam will be delivered to the upstream micro-diffraction experimental station.
- **Monochromatic nano-diffraction mode:** In this mode, focused monochromatic beam will be delivered to the downstream nano-diffraction experimental station.
- **Pink nano-diffraction mode:** In this mode, focused pink beam will be delivered to the downstream nano-diffraction experimental station.

Three principle experimental methods will be utilized by the 3DMN endstation instrument.

- **Polychromatic micro/nano diffraction:** For this technique pink beam is focused to a micro- or nano-sized spot and used to map heterogeneities in a multi-grained system. This technique will be utilized at both the micro-diffraction and nano-diffraction experimental stations.
- **Monochromatic micro/nano diffraction:** For this technique monochromatic beam is focused to a micro- or nano-sized spot and used to map heterogeneities in a multi-grained system. This technique will be utilized at both the micro-diffraction and nano-diffraction experimental stations.
- **Bragg Coherent Diffraction Imaging:** For this technique a monochromatic beam is focused to a coherent micro- or nano-sized spot and used to image the shape and strain of individual crystallites. This technique will be utilized at the micro-diffraction station.

A detailed description of the 3DMN Endstation instruments can be found in the 34-ID-D/E 3DMN Endstation Instrumentation ESD (ICMS Content ID: APSU_2030818).

### 4-9.9 Instrument Overview ATOMIC

#### 4-9.9.1 Scientific Scope

The ATOMIC beamline and endstation instrument will be dedicated to using x-ray coherent-diffractive imaging (CDI) for high-resolution studies of the interrelated structural, chemical and physical properties exhibited by advanced functional materials. To the achieve this goal the ATOMIC endstation instrument will have state-of-the-art x-ray focusing optics, sample and detector positioning systems, and x-ray detectors.

#### 4-9.9.2 Instrument Definition

The ATOMIC endstation instrument includes the, End-station Beam Pre-conditioning Platform, sample positioning diffractometer, the detector positioning diffractometer, and x-ray detectors.

#### 4-9.9.3 Instrument Location

The ATOMIC experimental instrument will be located at the site of a new 34-ID-F end station as indicated in Figure 4.68.

The ATOMIC endstation instrument will have two operational modes that will function independently of the 3DMN experimental instruments:

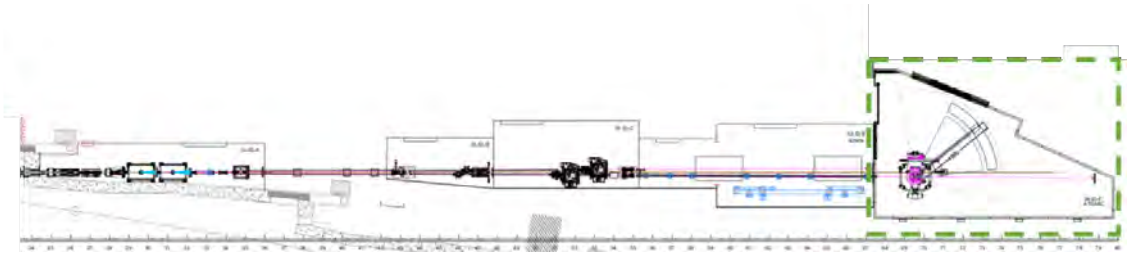

*Figure 4.69. 34-ID station layout. The 34-ID-F station is enclosed by the green dashed box.*

- **Monochromatic CDI mode:** In this mode, focused monochromatic beam will be delivered to the endstation instrument.
- **Pink Beam CDI mode:** In this mode, focused pink beam will be delivered to the endstation instrument.

## 4-10 ASL 25-ID

### 4-10.1 Introduction

The Advanced Spectroscopy (AS) and LERIX beamlines are a canted undulator expansion and relocation of the programs currently located at beamlines 20-ID and 11-ID-D. They consist of the advanced spectroscopy and LERIX branch lines operating independently, and will be located at sector 25. The advanced spectroscopy branch line expands on the capabilities of the current Sector 20 microprobe station to take advantage of the MBA source properties, and to optimize it for additional spectroscopy applications based on variable-resolution analysis of the sample fluorescence. Both beamlines will have multilayer options in the monochromator for maximum flux in non-resonant applications.

The LERIX branch will support the Lower Energy Resolution Inelastic X-ray (LERIX) spectrometer, additional high resolution spectrometers for various types of emission spectroscopy, and time-resolved spectroscopy and diffraction. Both miniXS style [30, 31] and bent crystal analyzers will be used for high energy resolution analysis of the emission, suitable for rapid measurement of resonant and non-resonant x-ray emission spectra for determination of valence, spin, and some aspects of local electronic environment in a complementary method to the typical x-ray absorption near edge structure (XANES) analysis. The LERIX-1 was the first spectrometer optimized for high-throughput, non-resonant inelastic x-ray scattering. The current LERIX-1B spectrometer is an upgrade providing improved sample handling, better low-energy capabilities, and a more flexible support frame. The LERIX spectrometer will be further enhanced as part of the beamline enhancement program to allow a more optimum placement of the analyzer crystals. The LERIX branch line will provide variable-energy resolution using a secondary monochromator to allow selection of the optimum resolution/flux tradeoff for the experiment. Part of the beamline will serve other types of techniques, such as laser-based time-resolved X-ray spectroscopy and scattering, which is the program of 11-ID-D today. This is program is focused on state-of-the-art laser-pump X-ray-probe experiments on the timescale of pico- to microseconds.The experimental setup of 11-ID-D including the laser will be transferred to the new LERIX beamline.

### 4-10.2 Scientific Objective

#### 4-10.2.1 Advanced Spectroscopy Beamline

The advanced spectroscopy branch line will support three classes of experiments: submicron-scale x-ray microprobe, x-ray absorption fine structure (XAFS) requiring the high flux and brilliance of an undulator source (i.e., very dilute systems, small samples as found in high-pressure cells, or glancing angle measurements of thin films), and fluorescence spectroscopy using miniXS or other high-resolution spectrometers. The first two categories include most of the applications at the current microprobe station. The current microprobe station that provides a 2-5 micron beam size has a diverse and active set of users averaging about 20 publications per year while using about 50% of the available beam time at 20-ID. These capabilities will be improved with the MBA source to provide higher flux at beam sizes down to 0.5 micron while retaining a good working distance and our unique capabilities such as high-resolution confocal detection.

As the detection resolution is improved, fundamentally distinct variants of spectroscopic informa-

tion become accessible. These include lifetime-broadening suppression, which occurs when selecting regions of individual emission channels, magnetic-state or valence-specific x-ray absorption spectroscopy (XAS) when selecting emission channels that couple directly to the spin- or charge-state of a metal ion, and the possibility of performing non-resonant and resonant x-ray emission spectroscopy (XES and RXES, respectively).

Nonresonant XES (or simply XES) is the spectral emission from the target species when the incident photon energy is at least ~100 eV above the binding energy, so that quantum mechanical coupling between the absorption and emission processes is only weakly relevant for the emitted spectrum. That means a core hole has been formed and some electrons from a less-tightly-bound shell will decay to fill the core-level vacancy. For hard x-ray applications, with ~30% to 70% probability, this will result in the emission of a fluorescence x-ray. This process is manifestly atomic in nature, with a weak, but still sometimes useful, influence of the nearest- neighbor species. Most critically, it is important to note that XES characterizes the occupied density of states – without the complications of final-state effects – while XANES is instead sensitive to the unoccupied density of states. For example, the many $K_\beta$ features for 3d transition metals often provide unique insight into spin, valence, ligand species, and ligand bonding. Such information could be of critical importance for studies of bulk and nanophase transition metal oxide compounds used in numerous energy science applications. Unfortunately, comparatively few XANES studies at hard x-ray energies are accompanied by XES measurements with resolution comparable to the core-hole lifetimes (e.g., 0.5 - 2 eV for 3d transition metals) even though many such studies would vastly benefit from the complementary information provided by XES. This is due to the complexity, cost, and sheer physical scale of high-throughput x-ray spectrometers based on arrays of spherically-bent crystal analyzers. Recent work at the APS has demonstrated a new type of "miniature" x-ray spectrometer (miniXS) [30, 31], which overcomes many of these issues while also providing better-than-order-of-magnitude improvement in measurement times. Using either the miniXS approach or a traditional spherically bent crystal analyzer (SBCA)-based system, as needed, x-ray emission spectrometers at sector 20 have been developed for operation from 3 to 12 keV. This energy range is of high scientific importance, as it spans the K-emission for 3d transition metals, the L-emission for lanthanides, and the M-emission for actinides.

A goal for the new microprobe line is the ability to carry out emission spectroscopy simultaneously with x-ray fluorescence imaging. This will provide a new capability of chemically sensitive imaging. To accomplish this we need the improved brightness provided by the MBA lattice. Currently a good emission spectrum requires 30-60 sec. With the MBA source we can expect for the same spot size that the spectrum will require approximately 1 sec, making imaging possible. To further decrease the time for non-resonant applications, we will use a multilayer monochromator that should provide an additional reduction of 10-20 in scan time.

#### 4-10.2.2 LERIX beamline

The LERIX branch line will support the LERIX spectrometer for x-ray Raman studies (XRS) as well as additional high-resolution spectroscopies, and pump-probe x-ray spectroscopy and scattering. X-ray Raman scattering, from semi-core and relatively low-lying electronic core levels, is an emergent branch of synchrotron-based science. XRS is a subset of nonresonant inelastic x-ray scattering (NIXS), which more broadly also includes the scattering from valence levels. In XRS or NIXS, a fixed-energy spectrometer and a scanning monochromator work in unison to generate energy loss

spectra which, at given momentum transfer Q, provide a direct probe of the electronic excitations in the system.

XRS is a very powerful tool for examining the chemical structure and environment in light elements embedded in thick or absorbing objects [32]. It combines the power of soft x-ray spectroscopy with the in situ capabilities of hard x-rays. This technique has been widely used in high-pressure research to examine light elements, including hydrogen. Recent work at the APS has demonstrated that XRS is applicable to work on Li-ion batteries, providing important information about the redox chemistry through measurement of all low-energy edges in the system (i.e., the oxygen K-edge, transition metal L- and M-edges, and in some cases, the Li K- edge). In addition, it is possible to explore the momentum transfer (Q) dependence of the scattering, move beyond the dipole approximation, and access a unique combination of S(Q,$\omega$),which cannot be observed with longer-wavelength, electromagnetic radiation [33, 34, 35, 36, 37].

Pump-probe X-ray (PPX) spectroscopy and scattering are unique tools to directly investigate multiple timescale structural dynamics underlying energy conversion processes at the atomic scale. The PPX capabilities have critical applications addressing the grand challenges of the 21st century across a broad range of scientific disciplines, including solar energy conversion, catalysis, geochemistry and fuel cells. Currently, this program is located at 11-ID-D, a dedicated beamline. 11-ID-D is currently oversubscribed by a factor of three and produces ~ 20 publications/year reflecting the high demand and impact. PPX uses laser pulses to initiate a reaction, then interrogates with stroboscopic X-ray pulse snapshots to track the electronic and structural evolution spanning the time domain from sub-nanoseconds to microseconds. This time domain will remain an important mission of synchrotron-based techniques, since it fills the gap between the femtosecond light sources (XFEL) and microsecond to millisecond time-scale of, rapid-scan synchrotron X-ray techniques, e.g. quick XAFS and scattering.

### 4-10.3 Beamline Requirements for the Insertion Devices (IDs)

This beamline will be configured to operate two independent branches fed by two independent insertion devices. The ID straight section will be instrumented with magnets to cant the two branches by 1 mrad so that they can be operated independently.

*Table 4.68. Source Parameters*

| **Unduator** | **Period** *(mm)* | **Length** *(m)* | $\mathbf{K_{max}}$ | **Power*** *(kW)* | **Power Density*** *($kW/mrad^2$)* | **Location** |
|---|---|---|---|---|---|---|
| Planar | 28.0 | 2.1 | 2.459 | 8.5 | 196 | Upstream |
| Planar | 28.0 | 2.1 | 2.459 | 8.5 | 196 | Downstream |

### 4-10.4 Beamline Requirements for the Front End

The ASL beamline will have a canted undulator (CU) front end capable of handling two beams separated by 1 mrad canting angle and 10 kW power each. The beamline will a windowless exit configuration with a 2 mm x 1 mm (H x V) exit aperture for each branch.

A detailed description of the ASL Front End and Insertion devices can be found in the APS-U

25-ID Beamline Front End and Insertion Devices Interface Control Document (ICMS Content ID: APSU_190953).

### 4-10.5 Beamline Layout

The beamline layout in Figure 4.70 shows three experimental hutches with 6 experimental stations. With the exception of the LERIX instrument, these stations are not part of the project and will be moved from their current locations at 20-ID and 11-ID-D. The LERIX instrument is planned to be upgraded as a beamline enhancement project.


*Figure 4.70. Layout of ASL beamline.*

#### 4-10.5.1 Beamline Component Table

### 4-10.6 Optics Overview

#### 4-10.6.1 Detailed Optical Layout

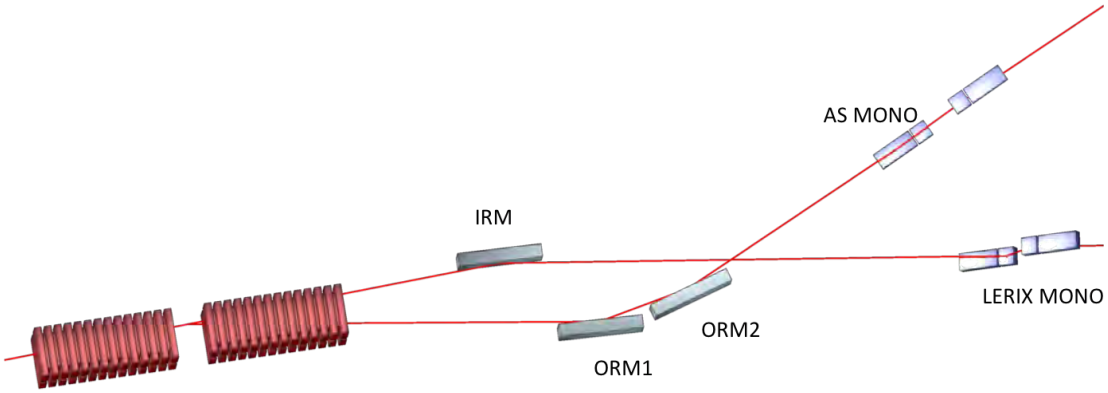


*Figure 4.71. Basic optical layout of the ASL beamline.*

Figure 4.71 shows the basic optical layout. Water-cooled mirrors serve as the first optics for each branchline: an Inboard Reflecting Mirror (IRM) will reflect one of the canted beams inboard to the LERIX monochromator and the 25-ID-D and E Stations. This mirror will be bendable and will increase the beam separation, as well as provide power filtering; higher-harmonic rejection; and

*Table 4.69. Beamline Component Table*

| Distance | Component | Description/Comments |
|---|---|---|
| 25.6 | FE Exit Mask | Standard HHL Front-End exit mask 2x2 aperture |
| 26.0 | FE Collimator | Standard HHL Front-End Exit Collimator. 5x5 aperture |
| 26.4 | Canted Undulator WB Slits | CU Variable Aperture Photon Absorber w/ Tungsten Edge inserts |
| 27.1 | Canted Undulator WB Slits | CU Variable Aperture Photon Absorber w/ Tungsten Edge inserts |
| 28.5 | Mirror | Flat Horizontal Mirror, Inboard (L) |
| 29.9 | Mirror | Flat Horizontal Mirror, Outboard (AS) |
| 30.7 | Mirror | Outboard Horizontal Mirror (AS) |
| 31.6 | Diagnostic | BPM Diagnostic |
| 32.1 | Photon Mask | WB Stop Photon Mask, 4105090405-130000 |
| 32.5 | Collimator | Bremsstrahlung Collimator, 4105090403-160000 |
| 36.3 | Diagnostic | BPM Diagnostic |
| 38.9 | Photon Mask | Outboard Pink Photon Mask, 4105091008-160000 |
| 39.0 | Photon Mask | Inboard Pink Photon Mask, 4105091008-160000 |
| 39.3 | Collimator | Tungsten Bremsstrahlung Collimator, 4105090403-180000 |
| 39.7 | Collimator | Lead Bremsstrahlung Collimator, 4105090403-190000 |
| 49.1 | Slits | Pink Slits (AS) |
| 50.5 | Monochromator | Monochromator (AS) |
| 51.3 | Photon Mask | Pink Stop Photon Mask, 4105090913-110000 |
| 51.9 | Photon Mask | Pink Stop Photon Mask, 4105090913-110000 |
| 52.5 | Monochromator | Monochromator (LERIX) |
| 53.5 | Shutter | P8-20 Mono Shutter (Outboard) |
| 54.0 | Shutter | P8-20 Mono Shutter (Inboard) |
| 55.2 | Slits | Mono Beam Conditioning Slits (AS-Existing) |
| 58.6 | Mirror | K-B Mirror System w/monochromatic slits (spectroscopy, exist) |
| 62.4 | Slits | Mono Beam Conditioning Slits (LERIX-Existing) |
| 69.3 | Beam Stop | Movable Mono Beam Stop |
| 76.3 | Beam Stop | Fixed Mono Beam Stop |

horizontal focusing to the LERIX branchline. The IRM will be located in the FOE and will operate at about 2 mrad horizontal incident angle (4mrad beam deflection). Two Outboard Reflecting Mirrors (ORMs) will reflect the other canted beam outboard to the 25-ID-C Station for the Advanced Spectroscopy (AS) branch. In addition to increasing the beam separation, these mirrors will also provide power filtering; higher-harmonic rejection; and focusing to the AS branch. They will be located in the FOE for maximum downstream beam deflection. They will operate at about 2.5-mrad horizontal incident angle (5mrad beam deflection for each mirror giving a total of 10 mrad). The first mirror will be flat, while the second will be bendable to potentially provide a horizontal focus at a downstream position. All three mirrors will have three reflecting stripes (bare Si, Rh, and Pt) to provide harmonic rejection and cover the operational energy range.

As shown the mirrors will be mounted in a geometry such that the reflected x-ray beams cross paths downstream of the mirrors. Therefore, the IRM with be located on the outboard source and the ORMs will be mounted on the inboard source. This mounting geometry will allow for the use of conventional horizontally-deflecting mirror designs.

The double crystal/multilayer monochromators (DCMM) will be located in the second optical enclosure where the beam separation is sufficient to allow them to be completely independent. Both monochromators will have liquid nitrogen cooled Si (111) crystals allowing an operational energy

range of 4-40 keV. The beam offset is chosen to be 9-11mm to allow for the use of multilayer crystals located in front and behind the first and second Si crystals. These crystals will be accessed by rotating to small angles and raising the monochromator rotation stage by 2mm such that the beam is below the rotation axis and strikes the multilayer. The multilayer crystals will have two reflecting stripes with different d-spacing, a high energy stripe with d≈24 Å, and a low energy stripe with d≈48 Å. A horizontal translation of nominally 10 mm is needed to choose between the stripes. The small offset allows a compact design for the multilayer option, and is possible because all of the potential bremsstrahlung radiation is stopped in the first optical enclosure.

## 4-11 1-ID Enhancements

The 1-ID beamline is a world-leading high-energy X-ray facility used for a wide range of materials research including the aerospace, automotive, biomaterials, energy storage and nuclear materials sectors. *Through recent developments of multi-modal scattering and direct-beam imaging techniques including SAXS/WAXS, μ-CT and High-Energy Diffraction Microscopy (HEDM), a wide range of size scales, ranging from Angstroms to mm's, can be evaluated with a single probe. One of the key developments in APS-U will be to extend the spatial resolution of these techniques from their current micron-level resolutions to the ~100 nm level. This will allow a more direct evaluation of nano-scale heterogeneity, which drives the function of many material classes.*

The 1-ID user base is broad and comprised of researchers from universities, national laboratories, defense and industry both within the U.S. and abroad, with oversubscription ratios of 5x common. This demand for non-destructive, high-energy x-ray capabilities is expected to continue, and the enhancements listed below put the APS in position to deliver the highest quality scientific output for the users.

### 4-11.1 New High-Energy X-Ray Monochromator

This enhancement entails changing the monochromator to a horizontal reflection configuration to meet the requirement of preserving the vertical and horizontal source emittance of the APS-U, and designing the monochromator to meet all performance specifications while withstanding the thermal load of a long superconducting undulator (SCU) source.

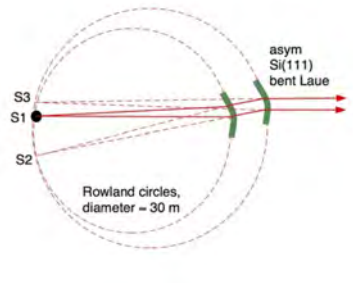


*Figure 4.72. Schematic of the bent double-Laue crystal system for fixed exit beam over the 40–140 keV energy range.*

The current 1-ID monochromator, in use for close to twenty years, consists of a vertically diffracting, cryogenically-cooled, bent double-Laue crystal system in sequential Rowland conditions to deliver a high-flux, fixed-exit beam that is fully tunable over 40–140 keV Figure 4.72. Laue crystals are known to distort the x-ray phase-space in the diffraction plane due to Bormann-fan type effects, with further complications arising from bending. However, in propagation through the specific two-crystal configuration in use here, there is a compensation effect where the second reflection undoes, to a large extent, the phase-space distortion from the first one, restoring the effective vertical source size and divergence to the original within a few microns and hundreds of nanoradians, respectively. This is sufficient to preserve the present APS vertical emittance ($\varepsilon_y$ = 40 pm) to within 20%. However, one would not expect this compensation effect to work for the 4.2 pm vertical emittance in the APS-U flat-beam lattice. Consequently, it is required that the same concept be implemented, but

in a horizontal diffraction plane. This would leave the APS-U vertical source emittance effectively unperturbed, as well as the APS-U horizontal emittance, as the latter is close to the present vertical emittance.

A new monochromator also offers the opportunity to be appropriately engineered to meet all specifications while handling the thermal load from the anticipated/upgraded insertion device—a long SCU.

### 4-11.2 SMS upgrade in 1-ID-E

The 1-ID-E hutch currently has two sample-manipulation-systems (SMS), which can be differentiated by high-load capacity (used for the MTS load frame and other applications needing >100 kg capacity) and high-resolution (the centerpiece being an air-bearing Aerotech ABRS300 single-axis rotary stage). Both SMS reside on floor rails allowing easy interchange between them. This enhancement will apply only to the high-resolution SMS, and will add two new features namely (i) allow for full and continuous rotation for the ABRS300 and components mounted above it and (ii) add tilting capabilities for these components. Item (i) will enable faster tomography (in both absorption and diffraction contrast) while item (ii) will turn the SMS into a full diffractometer enabling the use of additional imaging techniques such as dark-field microscopy.

### 4-11.3 1-ID-E extension

The extension of the 1-ID-E end-station, combined with the existing hutch infrastructure, is required to take full advantage of APS-U. The extension, combined with the enhanced brilliance, will allow the $q_{min}$ of pinhole SAXS to be significantly reduced, allowing correspondingly larger features to be measured (up to ~1 µm). This will also enable higher spatial resolution zoomed-in imaging with a high-energy transmission x-ray microscope (TXM). Such a full-field TXM, based on a refractive lens objective, has already been demonstrated at 45 keV having ~ 500 nm resolution, with the specimen, objective, and detector all fitting within a 6 m length in the current APS 1-ID-E end-station. Adding more distance (+4 m) in a new end-station will enable a TXM system with higher magnification, larger sample depth of field, and detector pixel oversampling to achieve < 200 nm imaging resolution at high energies. For both enhanced SAXS and TXM, the samples will be positioned at the same place/environment as for interrogation by other techniques including WAXS and imaging, for multi-scale characterization.

### 4-11.4 Beamline Description

At the downstream end of 1-ID-A is a multi-mode shutter/stop (P4). Its modes are: passing through white beam (no shuttering) or shuttering monochromatic beam (with white beam stopped). So, the B station can accept either white or monochromatic beam. At the downstream end of B is a single-mode shutter/stop (P5) that shutters and stops monochromatic and white beams, respectively. Stations C and E are for monochromatic radiation only.

The high-heat-load monochromator in A operates in a fixed-offset geometry with 40–140 keV tunability with ~$10^{-3}$ bandwidth. A high-resolution monochromator in B can subsequently narrow the bandwidth to $10^{-4}$–$10^{-5}$ levels when needed. Refractive optics (e.g., saw-tooth lenses, CRLs) are

placed at various locations for focusing or collimation. There are no modifications to the 1-ID-A, B, and C shielded enclosures in this Enhancement Project.

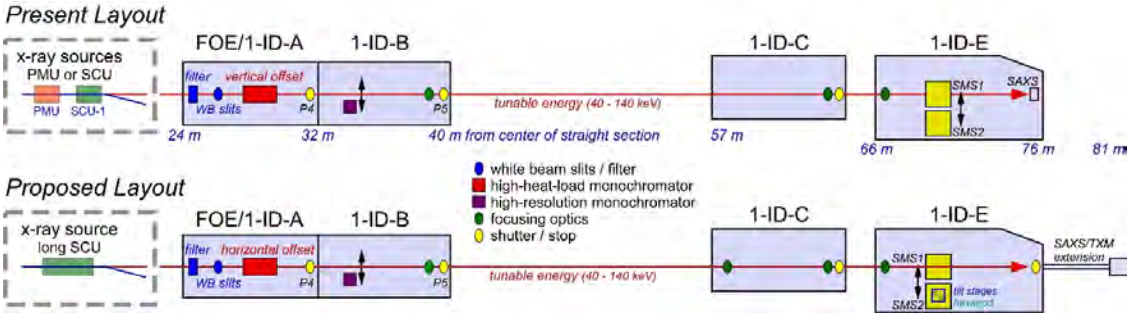


*Figure 4.73. Schematic of current and proposed/enhanced layouts for 1-ID.*

## 4-12 2-ID Enhancements

The stations 2-ID-D and E provide advanced scanning probe capabilities to diverse user communities such as materials science, energy science, environmental science, life science. Applications include, for instance, measuring microelectronics defects in 3D, local structure and electronics state in advanced photovoltaic materials, elemental content and oxidation state of aerosol particles, exogenous and endogenous metal distribution in cells and tissues. These experiments are currently performed on the XRF/XANES microprobe and the fast ptychography instrument (Velociprobe) at 2-ID-D, and the 2D/3D XRF microprobe at 2-ID-E. In 2019, the entire 2-ID beamline will be canted to provide independent operation of the 2-ID-D and 2-ID-E station. In the longer term, after the APS Upgrade, it is envisioned that the XRF/XANES microprobe at 2-ID-D will be replaced by the upgraded Bionanoprobe (BNP-II) relocated from 9-ID-B.

### 4-12.1 Vertically Reflecting Mirror

While the canted 2-ID will have horizontal bendable mirrors on the 2-ID-D and the 2-ID-E branchline to re-focus the source onto a set of beam defining apertures (BDAs) at 35 m, there is currently no focusing in the vertical direction. To utilize the APS-U each branchline requires the addition of a vertical focusing mirror. Used along with the existing horizontal focusing mirrors, it will allow one to create a well-controlled stigmatic secondary source. This will mitigate any beam instability due to vibration and drift of the source or optical components, which is particularly stringent in the vertical direction due to the smaller vertical source. In addition, spatial filtering by the BDA will provide more flexibility for the microprobe operation, allowing optimization between flux and resolution. The APS-U source parameters vary significantly between the Timing Mode and Brightness Mode, where the vertical source size changes by 2.5x. This variation in source size is difficult to accommodate by downstream nanofocusing optics; the addition of a vertical focusing mirror used in conjunction with the BDA will enable the microprobe to operate more independently from changes in the source parameters. It is required that the mirror operate up to energies of 30 keV and be able to meet all specifications under the full heat load of each beam.

### 4-12.2 2-ID-E Mirror System

In order to fully utilize the APS-U low emittance source requires upgrading the 2-ID-E microprobe to a KB-mirror-based system with advanced nanomotion capabilities. KB mirrors offer two significant advantages compared to zone plate optics: higher efficiency (60-80% versus 10-20%) and achromaticity. Being achromatic allows one set of fixed optics instead of multiple ZPs to be used for all energies, significantly simplifying the operation. Additionally, with focal length being independent of the energy, it not only enables true micro-XAS capability but also allows wider bandwidth (hence higher flux) to be used in micro-XRF mode. Because 2-ID-E is a pink beam station this enhancement will also allow the possibility of focusing pink beam without a monochromator. It is worthwhile to note that due to the low emittance of the APS-U source, the energy bandwidth of the undulator harmonic will be approaching its natural width (1/nN), typically ~ 1% or less. Thus, focusing pink beam will not significantly broaden the elastic or Compton scattered peak which is important for achieving low background in the XRF spectrum. In fact it offers the possibility of focusing multiple harmonics simultaneously, for instance using the $1^{st}$ harmonic to optimize excitation of low-Z elements while using the $3^{rd}$ harmonic to optimally excite high-Z elements, allowing

more elements to be imaged at the same time.

### 4-12.3 2-ID-E Advanced Positioning System

With the KB-mirror upgrade and the much higher source brightness from the APS-U, the focus intensity of the 2-ID-E microprobe will increase by 2 orders of magnitude in micro-XAS mode and by 4 orders of magnitude in micro-XRF mode. Utilizing these enhancements requires the deployment of advanced motion control and faster signal processing, which will substantially increase the throughput or "pixel counts" of 2D XRF images and make fluorescence tomography practical. This will require high-stiffness, fast-scanning sample stages with resolution $< 10$ nm and travel range $> 10$ mm optimized for high dynamical performance. This performance will be facilitated by advanced motion control and data acquisition system that are capable of sophisticated scanning patterns such as Lissajous trajectories, variable dwell time per pixel etc.

### 4-12.4 2-ID-D BNP-II

The Bionanoprobe (BNP) is so far the *only* XRF nanoprobe at the APS with cryogenic and cryo sample transfer capabilities. User demand is high, with 2-3x oversubscription. With the *unique* cryogenic capabilities, the BNP is especially suited to trace elements studies in biological materials and other soft matters with <100 nm spatial resolution. To utilize the APS-U characteristics and maintain the world-leading position requires that the instrument be upgraded to BNP-II capable of delivering <10 nm spatial resolution and a-few-atom sensitivity with cryogenic capabilities. It will enable both 2D survey of large samples and fast tomography for 3D visualization. It will offer the capability of complementing elemental mapping with simultaneous ultrastructure imaging via ptychography. The reconstructed probe function via ptychographic method will then be used to further improve the XRF images to reveal the features beyond the diffraction limit of X-ray optics. It will lead to great advancement in soft matter sciences. Meeting these new motion specifications while maintaining the cryogenic capabilities of the BNP-II instrument will require a redesign of the vacuum chamber as well as a number of critical cooling components such as the phase separator and the cold shield.

### 4-12.5 Beamline Description

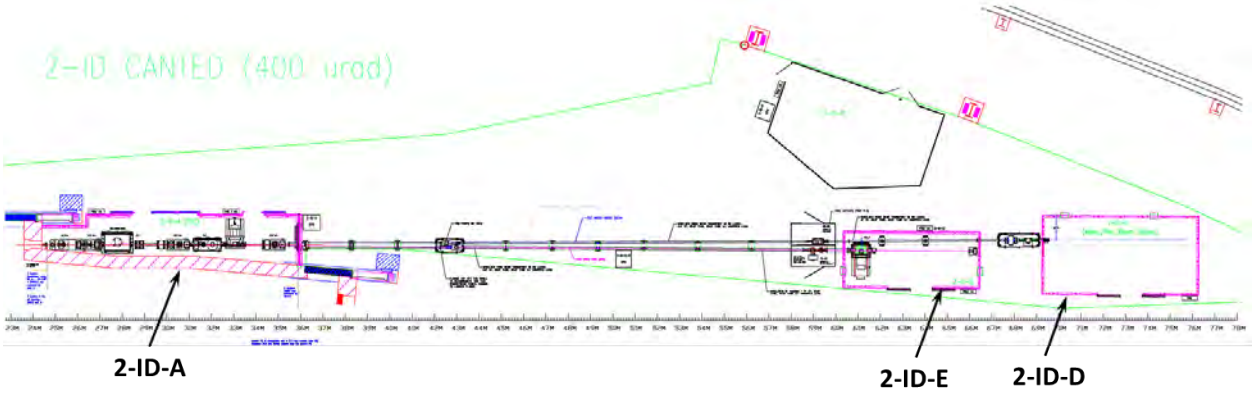


*Figure 4.74. Layout of the canted 2-ID beamline, with the 2-ID-D and 2-ID-E branchline.*

The 2-ID beamline is designed to provide highly coherent and stable beams for the scanning probes in the 2-ID-D and 2-ID-E station which will operate independently after the canting. Essentially both branchlines employ a mirror-first approach to refocus the source horizontally onto a BDA which acts as a stable virtual source for the scanning probe instruments downstream. The x-ray intensity and coherence can be selected by varying the BDA opening. The 2-ID-D branchline is served by a horizontal double crystal monochromator (H-DCM) upstream of the BDA, while the 2-ID-E branchline is served by a vertical double multilayer monochromator (DMM) upstream of the BDA and a Kohzu double crystal monochromator (DCM) in the 2-ID-E station.

### 4-12.6 Instrument Overview BNP-II

The upgrade of the BNP to BNP-II will enable performance capabilities that capitalizes on the unprecedented brightness of the APS upgrade. The highlights of the upgrade to the BNP include:

- 10 nm spatial resolution for XRF imaging with cryogenic conditions.
- 2D survey of large samples and fast tomography for 3D visualization.
- Capabilities of complementing elemental mapping with simultaneous ultrastructure imaging via ptychography.
- Further improvement to XRF images will result from the reconstructed probing function via ptychographic method, revealing features beyond the diffraction limit of X-ray optics.

#### 4-12.6.1 Instrument Definition

The BNP-II instrument is defined as a combination of

- A cryogenic in vacuum sample configuration, including staging.
- An optic configuration, including optic stages and any local beam conditioning.
- Dedicated detectors for diffraction and x-ray fluorescence measurements.
- Metrology and supporting hardware for monitoring sample and optic motion.
- A vacuum chamber housing the sample, optics, metrology and cryogenic hardware.
- Supporting structures and positioning needed to place the vacuum chamber in the beamline.
- All connected auxiliary hardware to the vacuum chamber needed to run the BNP-II.

#### 4-12.6.2 Cryogenic Operation

The following are capable x-ray measurement techniques of the BNP-II at cryogenic temperatures:

1. Ptychography (Ptycho)
2. X-ray fluorescence (XRF)
3. Tomography (Tomo)

The cryogenic system in the BNP-II facilitates a cryogenic sample environment by means of conductive cooling to the sample, a cold radiation shield, a sample storage shuttle, and a robot arm for sample exchange. A liquid nitrogen dewar is attached to the outside of the vacuum chamber with a cold finger and a reservoir inside the chamber. An airlock on one side of the chamber allows samples to be transferred in and out without breaking the vacuum. This system will be re-used

from the current BNP for the upgrade to BNP-II.

A detailed description of the 2-ID BNP II instrument can be found in the APS-U 2-ID Bionanoprobe II enhancement ESD (ICMS Content ID: APSU_2030653).

## 4-13 3-ID Enhancements

The 3-ID beamline engages in high-resolution spectroscopy that includes high energy-resolution inelastic X-ray scattering (IXS), nuclear resonant vibrational spectroscopy (NRVS), and synchrotron Mössbauer spectroscopy (SMS). These techniques are exploited by a wide range of research interests including geophysics, geochemistry, bioinorganic chemistry, and material science.

Nuclear resonant scattering (NRS) involves special isotopes ($^{57}$Fe, $^{151}$Eu, $^{119}$Sn, $^{161}$Dy) in samples to achieve the highest energy-resolutions possible with synchrotron radiation (sub-meV to nano-eV) and includes both SMS for measuring hyperfine interactions as well as NRVS to measure phonon density-of-states. IXS is used to measure phonon dispersion in materials with meV-resolution using the high energy-resolution inelastic X-ray spectrometer (HERIX-3). All three programs have developed a healthy scientific user base over the last two decades and will benefit significantly from the following three enhancements:

- A near doubling of the range of momentum transfers accessible with IXS by relocation of the IXS spectrometer to 3ID-D.
- Improving the monochromator for NRVS to offer sub-meV-energy resolution with direct XRD capability, greater energy-positioning stability, and significantly improved focusing – contingent upon available funding.
- Improving the spatial resolution (from 20µm to 1µm) for NRVS via a new KB mirror system – this requires funding for a new dispersion-compensated HRM.

In the following subsections, each of these enhancements will be presented in brief detail.

### 4-13.1 Relocating IXS spectrometer to 3ID-D station

The IXS spectrometer currently residing in the 3-ID-C station will be relocated to the 3-ID-D station. This will increase the range of momentum transfers accessible with the instrument by 80% and incur minimal cost ($<$ \$20k) that can be absorbed by the IXN group's operating budget. This will significantly increase the demand for this instrument, as the limited momentum range has been the primary obstacle to user-demand. A larger Q-range is possible because the reduced horizontal photon-divergence (that results from the lower storage ring emittance) allows a Si(111) horizontally-deflecting crystal to be employed to make maximal use of the available floor space in the D station. The C station does not allow this as it precludes positioning any of the crystal back-reflecting analyzers at 0°scattering angle, which is required during operations. This enhancement is not being paid by the APS Upgrade project, but is mentioned here because it represents a significant rearrangement of the beamline's existing components and is only possible because of the reduced horizontal beam divergence created by the new storage-ring parameters.

### 4-13.2 New High-resolution Monochromator for $^{57}$Fe-based NRS

A new inline, cryogenic high-resolution monochromator (HRM) for $^{57}$Fe-based NRVS will allow subsequent focusing to 1um, higher energy resolution, 100-fold improvement in energy-alignment stability, and switching between sub-meV and eV-bandpass beams for much-requested X-ray diffraction (XRD) capability using 14.4 keV and/or 43.2 keV X-rays (higher harmonic radiation) without

beamline re-alignment. This HRM will be installed in the B station (near beam-entrance port).

The current HRM exhibits a deleterious dispersion effect on the X-ray beam that makes the X-ray source appear 50 times larger in the vertical and precludes focusing the beam below ~8 um (vertical) for acceptable working distances, regardless of the focusing optic. To achieve 1 um requires the design and construction of a new "dispersion-compensated" HRM to be operated in conjunction with a new KB mirror system.

The current HRM for $^{57}$Fe-based measurements produces a 1-meV bandwidth, which determines the energy resolution of phonon data using NRVS. Many users would prefer improvements in both energy resolution and energy-alignment stability for more accurate phonon energy assignment in large metalloproteins as well as for measuring low-energy phonon behavior in hydrodynamic regimes, e.g. for more precise determination of sound velocity in materials under extreme conditions. A new HRM will deliver a bandwidth of 0.6 meV (FWHM) with substantially reduced spectral tails for exploring excitations close to the elastic line, and dramatically greater energy-alignment stability.

Unlike the current HRM, the new instrument will be a true inline optic allowing switching between a 0.6-meV bandwidth beam of 14.4-keV X-rays to a wide-bandwidth beam able to deliver either 14.4 keV or 43.2 keV photons (higher harmonic radiation) for XRD with 1µm spatial resolution. Currently, users need to remove their samples and go to other beamlines to collect x-ray diffraction data, and then return to re-install/re-align their sample before continuing. The inline character of the new HRM is critical to providing direct switching between NRVS and XRD.

The existing HRM is near its operating limit for heat load and is at risk for precluding reproducible energy positioning if the thermal load from the incident beam is increased by a factor of two or more. It is required that the new cryogenic HRM withstand any possible increases in heat load from the incident beam.

### 4-13.3 New Kirkpatrick-Baez Mirror System

A new Kirkpatrick-Baez mirror system (K-B) will be installed in the C station (near beam-entrance port) that will provide a 1µm (vertical & horizontal) focal spot size and be suitable for various X-ray energies (corresponding to resonant transitions in different isotopes) as well as having the option to focus 43.2 keV X-rays for XRD when needed with acceptable trade-off at 14.4 keV. The 1µm focal spot size is important for samples under extreme conditions of pressure and temperature, and will allow performing measurements up to 300 GPa and 3000K. Also, the K-B system will provide the necessary 2-D focusing required by the dual-fast-shutter system (for $^{57}$Fe-based SMS measurements), but with a somewhat increased focal-spot size of 5 µm at the sample position. The dual-fast-shutter system will be located 4 m downstream of the K-B mirror system and requires a very large depth of focus in order to provide a small beam at both shutters as well as at the sample position. This would be an improvement over the existing dual-shutter system that provides a 13 µm spot size.

### 4-13.4 Beamline Description

Beamline 3-ID performs high energy-resolution X-ray and Gamma-ray spectroscopies for a wide class of materials under a variety of thermodynamic environments. Owing to the narrow spectral

ranges (meV to neV bandwidths) involved, the source involves dual planar undulators operated simultaneously to provide maximum spectral power at the energy of interest.

Beamline 3ID has 4 stations, successively labeled A, B, C, and D:

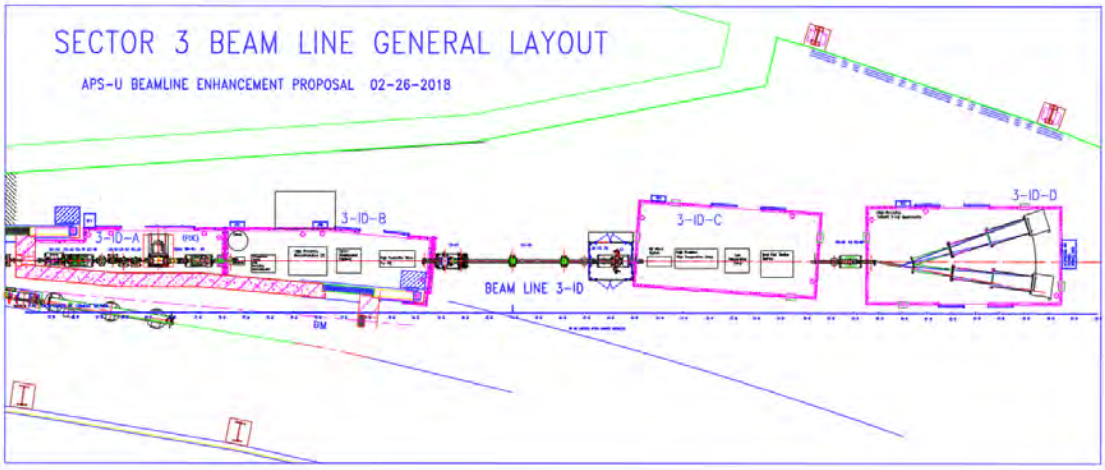


*Figure 4.75. Floor plan and optics layout for beamline 3-ID*

- Station A – This is a white-beam-rated enclosure that houses the first optical elements that are exposed to the raw radiation from the two inline insertion devices: each 2.3 m device will have a magnetic period of 2.5 cm. Both insertion devices will be used simultaneously to maximize the monochromatic power available for measurements. The optical components in this station include water-cooled mask, white-beam slits, and Be refractive lens, a $LN_2$-cooled Si(111) double-crystal monochromator, and an integrated photon shutter/white-beam-stop.
- Station B – This enclosure is rated for monochromatic beam only and will contain all HRMs as well as a development platform for ongoing optics development. HRMs are temperature-sensitive components that are best operated in a station that remains closed during user operations.

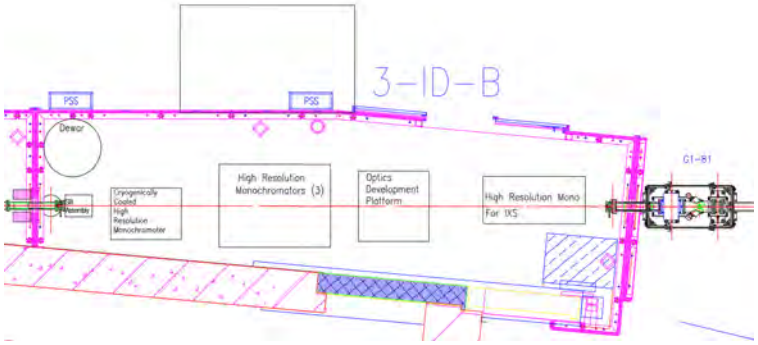


*Figure 4.76. Layout for new HRM and existing optics in station 3-ID-B.*

- Station C – This enclosure is rated for monochromatic beam only and will be the station for all NRS measurements. The K-B focusing system will provide focused beam for all experimental

setups within this station. User-measurements that require the smallest beam size (1Âţm x 1Âţm) will be performed immediately downstream of the K-B mirror system (delivering maximum demagnification). User measurements requiring the dual-fast-shutter setup (for $^{57}$Fe SMS) require a long depth-of-focus to support shutter operation (to convert native 48-bunch timing mode to artificial 6-bunch timing mode), and so is located at the end of this station.

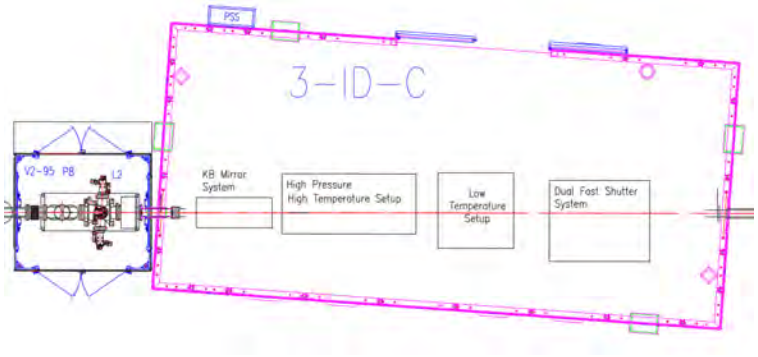


*Figure 4.77. Layout for new K-B mirror system and NRS measurement setups for station 3-ID-C.*

- Station D – This enclosure is rated for monochromatic beam only and will house the IXS meV-spectrometer. This station's layout (size and placement relative to the beam) allows the greatest range of momentum-transfers for user measurements using the existing analyzer arm.

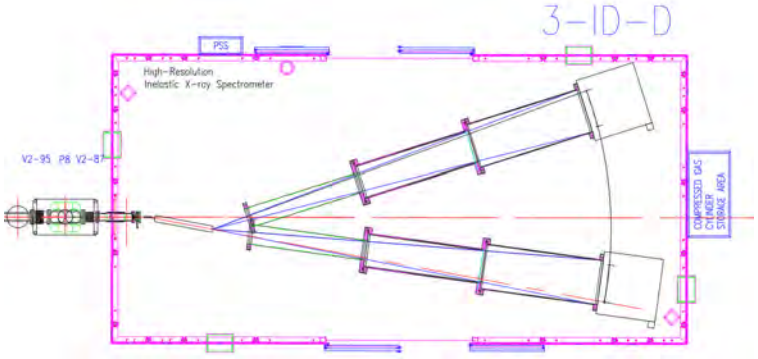


*Figure 4.78. Layout of IXS spectrometer in station 3-ID-D.*

## 4-14 5-ID Enhancements

DND-CAT is the original team that has designed, built, and operated Sector 5 at the Advanced Photon Source. For over 25 years our collaborative effort has worked extremely well delivering science and technology to the DND-CAT partners and General Users. As of today, 968 DND-CAT related publications are in the APS database.

DND-CAT plans to maintain vibrant scientific activity up to the APS Upgrade and plans to make excellent use of the exciting new source characteristics available after the APS Upgrade is completed. We expect to provide our user base with new and enhanced capabilities in multiple-length-scale x-ray scattering as well as new and enhanced capabilities for studies of surfaces, interfaces, and thin films. The enhancements scope for the DND-CAT beamline will be refinishing their mirrors and an upgraded monochromator as discussed in the next sections.

### 4-14.1 Refinished Mirrors

5-ID makes use of a pair of horizontally reflecting mirrors – the first one is flat, the second can be bent for focusing. Each mirror has three horizontal stripes – Rh coated, uncoated (the substrates are ULE glass), and Pt coated. The mirrors date from 1995 (made by Boeing) and have large slope errors compared to current mirror standards. Although they have been kept in a clean UHV (mid $10^{-9}$ mbar) environment, reflectivity measurements indicate a reduction in overall performance of the mirrors. To deliver the optimal beams to be produced by the upgraded APS, re-polishing and refiguring or replacing the mirror pair will be required.

### 4-14.2 Upgraded Monochromator

The DND-CAT 5-ID monochromator is a Daresbury design tank and theta circle, with a $LN_2$ side-cooled 3-inch cube of silicon as the first crystal. The second crystal is held rigidly in a pseudo-channel-cut configuration with no motions other than a coil driven angle adjustment and manual theta and chi adjustments. For this enhancement we seek to improve the monochromator's stability, flexibility, and upper energy limit (currently 18 keV). The stability upgrade is required to deliver the upgraded APS brightness to the experimental stations downstream, while the flexibility and increased energy range are greatly desired to enhance the experimental programs and take advantage of the unique higher x-ray energy capabilities of the upgraded APS. We would be very interested in moving quickly (pre APS-U shutdown) to implement APS designs for monochromators on our sector. (It is also possible that this request will be considered part of the baseline "do-no-harm" policy).

### 4-14.3 Beamline Description

Figure 4.79 shows a drawing of the beamline FOE and the components associated with the enhancements described above. The monochromator is positioned upstream of the mirrors ~29m from the source, meaning it receives the high-heat-load beam emanating from the white beam slits (L5). M1 and M2 are positioned ~32.5m and ~33.7m from the source respectively. Both mirrors reflect the beam in the outboard direction at an incidence angle of 3 mrad. Since they are positioned downstream of the monochromator and only receive the heat load associated with the monochromatic

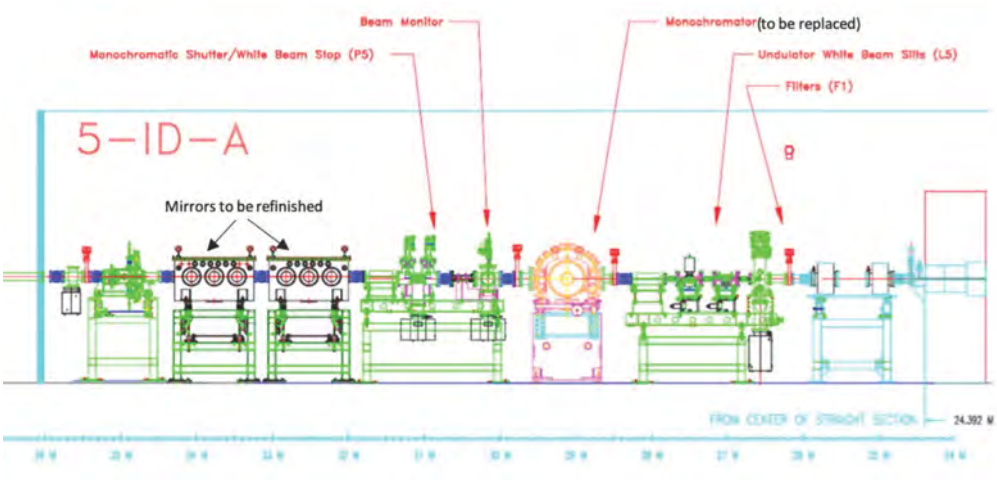


*Figure 4.79. Current drawing of the 5-ID FOE. The black text indicates the components associated with the required enhancements.*

beam.

## 4-15 6-ID Enhancements

### 4-15.1 6-ID-B and 6-ID-C CRL System

This enhancement will upgrade the resonant single crystal diffraction program at beamline 6-ID by taking advantage of both a small beam size (<1 µm) and the inherent coherence provided by APS-U.

This upgrade consists of beam conditioning to produce a high flux, stable <1 µm coherent beam across the 5 keV to 25 keV energy range with high precision positioning and rastering capabilities with energy scanning ~400 eV for spectroscopy. For these purposes, we will employ twin CRLs for horizontal and vertical focusing with a precision alignment mechanism upon a motion isolating mount.

Our sample environment program (funded elsewhere) envisions delivering Ultra-low Vibration (ULV) sample-cryo characteristics (<50-100 nm at 5-300 K) in open angular configuration with *in operando* capabilities. This will require both optical upgrades to the beamline including stability and focusing and the development of sample-stage stability engineering. We will employ compound refractive lens (CRLs) and pinhole technology to produce a beam size of ~1 µm/<1 µm with optimal coherence or optimal stability, respectively. Beam conditioning will consist of *in-vacuum* components and minimizing windows to maximize flux density across the energy range of interest to our user community and minimize decoherence effects.

Two CRL units will be acquired and separated, the first up-stream at the entrance to the B hutch and the second unit down-stream (3 m) in front of the PSI-diffractometer in 6-ID-B, to provide a focused beam in 6-ID-C for full field imaging.

### 4-15.2 6-ID-D CRL System

The increase in brightness of hard x-rays from APS-U dovetails into the use of CRLs, which have a relatively small beam acceptance area of ~170 µm diameter. Tests performed on 6-ID-D using the Sector 1 CRL lens system produced a flux density gain factor of approximately x108 compared to slit reduction, with the ultimate spot size being 50(h) x 3.7(v) µm at 60 keV.

### 4-15.3 Beamline Description

Figure 4.80 shows the planned layout of 6-ID.

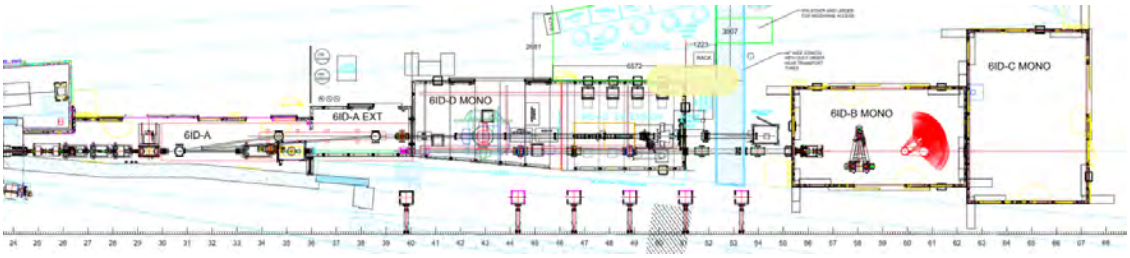


*Figure 4.80. Planned layout of the 6-ID beamline.*

As part of the upgrade the beamline will become canted with a 1 mrad separation between the sources. The upstream inline planar undulator with provide beam outboard through the 6-ID-A hutch to the experimental station in the 6ID-D hutch. The downstream SCU will provide beam to the inboard through the 6-ID-A and 6-ID-D hutches to experimental stations in the 6-ID-B and 6-ID-C stations.

## 4-16 7-ID Enhancements

The competition among multiple collective states in condensed-matter systems leads to coexisting phases (heterogeneities) at length scales from nm to µm and time scales from sub-ns to tens of Âţs. We have proposed enhancements to the 7-ID beamline that will provide critical insight into emergent problems in condensed matter physics and materials science. This facility is only possible at the APS-U because it is enabled by the unique timing structure and significantly enhanced coherent flux of the APS-U, which results in a single-bunch brightness that is 25 times better than available from the APS today and an order of magnitude greater than any other existing or proposed synchrotron. The instrumentation and scientific expertise at the beamline will allow researchers to directly visualize mesoscopic structural dynamics on characteristic length and time scales of 100 nm and 100 ps, respectively.

Three enhancements that have been evaluated as "highest priority" in the APS-U Beamline Enhancements Program are described here.

### 4-16.1 White-beam mirror

The first enhancement will be the beamline's first optical element, a horizontally deflecting white-beam mirror. This Si mirror with Rh and Pt stripes will have a 3.25 milliradian grazing angle, resulting in critical energies for the stripes of 9.8, 20.5, and 26.1 keV, respectively. It will be positioned upstream of the monochromator, which will greatly improve the thermal stability of the mono's indirectly cooled crystals.

### 4-16.2 Kirkpatrick-Baez nanofocusing optics

The second enhancement is fixed-figure Kirkpatrick-Baez (KB) mirrors for the nanodiffraction/ microscopy/ SNOM setup. These will replace the zone plate currently in use and will result in a ten-fold increase of focused x-ray flux. Calculated spot sizes with a working distance of 100 mm are about 90 nm vertical by 150 nm horizontal (FWHM), compared to current values of about 400 nm by 1200 nm. The relatively large working distance is intended to allow small sample-environmental chambers as well as provide optical access for the excitation beams and the SNOM.

### 4-16.3 High-resolution, decoupled detector arm

The third enhancement is a mechanically decoupled, extended detector positioning assembly for the multimodal imaging platform. A motorized detector arm decoupled from the sample stages is necessary to achieve the highest resolution and repeatability. This will include a separate detector and flight path positioning assembly. A sample-to-detector distance of 2.5 meters will permit the oversampling necessary for coherent diffraction imaging measurements while preserving the mechanical stability of the sample.

### 4-16.4 Beamline Description

The key driver in these enhancements is the optimization of the multimodal imaging platform currently located in 7-ID-C. Thus, the enhancements described here are intended to optimize the

use of this instrument with the APS-U and the brightness per bunch that the APS-U will provide. This instrument will be relocated to 7-ID-D providing slightly higher demagnification, less separation from the high-power ultrafast Ti:Sapphire laser, and a dedicated experiment space that can be used even when x rays are present in the upstream hutches. Complementarily, our vision is to increasingly optimize 7-ID-C for general-purpose and pump-probe diffraction and time-resolved spectroscopy and to dedicate 7-ID-B to time-resolved fuel spray imaging and levitator-enabled mixing and synthesis experiments that can run in 324-bunch mode.

A schematic of the enhanced 7-ID beamline is shown in Figure 4.81. A very brief description of the major components of the enhanced 7-ID beamline follows:

- 2.7-cm undulator
- Standard APS-U front end
- 7-ID-A: FOE
  - Masks, collimator, Be window
  - L5-20 white beam slits
  - Horizontal mirror (*enhancement*)
  - High heatload double-crystal monochromator: Si(111) or Si(311)
  - P4-20 mode shutter
- 7-ID-B: White-beam compatible experimental hutch
- 7-ID-C: Mono-beam hutch for spectroscopy and general diffraction
  - Multicircle diffractometer
- 7-ID-D: Mono-beam hutch for multimodal imaging
  - Fixed-figure KBs (*enhancement*)
  - Multimodal diffraction/imaging platform
  - Decoupled detector arm (*enhancement*)

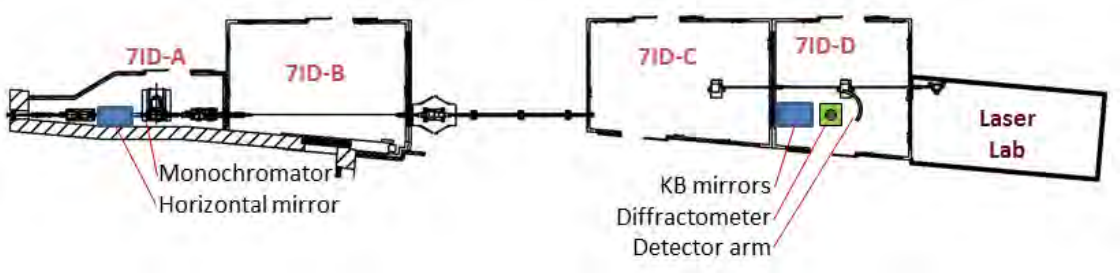


*Figure 4.81. A schematic of the enhanced 7-ID beamline.*

## 4-17 11-ID Enhancements

The microscopic ordering of a material drives its macroscopic properties. High-energy X-rays enable structural analysis of such materials from nearest neighbor ordering and the study of nanometer sized domains to long-range order over several micrometers. In the highly successful experimental stations 11-ID-B and 11-ID-C, structural analysis has led to a better understanding of the synthesis of materials, annealing processes, the function of materials, aging of devices, chemical reactions, and many more phenomena.

While the ensemble study of bulk material has given great insight into the average ordering of materials, information on the structure of materials with spatial resolution requires focusing the high-energy X-ray beam down to the submicron level. This will be enabled by the ultra-low emittance of the upgraded APS. Surfaces and interfaces are of particular interest for functional devices, chemical reactions, as well as for the synthesis of materials. Grazing incidence diffraction allows surface sensitive measurements while taking full advantage of high-energy X-rays for structural analysis.

The combination of WAXS/SAXS measurements will enable the addition of shape and size information to this structural analysis. Additionally, SAXS capabilities will allow us to study dynamics in domain fluctuations with XPCS, utilizing the coherence fraction of the beam. Fully utilizing the APS-U to achieve these goals will require the beamline enhancements described below.

### 4-17.1 Canting the Beamline

Exchanging the insertion devices and canting the new superconducting undulators will allow independent operation of the main and side stations. The superconducting undulators will provide a significant gain in flux, especially at 100 keV. The canting will allow uncompromised performance for 11-ID-D. This enhancement requires a new photon stop (moveable-mask + bremsstrahlung-stop), two tungsten collimators with masks, high-heat-load canted slits, and shielding modifications.

### 4-17.2 Multilayer Monochromator

A Double Multilayer Monochromator (DMM) will be used to vertically offset the beam to the 11-ID-D hutch. The DMM will diffract almost all the flux in a single undulator harmonic, while strongly suppressing higher harmonics. After successfully testing multilayer optics produced in-house by Ray Conley (Optics group) at 106 keV photon energy, we found that a water-cooled multilayer optic provides high flux and full tunability between 27 keV and 120 keV. If a higher energy resolution than that provided by the DMM is required, a secondary silicon crystal optic will be used downstream.

### 4-17.3 1D and 2D CRLs

The beamline will be equipped with focusing optics for 1D and 2D focusing by employing compound refractive lenses (CRLs). One set of lenses will be placed in the 11-ID-A hutch for 1:1 focusing or collimation and a second set in the experimental hutch 1-4 m in front of the sample.

### 4-17.4 11-ID-D Extension and Mini-enclosure

The 11-ID-D experimental station will be extended by 11 m to allow total scattering from very small q (SAXS) to large q (typical PDF). The laser hutch currently behind the station will be removed to make space for a large experimental station. This station will be equipped with a heavy load diffractometer capable of surface diffraction measurements. This extension will allow an area detector to be placed about 12-15 m away from the sample, enabling an extended range of SAXS measurements and potentially facilitating XPCS measurements as well. Figure 4.82 shows the extension of the 11-ID-D station in green outline.

A mini-enclosure, which will house a second monochromator to improve energy resolution (not part of this enhancement project), is located at the upstream end of 11-ID-D. The enclosure is outlined in green in Figure 4.82 and has a manual door access that does not require PSS interlocks.

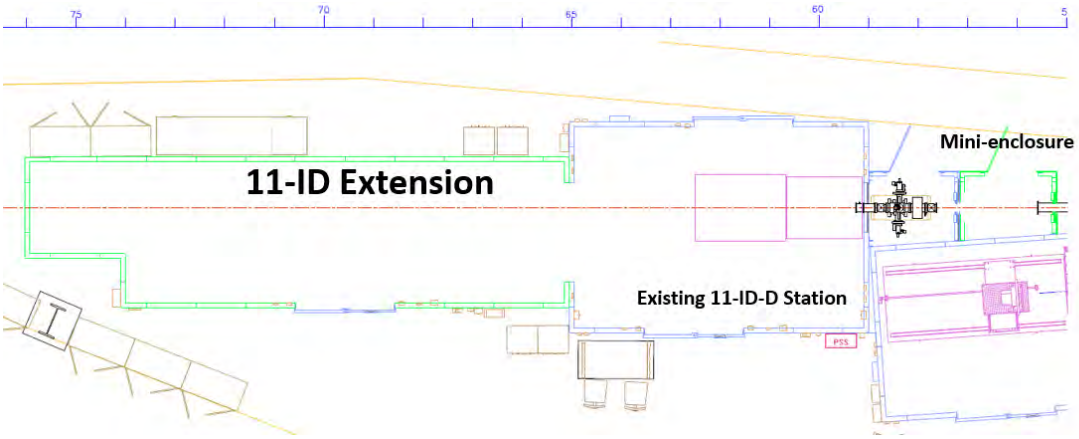


*Figure 4.82. The 11-ID-D station extension outline is shown in green on the left side of the drawing. The mini-enclosure is located on the upstream end of the station on the right side.*

### 4-17.5 Beamline Description

Sector 11 is composed of 4 beamlines: 11-BM, 11-ID-B (at a fixed angle of 7.4 degree), 11-ID-C (at a fixed angle of 3.9 degree) and 11-ID-D (straight). 11-ID-B and –C will share one insertion device, while 11-ID-D will operate independently with a canted beam from the second insertion device. The layout of 11-ID-B and C will constrain the optical design of 11-ID-D, since their monochromators cannot be moved and need to remain roughly 31 m from the source. 11-ID-D will use a DMM as first optic to offset the beam in the vertical plane enabling energy tunability between 27 to 120 keV.

Focusing optics (CRLs) at the end of the FOE (at 36 m) will allow 1:1 focusing. Lenses in the experimental station at about 60 m from the source will focus the beam at the sample position down to submicron length scales. If higher energy resolution is required, a secondary monochromator in the mini enclosure at 55 m can be used.

The optic layout is a complicated because it is designed to allow 3 beamlines to operate simultaneously. The stations B and C will use the inboard beam, and 11-ID-D will take the outboard beam. The monochromators for B and C will need to stay where they currently are to avoid the significant costs associated moving beam transport pipes. Therefore, the optics for the D station have to be

designed around this constraint. The spectral width of a given x-ray harmonic after the upgrade will be significantly narrower then they currently are, about 1%.

## 4-18 12-ID Enhancements

Sector 12 is home to three beamlines: 12-BM, 12-ID-B, and 12-ID-C/D. The bending magnet and the canted ID line support both chemistry and materials science user programs. The 12-ID beamline suite provides SAXS based techniques including grazing incidence SAXS (GISAXS), anomalous SAXS (ASAXS), SAXS/XAFS, and SAXS/WAXS in addition to other techniques used for studying nanoscale structures of materials

The proposed enhancements along the APS-U will improve the q and spatial resolution of each beamline. Microfocusing capability will be added to current SAXS/WAXS setup at the 12-ID-B station. The 12-ID-C station will become the highest $q_{min}$ and $\Delta q$ resolution SAXS facility in US by extending the length of current SAXS tube from max 4-5 m to 10 m. These improvements in both real and reciprocal space will enable new SAXS techniques including coherent SAXS, tomographic SAXS, 2D U-SAXS and scanning SAXS imaging. With these new capabilities, it will become possible to understand a material across multiple scales from atomic to nano, meso, and micro.

In addition to the enhancements described above, the USAXS program currently at 9-ID will move to 12-ID-C and undergo a significant instrumentation upgrade. This upgraded USAXS/SAXS/WAXS instrument will operate over a wide range of x-ray energies (currently, 7-24 keV, and extended in the future to least 30-keV or higher). Its spatial operational range will span six decades, with a largest measurement scale of over 20 microns. Temporal resolution will be reduce to 2-3 minutes; the dynamic range of the measured intensity will span over 10 decades. Combined with dedicated USAXS imaging and USAXS-XPCS capabilities this instrument will provide a combination of techniques not available anywhere else. The main target of this unique facility will be to measure materials under real (*in operando*) conditions.

### 4-18.1 Extension of the SAXS beamline

The low q resolution limit of the 12-ID-C SAXS beamline will be enhanced and the overall $\Delta q$ resolution will be improved by doubling the sample to detector distance. The SAXS vacuum flight tube in 12-ID-C, that currently limits the max sample to detector distance to 6 m, will be extended to 12m. Doubling the sample-to-detector distance will enhance both $q_{min}$ and $\Delta q$ resolutions by the same factor. Access to smaller q is essential for coherent SAXS and fast kinetic studies because the SAXS cross section generally decays with the $4^{th}$ power of q. The extension of the 12-ID-C beamline will allow the USAXS instrument to be relocated to the 12-ID-C hutch. This will enable 2D USAXS for the study of oriented samples, it will improve $\Delta q$ resolution while not compromising it for higher X-ray energies, it will enable coherent SAXS imaging, and it will allow fast kinetics studies enabled by the double-multilayer monochromator that has been built for the station. In order to facilitate these enhancements, it is required to lengthen the 12-ID-C station by partly removing the separating wall between 12-ID-C and 12-ID-D station. The newly designed 12 m long SAXS vacuum flight tube will span the 12-ID-C and 12-ID-D stations and include an in-vacuum 2D detector that will translate to cover q range of interest based on user's needs. Samples for SAXS will be located either on a new sample stage that will sit between the SAXS flight tube and USAXS instrument or on the USAXS sample table. In the latter case, the vacuum flight tube will be designed to give extra sample-to-detector distance.

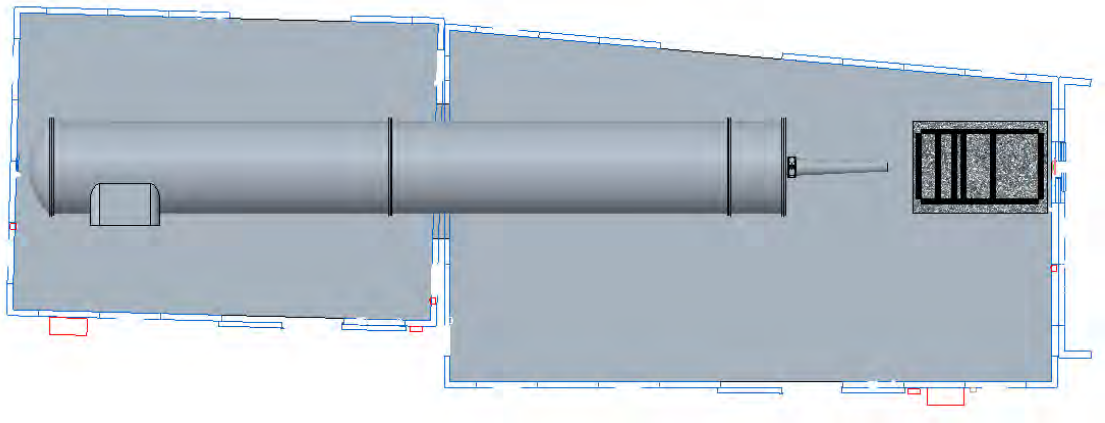

*Figure 4.83. Extension of the SAXS beamline, showing upgraded flight tube and modified hutch.*

### 4-18.2 Upgraded Focusing Optics

The current focusing device, one vertical mirror in the third mini hutch (MH3) will be upgraded to a CRL transfocator in the first mini hutch (MH1). The upgraded focusing optic will significantly enhance the low q resolution limit and the overall $\Delta q$ resolution up to an order of magnitude when combined with a longer sample-to-detector distance. MH1 will also be expanded to house the CRL transfocator and allow for the repositioning of the final Bremsstrahlung collimator for APS-U 200mA operation.

### 4-18.3 Upgrade of USAXS Instrument

USAXS/SAXS/WAXS instrument will be enhanced by a complete redesign to provide a suitable platform for growth and to take full advantage of the APS-U beam capabilities. The USAXS instrument will be redesigned so that the main scattering direction is reoriented horizontally (as opposed to vertically today). The increased stability that will come with this reorientation will make use of the high-resolution setup (Si(440) crystals) practical and will also enable use higher order (e.g. Si(660)) reflections in those cases when extreme resolutions are necessary. The use of high-resolution Si(440) optics extends the measurement range up to ~ 20 microns for large sample features, while preserving the ability to measure small features. High-resolution Si(440) measurements performed in the current vertical geometry yield noisy data and only work for strongly scattering materials. The enhanced capability will help meet growing demand by the user community for high-resolution measurements even for weakly scattering samples, such as bacteria. The horizontal scattering geometry will be also be more practical for 2D collimated USAXS, USAXS imaging, as well as for USAXS-XPCS. Use of the Si(660) reflection will extend the range of measurements to even larger sizes, positioning our instrument well ahead of any other currently existing or even planned (U)SAXS instruments in the world.

### 4-18.4 Beamline Description

In order to enhance the resolution of SAXS in the **12-ID-**C station, we propose to extend the length of the **12-ID-**C station and focus beam with CRLs. To do so,

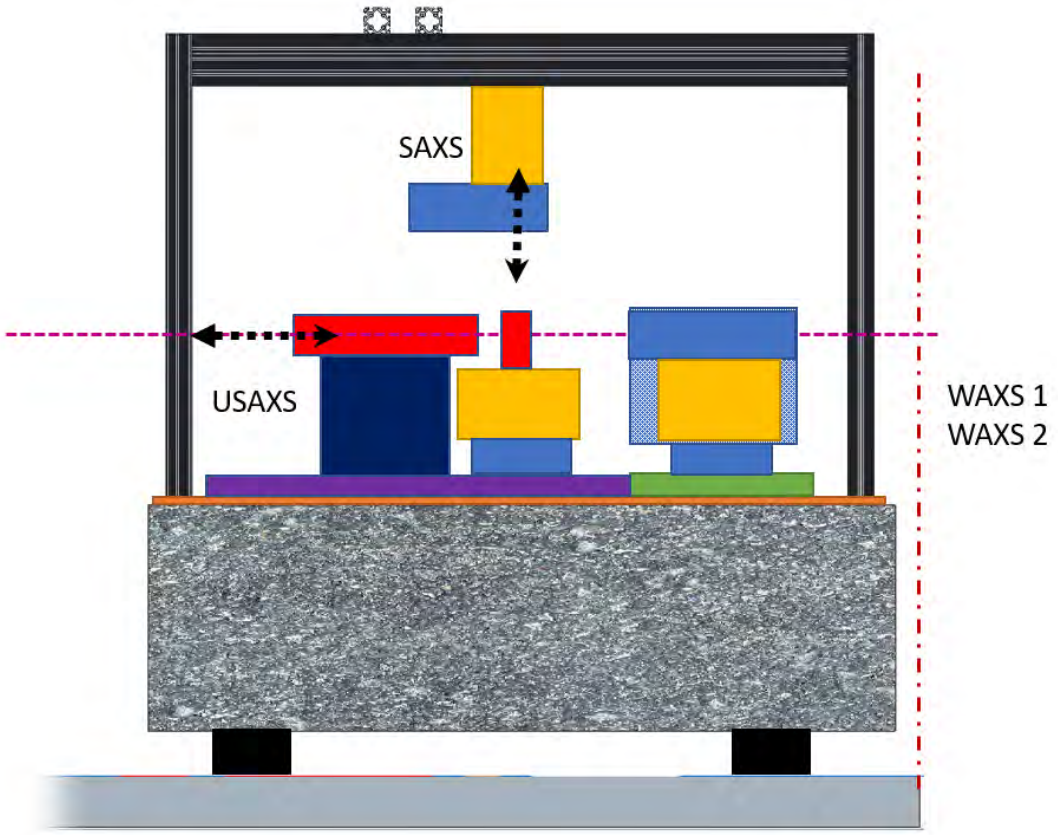


*Figure 4.84. General layout schematic of the USAXS instrument table*

- The wall between **12-ID-**C and **12-ID-**D stations will be partly removed.
- Through the hole in the wall, a long SAXS chamber will be built and located. Diameter and length of the chamber will be around 1.5 m and 12 m, respectively.
- A set of CRLs will be installed in MH1 at 43 m. This CRL system will focus beam at the detector in the SAXS chamber, the position of which will vary. X-ray energy of the beamline will range from 6 to 35 keV.
- MH1 will be expanded to house the new CRL transfocator and because the final Bremsstrahlung collimator that the MH1 is currently housing needs to be redesigned for APS-U 200 mA operation.
- Experimental setups of **12-ID-**C/D SAXS will be upgraded accordingly, including SAXS vacuum flight tube, SAXS sample table, and USAXS instrument.

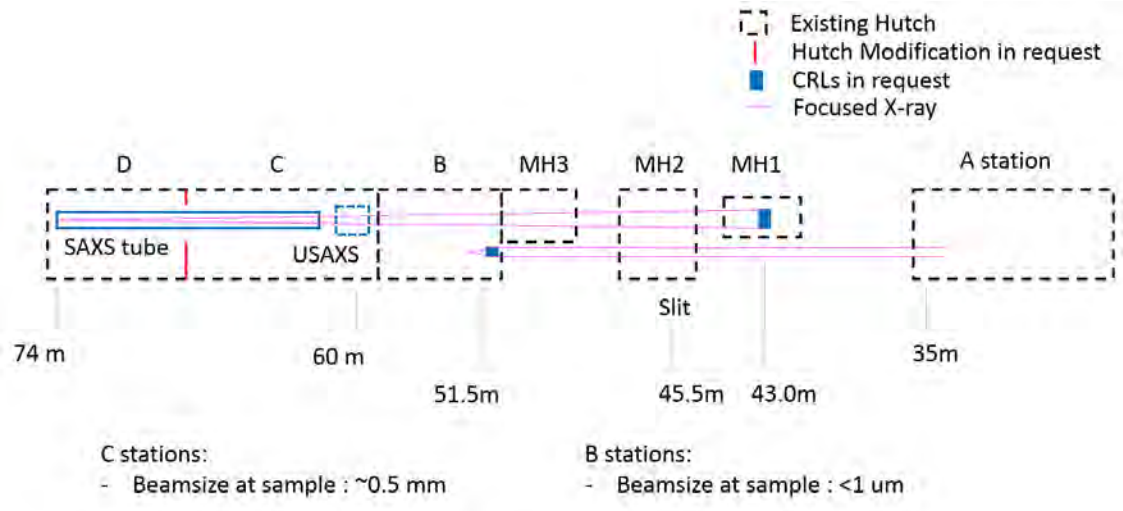


*Figure 4.85. Schematic drawing of upgraded 12-ID layout. Hutch walls at places in red need to be modified. For the C station, 12m long SAXS tube and a set of CRLs with a transfocator are required.*

## 4-19 15-ID Enhancements

The enhancements described here outline the required upgrades to the ChemMatCARS (15-ID) beamline focusing optics. The aim of this upgrade is to achieve the dual capabilities of both producing micro-beams at high energies (30 to 70 keV), with more than three orders of magnitude gain in flux density on samples, and performing energy scans in the range of 5 to 70 keV, so as to take full advantage of the APS-U low emittance and high flux density high-energy beam.

### 4-19.1 Conversion of bimorph mirror system to mechanical bender and mirror slope error reduction

Currently, the 15-ID beam delivery system employs two reflective mirrors: a vertically focusing bimorph mirror and a vertically deflecting flat mirror placed in the same mirror tank; the mirrors are 600 mm (L) x 50 mm (W) x 40 mm (T) and are located 32.5 m away from the undulator source, and 24 m and 29 m away from sample locations in Hutches C&D, respectively. X-rays of different energies, from 5 to 70 keV, are delivered via three different stripes on the mirrors: Si, Rh, and Pt. The performance of the bimorph focusing mirror has been problematic since it was installed by ACCEL in 2010. To begin with, the optimization process for the bimorph has been time consuming and not very reproducible. Additionally, the figure and reflecting surface of the mirror deteriorated over time, most notably on the uncoated silica surface used for the lower energies (below 12 keV). The vertical beam was 80 µm FWHM at 24 m (in Hutch-C) when measured during the initial commissioning period, corresponding to a combined RMS slope error of 0.7 µrad from the two mirrors, as specified by ACCEL. Currently, the vertical beam is 200 µm FWHM from the Si stripe and 120 Îijm FWHM from the Rh and the Pt stripes, corresponding to a combined RMS slope error of 1.8 µrad and 1.0 µrad, respectively. In addition, the profile of the focused beam with the Si stripe is asymmetric with a large diffuse background, containing undesired structures, and is irreproducible.

The required upgrades of the existing mirror system is to replace the existing bimorph-focusing dual-mirror system with a mechanically bent flat-silicon dual mirror system.

The combined RMS slope error for the two new mirrors is specified as 0.28 µrad (0.2 µrad each), which will produce a vertically focused beam of 35 µm FWHM in Station C. The new mirrors will improve not only the beam flux and profile, but also the efficiency of beamline operations because the mechanical bender is expected to outperform the bimorph in terms of beam optimization and reproducibility.

### 4-19.2 Addition of 95 2D CRLs to existing transfocator

This enhancement entails adding 95 aluminum parabolic lenses to the existing 2D CRL transfocator, which will significantly enhance the beamline capabilities in the energy range of 30 to 70 keV.

The 15-ID beamline has been upgraded to provide higher energy X-rays (up to 70 keV), as well as a new state-of-the-art high energy X-ray detector (Pilatus3X CdTe 1M). However, a limiting factor in the development of many new experiments is the large size of the beam. 15-ID uses reflective mirror optics to deliver vertically focused beams of 120 µm (FWHM) for the higher energies, with a horizontal beam size of 1.5 mm. A beam size in the vertical as small as 15 µm can be achieved by

passing the beam through an aperture, but this comes at the cost of reducing the beam intensity by a factor of ten. Coherence effects limit further reduction in the vertical dimension. Although this beam size is adequate for some experiments, many require smaller beams, on the order of 1 to 5 µm vertically, and for some, 10 to 15 µm horizontally.

The 2D CRLs will be placed in Hutch-B1, at a distance of 10 and 15 meters, respectively, from Hutch-C (liquid surface scattering), and Hutch-D (advanced crystallography). Our optical calculations for higher energies (30 to 70 keV) indicate that the 2D CRLs will produce a beam size of 2 to 3 µm vertically and 11 to 16 Îijm horizontally, while increasing the flux density on samples by more than three orders of magnitude (compared with a non-focused beam) in Hutches C and D.

The existing transfocator already includes the support, tank and global motion system which will serve the added 2D lenses. The added 95 2D lenses will be driven by 7 actuators.

### 4-19.3 Harmonic rejection mirrors

In conjunction with the 2D CRLs described in section 1.2, a mirror assembly located in each hutch (three in total), consisting of two flat mirrors of 100 mm (L) x 25 mm (W) x 20 mm (T), is required to reject higher harmonic X-rays that will pass through the CRL assembly. By using two mirrors, the higher harmonics are reduced by six orders of magnitude, which is sufficient to compensate for beam hardening due to attenuation.

### 4-19.4 Beamline Description

Figure 4.86 is a preliminary beamline layout for the upgrade. The 15-ID beamline is canted with 2 beamlines and 4 experimental stations (15-ID-B1, B2, C, D). Stations B1 and B2 are repeated top and bottom) as shown in in Figure 4.86. The top portion in Figure 4.86 is the upstream half of the beamline and the bottom postion is the downstream portion of the beamline. In Figure 4.86 the labels are as follows: FOE: First Optics Enclosure. SOE: Second Optics Enclosure. Canted Beamline: (c1-c2) Side-bounce monochromator, (c3) CRL, (c4) interface scattering, (c5) crystallography. Straight Beamline: (s1) monochromator, (s2) reflection mirrors, (s3) CRL, (s4) interface scattering, (s5) crystallography and ASAXS, and (s6) high harmonic rejection mirrors.

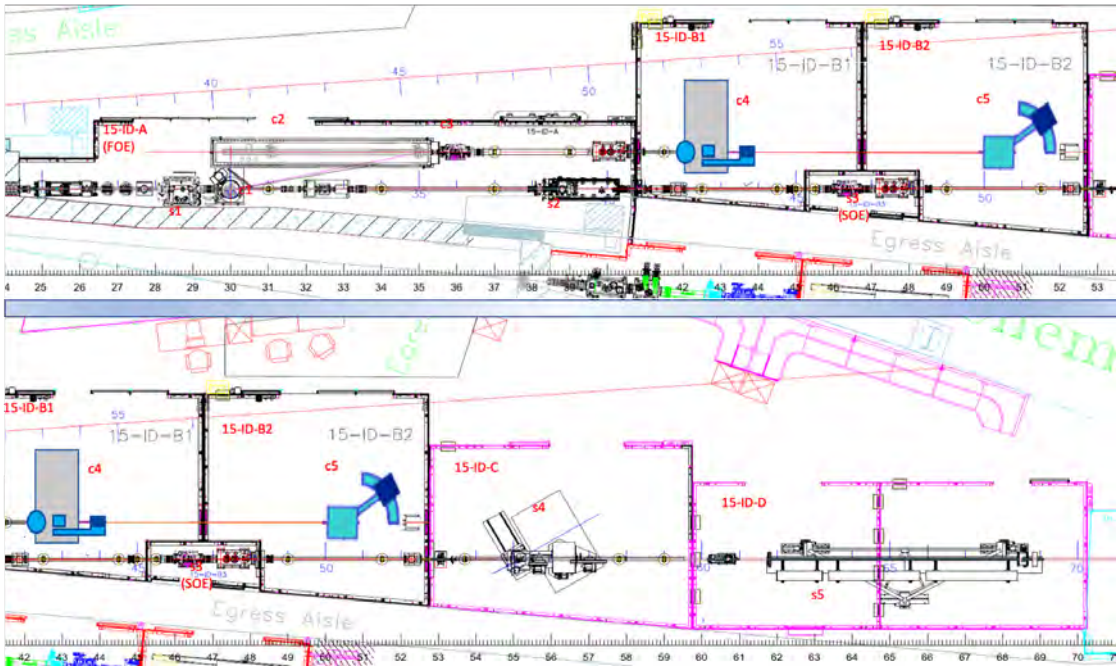


*Figure 4.86. Schematic layout of sector 15-ID.*

## 4-20 26-ID Enhancements

The Sector 26 Enhancement Project will deliver a new 4D Nanoprobe (N4D) visualization tool for the dynamic manipulation of nanoscale strain and heterogeneous crystallinity in space and time. The N4D project will significantly advance the capabilities of the existing CNM/APS Hard X-ray Nanoprobe, particularly in coherent nano-focused Bragg diffraction microscopy. The key instrumentation development is a rebuild of the Nanoprobe chamber to allow for: (i) rapid scanning and (ii) optical pump- x-ray probe capabilities intended to capture both reversible and irreversible nanoscale structural phenomena in the time domain. Enabling beamline developments include a first mirror with state-of-the-art figure error, a monochromator optimized for coherent throughput, and nano-focusing Fresnel zone plate optics targeted to high x-ray energy (15-25keV). This facility enhancement will allow the CNM / APS Hard X-ray Nanoprobe to take full advantage of both the unique brightness of the diffraction limited storage ring and the ring time structure planned under the APS Upgrade.

### 4-20.1 Rebuild Nanoprobe scanning capabilities

The first enhancement target is a redesigned Nanoprobe Instrument (NPI) built to enable rapid nanobeam diffraction and scattering imaging capitalizing on the unprecedented brightness of the APS Upgrade. We intend to create a rapid Bragg nanodiffraction scanning mode for strain imaging correlative with chemical imaging at speeds approaching video frame rate (target is a 1 micron 2D scanning area imaged with ~10nm spatial resolution at ~10-100ms total scan acquisition time). Rapid 2D imaging will be combined with slower (seconds to minutes) high resolution 3D coherent diffractive visualization of strain in volumes of interest. Beyond strain, these capabilities will enable a diverse user community using the many structural contrast mechanisms available with x-ray diffraction such as unit cell polarization, orbital ordering or magnetic ordering. Rapid scanning diffraction when combined with x-ray fluorescence will also enable irreversible structural/chemical processes in materials to be correlatively visualized, providing critical insight in areas such as diffusion in chemically driven structural transitions of cathode materials, self-assembly of quasi-crystals, or structural transformation kinetics in oxygen conductors used for solid oxide fuel cells. This capability will also enable efficient, direct observation of statistically relevant populations of nanoscale structures within single-shift (8-hour) time frames under operating conditions, closing a key gap in x-ray methodology.

### 4-20.2 Rebuild of mirror system M1

The second enhancement target is to rebuild the interior components of the M1 mirror system to optimize figure error, coherent flux transfer, and mechanical stability. This thrust combines the re-polishing of the M1 first mirror with an optimization of mirror interior components to take advantage of current best practice design elements for stability in reflection based synchrotron optics. This is a critical development as current beamline operation uses a horizontal Beam Defining Aperture (BDA) downstream of the mirror system as a virtual x-ray source to correct for current source astigmatism, in large part hiding the current mirror performance. This aperture will be removed due to the upgraded source characteristics, dramatically increasing the sensitivity of microscope operation to mirror performance.

### 4-20.3 Rebuild of Double Crystal Monochromator (DCM)

The third enhancement target is a rebuild of interior components of the Double Crystal Monochromator (DCM) to improve high-heat load angular stability and coherent flux transfer. The motivation for this development is also a consequence of the removal of the BDA in the beamline upgrade plan – as current beamline operations only use a coherent fraction of the x-ray beam to illuminate the DCM, the effective heat load on this component will increase by ~100x under the upgrade. The interior components are currently designed to take advantage of the BDA by using low-cooling-power / low-vibration connections which will be insufficient for the upgrade scenario.

### 4-20.4 Fresnel zone plate optics for 20keV

The fourth enhancement target is a set of nano-focusing Fresnel zone plate optics with ~20nm effective outermost zones compatible with high x-ray energy (15-25keV) operation. This development will make full use of the continuous energy selection of our planned APSU 2.7cm undulator from 6-25keV, complementing our current 6-15keV optics. These optics will be mounted with central stops and a vacuum-compatible interface layer by Zeiss.

### 4-20.5 Beamline Description

The first optical element 30m from the source is a double horizontal mirror system in 26-ID-A. The Double Crystal Monochromator (DCM) is located 63m from the source in 26-ID-B. The Nanoprobe Instrument is 75m from the source in the end station, 26-ID-C. The current beamline configuration uses the horizontal mirror system to focus the pink beam onto a horizontal beam defining aperture (BDA) 40m from the source – under the APS Upgrade this operating mode will change to a flat mirror / open BDA configuration changing the heat and stability requirements for both the mirror and DCM.

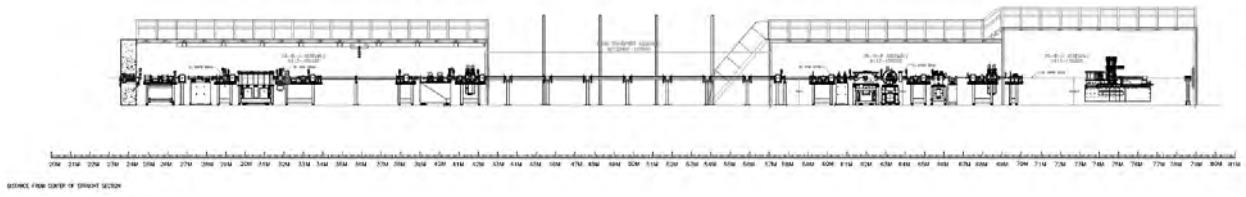

*Figure 4.87. Beamline layout and location of the NPI instrument at 26-ID-C*

### 4-20.6 Instrument Overview NPI

The NPI is defined as a combination of:

- A sample configuration, including staging and the experimental environment.
- An optic configuration, including optic stages and any local beam conditioning.
- Dedicated detectors for diffraction and x-ray fluorescence measurements.
- Metrology and supporting hardware for monitoring sample and optic motion.
- Vacuum chamber housing the sample and optics.
- Supporting structures and positioning needed to place the vacuum chamber in the beamline.

- Laser delivery system to the sample.
- All connected auxiliary hardware to the vacuum chamber needed to run the NPI.

A visualization of the upgraded instrument is shown in Figure 4.88.

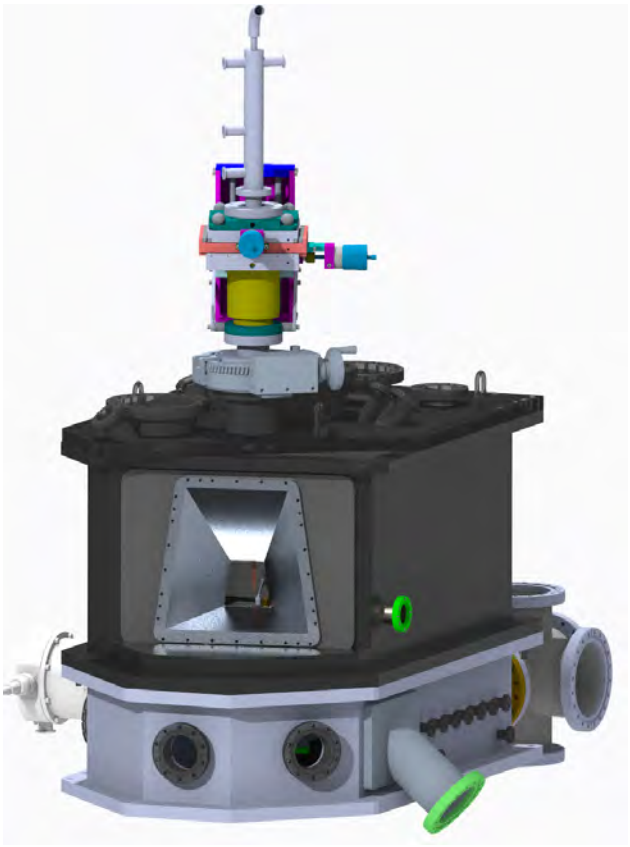

*Figure 4.88. A schematic of the NPI upgrade planned.*

The NPI resides in 26-ID-C. A layout of 26-ID including the instrument location in the hutch is shown in Figure 4.87 and Figure 4.89. The upgrade to the NPI will not change the location of the instrument.

The NPI will only operate with a selected mono-beam at a fixed height. The NPI will be stationary and will not have to move out of beam for other beamline modes of operation.

The following are capable x-ray measurement techniques of the NPI:

1. Scanning x-ray diffraction microscopy (SXDM).
2. Bragg fast scanning nano x-ray diffraction (BXRD)
3. X-ray fluorescence (XRF).

A detailed description of the 26-ID Nanoprobe enhancements can be found in the APS-U 26-ID Nanoprobe enhancement ESD (ICMS Content ID: APSU_2030657).

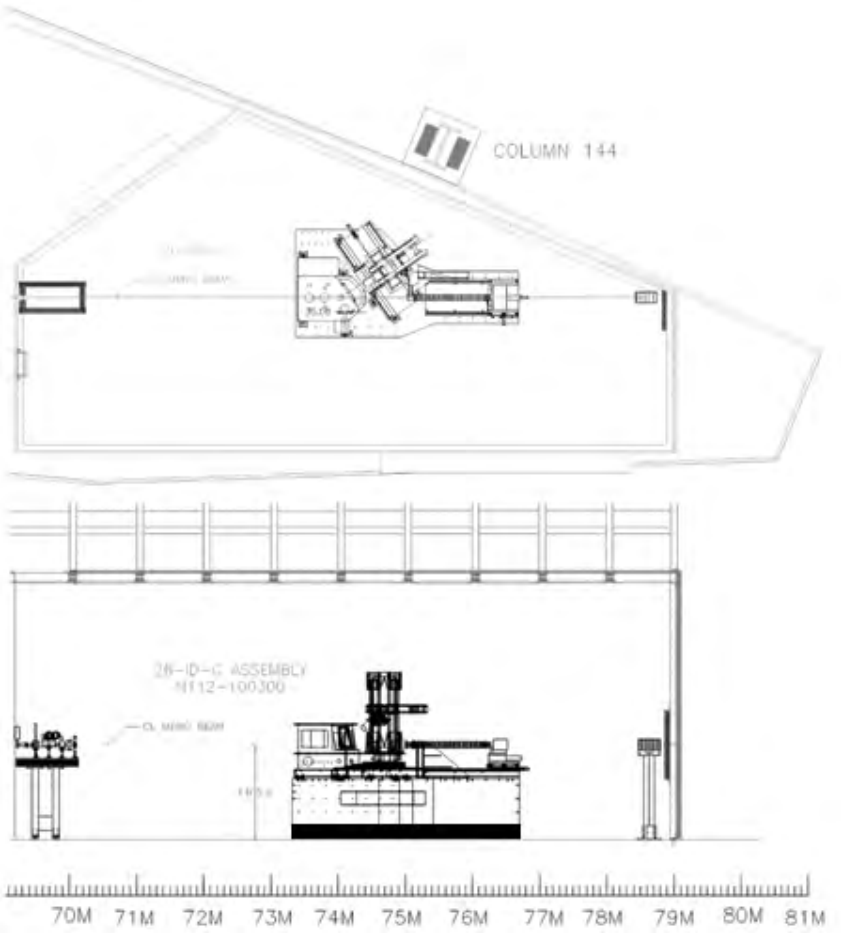


*Figure 4.89. Zoomed in view of NPI beamline location*

## 4-21 27-ID Enhancements

For resonant inelastic x-ray scattering (RIXS) at beamline 27-ID, the upgrade of the APS offers unprecedented opportunities for enhancements of the technique and the beamline, which will greatly benefit the users of the facility. These enhancements become possible due to the vastly increased brightness of the x-ray source, enabling focal spots at the sample position at 27-ID of 500 nm or smaller. Secondly, the increase in flux for this photon-hungry technique will permit measurements that are not feasible today, even at the very limited band passes required for ultra-high resolution measurements. In order to fully utilize the characteristics of the future x-ray source at the APS, the following beamline enhancements are proposed in order of priority.

### 4-21.1 Extension of the high-energy-resolution monochromator

Beamline 27-ID employs an older, in-vacuum, high-resolution monochromator that was designed to be tunable over a wide range of energies (5 keV to 15 keV), but is limited to a best resolution of 70 meV. Higher resolution measurements are currently performed using ad hoc, in-air assemblies, consisting of single or double monolithic channel cut crystals of appropriate orientation.

It is required that the mechanical in-vacuum assembly be extended from the 2 existing to 4 high-precision motion stacks (Only 1 by APS-U). These are required to be equipped with crystals that yield multiple choices of resolutions in the 5 meV to 80 meV regime. The tunability range is required to be between 6 keV and 20 keV for lower resolutions and 9 keV to 12 keV for the highest resolutions.

The current vacuum vessel will be re-used. Only one-half of the existing vacuum vessel is currently occupied, the extension can be accommodated in the other half. Thus, only motion stages, crystals and vacuum feed-throughs will have to be procured.

### 4-21.2 Upgrade of the RIXS spectrometer

The biggest impediment to a full utilization of the upgraded source characteristics is the custom-built 7-circle diffractometer, in use as RIXS spectrometer at 27-ID. Principal mechanical components of this instrument include motion stages that are more than 30 years old, causing a sphere-of-confusion of ~200 µm or larger, even after a thorough re-alignment. In order to properly manage measurements with future small beams and maintain proper alignment of the complex analyzer assemblies, these stages are required to be replaced by modern devices. In addition, the sample stages are currently rigidly connected to the horizontal detector arm motion. An independent 3-circle Euler-type sample environment mounted on the fixed spectrometer base is required to properly decouple sample and detector circles. An overall sphere-of-confusion of 5 µm is required for the spectrometer upgrade.

### 4-21.3 Beamline Description

The RIXS beamline is located in sector 27 at the APS and consists of two back-to-back shielding enclosures, 27-ID-A and 27-ID-B, and an enclosed control room, providing temperature stability for the experimental areas of the beamline and a space for beamline control components, sample preparation facilities, and user accommodations. There will be no modifications to these enclosures.

The overall layout of the beamline is shown in Figure 4.90. The first enclosure, 27-ID-A, serves as a First Optics Enclosure (FOE), housing all white-beam equipment. The most upstream component is a differential pump, providing a window-less transition between the front end and the beamline and defining the size of the entrance aperture through its intrinsic mask. The aperture size is approximately 2 x 2 $mm^2$ (h x v). The differential pump is followed by a white-beam slit, which provides a user-selectable aperture between 0x0 $mm^2$ and 5x5$mm^2$. The heart of the FOE is a water-cooled, double-crystal, diamond high-heat-load monochromator. The FOE is terminated by a white-beam stop, a Bremsstrahlung stop and a monochromatic shutter assembly. The white beam stop blocks the white beam while passing the monochromatic, the Bremsstrahlung stop stops Bremsstrahlung radiation, and the shutter will allow user access to the downstream portion of the beamline while beam is present in the FOE. The transition for the monochromatic x-ray beam between the 27-ID-A and 27-ID-B enclosures is accomplished with a shielded transport pipe.

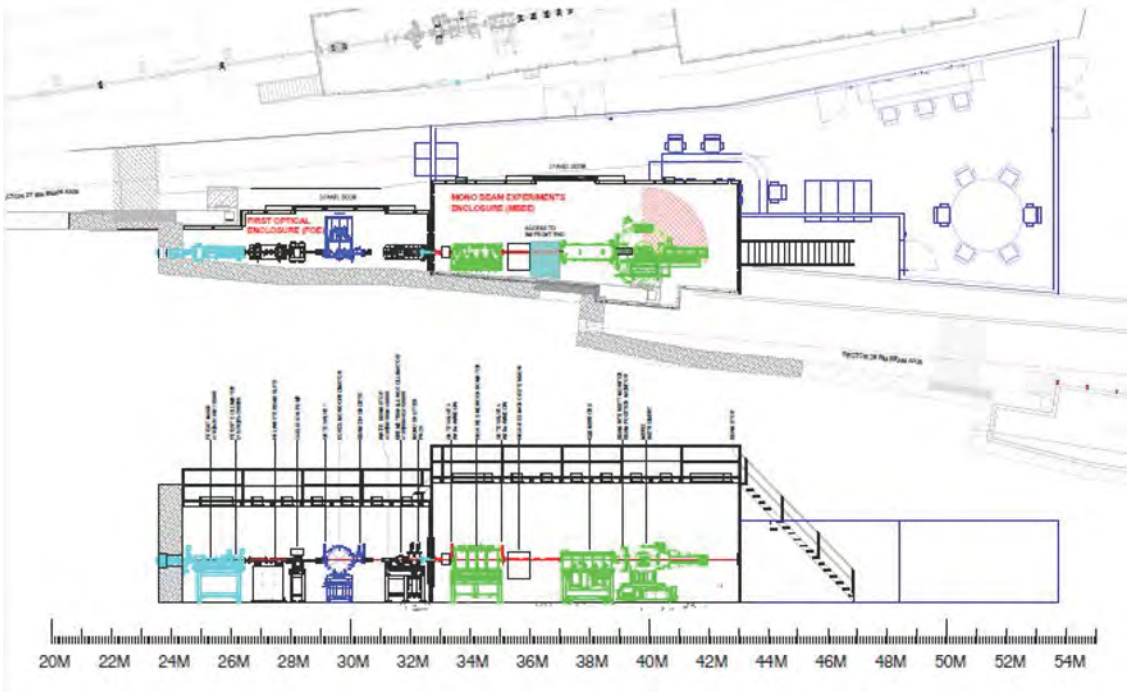


*Figure 4.90. Plan and elevation view of beamline 27-ID*

The second shielding enclosure, 27-ID-B, serves as a user-accessible experimental station. It houses a set of high-resolution monochromators, focusing mirrors and the main instrument, the RIXS spectrometer. This enclosure is surrounded by an enclosed control room and user work space.

In regards to radiation safety, the enclosure 27-ID-A is a white beam station while 27-ID-B is a monochromatic station. The beamline shielding conforms to all APS standards. A photon shutter is installed between the A and B stations, which allows safe access to the B station even while beam is present in the A station.

## 4-22 30-ID Enhancements

The 30-ID enhancements will directly benefit the General User Programs (GUPs) at 30-ID and will greatly increase the scientific productivity of the beamline. At Sector 30, there are two techniques to measure atomic vibrations in condensed and soft matter. The two techniques are: 1) momentum resolved High Energy-Resolution Inelastic X-ray scattering (HERIX) at E = 23.724 keV and 2) Nuclear Resonant x-ray Scattering (NRS) at $^{119}$Sn isotope at E = 23.88 keV. Both techniques currently utilize the same high energy-resolution monochromator. Achieving 1.5 meV energy resolution at 23.7 keV with sufficient flux to measure phonon dispersions in solids is only possible at high-energy synchrotron radiation (SR) facilities like the APS. The APS-U will provide higher flux as well as smaller beam which are critical factors for any x-ray spectroscopy techniques in general and for high energy-resolution spectrometer at Sector 30 specifically. In order to utilize the characteristics of the new ring efficiently, the following improvements are required:

### 4-22.1 Cryogenic high energy-resolution monochromator

Part of the planed enhancement within the APS-U is to improve the overall energy stability and energy drift of the beamline, which are crucial for measuring a small shift in the phonon energy position and life time. Additionally, better energy stability increases the efficiency of data acquisition and accuracy. Energy instability is caused by thermal and/or angular drift. As a solution, we will install a new high energy-resolution monochromator (HRM) which operates at cryogenic temperatures with an exchange gas to minimize temperature gradient on the crystal surfaces. The copper box containing the exchange gas will be placed in a vacuum tank. The new HRM will have an active feedback on temperature as well as Bragg angles to provide the required energy stability as demonstrated at 3-ID where an energy stability of ~0.05 meV over a 3-to-4 day period was achieved. This is more than a factor of 100 better than the current beamline can deliver [38]. The new HRM will have a limited energy tunability and will not reach 23.88 keV ($^{119}$Sn NRS energy) and therefore, the current HRM will be dedicated to NRS and the new HRM will be used for HERIX.

### 4-22.2 High-heat-load monochromator cryogenic conversion

The second enhancement for the beamline is to convert the current high-heat-load monochromator (HHL) from water-cooled diamond crystals to cryogenically cooled high-quality silicon crystals to increase the throughput and stability as was demonstrated recently at sector 3. The present monochromator is a Kohzu HLD monochromator with on-axis water feedthroughs.

### 4-22.3 Beamline Description

The beamline is designed to enable high-energy-resolution inelastic experiments with 1.5 meV overall energy resolution at an incident energy 23.72 keV with a maximum momentum transfer of 72 nm$^{-1}$. This beam is used for the HERIX spectrometer in 30-ID-C station and with 1 meV energy resolution at incident energy 23.88 keV for NRS spectrometer in 30-ID-B station.

Sector 30 consists of three stations 30-ID-A, 30-ID-B and 30-ID-C. Station 30-ID-A is designed to be compatible with white beam, while stations 30-ID-B and 30-ID-C are compatible with monochromatic beam only, the beamline layout is shown in Figure 4.91. The major components are:

- Two tandem undulators, simultaneously optimized for HERIX spectrometer
- Water cooled double Be window (total thickness of 0.5 mm)
- Water cooled white beam slits
- A white beam Be-compound refractive lens (CRL) that collimates the beam for increased performance of the downstream optical elements for HERIX experiments above 20 keV
- A double crystal high-heat-load monochromator, with 25 mm vertical off-set
- An "in-line", high energy-resolution monochromator
- An in-vacuum, KB focusing mirror pair, housed in 30-ID-C station, with bimorph adaptive bending technology, dedicated to the HERIX instrument
- The HERIX spectrometer, also housed in 30-ID-C station, with 9 m long horizontal arm, currently fitted with 9 analyzers and expandable to 21 analyzers
- The FOE (30-ID-A) houses the beam-defining components, like the slits and a white beam refractive lens for collimation; in addition, it houses the bremsstrahlung stop and an integral shutter. Station 30-ID-B is a monochromatic station and houses the high-resolution monochromators, KB mirrors for NRS experiments and a table with sample mounting goniometer. The monochromatic photon shutter for the next station is also located here. Station 30-ID-C (HERIX), a monochromatic station, houses KB mirrors, sample mounting goniometer and motorized table, and the HERIX spectrometer. A work-area enclosure encompasses the two monochromatic stations for operating the beamline

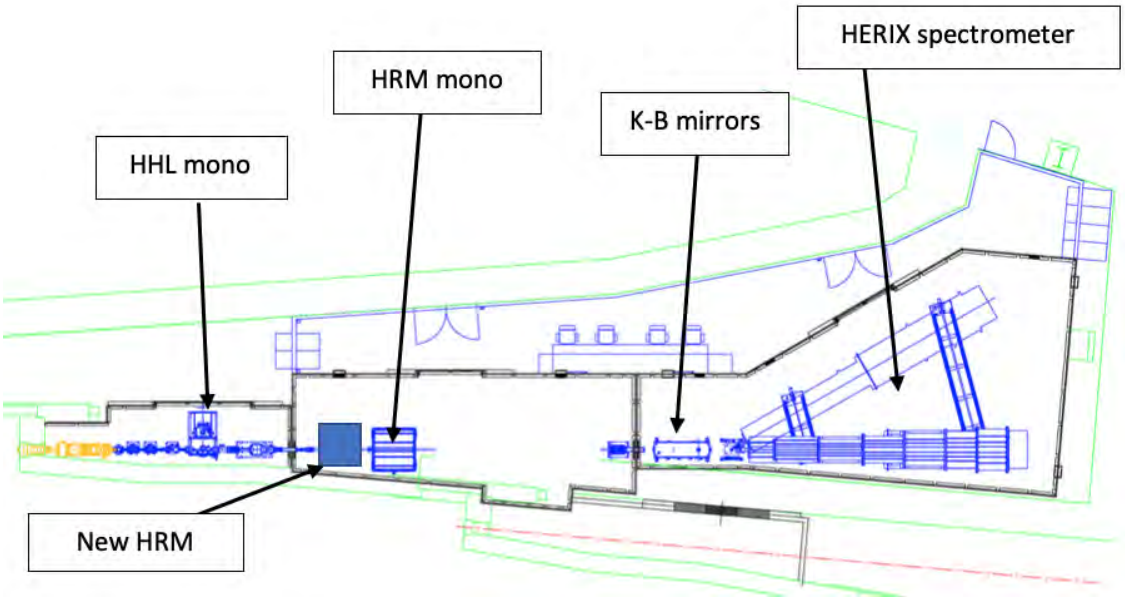


*Figure 4.91. 30-ID beamline layout*

## 4-23 32-ID Enhancements

The new APS-U source enables x-ray full-field imaging technique to extend its spatial resolution well below 1 µm, without a major sacrifice in time resolution providing hierarchical characterization of dynamic systems and materials. The new APS-U source, besides increasing sensitivity and resolution for parallel beam full-field imaging (by reducing the projected horizontal source size on the detector), enables a Kirkpatrick-Baez (KB)-based Cone Beam projection x-ray Imaging (CBI) to bridge the existing full-field imaging resolution gap in the 50-1000 nm range for dynamic systems while preserving the single pulse (~ 100s of ps) time resolution that currently only parallel white-beam imaging can afford.

We will exploit the new source characteristics by implementing projection x-ray imaging for the high-speed imaging program. This will increase the spatial resolution of the high-speed imaging instrument from 1 µm to below 100 nm and increase the temporal resolution of the nano-imaging tomography instrument from 500 ms to tens of µs. Other unique advantages offered by this particular instrument geometry are i) the zooming capability that fills the gap in terms of resolution and field of view between the currently available µ-computed tomography (µ-CT) and the transmission x-ray microscopy (TXM) based nano-computed tomography (nano-CT), and ii) the multi-modality capability coming from the simplicity of using the focused beam as a probe.

We will also enable the dual beam operation by canting the two existing undulators. We will use one beam for full-field imaging while we focus and deflect the second undulator beam back on the sample for simultaneous diffraction or WAXS/SAXS. This dual beam mode will make the beamline a unique and world-class facility for studying highly dynamic and irreversible processes.

### 4-23.1 Canting the Beamline

Two undulators in a canted geometry are required to achieve the dual beam imaging configurations described above. A number of beamline components will need to be either redesigned or repositioned to accommodate the canted beams.

### 4-23.2 Relocation of the TXM instrument to 32-ID-B

The TXM will be relocated to the 32-ID-B hutch. It will be positioned and configured in such a way that it can easily be moved to allow transport of the beam to the 32-ID-C hutch. This relocation will require new optical tables and new focusing optics. These requirements are described in detail in the 32-ID ESD.

### 4-23.3 Dual beam Imaging Instrument

To achieve the dual imaging configuration described above will require optics for deflecting and refocusing the canted beam onto the sample as well as a detector for measuring the diffracted signal. The required instrumentation is described in detail in the 32-ID ESD.

### 4-23.4 New Nano-CT Instrument

A new instrument for performing nano-CT measurements will be constructed and installed in the 32-ID-C hutch. This instrument will include focusing optics, a nano-positioning motion stack, optical tables, and stages for detector positioning. The technical specifications for this instrument are included the 32-ID ESD.

### 4-23.5 Beamline Description

Figure 4.92 (a) is the current operating mode, with two collinear beams from U33 and U18. The enhancements will allow for (b), (c), and (d). The current undulators will be replaced with equivalent ones (U28 and U13.5). For the enhancement, the beamline will be canted, Figure 4.92(b) is the dual-beam operation, where the single-line beam from U13.5 will be focused (with CRLs) and deflected with a small (multilayer) mirror toward the sample for local diffraction (or scattering) while we maintain the beam from U28 to do full-field imaging, all at ultrafast speed. Figure 4.92(c) is the high speed sub-micron ($>$ 50 nm) imaging, in a projection mode with variable resolution and field of view, using a KB system. Figure 4.92(d) is a variation of 1(c) where a secondary source is created with a set of CRLs. Sub- 50 nm resolution is expected, at an expense of some loss in the temporal resolution.

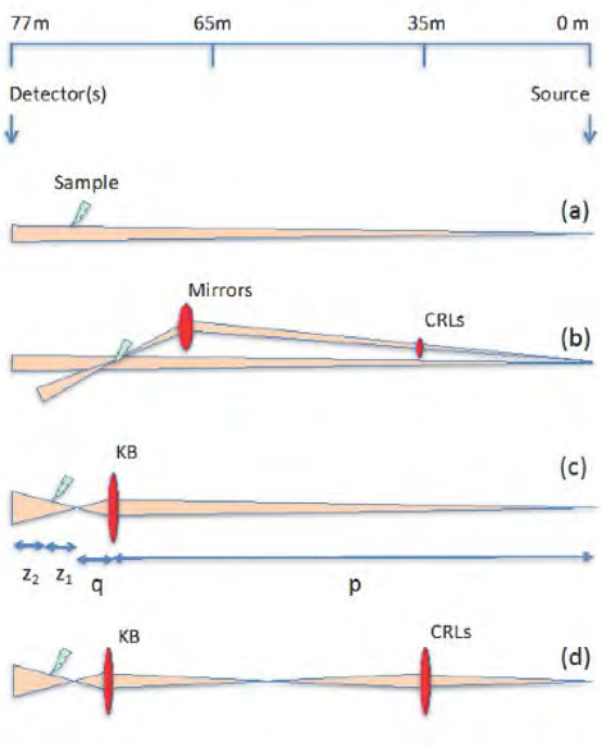


*Figure 4.92. The different operating modes for 32-ID beamline*

Figure 4.93 shows the planned beamline layout.

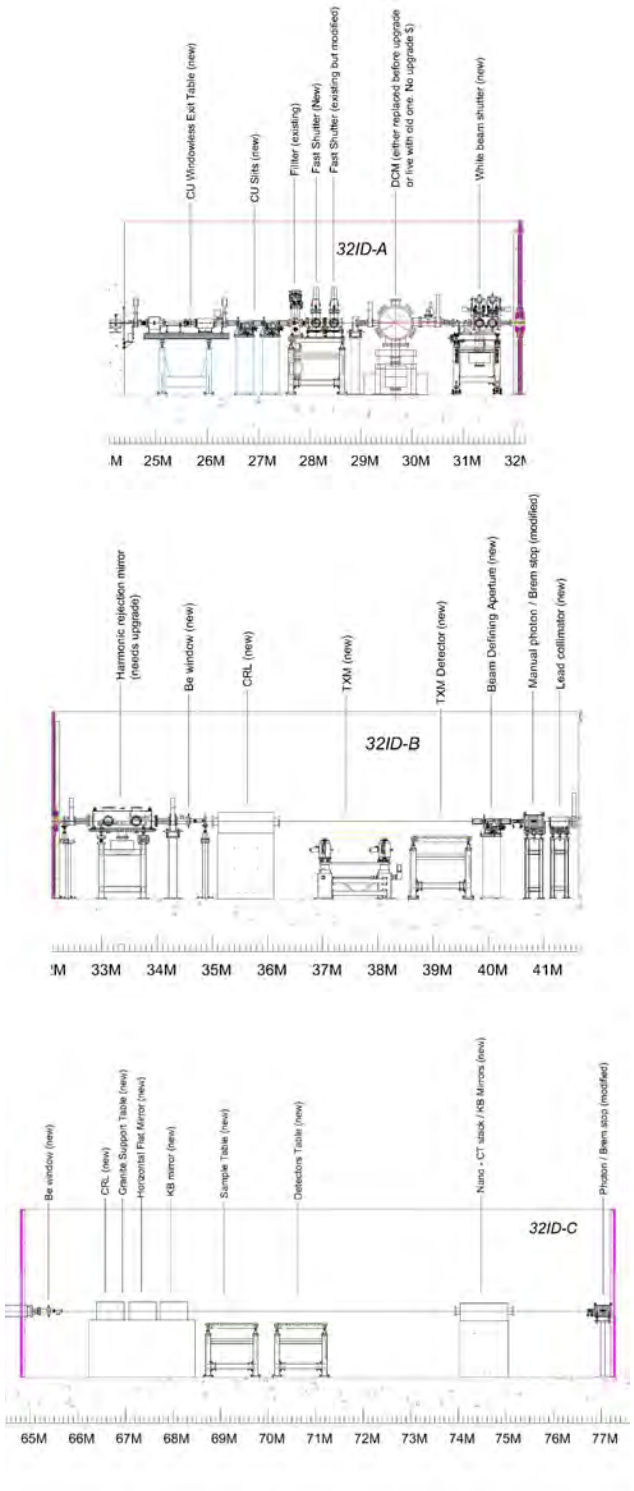


*Figure 4.93. Modified 32ID beamline layout showing 32-ID-A, 32-ID-B, and 32-ID-C stations.*

### 4-23.6 Instrument Overview n-CT

The new n-CT instrument will exploit the new APS-U source characteristics by implementing projection x-ray imaging for the high-speed imaging program at APS. A visualization of the instrument is shown in Figure 4.94.

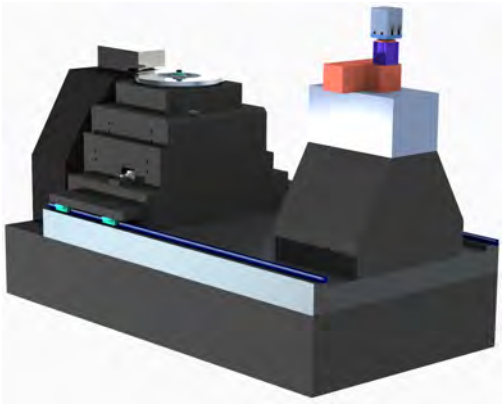

*Figure 4.94. n-CT instrument visualization.*

The following are capable measurements techniques of the new n-CT instrument:

1. Full field nano-computed tomography (FFnCT)
2. Nano scale x-ray fluorescence probing (XRF)

The difference between these modes of operation is the ability to change the working distance to the sample and thereby change the magnification and field of view of the instrument. Probing is considered when the sample is directly on the focal center of the KB optic. A detailed description of the 32-ID-C instrument can be found in the 32-ID-C Endstation Instrumentation ESD (ICMS Content ID: APSU_2030652).

## References


[1] Early Science at the Upgraded APS. https://www1.aps.anl.gov/files/download/Aps-Upgrade/Beamlines/APS-U%20Early-Science-103015-FINAL.pdf, 2015.

[2] G.G. Lonzarich. *Nat. Phys.*, 1:11, 2005.

[3] C. Pfleiderer. *Rev. Mod. Phys.*, 81:1551, 2009.

[4] L. Dubrovinsky and et al. *Nature*, 525:226–229, 2015.

[5] M. Eremets and et al. *Nature*, 411:170, 2011.

[6] Drozdov and et al. *Nature*, 525:73, 2015.

[7] L. Mirebeau and et al. *Nature*, 420:54, 2002.

[8] Aronson and et al. *Phy. Rev. Let.*, 63:2311, 1989.

[9] N. Souza-Neto and et al. *Phy. Rev. Let.*, 109:026403, 2012.

[10] N. Ishimatzu and et al. *Phy. Rev. B*, 83:180409, 2011.

[11] R. Torchio and et al. *PHY. REV. B*, 84:060403, 2011.

[12] Challenges at the Frontiers of Matter and Energy: Transformative Opportunities for Discovery Science. Technical report, Basic Energy Sciences Advisory Committee, November 2015.

[13] A Boker, Y Lin, K Chiapperini, R Horowitz, M Thompson, V Carreon, T Xu, C Abetz, H Skaff, A D Dinsmore, T Emrick, and T P Russell. Hierarchical nanoparticle assemblies formed by decorating breath figures. *Nature Materials*, 3(5):302–306, May 2004.

[14] Wei Bu, Hao Yu, Guangming Luo, Mrinal K Bera, Binyang Hou, Adam W Schuman, Binhua Lin, Mati Meron, Ivan Kuzmenko, Mark R Antonio, L Soderholm, and Mark L Schlossman. Observation of a Rare Earth Ion-Extractant Complex Arrested at the Oil Water Interface During Solvent Extraction. *Journal of Physical Chemistry B*, 118(36):10662–10674, 2014.

[15] Sahil R Vora, Brice Bognet, Huseini S Patanwala, Francisco Chinesta, and Anson W K Ma. Surface Pressure and Microstructure of Carbon Nanotubes at an Air-Water Interface. *Langmuir*, 31(16):4663–4672, 2015.

[16] Philipp Erni, Peter Fischer, Vishweshwara Herle, Martina Haug, and Erich J Windhab. Complex interfaces and their role in protein-stabilized soft materials. *Chemphyschem*, 9(13):1833–1837, 2008.

[17] Y Lin, A Boker, H Skaff, D Cookson, A D Dinsmore, T Emrick, and T P Russell. Nanoparticle assembly at fluid interfaces: Structure and dynamics. *Langmuir*, 21(1):191–194, 2005.

[18] F Bresme, Lehle H., and Oettel M. *J. Chem. Phys*, 130:214711, 2009.

[19] V Prasad, D Semwogerere, and Eric R Weeks. Confocal microscopy of colloids. *Journal of Physics: Condensed Matter*, 19(11), 2007.

[20] Mingwei Chen. A brief overview of bulk metallic glasses. *NPG Asia Materials*, 3(9):82–90, September 2011.

[21] Jan Schroers. Bulk Metallic Glasses. *Physics Today*, 66(2):32, 2013.

[22] W H Wang, C Dong, and C H Shek. Bulk metallic glasses. *Materials Science and Engineering: R: Reports*, 44(2-3):45–89, June 2004.

[23] C J Byrne and M Eldrup. Bulk Metallic Glasses. *Science*, 321:502, July 2008.

[24] W L Johnson, G Kaltenboeck, M D Demetriou, J P Schramm, X Liu, K Samwer, C P Kim, and D C Hofman. Beating Crystallization in Glass-Forming Metals by Millisecond Heating and Processing. *Science*, 332(6031):828, May 2011.

[25] E Nazaretski, Jungdae Kim, H Yan, K Lauer, D Eom, D Shu, J Maser, Z Pešić, U Wagner, C Rau, et al. Performance and characterization of the prototype nm-scale spatial resolution scanning multilayer laue lenses microscope. *Review of Scientific Instruments*, 84(3):033701, 2013.

[26] Mirko Holler and Jörg Raabe. Error motion compensating tracking interferometer for the position measurement of objects with rotational degree of freedom. *Optical Engineering*, 54(5):054101, 2015.

[27] F. Villar and et al. *MEDSI*, 2014.

[28] H.M. Jaeger and A.J. Liu. *cond-mat.soft*, 2010. arXiv:1009.487v1.

[29] T.Sun, Z. Jiang, J. Strzalka, L. Ocola, and J. Wang. *Nat. Photon*, 6:586–590, 2012.

[30] B Dickinson, GT Seidler, ZW Webb, JA Bradley, KP Nagle, SM Heald, RA Gordon, and I-Ming Chou. A short working distance multiple crystal x-ray spectrometer. *Review of Scientific Instruments*, 79(12):123112, 2008.

[31] BA Mattern, GT Seidler, M Haave, JI Pacold, RA Gordon, J Planillo, J Quintana, and B Rusthoven. A plastic miniature x-ray emission spectrometer based on the cylindrical von hamos geometry. *Review of Scientific Instruments*, 83(2):023901, 2012.

[32] Uwe Bergmann, Pieter Glatzel, and Stephen P Cramer. Bulk-sensitive xas characterization of light elements: from x-ray raman scattering to x-ray raman spectroscopy. *Microchemical Journal*, 71(2-3):221–230, 2002.

[33] JA Soininen, AL Ankudinov, and JJ Rehr. Inelastic scattering from core electrons: A multiple scattering approach. *Physical Review B*, 72(4):045136, 2005.

[34] JA Bradley, GT Seidler, G Cooper, Maarten Vos, Adam Percival Hitchcock, AP Sorini, C Schlimmer, and KP Nagle. Comparative study of the valence electronic excitations of n 2 by inelastic x-ray and electron scattering. *Physical review letters*, 105(5):053202, 2010.

[35] T Gog, GT Seidler, DM Casa, MH Upton, J Kim, Y Shvydko, S Stoupin, KP Nagle, M Balasubramanian, RA Gordon, et al. Momentum-resolved resonant and nonresonant inelastic x-ray scattering at the advanced photon source. *Synchrotron Radiation News*, 22(6):12–21, 2009.

[36] Timothy T Fister, Fernando D Vila, Gerald T Seidler, Lukas Svec, John C Linehan, and Julie O Cross. Local electronic structure of dicarba-closo-dodecarboranes c2b10h12. *Journal of the American Chemical Society*, 130(3):925–932, 2008.

[37] RA Gordon, GT Seidler, TT Fister, MW Haverkort, GA Sawatzky, A Tanaka, and TK Sham. High multipole transitions in nixs: Valence and hybridization in systems. *EPL*, 81(2):26004, 2008.

[38] TS Toellner, J Collins, K Goetze, MY Hu, C Preissner, E Trakhtenberg, and L Yan. Ultra-stable sub-mev monochromator for hard x-rays. *Journal of synchrotron radiation*, 22(5):1155–1162, 2015.